Development of Amine Functionalized Mesoporous Silica (KIT-6) for Carbon Dioxide Capture

Thesis

Submitted for the partial fulfillment for the degree of

DOCTOR OF PHILOSOPHY

by

RUPAK KISHOR

September 2017
Department of Chemical Engineering
Indian Institute of Technology Guwahati
Guwahati 781 039, Assam, India

Department of Chemical Engineering
Indian Institute of Technology Guwahati
Guwahati 781039 (India)

CERTIFICATE

It is certified that the work described in this thesis entitled **"Development of Amine Functionalized Mesoporous Silica (KIT-6) for Carbon Dioxide Capture** by **Rupak Kishor** for the award of degree of **Doctor of Philosophy** has been carried out under our supervision. This work has not been submitted elsewhere for any degree.

(**Dr. Sasidhar Gumma**), Administrative Supervisor

Professor

Department of Chemical Engineering

Indian Institute of Technology Guwahati

Guwahati 781039 (India)

ACKNOWLEDGEMENTS

First of all, I would like to express my sincere thanks to my thesis adviser, Professor Sasidhar Gumma and Professor A. K. Ghoshal, for providing me an opportunity to work under his guidance at Indian Institute of Technology Guwahati to explore the chemical engineering and science. I am deeply grateful for his valuable advice, motivation and competent guidance during my doctoral work.

I wish especially to thank my doctoral committee members Prof. Bishnupada Mandal, Dr. Mahuya De, Prof. Gopal Das for their fruitful suggestions and advices during my doctoral work. I am very thankful to Prof. Bishnupada Mandal, Prof. G. Pugazhenthi and Prof. Prabir Kumar Saha and all other faculty members for their advices and help during my doctoral work.

Special thanks to Central Instruments Facility for fulfill the need of sophisticated instruments (FESEM, TEM, N_2 adsorption/desorption, and CO_2/N_2 adsorption analysis) required during my doctoral work. I am also thankful of Prof. G. Krishnamoorthy (Head of the Central Instruments Facility) Mr. M. Borah, Dr. K. K. Senapati, Mr. C. Borgohain, Mr. K. K. Singh and others staffs for constant help.

I am very grateful for the help from all my co-research fellows Abhik Bhattacharjee, Sravanthi Loganathan, Satyannarayana Edubilli, Prashant Mishra, Kishant Kumar, Prudhvi Medikonda, Sanjeeb Barma, D. Sahu, Sohanbir singh, Supriyo Kumar Mondal, Pradip Das, and Patrali for

their help in several forms during my doctoral work. I am also thankful to all the technical staffs Mr. Debojit, Mr. Harsha, Mr. kaustav, Ms. Ritumoni, Mr. Lukumoni, Mr. Prasun and non-technical staffs of chemical engineering department.

Finally, I wish to thank my family for their invaluable personal and financial support, their understanding and patience.

(Rupak Kishor)

ABSTRACT

The doctoral work focuses on the development of amine functionalized mesoporous silica based CO_2 adsorbent. Mechanical, thermal, hydrothermal and hydrolytic stability of material are important parameters in designing an adsorbent. They decide the working limitation of the material during practical application. Additionally, physical properties such as specific surface area, pore volume, pore diameter and pore structure also affect the performance during application. In last few years, large varieties of mesoporous silica were discovered. Three dimensional mesoporous KIT-6with large interconnected pores is selected in this study based on its stability in extreme external conditions. KIT-6 shows the high mechanical stability (up to 4680 bar) and thermal stability (upto 900°C); possibly due to the presence of thicker pore wall and cubical structure. It also shows the stable structural properties even after ageing for six months in atmospheric conditions and one month in water at room temperature. In addition, after three days of ageing in boiling water, KIT-6 still retains its porosity. At high pressure, a good surface interaction is seen between KIT-6 and CO_2 without significant damage to the structure. KIT-6 also shows 2.38 wt% H_2 storage capacity at 30 bar and −196 °C. The highly stable KIT-6 is considered to be a good material for adsorbent, catalyst support and nanostructure synthesis. But low CO_2 sorption capacity at low partial pressure suggests further improvement in KIT-6 for practical application.

The CO_2 sorption capacity at low partial pressure is improved by grafting of APTES in highly stable mesoporous KIT-6. The grafting capacity of APTES on KIT-6 is tailored with increase in water concentration in the grafting solution (toluene). Presences of water in the grafting solution improves the APTES loading through double condensation. It shows an agglomeration of APTES and leading to a non-uniform distribution on KIT-6. However, the CO_2 sorption capacity is improved from 0.48 mmol/g (KIT-6) to 1.56 mmol/g (0.20KIT 9.0AP) at 1 bar and 30 °C.

The sorption capacity depends on the accessible amine group present for CO_2 in the adsorbent. The intensity of amine in the KIT-6 is further improved by grafting of TMPTA and compared the sorption performance with MCM-41 and SBA-15. It is found that the sorption capacity of KIT-6 is increased up to 2.59 mmol CO_2/g (WK30T) at 30°C and 1 bar. However, MCM-41 and SBA-15 show the maximum sorption capacity of 1.34 mmol CO_2/g (M20T) and 1.54 mmol CO_2/g (S20T), respectively at 30°C and 1 bar. After aqueous grafting of TMPTA, the sorption capacity of MCM-41 and SBA-15 are sharply decreased because of pore blocking and reduction in the accessible amine group.

CO_2 sorption capacity of aminosilane grafted KIT-6 gradually decreases with increase in adsorption temperature. Hereafter, CO_2 sorption capacity is further improved by impregnation of wide varieties of polyethyleneimines (DETA, TEPA, PEHA, PEI-800, PEI-1200 and PEI-25K) in KIT-6. The sorption capacity of polyethyleneimine impregnated KIT-6 is gradually increased with increase in temperature from 30 °C to 105 °C. In addition, KIT-6 shows better CO_2 adsorption performance than more traditional MCM-41, SBA-15 and HV MCM-41. The 60 wt% PEHA impregnated KIT-6 (K/60 PEHA) shows the maximum sorption capacity of 4.0 – 4.5 mmol CO_2/g at 90 −105 °C at 1 bar. The adsorbent is further improved by impregnation of polyethyleneimine in as-synthesized KIT-6 (ASK) in minimum time and energy. The confiscated

structure directing agent within ASK improves the thermal stability as well as kinetics of adsorbent during CO_2 adsorption. The 60 wt% PEHA impregnated ASK shows the stable sorption capacity of 3.86 – 4.18 mmol CO_2/g at 90−105 ℃ and 1 bar. Thus, high sorption capacity at low partial pressure and high temperature illuminate ASK (particularly, 60wt% PEHA impregnated ASK) a promising candidate for CO_2 capture from large anthropogenic source.

CONTENTS

LIST OF FIGURES

LIST OF TABLES

LIST OF ABBREVIATIONS	
AC	Activated carbon
AEEA	(2-aminoethyl)ethanolamine
AHPD	2-amino-2-hydroxymethyl-1,3-propanediol
BET	Brunauer–Emmett–Teller
BJH	Barrett, Joyner, and Halenda
GHG	Greenhouse gas
CCSU	Carbon capture sequestration and utilization
CCU	Carbon capture and utilization
CTAB	cetyltrimethylammoniumcation
DRIFT	Diffuse reflectance infrared fourier transform spectroscopy
DEA	Diethanolamine
DETA	Diethylenetriamine
DGA	Diglycolamine
DEC	Dimethyl carbonate
DMDA	Dimethyl decylamine
FESEM	Field emission scanning electron microscope
FTIR	Fourier transform infrared spectroscopy
HAS	hyperbranched aminosilica
HV MCM-41	High pore volume MCM-41
MOFs	Metal organic freamworks
MEA	Monoethanolamine
NGCC	Natural gas combined cycle
OMS	Ordered mesoporous silica
PZ	Piperazine
PE	2-piperidineethanol
PEHA	Pentaethylenehexamine
PEI	Polyethylenimine
ppm	Parts per million
ppb	Parts per billion

TSA	Temperature swing adsorption
PSA	Pressure swing adsorption
PEO	Poly(ethylene oxide)
PEG	Poly(ethylene glycol)
PPO	Poly(propylene oxide)
TEM	Transmission electron micrograph
TGA	Thermogravimetry analyzer
XRD	X-ray diffraction
TMPTA	N^1-(3-trimethoxysilylpropyl)diethylenetriamine
TEPA	Tetraethylenepentamine

NOMENCLATURE	
a_0	Unit cell parameter
b	Affinity parameter (/bar)
$d_{(211)}$	Interplanar spacing (nm)
ΔH	Heat of adsorption (kJ/mol)
q	Adsorption capacity (mmol/g)
R	Universal gas constant (J/mol.K)
W	Pore size (nm)
p	Pressure
Δr	Heat of reaction (kJ/mol)
S	Specific surface area (m^2/g)
t	Time
T	Temperature (°C)
V_t	Total pore volume (cc/g)

CHAPTER 1

INTRODUCTION

CHAPTER 1

The chapter provides a brief introduction to different energy sources and their impact on global warming. The advantage of the solid based adsorption over other CO_2 separation techniques such as amine-based absorption, porous membrane and by algae biomass is comprehensively discussed. The selection criteria of an adsorbent for economic separation of CO_2 are listed. At the end of this Chapter, the outlines of the doctoral work are presented.

1.1 Motivation

World energy demand gradually increases with time in view of growing global population and industrialisation [1,2]. Today, India is home to one-sixth of the world's population with the third-largest economy but accounts for only 6% of global energy use. One in five of the population (~240 million people) still lacks access to electricity. With the policies in place to accelerate the country's modernization and develop its manufacturing base (via the "Make in India" programme), population and income are on the rise. An additional 315 million people are anticipated to live in Indian cities by 2040. Thus, India is entering into an era of rapid growth in energy consumption. Coal based power plants in India, with an installed capacity of over 130 GW account for more than half of the energy production in the country and approximately 650 $MtCO_2$ annually i.e. 37.5% of the total GHG emissions of the country [3,4]. With a large number of new coal power plants (~ 450 plants with about 520 GW capacity) being proposed, the problem of greenhouse gases (GHGs) emissions is going to persist [5].

Since long, conventional fossil fuel such as coal, oil and natural gas is a major source of energy production (Figure 1) [1]. It is also a major anthropogenic source of GHGs such as CO_2, CH_4, N_2O and fluorinated gas in the atmosphere. The concentration of GHGs in the atmosphere increased from about 310 ppm CO_2, 1147 ppb CH_4 and 289 ppb N_2O in 1950 to 389 ppm CO_2, 1810 ppb CH_4 and 323 ppb N_2O in 2010 (Figure 2) [2]. CO_2, N_2 and H_2O are the major components in flue gas (Table 1). Additionally, CO_2 is a major GHG [6]. Its concentration is gradually increasing in the atmosphere by burning the fossil fuels. The emission of CO_2 can be reduced by capturing from scientific method and utilising for useful product synthesis as well as sequestration. The CO_2 concentration already reached to ~ 407 ppm (the year 2016) in the atmosphere [7]. The increment in CO_2 concentration gradually increases the global surface temperature, which is dragging it towards the global warming limit of +2 ºC [8]. The global surface temperature has already increased to +1.5 ºC from pre-industrial era. Before any catastrophic event, it is essential to control the CO_2 emissions in the atmosphere.

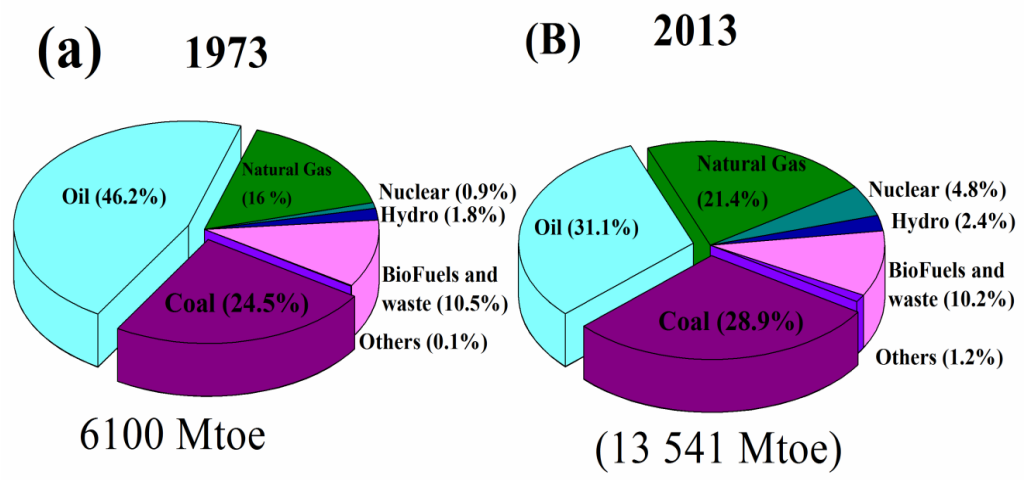

Figure 1.1 Sources of energy in (a) 1973 and (b) 2013

Table 1.1

Typical properties of major components in the flue gas emitted from coal based thermal power plant [6].

Carbondioxide, CO_2 (mol %)	13
Nitrogen, N_2 (mol %)	62
Oxygen, O_2 (mol %)	3.5
Water, H_2O (mol %)	20.5
Argon, Ar (mol %)	0.8
Nitrous oxide, NOx (ppmv dry basis)	151
Sulfur dioxide, SOx (ppmv dry basis)	212

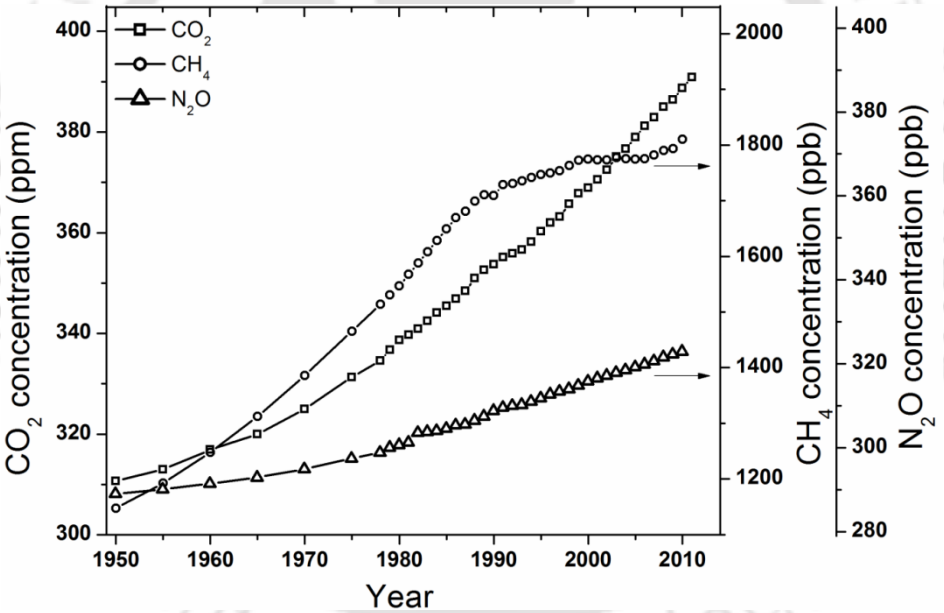

Figure 1.2 Major greenhouse gas concentration in atmosphere

Carbon capture sequestration and utilisation (CCSU) is a promising option to control the GHG emissions in the atmosphere. Under this concept, CO_2 is captured from an anthropogenic source such as coal and petroleum oil based thermal power plants. Then the captured CO_2 is converted

into a useful products such as methanol, plastic and other hydrocarbons for economic benefits [9–11]. However, the excess CO_2 is injected into geological formations, such as depleted oil and gas fields, saline formations, and unmineable coal seams [12]. During this step, CO_2 would be locked up (sequestered) for more than 100 to 1000 years. The feasibility of using this phenomenon (sequestration) as a mitigation measure has been demonstrated successfully at various projects around the world. For example, at Sleipner (Norway), CO_2 is being stored in a saline aquifer under the North Sea [13]. However, according to the Global Energy Assessment Report, India has limited geological storage capacity. The Deccan volcanic province exposed in the western and central India cover an area of approximately $5x10^5$ km^2 and could be considered for a large sink of CO_2 storage.

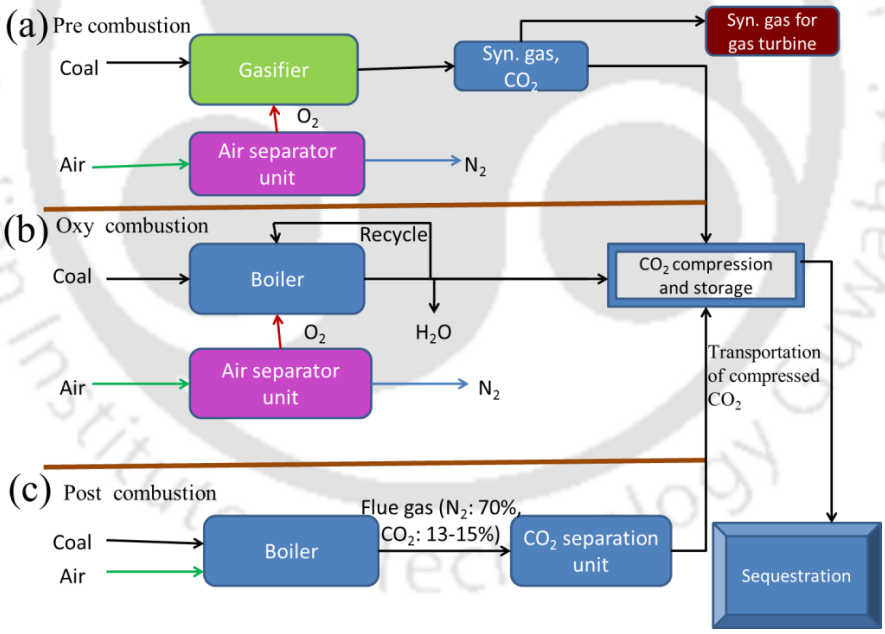

Figure 1.3 Schematic illustration of CCSU by pre-combustion, oxy-combustion and post-combustion systems

1.2 Carbon Capture Technologies

Each step in CCSU is a landmark in itself. Thus, carbon capture step is most important as it also decides the economics of CCSU process as a whole. Three technological pathways can be pursued for CO_2 capture from coal-derived power generation: pre-combustion capture, oxy-combustion and post-combustion capture, as illustrated in Figure 1.3.

Pre-combustion strips the CO_2 out of the fuel before it is burned, via a series of interlinked chemical reactions (Figure 1.3a). The fossil fuel is converted to syngas (carbon monoxide and hydrogen), which is then reacted with water vapour (a "shift reaction") to form an easily separable mixture of hydrogen and CO_2. The hydrogen is then burned as high calorific energy fuel. It is mainly applicable to new power plant. In Oxy-fuel combustion process, pure oxygen is separated from the air (Figure 1.3b) and the fuel is almost pure oxygen instead of air. Thus, the exhaust gas from the boiler mostly consists of a separable mixture of CO_2 and water. However, production of pure oxygen is an expensive and energy-intensive process. Additionally, oxy-combustion can be applied to new plants or retrofitted to existing plants by extensive modification. Post-combustion CO_2 captures process is illustrated in Figure 1.3c. It is the last section of a process plant and can be easily retrofitted to existing and new power plants. Existing power plants use air for combustion and generate a flue gas at atmospheric pressure with a CO_2 concentration of less than 15%. Thus, the thermodynamic driving force for CO_2 capture from flue gas is low as CO_2 partial pressure is typically less than 0.15 atm. This is a technical challenge for the development of cost-effective advanced capture process [6]. In spite of this difficulty, post-combustion carbon capture is having the greatest near-term potential for reducing GHG emissions, because of its retrofitting possibility to existing units in the power sector that

generate two-thirds of the CO_2 emissions. Some of the major options for post-combustion CO_2 capture are discussed in the following section.

1.3 State of the Art Current CO_2 Separation Techniques

The flue gas composition varies with feed composition, but a typical composition is summarised in Table 1. There are different separation techniques as follows:

1.3.1 *Amine-based absorption system*

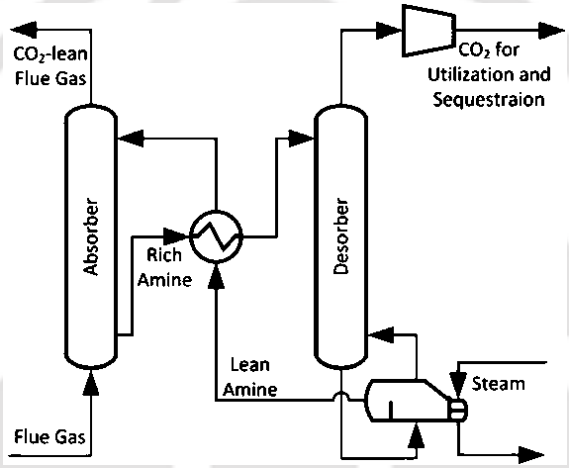

Figure 1.4 Schematic illustration of carbon capture by amine absorption process

CO_2 absorption process using aqueous amine solution for a power plant is shown in Figure 1.4. Flue gas is bubbled through a column containing the aqueous amine, which absorbs the CO_2. The CO_2-rich amine is then sent to a stripper, typically heated with steam where the CO_2 is released from the solution which is compressed afterwards for transport and sequestration. There are numerous studies available for CO_2 capture from thermal power plants, refineries and natural gas conditioning units using aqueous amine solution. The amines such as monoethanolamine (MEA) [14−18], diethanolamine (DEA) [16], diglycolamine (DGA) [19], (2-aminoethyl)ethanolamine (AEEA) [16], 2-amino-2-hydroxymethyl-1,3-propanediol (AHPD) [20] and 2-piperidineethanol

(PE) [21] are widely used. In addition, dimethyl carbonate (DMC) [22] and sodium glycinate [23] are also used for CO_2 absorption. More recently, aqueous piperazine (PZ) opened a new window for CO_2 capture [17,18,24]. Piperazine requires lower regeneration temperature, increases resistance to oxidative degradation and most importantly is not corrosive to stainless steel [18,24]. Presently in the world, there are four amine based projects in whichthe capture; transport and storage of carbon dioxide are beingsimultaneously demonstrated. They are the projects Sleipner (Norway), Weyburn (USA–Canada), In Salah (Algeria) andSnøhvit (Norway). The amount of stored carbon dioxide of thefour projects totals to about 7 million ton per annum.

Improvements to amine-based systems for post/pre-combustion CO_2 capture are being pursued by a number of process developers; a few of these are Fluor, Mitsubishi Heavy Industries (MHI), and Cansolv Technologies.Fluor's Econamine FG Plus has demonstrated the 350 ton/day CO_2 capture from natural gas fire power plant in Bellingham, MA. MHI has developed a new absorption process, referred to as KS-1. Furthermore, the German activities comprise theconstruction of post-combustion plants (Wilhelmshaven andJänschwalde), a pre-combustion plant at the site Hürth and thebuilding of an Oxy-fuel plant at the power-plant site Jänschwalde.

However, the major challenge for CO_2 capture from the thermal power plant is the large volumetric flow rate of flue gas at moderate temperature (~100 −150 ºC). The integration of CO_2 absorption unit leads to a reduction in net power output, where the largest contributors to the power loss are the parasitic heat required during solvent regeneration and CO_2 compression [25,26]. Additionally, amine degradation results in increased environmental impacts as volatile degradation products are emitted to air with flue gas exhaust [17,24,26,27]. Veltman et al. [27] compared the three scenarios (1) post-combustion CO_2 capture from 400 MW NGCC (natural gas combined cycle) using aqueous MEA, (2) a conventional 420 MW coal-fired power plant;

and (3) a 420 MW NGCC without capture on human and environmental impact. They concluded that the emissions of the amine-based scrubbing solvent MEA, result in a 10-fold increase in freshwater toxicity impacts. Thus, the above literature indicates that amine-based absorption process is still associated with many challenges and needs further research for better performance.

Emerging Technologies

1.3.2 *Membrane based separation*

Membranes are used for separating gas mixtures where they act as a permeable barrier through which different compounds move across at different rates. It is basically size selective method and permeates concentration increases with increasing the pressure. It is basically made from polymers [28−30], ceramics [31,32,33] and metallic substance [29,30]. Li et al. [31] tested the permeabilities of several gases (H_2, N_2, O_2, Ar, He, H_2S, CO_2 and C_3H_6) through a silicon based inorganic membrane measured in the pressure range of 10 to 50 psi and temperature range of 25 to 700°C. The permeabilities of all the gases decrease with increasing temperature. However, the permeability of condensable gases such as CO_2, C_3H_6 and H_2S decreased faster than those of noncondensable gases such as N_2, He, Ar and O_2. Prabhakar et al.[34] studied the permeabilities of N_2, O_2, CO_2, CH_4, C_2H_6, and C_3H_8 on Hyflon AD 80 membrane. The penetrant permeability decrease as molecular size increases. The penetrant permeability of different gases are as follow: $CO_2 > O_2 > N_2 > CH_4 > C_2H_6$. However, most of the membranes showed low CO_2/N_2 selectivity.

In the recent time, membrane was functionalized with different active materials such as amine [29,33,34], metal organic frameworks (MOFs) [29] and different type of zeolites [36] to improve the CO_2/N_2 selectivity. More recently, Shahid et al. [29] dispersed 0 to 30 wt% of the three

distinctively different MOFs (MIL-53(Al) (breathing MOF), ZIF-8 (flexible MOF) and Cu_3BTC_2 (rigid MOF)) into Matrimids-PI membrane. The CO_2 permeability for these functionalized membranes was increased by 132%, 144% and 89%, respectively as compared to native Matrimids-PI membranes. The enhanced CO_2 permeability is partly attributed to the higher diffusivity of CO_2 through the MOFs. Roussanaly et al. [37] compared the CO_2 selective membrane process with more traditional MEA based CO_2 absorption process. They concluded that the membrane permeance and selectivity have to be at least superior to 3 m^3(STP)/(m^2 h bar) and 65, when high selectivities and high permeances are considered, respectively. However, with more advanced configured (for example with recycling, sweep, counter-current flow pattern, etc.) membranes processes with permeances as slow as 1 m^3(STP)/(m^2 h bar) with high selectivities, and membranes of low selectivities as 30 with high permeances could compete with MEA-based capture process. Ho et al. [38] studied the economics of membrane process and compared with MEA process. They concluded that lower costs and higher tonnages of CO_2 avoided could be achieved using an amine-based absorption capture process. The lower CO_2/N_2 selectivity and low permeate flux for a higher volume of flue gas pay further attention to future research for improvement in membrane properties.

1.3.3 *Microalgae-based process*

Microalgae are prokaryotic or eukaryotic photosynthetic microorganisms that can grow rapidly and live in harsh conditions due to their unicellular or simple multicellular structure. They are unique to other microorganisms due to the presence of chlorophyll. They have the photosynthetic ability in a single algal cell, which allows easy operation for biomass generation and effective genetic and metabolic research in a much shorter period than conventional plants [39].

Figure 1.5 Production of microalgae

Photosynthesis occurs in two main stages: light-dependent reactions and light independent reactions. Light-dependent reactions occur only when the cells are illuminated. Carbon-fixation reactions, also known as dark reactions, occur both in the presence and absence of light. The following empirical equation is frequently used to describe the overall reaction of photosynthesis [40]: $6\,CO_2 + 6\,H_2O \longrightarrow C_6H_{12}O_6 + 6\,O_2$

CO_2 is utilised as a carbon source by microalgae during photosynthesis and is converted to different organic cell components including carbohydrates, lipids, proteins, and nucleic acids [41]. One kilogram of algal dry cell weight utilises around 1.83 kg of CO_2. Annually around 54.9 − 67.7 tonnes of CO_2 can be sequestered in raceway ponds corresponding to annual dry weight biomass production rate of 30−37 tonnes per hectare [42]. Algal biomass can be used for the production of biofuels (e.g. biodiesel, bioethanol, biohydrogen, which are alternative renewable fuels to existing fossil diesel and gasoline) and other commercially and scientifically important products utilised for medications, cosmetics and nutritious foods, representing additional benefits from the microalgal CO_2 reduction process [43]. Microalgae can utilise CO_2 from different sources such as atmospheric, industrial exhaust gases and soluble carbonates (e.g. $NaHCO_3$ and Na_2CO_3) [44]. *Scenedesmus* sp. and *Chlorella* sp. have been identified as promising microalgae strains for CO_2 sequestration. Depending on the microalga strain, a supplement of 1-20% CO_2 is generally suitable for microalgal cultivation [45]. This approach would be a win-win situation

where CO_2 mitigation and renewable energy production are created on the same platform in order to have sustainability of the microalgae industry.

As a contrary, due to the lack of understanding of this technology, several issues and problems are normally ignored, such as a heavy requirement of inorganic nutrients and intensive energy in cultivating, harvesting and drying of microalgal biomass [43]. The consequence of these limitations may lead to serious negative CO_2 and energy balance in the life cycle of microalgae biodiesel production. On the other hand, some of the microalgae strains are highly sensitive to the contaminants and a high temperature of flue gas. Apart from that, low solubility of CO_2 in water is another problem that needs further attention.

1.3.4 Solid based adsorption process

Among the many process technologies for CO_2 capture from flue gases, there is a growing interest towards adsorption process as a promising alternative. The low regeneration energy requirement for CO_2 adsorbed sorbent makes it a great alternative compared to traditional aqueous MEA based absorption process. Adsorption process using novel sorbent can reversibly adsorb the CO_2 from a gas mixture with very high selectivity [47]. In last few years, several adsorbents such as ordered mesoporous silica (OMS), metal organic frameworks (MOFs), activated carbon (AC) and zeolites, etc. have been discovered for CO_2 separation [47]. Several CO_2 adsorptive separation mechanisms have been proposed, and they are highly dependent on the properties of adsorbents used, as well as the associated interactions. Numerous efforts have been carried out by many researchers to improve the surface properties of the material. The sorption capacity of AC has been improved by incorporation of amine [47,48]. Research Triangle Institute (RTI, Nelson,2009) is investigating a dry, inexpensive, regenerable, supported

sorbent sodium carbonate (Na_2CO_3), which reacts with CO_2 and water to form sodium bicarbonate ($NaHCO_3$) [49]. A temperature swing is then applied to regenerate the sorbent and produce a pure CO_2/water stream. J. R. Long has shown the adsorption capacity about 9.0 mmol CO_2/g of Mg_2(dobdc) at 1bar and 20 ºC [50]. Sayari et al. have improved the pore size and pore volume of traditional MCM-41 by adding the dimethyl decylamine (DMDA) swelling agent in synthesis solution [51]. Additionally, they improved the amine loading and CO_2 sorption capacity over traditional MCM-41 [52]. But, sorbent selection for practical application for CO_2 capture from the flue gas is a complex problem, and it should fulfil the following criteria to become a good adsorbent [47,52].

1. *Sorption capacity*: It is the maximum amount of CO_2 adsorbed at a specific pressure and temperature. It is represented by equilibrium adsorption isotherm. The high adsorption capacity reduces both adsorbent and operational costs.

2. *Selectivity*: it is simply expressed as $S_{ads} = (q_i/q_j)/(y_i/y_j)$; where q_i and y_i is the mole fraction of the species *i* in the adsorbed phase and in the bulk phase, respectively. For the efficient separation of CO_2 from the flue gas or a gas mixture, selectivity should be very high.

3. *Adsorption/desorption kinetics*: Adsorption/desorption kinetics directly control the cycle time of the fixed bed adsorption process. Fast adsorption/desorption kinetics is desirable properties of an adsorbent-adsorbate system as it reduces the time span between successive operations.

4. *Tolerance of moisture/impurities*: In addition to CO_2 andN_2, flue gas also contains other components such as CO, N_2O, SO_2 and moisture. High tolerance to moisture/impuritiespreserves the structural properties as well as CO_2 adsorption performance of adsorbent for a longer time.

5. *Thermal/Mechanical stability*: Thermal/mechanical property is an important parameter of the material. High thermal stability of adsorbent is favourable for sustaining the wide range of temperature for adsorption/desorption. High mechanical stability is required to avoid breakage during real adsorbent synthesis (pellet form) for an application.

5. *Cyclic stability*: Cyclic performance is indirectly associated with the replacement of the adsorbent after its usage. In gas adsorption, the sorbent is regenerated by changing the temperature (temperature swing adsorption, TSA), pressure (Pressure swing adsorption, PSA) else both temperature and pressure (TSA and PSA) simultaneously. Higher cyclic stability reduces the replacement cost of the adsorbent and also the operational complexity.

6. *Low Cost*: Apart from the above characteristics, sorbent cost is the most important criterion. The Higher sorbent may become an obstacle during scale up for an application. Tarka et al. used a base line of ca. $10/kg of adsorbent for fruitful application [53]. According to them, sorbent cost near about $15/kg adsorbent is not economical and $5/kg-adsorbent is more favourable for the process.

The above-mentioned criteria are desirable to become an ideal adsorbent for CO_2 separation from flue gas and gas mixture.

The technologies discussed earlier are associated with certain merits and demerits. A techno-economic and environmental assessment study suggests an 80% increase in the cost of electricity when CO_2 capture with aqueous MEA (30 wt%) absorption is employed in coal based thermal power plant [54]. CO_2 separation by membrane process is yet not economical compared to MEA process based absorption and not suitable for a large volume of CO_2 emitted with low concentration from the coal based thermal power plant [38]. Microalgae have the potential to

utilise the CO_2 by photosynthesis, but slow uptake reaction and long-time requirement during growth are yet to prove it suitable for CO_2 utilisation [38]. Adsorption based CO_2 separation is capable to capture high adsorption capacity through the use of novel adsorbent having low cost and high selectivity. However, low regeneration energy requirement over amine-based absorption makes it more attractive for industrial application.

Every adsorbent has certain merits and demerits. Activated carbon and alumina have low adsorption capacity. Zeolites require high heat of regeneration and susceptible to moisture. Low adsorption capacity and high regeneration temperature make it less favourable for CO_2 adsorption. In last few years, a wide variety of MOFs received special attention in gas separation and storage. But difficulties in storing, handling and susceptibility to moisture during real application need to be addressed and thus requires further improvement in its properties [55]. On the other hand, amine-functionalized mesoporous silica shows positive effect during CO_2 sorption in the presence of moisture. High CO_2 sorption capacity in low partial pressure and a wide range of temperature makes it a promising candidate over other adsorbents [55].

In early 1990's, the discovery of ordered mesoporous silica M41S with uniform hexagonal pore array structure and large internal surface area by researchers at the Mobil Oil Corporation using quaternary ammonium ($C_nH_{2n+1}(CH_3)_3NX$, X = Cl or Br) ionic template by liquid crystal templating sol-gel method in highly basic medium was a great embodiment in material science and engineering [56]. It has attracted great attention in wide range of applications such as host-guest chemistry, size selective separation, nano-material synthesis and enzyme immobilization due to their aloof intrinsic properties like high specific surface area (> 600 m^2/g), pore volume (> 0.5 cc/g), narrow pore size (2–30 nm) and presence of silanol group on the surface [55,57].There have been numerous efforts carried out to improve their physicalproperties. MCM

pores were tailored between 1.5 to 10 nm by using surfactants withvariable chain length and swelling organic compounds [58].Incorporation of aluminiumand fluoride anionsin ordered mesoporous silica (OMS) frameworks led to an improvement of the hydrothermal stability [59]. After the discovery of MCM using an ionic template, nontoxic and biodegradable polymers like polyethyleneoxide (PEO) and triblock copolymer poly(ethylene oxide)-poly(propylene oxide)-poly(ethylene oxide) (Pluronic, PEO_x–PPO_y–PEO_x) were identified as possible non-ionic templates for synthesis of OMS [60−62]. Zhao and coworkers synthesized wide varieties of mesoporous silica (lamellar, hexagonal and cubic) using wide various non-ionic templates (alkyl ethylene oxide, tween, span, triton, teritor, pluronic and tetronic surfactant) [61].The synthesized silica with non–ionic template remarkably improved the pore size (4 – 30 nm), wall thickness (up to 6 nm), thermal and hydrothermal stability. Subsequently, Ryoo et al. [62] modified the 2D hexagonal structure (SBA-15) to 3D cubical (KIT-6) by incorporating additional co-structure directing agent (n-butanol) in the synthesis solution. Additionally, the 3D mesoporous silica with large interconnected pores showed better kinetics performance in catalyst activityand gas adsorption/purification compared to the other OMSs like MCM-41, MCM-48, MCM-50 and SBA-15 [63,64].

Amine functionalized mesoporous silica received great attention among the researchers in past few years for CO_2 capture application. Zeleňák et al.[65] reported the CO_2 adsorption on aminopropyle grafted 2D hexagonal MCM-41, SBA-15 and 3D cubical SBA-12. They concluded that the three-dimensional structure with interconnecting pore provides better grafting surface for aminopropyle and thus shows better CO_2 adsorption.They further reported that the amine-functionalized mesoporous silica showed an increase in adsorption capacity with increase in pore size. The pore size and adsorption capacity as per their result are as follow: MCM-41 (3.3

nm; 0.57 mmol/g), SBA-12 (3.8 nm 1.04 mmol/g) and SBA-15 (7.1 nm 1.54 mmol/g) at 25°C [66]. More recently, synthesized mesoporous KIT-6 by Ryoo in mild acidic condition possessed lucrative intrinsic properties such as 3D cubical structure with large interconnected pore, high surface area and pore volume [62]. After amine functionalization, it is capable of becoming a good adsorbent for CO_2 separation.

Application of mesoporous silica as an industrial catalyst and commercial adsorbent has been carried out by surfacemodification and specific structure formation through post-synthesis treatment in extreme external conditions such as high temperature and pressure. Therefore, it is essential to understand the behavior of mesoporous KIT-6 in conditions like high pressure, high temperature and high moisture content. Additionally, amine-functionalized mesoporous silica sharply improved the CO_2 equilibrium adsorption capacity. In view of this, an effort has been undertaken in this doctoral work to develop a highly stable and efficient mesoporous KIT-6 for effective CO_2 capture.

1.4 Organization of Thesis

Chapter 1 of the thesis provides a brief introduction about energy production and CO_2 emissions by different sectors across the globe. In view of this, various CO_2 capture technology with the possible CO_2 separation techniques are discussed. The advantages of adsorption process over other separation techniques are thoroughly discussed in this section. Thereafter, this chapter presents the outline of the thesis work. In Chapter 2, performances of the various adsorbents available in the literature for CO_2 capture application are discussed along with the merits and demerits. The sorption capacities of various adsorbents for different gases are also summarized. This chapter at its end covers the objectives of the present work along with the detailed measurable objectives. Chapter 3, discusses the synthesis of amine functionalized ordered

mesoporous KIT-6 and explains the gas adsorption/desorption analysis by the volumetric and gravimetric method. It also explains the different analytical techniques for characterization of materials. In chapter 4, the comprehensive study such as hydrothermal, thermal, mechanical and hydrolytic stability of KIT-6 in extreme conditions is reported. Chapter 5 reports the comprehensive study of the CO_2/N_2 adsorption/desorption behaviour on (3-aminopropyl)triethoxysilane (APTES) functionalized KIT-6. Additionally, it also discusses the grafting mechanism of APTES on KIT-6. Further, the improvement in CO_2 adsorption capacity by the grafting of *N*[1]-(3-trimethoxysilylpropyl)diethylenetriamine (TMPTA) in KIT-6 and comparison of its performance with more traditional MCM-41 and SBA-15 are presented in Chapter 6. The extended study for CO_2 adsorption by functionalization of calcined KIT-6 with different polyethylenimine by wet impregnation method is discussed in Chapter 7. In this chapter, characterization of functionalized KIT-6 by different analytical techniques and study of the CO_2/N_2 selective separation in wide range of temperature and pressure are also included. Chapter 8 reports the development of an easy and facile way to synthesize the CO_2 adsorbent by impregnation of different polyethylenimine in KIT-6 with confiscated structure directing agent in minimum time and energy. The functionalized adsorbents are studied for the CO_2/N_2 adsorption over a wide range of temperature and pressure. Finally, the major inferences drawn from the doctoral work and an outlook for future studies are incorporated in Chapter 9.

1.5 Conclusions

This chapter provides a brief introduction about amine based absorption process, solid based adsorption process as well as membraneand algal technology for CO_2 separationfrom flue gas. Significant works for the development of amine functionalized mesoporous silica as an adsorbent as well as selection criteria for CO_2 separation from flue gas has also been illustrated.

References

[1] Key world energy statistics 2015, The international energy agency. http://www.iea.org/publications/freepublications/publication/KeyWorld_Statistics_2015.pdf

[2] The European Environment Agency (http://www.eea.europa.eu/themes/air)

[3] CEA, 2013: Monthly all India generation capacity report, December 2013, available at the central electricity authority, India's website: (http://www.cea.nic.in/reports/monthly/executive_rep/dec13.pdf)

[4] INCCA, 2010: "India – Greenhouse Gas Emission 2007", A report by Indian network for climate change assessment, ministry of environment and forests, Government of India, http://moef.nic.in/sites/default/files/Report_INCCA.pdf

[5] WRI, 2012: "Global coal risk assessment – data analysis and market research", a working paper by world resource institute, available at: http://www.wri.org/publication/global-coal-risk-assessment

[6] K.A. Mumford, K.H. Smith, C.J. Anderson, S. Shen, W. Tao, Y.A. Suryaputradinata, A. Qader, B. Hooper, R.A. Innocenzi, S.E. Kentish, G.W. Stevens, Post-combustion capture of CO_2: results from the solvent absorption capture plant at Hazelwood power station using potassium carbonate solvent, Energy Fuels, 26 (2011), 138–146

[7] Earth system research laboratory global monitoring division. https://www.esrl.noaa.gov/gmd/ccgg/trends/

[8] M. Steinacher, F. Joos, T. F. Stocker, Allowable carbon emissions lowered by multipleclimate targets, Nature 499 (2013) 197–201.

[9] J. Kothandaraman, A. Goeppert, M. Czaun, George A. Olah and G. K. S. Prakash, Conversion of CO_2 from air into methanol using a polyamine and a homogeneous ruthenium catalyst, J. Am. Chem. Soc., 138 (2016) 778−781.

[10] N. M. Rezayee, C. A. Huff and M. S. Sanford, Tandem amine and ruthenium-catalyzed hydrogenation of CO_2 to methanol, J. Am. Chem. Soc., 137 (2015) 1028−1031.

[11] P. Markewitz, W. Kuckshinrichs, W. Leitner, J. Linssen, P. Zapp, R. Bongartz, A. Schreibera and T. E. Müller, Worldwide innovations in the development of carbon capture technologies and the utilization of CO_2, Energy Environ. Sci., 5 (2012) 7281–7305.

[12] J.D. Figueroa, T. Fout, S. Plasynski, H. McIlvried, R.D. Srivastava, Advances in CO_2 capture technology—The U.S. department of energy's carbon sequestration program, Int. J. Greenh. Gas Control, 2 (2008) 9–20.

[13] Sleipner project, 1996: Project details available at the website:http://www.statoil.com/en/OurOperations/ExplorationProd/ncs/sleipner/Pages/default.aspx

[14] M. S. Jassim, G. T. Rochelle, Innovative absorber/stripper configurations for CO_2 capture by aqueous monoethanolamine, Ind. Eng. Chem. Res. 45 (2006) 2465-2472.

[15] K. Maneeintr, R. O. Idem, P. Tontiwachwuthikul, A. G. H. Wee, Comparative mass transfer performance studies of CO_2 absorption into aqueous solutions of DEAB and MEA, Ind. Eng. Chem. Res. 49 (2010) 2857–2863.

[16] A. Bajpai, M.K. Mondal, Equilibrium solubility of CO_2 in aqueous mixtures of DEA and AEEA, J. Chem. Eng. Data, 58 (2013) 1490−1495.

[17] T. Nguyen, M. Hilliard, G.T. Rochelle, Amine volatility in CO_2 capture, Int. J. Greenh. Gas Control, 4 (2010) 707−715.

[18] G. Rochelle, E. Chen, S. Freeman, D. Van Wagener, Q. Xu, A. Voice, Aqueous piperazine as the new standard for CO_2 capture technology, Chem. Eng. J., 171 (2011) 725-733.

[19] M. Al-Juaied, G. T. Rochelle, Absorption of CO_2 in aqueous diglycolamine, Ind. Eng. Chem. Res., 45 (2006) 2473-2482.

[20] F. Bougie, M. C. Iliuta, CO_2 Absorption into mixed aqueous solutions of 2-amino-2-hydroxymethyl-1,3-propanediol and piperazine, Ind. Eng. Chem. Res., 49 (2010) 1150–1159.

[21] K.-P. Shen, M.-H. Li, Kinetics of carbon dioxide reaction with sterically hindered2-Piperidineethanol aqueous solutions, Ind. Eng. Chem. Res., 30 (1991) 1811-1813.

[22] X. Gui, Z. Tang, W. Fei, Measurement and prediction of the solubility of CO_2 in ester mixture, Low Carbon Economy, 02 (2011) 26-31.

[23] S. Lee, S.-I. Choi, S. Maken, H.-J. Song, H.-C. Shin, J.-W. Park, K.-R. Jang,J.-H. Kim, Physical properties of aqueous sodium glycinate solution as an absorbent for carbon dioxide removal, J. Chem. Eng. Data, 50 (2005) 1773-1776.

[24] S. A. Freeman, G. T. Rochelle, Thermal degradation of aqueous piperazine for CO_2capture: 2: Product types and generation rates, Ind. Eng. Chem. Res., 51 (2012) 7726–7735.

[25] H. Kim, S.J. Hwang, K.S. Lee, Novel shortcut estimation method for regeneration energy of amine solvents in an absorption-based carbon capture process,Environ. Sci. Technol., 49 (2015) 1478–1485.

[26] J. Oexmann, A. Kather, S. Linnenberg, U. Liebenthal, Post-combustion CO_2 capture: chemical absorption processes in coal-fired steam power plants, Greenhouse Gases Sci. Technol., 2 (2012) 80-98.

[27] K. Veltman, B. Singh, E. G. Hertwich, Human and environmental impact assessment of postcombustion CO_2 capture focusing on emissions from amine-based scrubbing solvents to air, Environ. Sci. Technol. 44 (2010) 1496–1502

[28] W. Yave, A. Car, S.S. Funari, S.P. Nunes, K.-V. Peinemann, CO_2-Philic polymer membrane with extremely high separation performance, Macromolecules 43 (2010) 326-333.

[29] S. Shahid, K. Nijmeijer, Performance and plasticization behavior of polymer–MOF membranes for gas separation at elevated pressures, J. Membr. Sci., 470 (2014) 166-177.

[30] O.G. Nik, X.Y. Chen, S. Kaliaguine, Functionalized metal organic framework-polyimide mixed matrix membranes for CO_2/CH_4 separation, J. Membr. Sci., 413-414 (2012) 48−61.

[31] D. Li, S.-T. Hwang, Gas separation by silicon based inorganic membrane at high temperature, J. Membr. Sci., 66 (1992) 119-127.

[32] M. Ostwal, R.P. Singh, S.F. Dec, M.T. Lusk, J.D. Way, 3-Aminopropyltriethoxysilane functionalized inorganic membranes for high temperature CO_2/N_2 separation, J. Membr. Sci., 369 (2011) 139-147.

[33] P. Castellazzi, M. Notaro, G. Busca, E. Finocchio, CO2 capture by functionalized alumina sorbents: diethanolAmine on γ-alumina, Microporous Mesoporous Mater., 226 (2016) 444-453.

[34] R. S. Prabhakar, B. D. Freeman, I. Roman, Gas and vapor sorption and permeation in poly(2,2,4-trifluoro-5-trifluoromethoxy-1,3-dioxole-co-tetrafluoroethylene), Macromolecules 37 (2004) 7688−7697.

[35] Y. Chen, W.S.W. Ho, High-molecular-weight polyvinylamine/piperazine glycinate membranes for CO2 capture from flue gas, J. Membr. Sci., 514 (2016) 376-384.

[36] L. Zhao, Y. Chen, B. Wang, C. Sun, S. Chakraborty, K. Ramasubramanian, P.K. Dutta, W.S.W. Ho, Multilayer polymer/zeolite Y composite membrane structure for CO_2 capture from flue gas, J. Membr. Sci., 498 (2016) 1-13.

[37] S. Roussanaly, R. Anantharaman, K. Lindqvist, H. Zhai, E. Rubin, Membrane properties required for post-combustion CO_2 capture at coal-fired power plants, J. Membr. Sci., 511 (2016) 250-264.

[38] M. T. Ho, G. Leamon, G. W. Allinson, D. E. Wiley, Economics of CO_2 and mixed gas geosequestration of flue gas using gas separation membranes, Ind. Eng. Chem. Res. 45 (2006) 2546-2552.

[39] L. Brennan, P. Owende, Biofuels from microalgae—A review of technologies for production, processing, and extractions of biofuels and co-products, Renewable Sustainable Energy Rev., 14 (2010) 557-577.

[40] M.G. de Morais, J.A. Costa, Biofixation of carbon dioxide by Spirulina sp. and Scenedesmus obliquus cultivated in a three-stage serial tubular photobioreactor, J. Biotechnol., 129 (2007) 439−445.

[41] A. Kumar, S. Ergas, X. Yuan, A. Sahu, Q. Zhang, J. Dewulf, F.X. Malcata, H. van Langenhove, Enhanced CO(2) fixation and biofuel production via microalgae: recent developments and future directions, Trends Biotechnol., 28 (2010) 371-380.

[42] K. Kumar, C. N. Dasgupta, B. Nayak, P. Lindblad, D. Das, Development of suitable photobioreactors for CO_2 sequestration addressing global warming using green algae and cyanobacteria. Bioresour. Technol, 102 (2011) 4945-4953.

[43] M. K. Lam, K. T. Lee, A. R. Mohamed, Current status and challenges on microalgae-based carbon capture. Int. J. Greenhouse Gas Control, 10 (2012) 456-469.

[44] T. M. Mata, A. A. Martins, N. S. Caetano, Microalgae for biodiesel production and other applications: A review. Renewable Sustainable Energy Rev., 14 (2010) 217-232.

[45] P. Spolaore, C. Joannis-Cassan, E. Duran, A. Isambert, Commercial applications of microalgae. J. Biosci. Bioeng., 101(2) (2006) 87-96.

[46] B. Zhao, Y. Su, Process effect of microalgal-carbon dioxide fixation and biomass production: A review. Renewable Sustainable Energy Rev., 31(0) (2014) 121-132.

[47] A. Samanta, A. Zhao, G.K.H. Shimizu, P. Sarkar, R. Gupta, Post-Combustion CO_2 capture using solid sorbents: A review, Ind. Eng. Chem. Res., 51 (2012) 1438–1463.

[48] G. Sethia, A. Sayari, Nitrogen-doped carbons: Remarkably stable materials for CO_2 capture, Energy Fuels 28 (2014) 2727-2731.

[49] T.O. Nelson, L.J.I. Coleman, D.A. Green, R.P. Gupta, The dry carbonate process: Carbon dioxide recovery from power plant flue gas, Energy Procedia 1 (2009) 1305-1311.

[50] J.A. Mason, K. Sumida, Z.R. Herm, R. Krishna, J.R. Long, Evaluating metal–organic frameworks for post-combustion carbon dioxide capture via temperature swing adsorption, Energy Environ. Sci., 4 (2011) 3030-3040.

[51] R. Serna-Guerrero, A. Sayari, Applications of pore-expanded mesoporous silica. 7. adsorption of volatile organic compounds, Environ. Sci. Technol. 41 (2007) 4761-4766.

[52] A. Sayari, Y. Belmabkhout, R. Serna-Guerrero, Flue gas treatment via CO_2 adsorption, Chem. Eng. J., 171 (2011) 760-774.

[53] T. J. Tarka, J. P. Ciferno, M. L. Gray, D. Fauth, CO_2 capture systems using amineenhanced solid sorbents, 5th annual conference on carbon capture &sequestration. https://www.netl.doe.gov/publications/proceedings/06/carbonseq/Tech%20Session%20152. pdf

[54] A. B. Rao, E. S. Rubin, A technical, economic, and environmental assessment of amine-based CO_2 capture technology for power plant greenhouse gas control, Environ. Sci. Technol., 36 (2002)4467-4475.

[55] J.A. Mason, T.M. McDonald, T.H. Bae, J.E. Bachman, K. Sumida, J.J. Dutton, S.S. Kaye, J.R. Long, Application of a high-throughput analyzer in evaluating solid adsorbents for post-combustion carbon capture via multicomponent adsorption of CO_2, N_2, and H_2O, J. Am. Chem. Soc., 137 (2015) 4787-4803.

[56] J. S. Beck, J. C. Vartuli, W. J. Roth, M. E. Leonowicz, C. T. Kresge, K. D. Schmitt, C. T-W. Chu, D. H. Olson, E. W. Sheppard, S. B. McCullen, J. B. Higgins, J. L. Schlenker, A new family of mesoporous molecular sieves prepared with liquid crystal templates, J. Am. Chem. Soc., 114 (1992) 10834-10843.

[57] V. Valtchev, L. Tosheva, Porous nanosized particles: preparation, properties, and applications, Chem. Rev., 113 (2013) 6734-6760.

[58] A. Corma, Q. Kan, M. T. Navarro, J. Pérez-Pariente, F. Rey, Synthesis of MCM-41 with different pore diameters without addition of auxiliary organics, Chem. Mater. 9 (1997) 2123-2126.

[59] M. A. Springuel-Huet, J.-L. Bonardet, A. Gedeon, Y. Yue, V.N. Romannikov, J. Fraissard, Mechanical properties of mesoporous silicas and alumina-silicas MCM-41 and SBA-15 studied by N_2 adsorption and ^{29}Xe NMR, Microporous Mesoporous Mater., 44-45 (2001) 775−784.

[60] S. A. Bagshaw, E. Prouzet, T. J. Pinnavaiat, Templating of mesoporous molecular sieves by nonionic polyethylene oxide surfactants, Science, 269 (1995) 1242-1244.

[61] D. Zhao, Q. Huo, J. Feng, B. F. Chmelka, G. D. Stucky, Nonionic triblock and star diblock copolymer and oligomeric surfactant syntheses of highly ordered, hydrothermally stable, mesoporous silica structures, J. Am. Chem. Soc.,120 (1998) 6024−6036.

[62] T.-W. Kim, F. Kleitz, B. Paul, R. Ryoo, MCM-48-like large mesoporous silicas with tailored pore structure facile synthesis domain in a ternary triblock copolymer-butanol-water system, J. Am. Chem. Soc., 127 (2005) 7601−7610.

[63] W.-J. Son, J.-S. Choi, W.-S. Ahn, Adsorptive removal of carbon dioxide using polyethyleneimine-loaded mesoporous silica materials, Microporous Mesoporous Mater., 113 (2008) 31-40.

[64] C. Pirez, J.-M. Caderon, J.-P. Dacquin, A.F. Lee, K. Wilson, Tunable KIT-6 mesoporous sulfonic acid catalysts for fatty acid esterification, ACS Catal., 2 (2012) 1607−1614.

[65] V. Zeleňák, M. Badaničová, D. Halamová, J. Čejka, A. Zukal, N. Murafa, G. Goerigk, Amine-modified ordered mesoporous silica: effect of pore size on carbon dioxide capture, Chem. Eng. J., 144 (2008) 336–342.

CHAPTER 2

LITERATURE REVIEW

CHAPTER 2

This chapter outlines the adsorption phenomena as well as the designing of adsorbent. The adsorption capacity of various promising adsorbents reported so far for the carbon capture application is discussed. The merits and de-merits of literature reported pure and amine functionalized activated carbon, zeolites, metal-organic frameworks, and mesoporous silica are discussed. At the end, objectives of the thesis are discussed.

2.1 Adsorption

The separation of CO_2 from the gaseous mixture such as natural gas has been practised for decades. More recently, there has been an emphasis on separating CO_2 from the flue gases associated with combustion processes at fixed point sources. This interest is directly associated with the mitigation of excess CO_2 in the atmosphere and reduce the global warming potential. There are different separation techniques such as amine-based absorption, solid based adsorption, membrane purification and microalgae-based process (discussed in Chapter 1). Adsorption has gained special attention over other separation techniques in CO_2 separation for its high adsorption capacity, ease in handling and easy regeneration.

Solid adsorbents have the capability to attract gaseous molecules through their surfaces. These adsorbed molecules are usually referred to as the adsorbate. Nowadays, the porous solids such as mesoporous silica, porous carbons, zeolites, alumina, metal organic frameworks (MOFs) and covalent organic frameworks (COFs) have been emerging as a highly promising adsorbents for CO_2 capture due to their higher adsorbing capacity of gases[1-4]. This is attributed to their large

surface area, high pore volume and easy accessibility of pores during gas adsorption/separation [2-4].

Adsorption is classified as physical adsorption (physisorption) and chemical adsorption (chemisorption) [2]. In physisorption, the adsorption mainly takes place by van der Waals and electrostatic forces of attraction between adsorbate and the solid surface with low heat of adsorption (5−30 kJ/mol) [1, 2]. For example, CO_2 can be adsorbed by varieties of physical solid adsorbent materials such as zeolite, activated carbon, carbonaceous material, MOFs and COFs [2, 4] through van der Walls forces as shown in Figure 2.1a. Apart from this, the adsorption capacity of the adsorbent is also influenced by the number of ionic sites present on the surface [3]. In the case of chemisorption, the adsorption is through direct chemical interaction of sorbent with the active sites (Figure 2.1b) [5, 6]. The energy generated during this process is the same as the heat of reaction in terms of magnitude, ranging from 30 to 140 kJ/mol.

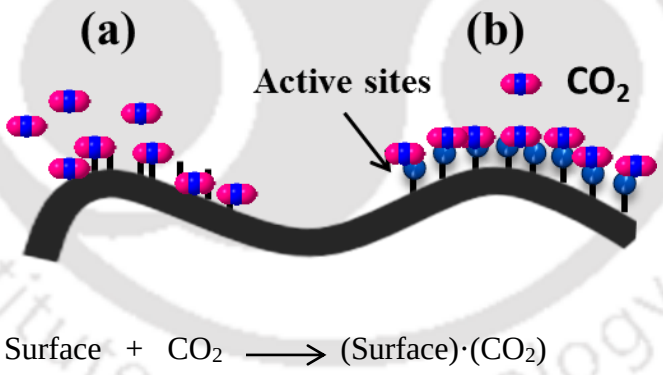

Figure 2.1 CO_2 adsorption phenomena on the surface (a) physisorption and (b) chemisorption

2.2 Classification of Adsorbents

The amount of gas adsorbed is a function of temperature, pressure, nature of the adsorbent and its physical properties [2]. Gas adsorption is commonly utilized for characterization of the porous solid materials, allowing one to determine the specific surface area, pore volume, and

pore size distribution [7]. The shape of the gas adsorption isotherms gives the qualitatively structural information. According to the IUPAC classification, gas adsorption isotherms fall into six categories [7] as shown in Figure 2.2.

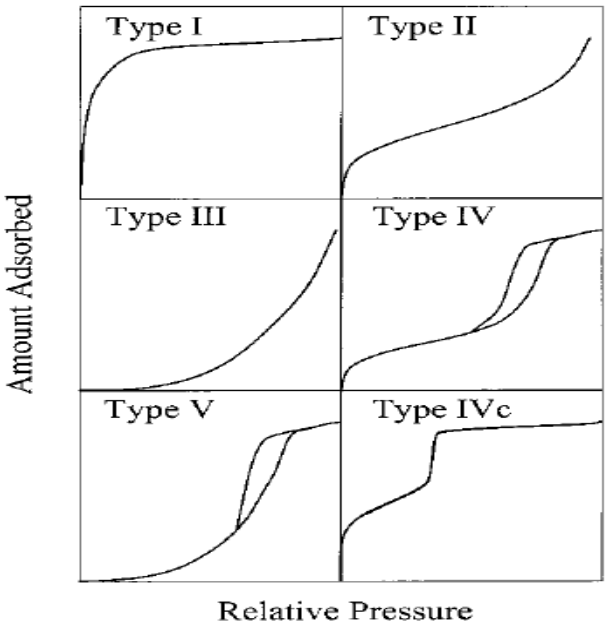

Figure 2.2 Classification of gas adsorption isotherms [7]

Type I isotherm exhibits prominent adsorption at lower relative pressure and then it gets level off. This isotherm occurs with adsorbent which contains micropores (≤ 2 nm pore diameter) or monolayer volume adsorption. This type of isotherms is usually called as Langmuir-type isotherm. However, Type I isotherms is also observed for mesoporous (cylindrical pore) materials having pore size close to the micropore range. Adsorption on many macroporous (pore diameter ≥ 50 nm) solids proceeds *via.*, multilayer formation and sorption capacity gradually increases with pressure. This type of isotherm comes under Type II and Type III. Adsorption on mesoporous (pore diameter lies between 2 to 50 nm) material proceeds via multilayer formation followed by capillary condensation. Such adsorption isotherm comes under Type IV and V

isotherms. In mesoporous material, initially the gas adsorption increases gradually with pressure but at higher pressure sorption capacity sharply increases due to capillary condensation in mesopores. Similarly, type V isotherm represents for macroporous material with capillary condensation. Type IVc isotherm is rare. It represents for mesoporous material with broad pore size distribution.

2.3 Selection of Adsorbent

Numerous factors describe the quality or utility of CO_2 adsorbents. In general, adsorbent with large adsorption capacity, fast adsorption and desorption kinetics, infinite regenerability and stability, and awide tunable range of operating conditions might become an ideal adsorbent. In last 20 years, large varieties of solid adsorbents have been reported in the literature. The characteristic property for useful adsorbent includes the effective and economical capture of CO_2 from flue gas over a wide range of temperature and pressure. The behaviour of the various classes of adsorbents utilized for CO_2 separation is reviewed and classified below.

2.3.1 *Activated carbon*

Activated carbon materials have been widely used in industry for gas separation [8-10], water purification[11] and removal of coloring matter[12] because of the low cost of the raw material, high surface area and high thermal stability. Over the past three decades, there have been attempts by several researchers to synthesize the carbon based adsorbent for CO_2 capture [2, 9, 10, 13-16]. It is synthesized by carbonization of organic material such as coal, olive stone and wood. Carbon is available in various forms, such as porous activated carbons (ACs), carbon nanotubes (CNTs), graphenes and ordered mesoporous carbon[11-36]. The CO_2 sorption

performances of different carbon-based adsorbents have been studied by several authors as illustrated below.

Wu et al. [14] have studied the sorption performance of AC bed for pure and binary CO_2, CH_4 and N_2 gas up to 40 bars. The adsorption capacity of pure component under the same pressure and temperature followed the order $CO_2 > CH_4 > N_2$. However, the selectivity of CO_2/CH_4 (3.6) and CH_4/N_2 (5.5) was low. Plaza et al. [21] synthesized the AC from olive stone and showed the sorption capacity ~ 2.0 mmol CO_2/g at 1 bar and 30 ºC. The adsorption capacity was decreased with increase in temperature. During the breakthrough experiment with 8, 14 and 30% CO_2 (rest N_2), adsorbent got saturated within ~20 min in all the cases. The sorption capacity was increased with increasing concentration 0.7 mmol/g, 0.91 mmol/g and 1.48 mmol/g for 8%, 14% and 30 wt% CO_2 feed gas, respectively. The sorption capacity of adsorbent was less than 1.0 mmol CO_2/g at 30°C and 0.2 bar. Siriwardane et al.[16] compared the sorption capacity of AC with more traditional 13X and 4A zeolite at 25 °C and 20 bars. At low partial pressure (< 2 bar) sorption capacity of AC was much lower than the 13X and 4A zeolite, but at pressure ~ 20 bar AC exhibited significantly higher adsorption capacity 8.5 mmol CO_2/g than 13X (5.2 mmol CO_2/g) and 4A zeolites (4.8 mmol CO_2/g). It was probably for the higher surface area and pore volume of the AC than 13X and 4A molecular sieves. Vargas et al.[28] showed that the CO_2 sorption capacity of AC with honeycomb monoliths was 0.89 mmol/g at 30 °C and 0.15 bar. An et al.[23] studied the CO_2 adsorption capacities of AC fibre-phenolic resin composites. The adsorption capacity lied between 2.8 – 2.9 mmol/g for a series of AC. Bhagiyalakshmi et al. [26] reported the adsorption capacity of polythiophene–mesoporous carbon as 2.7 mmol CO_2/g at 25°C and 1 bar. More recently, Wickramaratne [30] synthesized the AC spheres with ultrahigh surface area up to 2930 m^2/g. The maximum sorption capacity of the sorbent was 8.05 mmol

CO_2/g and 4.40 mmol CO_2/g at 0 °C and 25 °C, respectively. However, in all the above adsorbents, CO_2 sorption capacity sharply decreased with increase in temperature.

There are several research attempts to improve the CO_2 sorption performance by surface modification of AC with amine and metal oxide. Kongnoo et al. [11] synthesized the amine impregnated adsorbent by MEA and DEA impregnation in native AC and subjected to CO_2 sorption. The sorption capacity was increased with increasing amine concentration in adsorbent following the order native AC (1.70 mmol CO_2/g) < AC-MEA (1.79 mmol CO_2/g) < AC-DEA (2.11 mmol CO_2/g) at 40°C and 1 bar. As observed earlier, the sorption capacity of AC was gradually decreased with temperature. However, the sorption capacity was increased in amine impregnated AC till 70 °C. Wang et al. [20] synthesized a series of nitrogen doped templated carbon and studied the CO_2 adsorption performance over it. They found that the adsorption capacity increases with increase in surface area of adsorbent. The adsorption capacity of different adsorbents are as follows: TC-Y2 (1815 m^2/g; ~ 1.6 mmol CO_2/g) < Maxsorb (3311 m^2/g; ~ 2.7 mmol CO_2/g) < TC-Y1 (3519 m^2/g; ~ 2.95 mmol CO_2/g) < TC-EMC (3840 m^2/g; ~ 3.2 mmol CO_2/g) [20]. After nitrogen doping, the surface area of the adsorbent was decreased and simultaneously the sorption capacity was increased following the order: N-TC-Y2 (1361 m^2/g; 2.6 mmol CO_2/g) < N-TC-Y1 (1762 m^2/g; 3.2 mmol CO_2/g) < N-TC-EMC (2559 m^2/g; ~ 4.0 mmol CO_2/g) at 25°C and 1bar. Shahkarami et al. [27] synthesized the porous AC/MgO composite for CO_2 separation. The study revealed a correlation that adsorption capacity increased proportionally to MgO concentration in the AC. The CO_2 sorption capacity was enhanced from 0.79 mmol/g to 1.11 mmol/g, at 25°C and 1 bar with 10 % MgO adsorbent. Additionally, the breakthrough time had also increased from 10 min to 14 min.

Garcia-Gallastegui et al. [22] synthesized the graphene oxide (GO) supported Mg-Al Layered Double Hydroxides (LDH) based adsorbent for CO_2 adsorption at high temperature. GO/LDH nano-composite (20 wt%) showed 0.45 mmol CO_2/g adsorption capacity at 300ºC and 1 bar. Further, Iruretagoyena et al. [35] incorporated Na, K, and Cs alkali metals by impregnation in LDH supported GO. Alkali cations were found to modify the distribution and density of chemisorption sites resulting in higher CO_2 adsorption capacities at 300 °C (0.56−0.69 mmolCO_2/g) compared to the unpromoted adsorbents (0.29 mmol CO_2/g) (LDO and LDO/GO hybrids) at 300 ºC and 0.2 bar. However, incorporation of GO did not significantly affect the adsorption capacity of the material.

These examples of pure, nitrogen rich and metal oxide functionalized porous carbons opened a new window for the preparation of effective adsorbent. But the sharp reduction in CO_2 sorption capacity at moderate temperature, the presence of micropores and low pore volume in the AC did not suggest it as an ideal structure for designing an amine impregnation adsorbent. The presence of metal oxides in the carbon based adsorbent also did not improve the CO_2 adsorption capacity much.

2.3.2 *Zeolite sorbents*

Amongst all the porous inorganic solids, highly crystalline microporous zeolite frameworks have received greater attention in gas separation and purification [37, 38], catalysis[39, 40] and structural support for synthesis of nanomaterials [41]. They are widely available in both synthetic and natural form [37, 41]. Conventional zeolites are based on aluminosilicate framework in which substitution of some of the Si with Al (or other metal) leads to the negative charge on the framework leaving the cations within the pore structure. The cations present in the zeolites plays

an important role in the CO_2 adsorption [42, 43]. The gases with high quadrupole moment strongly interact with cations. In last few years, CO_2, N_2 and O_2 adsorption performance over a large variety of zeolites have been studied. Zeolites have shown some promising result as discussed below.

Siriwardane et al.[44] studied the CO_2, N_2 and O_2 adsorption on the natural zeolite. The Na cations present in the adsorbent played an important role in the CO_2 adsorption. Zeolite with high Na content showed high adsorption capacity along with the highest sorption rate. CO_2 was adsorbed on the natural zeolite either by physically or by the formation of bicarbonate/ bidentate carbonate. Physically adsorbed CO_2 was desorbed under vacuum. However, bicarbonate or bidentate carbonate required heating up to 115°C. Cavenati et al. [45] performed the CO_2, CH_4 and N_2 adsorption up to 50 bar on 13X zeolite using gravimetric method. The adsorption capacity was gradually increased with pressure and maximum adsorption capacity was ~ 0.71 mmol CH_4/g, 4.6 mmol CO_2/g and 0.26 mmol N_2/g at 1 bar and 25 °C. The isosteric heat of adsorption was −15.29 kJ/mol, −37.22 kJ/mol and −12.764 N_2 kJ/mol for CH_4, CO_2 and N_2 respectively. They concluded that zeolite 13X is highly selective for CO_2 separation. Wang et al. [46] studied CO_2 adsorption on a wide variety of synthetic zeolites, and the sorption capacity followed the order NaM > 4A > 13X > 5A > NaY, HM, USY, which is almost the same as the order of N_2. The interaction through quadrupole moment was dominant in low CO_2 pressure. The sorption capacity at higher pressure was dependent on the surface polarity and pore geometry of zeolites. Yang et al. [47] exchanged the surface ions (Na^+) of zeolite beta with various alkali and alkaline earth metal ions (Li^+, K^+, Cs^+, Mg^{2+}, Ca^{2+}, and Ba^{2+}) and studied the CO_2 adsorption performance. The CO_2 adsorption capacity was increased following the sequence $K^+ > Na^+ > Li^+ > Ba^{2+} > Ca^{2+} \sim Cs^+ > Mg^{2+}$. It indicates that the CO_2 sorption capacity in zeolite depends not

only on pore size and surface cations but also its density and distribution. Further, Yang et al.[38] increased the [K^+] in NaA zeolite from 10.2 to 29.3%. With increase in [K^+], CO_2 and N_2sorption capacity was gradually decreased. The sorption capacity of NaKA with 10.2 % was 3.55 mmol CO_2/g and 0.22 mmol N_2/g at 20 °C. Further increase of [K^+] (14.7%) in NaKA, reduced the CO_2 sorption capacity to 3.10 mmol/g and N_2 adsorption was negligible. The incorporation of K^+ in NaA reduces the micropore size and inhabiting the CO_2 and N_2 entry in the adsorbent. Bacsik et al.[48] synthesized wide varieties of zeolites such as 4A (Na12)-LTA, AlPO-5, $Na_{12-x}K_x$, SAPO-56, AlPO-17, SAPO-CHA and HKUST and compared the CO_2 sorption performance with commercially available 13-X, Norit-1 and HKUST-1. The CO_2 sorption capacity was gradually decreased with increase in [K^+] in zeolite 4A as was also reported by Yang et al. [47] earlier and similar behaviour was observed for CH_4 adsorption also. The CO_2 sorption capacity followed the order 13X (5.1 mmol/g) > 4A (4.5 mmol/g) > $Na_{8.8}K_{3.2}$ (4.0 mmol/g) ~ SAPO-56 (4.0 mmol/g) > AlPO-17 (1.8 mmol/g) > SAPO-CHA (1.5 mmol/g). The CO_2/CH_4 (50:50) selectivity followed the order zeolite-4A < 13-X < SAPO-56 < SAPO-CHA < AIPO-17 at zero coverage. The higher selectivity of zeolite-4A and 13-X was due to the interaction of CO_2 with the cations. Li et al. [49] showed that CO_2 adsorption performance of different zeolites followed the order: NaX > CaX > CaA > NaA > ZSM-5 > Y, and the affinity order towards CO_2 was CaA > NaX > NaA > CaX > ZSM-5 > Y. Zeolite type-X showed much better adsorption performance for CO_2 than ZSM-5 and type-Y. The difference in adsorption capacity could be understood by surface properties of the material. Zeolites with lower Si/Al ratio have higher electric field gradient which can strongly interact with the quadrupole of CO_2 molecules. The CaA showed the highest CO_2 adsorption capacity at low pressure, and this became a good adsorbent for separating CO_2 from gaseous mixture. The CH_4 adsorption capacity

followed the order: ZSM-5 > NaX ~ NaA > CaX ~ CaA ~ Y at 1 bar. The affinity order was ZSM-5 > CaA ~ NaX > Y > CaX ~ NaA. CH_4 (without quadrupole and dipole moment) was adsorbed by the van der Waals interaction with the surface. Thermal swing regeneration (~ 300 °C) completely desorbed the CO_2. However, the presence of moisture significantly reduced the separation performance of zeolites[50].

The effect of microporous surface area on CO_2 adsorption capacity was studied by Pham et al.[51]. The CO_2 adsorption performance of adsorbents followed the order on siliceous zeolites as Chabazite (CHA, ~ 3.5 mmol/g) > SSZ-23 (STT, ~3.35 mmol/g) > Ferrierite (FER, 2.55 mmol/g) ~ Silicalite-1 (MFI, 2.55 mmol/g), and beta (BEA, 2.4 mmol/g), at 1 bar and 0 °C. The interaction towards the zeolite surface was following the order: FER > STT > MFI ~ CHA > BEA. Thus, the higher CO_2 adsorption capacity of CHA is for higher microporous surface area of the adsorbent. Pham et al. [52] improved the specific surface area and pore volume compared to natural zeolite by synthesizing nanocrystalline zeolite. It improved the sorption capacity upto 4.81 mmol CO_2/g at 20 °C and 1 bar. The sorption capacity was sharply reduced in the presence of moisture. The CO_2/N_2 selectivity of nano- crystalline zeolite was decreased from 18.65 to 13.27 with increase in the sorption temperature from 20 to 50 °C. The isosteric heat of adsorption of nano-crystalline zeolite was 34.2 kJ/mol CO_2, which is similar to 13X zeolite (33kJ/mol CO_2). The sorption performance of nano-crystalline zeolite was reduced to 6.33% of the initial sorption capacity only after 10 cycles.

Siporin et al.[53] synthesized the KX, BaX and LaX zeolites by exchanging the zeolite-X ions with K, Ba or La. KX strongly adsorbed CO_2 through the formation of bidentate carbonate, but BaX and LaX adsorbed via. physisorption. Arletti et al.[50] studied the CO_2 adsorption/desorption behaviour on Na-Y zeolite. The synchrotron X-ray powder diffraction

experiments confirmed that the CO_2 molecule adsorbed on moist Na-Y formed the original tetrameric cluster of CO_2 molecules connected to the sodium cations of two adjacent faujasite supercages by water bridges. The hydrated CO_2 was completely desorbed at applied temperature between 250 – 300 °C. The high thermal stability of CO_2 in hydrated zeolite made it less effective for CO_2 separation from flue gas.

More recently, amine functionalized zeolite also showed some positive performance over non-functionalized one. In the last few years, several authors functionalized the zeolites with amine and subjected them to CO_2/N_2 separation. Kim et al. [54] functionalized the mesoporous SAPO-34 by (3-Aminopropyl)triethoxysilane (APTES) grafting. Despite the decrease in CO_2 adsorption capacity due to the loss in surface area and pore volume of SAPO-34, CO_2/N_2 selectivity of amine grafted adsorbent was improved because of the preferential adsorption of CO_2 over N_2. Zukal et al.[55] functionalized the mesoporous ITQ-6 by grafting of 3-aminopropyl (AP), 3-(methylamino)propyl (MAP), and 3-(phenylamino)propyl (PAP) organic ligands. The sorption capacity was significantly improved for ITQ-6/AP and ITQ-6/MAP at low CO_2 partial pressure following the order ITQ-6/AP > ITQ-6 > ITQ-6/MAP > ITQ-6/PAP at 1 bar and 20 °C. More recently, Madden et al.[56] impregnated the APTES and TEPA in zeolite-β. The 40% APTES impregnated zeolite showed exceptionally high adsorption capacity ca. 4.70 mmol CO_2/g at 35 °C and 0.15 bar. Su et al.[57] have impregnated the Y-type zeolite (Si/Al = 60) with TEPA. The adsorbent showed the adsorption capacity 4.27 mmol of CO_2/g of sorbent at a water vapour of 7%. Similar adsorption behaviour was also observed with PEI-impregnated ZSM-5, 13X and zeolite-silica (5A@MSA) [58, 59].

In summary, zeolites have been studied extensively for CO_2 adsorption by modification of surface with different cations and it improved the CO_2/N_2 selective separation. However,

complete regeneration of zeolite required high temperature and low pressure. The presence of moisture in the feed gas strongly influenced the CO_2 sorption capacity as well as the cyclic performance. The incorporation of amine in different zeolites improved the CO_2 adsorption performance, but further research is still to improve the stability in moist condition and regenerability.

2.3.3 *Metal-organic frameworks*

Metal-organic frameworks (MOFs) represent fundamentally new class of porous materials. The crystalline porous materials are constructed from transition metal ions and bridging polyatomic organic ligands, which have a vast, sturdy and open crystalline structure [60-64]. Owing to their extra-high porosity, ordered, and well characterized porous structures and adjustable chemical functionality various MOFs have been identified [60-64]. In the last few years, MOFs are attracting attention towards application like adsorption, CO_2 separation, gas storage, and heterogeneous catalysis [60,63,64].

Some of the literature reported MOFs showed exceptionally high CO_2 adsorption capacity. Mason et al.[65] reported CO_2 sorption ~ 9.0 mmol/g of Mg_2(dobdc) at 20ºC and 1 bar. The sorption capacity was gradually decreased with increasing sorption temperature like other physisorbents such as zeolites and AC [16,37]. Kapelewski et al.[66] tailored the surface of M_2(m-dobdc) (M = Mg, Mn, Fe, Co, Ni) for H_2 storage. Huang et al.[67] improved the CO_2 sorption capacity of Cu-BTC (6.49 mmol/g) by synthesizing its composite with graphite oxide GO@Cu-BTC (8.19 mmol/g) at 0 ºC and 1 bar. Liu et al.[68] confirmed that CO_2 was first adsorbed on the active metal sites and then on organic linker sites due to the difference in adsorption energy between these two sites.

Yaghi et al. [61] synthesized a series of IRMOF-j (j = 2, 3, 6, 9, 13, 20), HKUST-1 and MOF-74 with maximum surface area (S_{BET} =3409 m^2/g) and pore volume (Vt = 1.52 cc/g). Zhao et al.[69]showed that the CO_2 sorption capacity of IRMOF-1 was 2.10 mmol/g at 23 ºC and 1 bar. The sorption capacity of HKUST-1 was much lower than Ni/DOBDC [70]. Cavka et al.[71] synthesized the Zr-based MOFs, UIO-66 (S_{BET} = 1013 m^2/g, Vt = 0.36 cc/g), UIO-67 (S_{BET} = 2556 m^2/g, Vt = 0.83 cc/g) and DUT-52 (S_{BET} = 1615 m^2/g, Vt = 0.66 cc/g) and performed the CO_2/CH_4 sorption at high pressure. The sorbent showed that the sorption capacity was proportional to surface area and followed the order UIO-66 < DUT-52 < UIO-67. Jasuja et al.[72] improved the CO_2 sorption performance of UIO-66 by incorporation of dimethyl.

Férey et al.[62] synthesized porous chromium terephthalate, MIL-101, with the wide range of pore sizes (~ 1.2 – 3.4 nm) and surface area 4500 − 5500 m^2/g. MIL-101 was stable over months under air atmosphere and also when treated with various organic solvents at room temperature or under solvothermal conditions. These properties together with high adsorption capacities made MIL-101 an attractive candidate for the adsorption of gas or large molecules. Zhang et al.[73] reported the CO_2 sorption capacity 2.60 mmol/g of MIL-101 (Cr) at 1 bar and 25°C. Later they [74] improved the sorption capacity of MIL-101 (3.62 mmol CO_2/g at 1 bar and 25 °C) by microwave assisted chromium terephthalate method. Llewellyn et al. [75] reported the sorption capacity 2.8 mmol CO_2/g of MIL-91 (Al) at 1 bar and 30 ºC. The CO_2 sorption isotherm sharply increased at low partial pressure and got saturated at about ~ 15 bar.

More recently, amine functionalized MOFs also received a special attention due to their high CO_2 adsorption capacity at low partial pressure.Nitrogen-rich organic ligands were designed and synthesized for the fabrication of MOFs by employing the versatile click chemistry. As an example, in work reported by Wang et al.[76] a nitrogen-rich tetratopic ligand, 5,5’(1H-1,2,3-

triazole-1,4-diyl)-diisophthalic acid was synthesized followed by the construction of a corresponding triazole-containing MOF, NTU-101-Zn. This has a three-dimensional Pt S-type network. Couck et al. [77] synthesized the amine functionalized MIL-53 (Al) using 2-aminoterephthalic acid as a linker for CO_2/CH_4 separation. Wang et al.[76] prepared TEPA-MIL-101 by grafting of TEPA on unsaturated Cr(III) sites of MIL-101 for CO_2 selective separation over CO. Further, Xian et al. [78] prepared the PEI-impregnated UIO-66 for CO_2/CH_4 selective separation. However, Martínez et al.[79] impregnated the TEPA in HKUST-1, MIL-53(Al) and ZIF-8. The CO_2 sorption capacity of HKUST-1 and MIL-53 (Al) was sharply reduced compared to non-impregnated ones. Whereas, ZIF-8 impregnated with TEPA showed an improved performance. Maity et al. [80] synthesized the nitro functionalized Cu-based MOF for CO_2 separation.

Sensitivity to water vapour is considered widely to be a major weakness of MOFs that could negate potential advantages of the hybrid materials from an application perspective. Schoenecker et al. [81] studied the structural stability of HKUST-1, Mg MOF-74, UiO-66(-NH_2) and Zn-COOH containing MOFs (DMOF-1; DMOF-1-NH_2; UMCM-1) in the presence of moisture. The Zn-MOFs completely lost their structure in the presence of moisture. Others were able to keep their structure intact. Küsgens et al.[82] studied the stability of HKUST-1, ZIF-8,MIL-101, MIL-100(Fe) and DUT-4 in the presence of water through the measurement of N_2 adsorption/desorption. Both HKUST-1 and DUT-4 turned out to be unstable in direct contact with water, whereas the MIL-materials and ZIF-8 showed some stability. Liu et al.[83] studied the stability of Ni/DOBDC and Mg/DOBDC in flue gas condition/steam conditioning. Ni/DOBDC could maintain its CO_2 capacity after steam conditioning, whereas Mg/DOBDC could not. Mason et al.[84] studied the adsorption performance using wide range of MOFs,

zeolites and amine-functionalized mesoporous silica under flue gas condition. Most of the MOFs and zeolites lost their stability in the presence of flue gas. Thus, in view of the above literatures, it can be stated that MOFs are promising materials for CO_2 capture but susceptible to moisture which demands further research. In addition, the sharp reduction in adsorption capacity at moderate temperature also needs to be addressed before their practical application.

2.3.4 *Mesoporous silica*

Silicon is the most abundant element in the earth's crust and evidence of silicate hydrolysis and condensation to form polysilicate gels and particles are seen in many natural systems. Man-made syntheses of polysilicate gel from alkoxide precursors closely follow the first preparation of silicon tetrachloride ($SiCl_4$). Further, tetraethyl orthosilicate (TEOS), prepared by alcoholysis of silicon tetrachloride, undergoes repeated condensation reactions to form high-molecular weight polysiloxanes [85]. The overall hydrolysis of TEOS and subsequent dehydration of product can be understood by equations (1, 2) given below [86]. Depending on the conditions, one or both of these consecutive reactions may take place partly leaving some ethoxy or hydroxyl groups unreacted. Aelio et al.[86] showed that the rate of condensation of TEOS in water is extremely slow and its value is 4.16×16^{-6} litre mol^{-1} sec^{-1}. However, the rate of hydrolysis of TEOS changes with the pH of the solution. In highly acidic/basic medium, rate of condensation is much faster compared to that in distilled water. In the decade of 1960's, different types of silica were synthesized but breakthrough was obtained to Stöber [87-89]. They developed a methodology for a controlled growth of spherical silica particles of uniform size (0.05 to 2μ) by hydrolysis of TEOS (Figure 2.3). They showed that the size of spherical silica increases upon reduction of the pH of the solution.

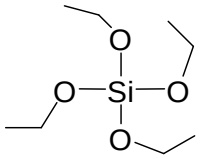

Tetra ethylorthosilicate

$$+ \quad 4nH_2O \xrightarrow{1} nSi(OH)_4 + 4nC_2H_5OH \qquad (1)$$

$$nSi(OH)_4 \xrightarrow{2} (SiO_2)n + 2nH_2O \qquad (2)$$

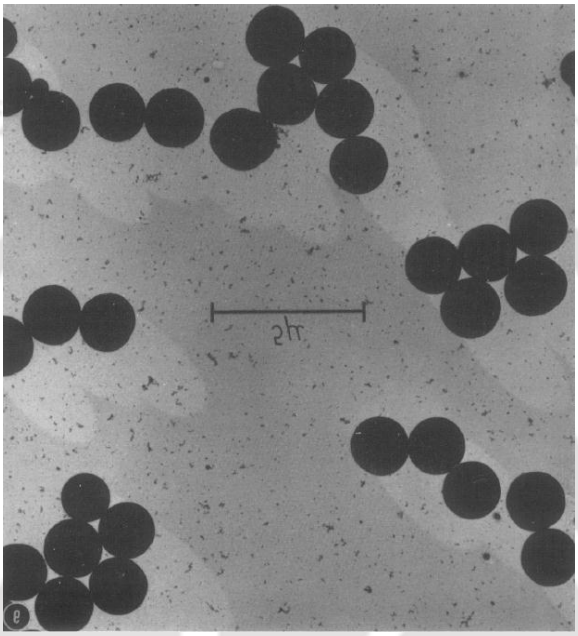

Figure 2.3 Electron micrograph of a Stöber silica spheres [5]

In the early 1990s, Japanese researchers[90] as well as Mobil scientists[91, 92] reported for the first time the successful synthesis of novel periodic mesostructured materials. They were synthesized with the help of cationic structure directing agent cetyltrimethylammoniumcation (CTAB) in the basic medium by liquid crystal templating mechanism (LCTM). This led to the discovery of the so-called M41S family of mesoporous materials [93]. These have been grouped into three major categories (Figure 2.4), the highly ordered hexagonal MCM-41, cubical MCM-48 and lamellar MCM-50. All these materials exhibited well-defined X-ray diffraction pattern as shown in Figure 2.4. The synthesis mechanism of MCM-41can be understood from Figure

2.5[91, 94]. During synthesis, surfactant forms the ordered micelles under prevailing conditions (pH and temperature) in the solution. Then TEOS forms a highly ordered structure by condensation reaction. Kruk et al. comprehensively studied the physical properties of MCM-41 and MCM-48 using X-ray diffraction analysis and nitrogen adsorption/desorption studies [95, 96].

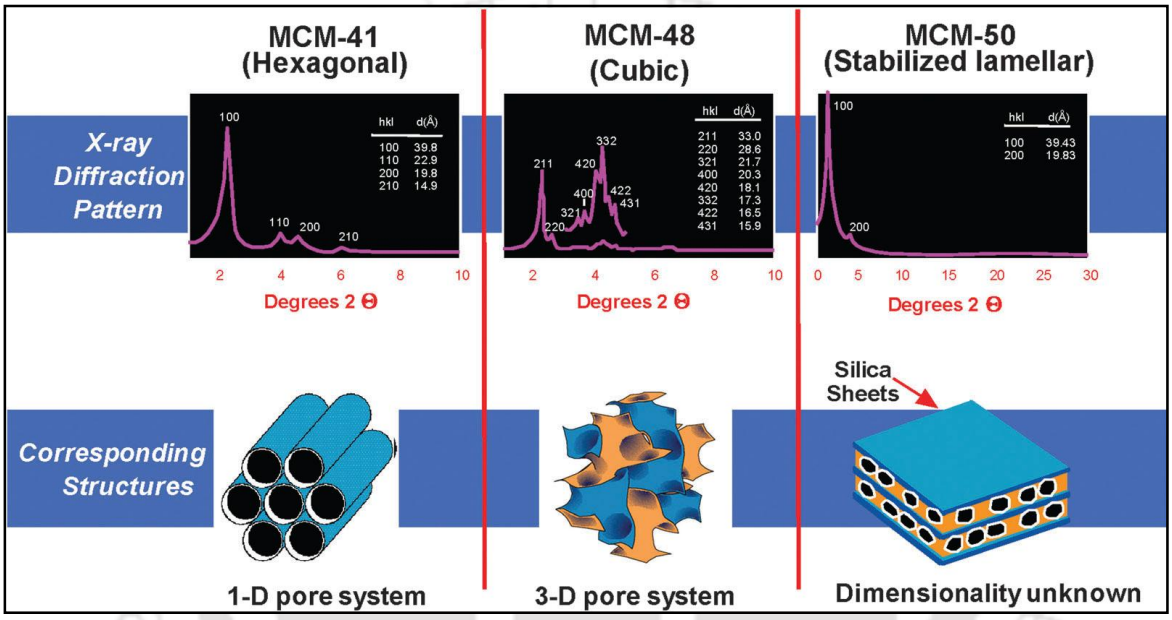

Figure 2.4 The M41S family of mesoporous molecular sieves including MCM-41, MCM-48, and MCM-50 [94]

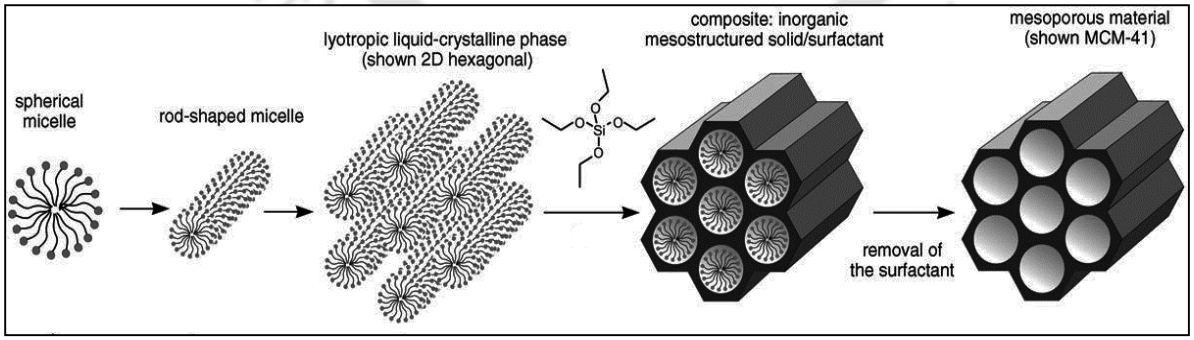

Figure 2.5 Formation of mesoporous materials with the help of structure-directing agent by liquid-crystal template mechanism [92,95].

In the last few decades, different types of mesoporous silica have been discovered as well as their physical properties were also improved. Sayari et al. [97] synthesized with high-yield of exceptionally good quality MCM-48 using fumed silica source. Vartuli et al.[98] synthesized the MCM-41 (hexagonal), MCM-48 (cubic), thermally unstable M41S, and a molecular species, the cubic octamer $[(CTMA)SiO_{25}]_8$ by changing the surfactant/Si molar ratio from 0.5 to 2. Huo et al. [99] synthesized varieties of mesoporous materials by changing the ionic surfactant/inorganic precursor. Beck et al. [100] and Corma et al.[101] improved the pore size of MCM-41 up to 6.6 nm by increasing the surfactant alkyl chain length (n = 8, 10, 12, 14 and 16). Sayari et al. [102] tailored the pores of MCM-41 by hydrothermal treatment. They concluded that the high-quality MCM-41 with maximum pore size up to 6.5 nm can be synthesized by hydrothermal treatment. Further the author also improved the pore sized from 3.5 to 9.2 nm by addition of swelling agent dimethyldecylamine (DMDA) in the solution [103].

Hartmann et al.[104] studied the mechanical stability of MCM-48 using N_2 adsorption/desorption and X-ray diffraction pattern. The structural properties were destroyed to a large extant under 480 MPa, which was confirmed by the reduction in adsorption of benzene, n-heptane, and cyclohexane. Liu et al. [105] synthesized the ordered MCM-41 by the adjustment of pH at 9, 7, 5, and 3 using UTM-1 zeolite. After being treated in boiling water for 312 h, the obtained MCM-41 exhibited remarkable hydrothermal stability than regular MCM-41. Kim and Ryoo[106] synthesized pure, and Al incorporated MCM-41 and MCM-48 mesoporous silica. They found that structure of MCM-41 and MCM-48 were completely disintegrated in boiling water within overnight. However, the addition of Al remarkably improved the hydrothermal stability of MCM-41 and MCM-48. MCM-41 and MCM-48 got their architecture collapsed and physicochemical properties destroyed under high pelletization pressure and moist condition due

to thinner pore wall. The addition of salt like NaCl, KCl, sodium acetate, ethylenediaminetetraacetic acid and tetrasodium salt during post-synthesis remarkably improved the hydrothermal stability of MCM -41 and MCM-48[105, 107-111]. However, the salt treatment required long time at moderate temperature to be effective.

After the discovery of M41S mesoporous family, wide variety of mesoporous silica was discovered by using the non-ionic surfactant as a structure directing agent with improved physical properties. In the late 90's, hexagonal mesoporous structures with large pore size (up to ~ 30 nm) SBA-15 (Santa Barbara Amorphous) was discovered by Zhao [112]. They further extended the study with wide variety of silica (lamellar, hexagonal and cubic) using several non-ionic block copolymer templates (alkyl ethylene oxide, tween, span, triton, teritor, pluronic and tetronic) and concluded that pluronic provided uniform structure, larger pore size (4 – 30 nm) with thicker wall (up to 6 nm) [113]. In addition, large varieties of mesoporous silica such as SBA series [114-116], MSU (Michigan State University) series[117, 118], HMS (Hexagonal mesoporous silica) series[6, 118], ultra large pore MCF (Mesostructured cellular foams)[119], HMU (Hannam university meso-structure)[6, 118] and KIT (Korea Institute of Technology)[120, 121] were discovered using non-ionic structure directing agent. This opened a new platform for applications to catalysis, adsorption (including CO_2 adsorption/separation), drug delivery and engineering devices.

Many studies have examined CO_2 adsorption on pure mesoporous silica such as MCM-41, SBA-15, PE-MCM-41 and KIT-6. All these mesoporous silica have lower adsorption capacity and selectivity toward CO_2 at low partial pressure. Sayari et al. [122] studied the CO_2 adsorption performance on pore-expanded MCM-41 and reported the sorption capacity ~ 0.6 mmol CO_2/g at 25 °C and 1 bar. Sorption capacity was further increased with increasing CO_2 pressure.

Loganathan et al. [123] comprehensively studied the CO_2 adsorption over wide range of temperature and pressure on MCM-41. Son et al.[120] showed the CO_2 adsorption performance of ordered mesoporous KIT-6 (0.02 mmol/g) and reported that the sorption capacity was gradually decreased with increase in temperature similar to physisorbent AC, MOFs and zeolites. The low CO_2 sorption capacity of pure mesoporous silica makes it less efficient material for CO_2 separation from large anthropogenic sources. However, high pore volume, abundant surface silanol groups and wide range of mesopores can facilitate chemical modification to improve their CO_2 adsorption capacity and selectivity.

Considering the merits of aqueous amine (MEA and DEA) based absorption technology, silica supported amine functionalized adsorbent have emerged as a promising adsorbent for CO_2 capture from large anthropogenic sources. Amine reacts with CO_2 following acid-base reaction pathway. Primary and secondary amines can react directly with CO_2 to form cabamates through the zwitterionic intermediates [124, 125]. Tertiary amine reacts with CO_2 to form bicarbonate.

Many studies have examined CO_2 adsorption in amine modified porous silica. For the first time, amine-functionalized silica was used for CO_2 capture by Tsuda in 1992[126]. The adsorbent was prepared by attachment of amine (polyethyleneimines or macrocyclic polyamines) on the surface of silica gel and was subjected to CO_2 adsorption. Leal et al.[127] reported the first aminosilane grafted silica gel adsorbent in 1995 and used for reversible CO_2 separation. The CO_2 sorption capacity of amine-functionalized silica gel was much higher than the pure one. However, first amine impregnated "molecular basket" using MCM-41 was prepared by Song in 2002 [128]. They used wet impregnation of hydrothermally synthesized MCM-41with high molecular weight polyethylenimine (PEI) to create an adsorbent termed as “molecular basket”. The CO_2 adsorption capacity as high as 4.8 mmolCO_2/g-PEI was obtained with MCM-41-PEI-50 at 75 °C, which is

24 times higher than that of MCM-41 and is even 2 times higher than pure PEI[128]. Subsequently, several groups have reported the use of aminosilane/polyethylenimine functionalized silica as CO_2 selective adsorbent [6, 114-117, 119-124, 129-147]. They opened a broad window for researchers to design an adsorbent with high CO_2 sorption capacity and high selectivity. There have been a number of amines investigated for functionalization of mesoporous silica supports (Figure 2.6). Mesoporous silica has been functionalized by (a) grafting of aminosilane and (b) impregnation of PEI and (c) by direct co-condensation reaction between amine and silica source during synthesis [6, 132, 133].

2.3.4.1 *Aminosilane grafted mesoporous silica*

Aminosilane grafting is one of the most commonly reported methods used for functionalization of mesoporous silica by condensation reaction[144]. In general, aminosilane reacts with the silanol group present on the mesoporous silica *via* condensation reaction. The amisosilane grafting capacity is highly dependent on surface silanol concentration over mesoporous silica, nature of the grafting solvent, presence of moisture in grafting solution and solution temperature. McGovern et al.[148] performed the grafting of octadecyltrichlorosilane over the glass in different grafting solvent namely, benzene, toluene, carbon tetrachloride, chloroform, n-pentane, cyclohexane, n-hexane, n-octane, dioxane, dichloromethane, cyclooctane, and n-hexadecane. They concluded that toluene provides uniform grafting over the surface. Gartmann et al.[149] grafted APTES in MCM-41 by changing the water concentration in grafting solvent. Chong et al.[150] characterized the APTES grafted SBA-15. The linker length of aminosilane strongly affects the CO_2 adsorptive separation process. Jones et al.[151] performed the aminosilane grafting after varying the alkyl linker length from C1 (methyl) to C5 (pentyl) over SBA-15. The C3(propyle)chain length of aminosilane gave better adsorption performance over others.

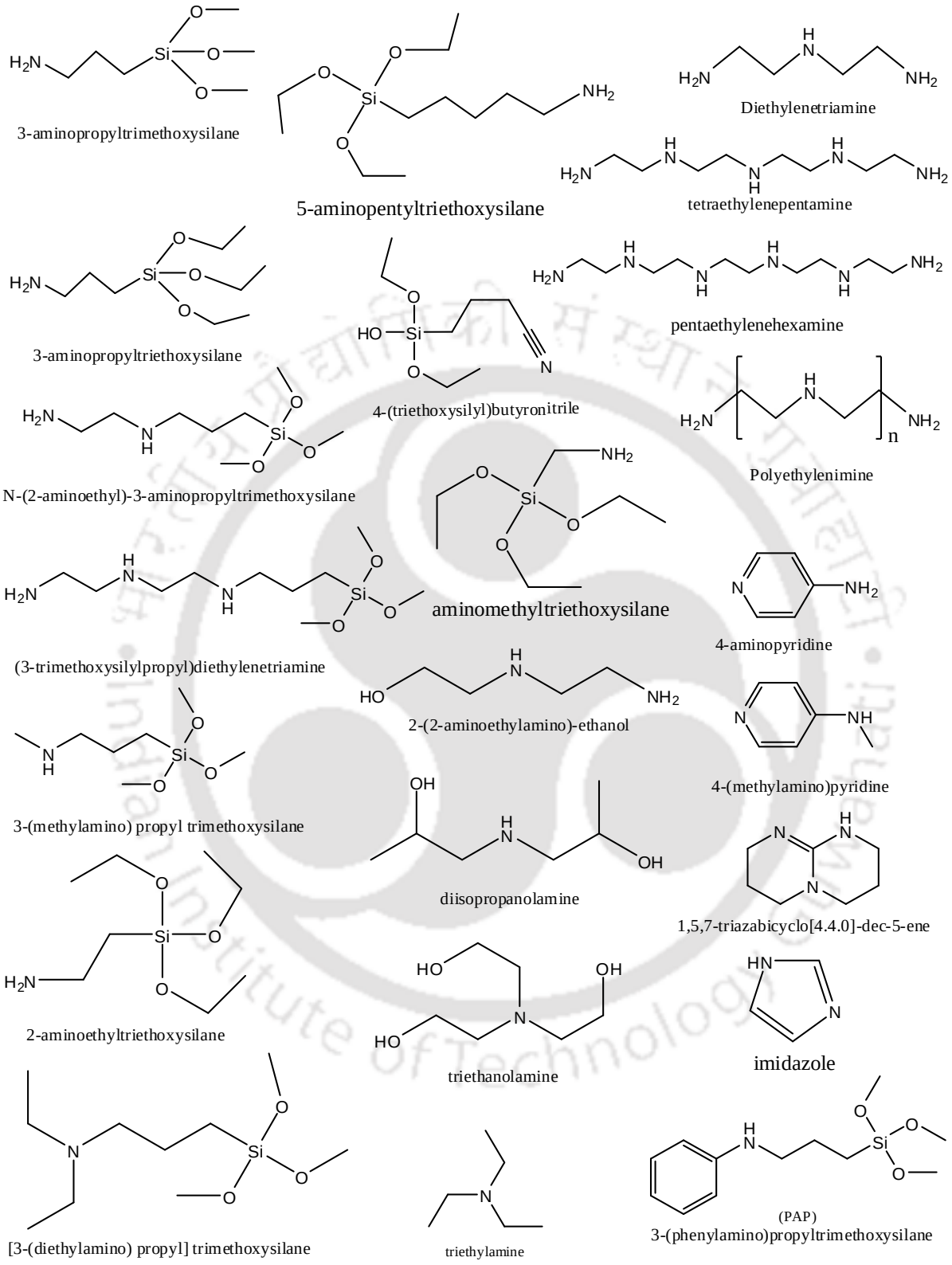

Figure 2.6 List of aminosilane and polyethyleneimine used in mesoporous silica functionalization

The most common aminosilanes used so far are shown in Figure 2.6 and their CO_2 adsorption performance in wide varieties of mesoporous silicas are summarized in Table A.1. Yang et al.[147] functionalized MCM-48 by APTES and utilized for CO_2 removal from the natural gas. APTES concentration was improved in SBA-15 by increasing the surface silanol groups [136]. This increased the CO_2 sorption capacity from 1.54 mmol CO_2/g to 1.86 mmol CO_2/g at 25°C and 1 bar. Knowles et al.[144] functionalized several silica materials using APTES and utilized in CO_2 capturewith maximum sorption capacity of 1.14 mmol/g at 25 °C and 0.05 bar. Mello et al.[137] improved the CO_2 adsorption performance of MCM-41 (0.12 mmol/g) by grafting of APTES (0.70 mmol/g) at 0.1bar and 25 °C.

The concentration of accessible amine groups defines the CO_2 adsorption capacity of the amine-functionalized mesoporous silica. Increase of the amine chain in aminosilane is the simplest way to increase the amine concentration in the mesoporous silica. Linneen et al.[132] prepared the mono, di and tri aminosilane grafted silica aerogel based adsorbents. The sorption capacity was increased with increasing amine group numbers as followed: mono (0.67 mmol CO_2/g) < di (1.2 mmol CO_2/g) < tri (1.86 mmol CO_2/g) in the grafted silica aerogels. Similar adsorption behaviour was also observed over amine-grafted platelet SBA-15 [131], double-walled silica nanotubes [134], magnesium phyllosilicates[152] and periodic mesoporous benzenesilicas[153]. However, Santos et al.[130] found the nearly constant adsorption capacity (~1.01mmol CO_2/g) over mono, di and tri aminosilane grafted MCM-41. This implies that the smaller pore size mesoporous silica is not much effective for aminosilane grafting.

Zelenak et al.[142] (2008) investigated the effect of pore size on the performance of amine functionalized mesoporous silica. In their study, three mesoporous silica supports namely, MCM-41 (3.3 nm), SBA-12 (3.8 nm) and SBA-15 (7.1 nm) were functionalized with

aminopropyl legends by grafting process. The SBA-15 (1.54 mmol/g) showed the largest CO_2 adsorption capacity over MCM-41 (0.57 mmol/g) and SBA-12 (1.04 mmol/g). It was concluded from the study that molecular sieves with larger pores and higher surface density of amines possess higher sorption capacity. The lower limit for pore size of mesoporous silica, to be used in preparation of efficient amine-based sorbents is approximately 3.5 nm. The similar adsorption behaviour was also observed with APTES grafted pore-expanded MCM-41 over traditional MCM-41[123].

Choi et al. [124] demonstrated the role of primary (APTES), secondary (MAPTMS) and tertiary (DEAPTMS) amine during CO_2 adsorption. SBA-15 was functionalized by grafting of primary, secondary and tertiary aminosilane. The maximum capacities of SBA-15-NH_2, SBA-15-NH–CH_3, and SBA-15-N$(CH_2CH_3)_2$ were 0.95, 0.75, 0.17 mmol CO_2/g adsorbent, respectively. The CO_2 adsorption rate constants for three types of adsorbents are comparable. However, the desorption rate constant for the SBA-15-NH_2 is almost four times lower than that for the SBA-15-N$(CH_2CH_3)_2$. This implies that the adsorbate molecules are more tightly bound with the primary amine. Similar adsorption behaviour was observed with primary, secondary and tertiary aminosilane functionalized double-walled silica nanotube.

Harlick and Sayari [103] synthesized the pore-expanded MCM-41 (~ 10 nm) and utilized in acidic gas such as CO_2 and H_2S separation by grafting of 3-[2-(2-aminoethylamino) ethylamino]-propyltrimethoxysilane (TRI). They focused on the optimization of TRI grafting condition in dry and wet solution. It was found that the wet aminosilane grafting via co-addition of water at 85 °C sharply improved the aminosilane grafting capacity. The optimal TRI grafted PE-MCM-41 exhibited 2.65 mmol CO_2/g at 25°C and 1 bar for a dry 5% CO_2 in N_2 feed mixture. They further showed that TRI-PE-MCM-41 gave stable sorption performance over more than 600 cycles in

humid feed gas condition over dry one[141]. Hiyoshi et al.[146] demonstrated the potential of aminosilane-modified mesoporous silica for the separation of CO_2 from a gas stream containing moisture. They modified the SBA-15 by wide variety of aminosilane namely, APTES, APTMS, TAMS, N-methylaminopropyl- trimethoxysilane (MAPS), (N,N-dimethyl-3aminopropyl) trimethoxysilane, DMAPS, N-(2-aminoethyl)-3-aminopropylmethyldiethoxysilane (AEAPMS) and utilized for CO_2 capture. They found that the adsorption capacity was increased in the presence of water[146]. Cui et al. [139] modified the silica aerogel by APTES grafting. The sorption capacity of functionalized aerogel was 1.95 mmol CO_2/g adsorbent [139].

2.3.4.2 *Polyethylenimine impregnated silica sorbents*

Previous studies have examined the CO_2 sorption in mesoporous silica, in which it has been functionalized by grafting of aminosilane. The maximum CO_2 uptake capacity of these adsorbents is nearly 2 mmol/g of the adsorbent (Table A.1). Polyethylenimine-impregnation is the simplest way to increase the amine concentration further in the mesoporous silica. Song et al.[128] developed the “molecular basket” adsorbents by loading PEI into MCM-41 and showed the maximum adsorption capacity 4.88 mmolCO_2/g-PEI at 75°C. The same research group extended the study with flue gas in the presence of moisture over PEI-impregnated MCM-41[154]. They reported that, moisture have positive impact during CO_2 adsorption with PEI-impregnated MCM-41. Sayari et al. [141] showed the stable CO_2 sorption performance with PEI/TEPA impregnated PE-MCM-41 in flue gas (in the presence of moisture) till more than 600 cycles. Wang et al.[155] prepared the PEI-impregnated SBA-15 based "molecular basket" and subjected to the CO_2 capture from flue gas at wide range of temperature. They reported the sorption capacity to be nearly 3.14 mmol CO_2/g at 75 °C in flue gas condition. Jiang et al.[156] prepared the PEI impregnated nano-silica composite and showed that the sorption capacity was

gradually increased with increasing the PEI loading at moderate temperature (75 – 105 °C). The adsorbent having 60 wt% PEI showed capture capacity of 4.2 mmol CO_2/ g at 105 °C under pure CO_2, and the PEI utilization efficiency was also increasedup to 6.9 mmol CO_2/g. Al-Marri et al.[157] showed that PEI impregnated mesoporous silica got saturated in less than 20 minutes over a wide range of pressure and temperature with high adsorption capacity.

Sanz et al. [158] studied on PEI and TEPA impregnated SBA-15 and PE-SBA-15. They reported that CO_2 sorption capacity increased with an increase in temperature.The maximum sorption capacity was 1.82 and 2.15 mmol CO_2/g for PEI and TEPA respectively at 75°C. They further extended the adsorption study by double functionalization (grafting with impregnation) over pore-expanded MCM-41 [5]. Liu et al. [159] studied the dynamic CO_2 sorption performance of TEPA impregnated three-dimensional KIT-6. The dynamic adsorption capacity was increased from 1.5 mmol CO_2/g to 2.9 mmol CO_2/g adsorbents when the amount of loaded TEPA was increased from 10 wt.% to 50 wt.% at 333 K. Wei et al. [160] reported the sorption capacity 3.5 mmol CO_2/g at 80 °C and 1 bar for 50 wt% PEHA impregnated SBA-15.

The structure of the mesoporous silica influences the CO_2 sorption capacity of the amine functionalized adsorbents. Son et al.[120] synthesized the series of ordered mesoporous silica, namely, MCM-41, MCM-48, SBA-15, SBA-16 and KIT-6 and functionalized them with 50 wt% PEI. The CO_2 adsorption capacities were found to be in the following order: KIT-6 > SBA-15 ~ SBA-16 > MCM-48 > MCM-41. However, 50 wt% PEI impregnated KIT-6 with the largest pore in 3D arrangement showed the highest CO_2 adsorption capacity (135 mg/g-adsorbent) in the fastest response time. Further, Song et al.[6] prepared PEI impregnated 3D molecular baskets, namely MCF, MSU-J and HMS with different pore properties for CO_2 separation and compared with MCM-41, SBA-15 and CB-based1D/2D MBS[6]. The rate of CO_2 sorption was increased in

the order of PEI(50)/MCM-41 < PEI(50)/SBA-15 < PEI(50)/MSU-J ≈ PEI(50)/HMS < PEI(50)/MCF, and the values were 0.79, 0.97, 1.21, 1.24,and 1.41 mg-CO_2/g-sorb/s, respectively. They concluded that 3D supports displayed a much better synergistic effect with PEI for CO_2 sorption than 1D/2D mesoporous materials as was previously observed by Son et al [120].

Jones group prepared adsorbents with high amine content SBA-15 through polymerization of aziridine inside the pore which they named hyperbranched aminosilica (HAS) [161, 162]. During functionalization, aziridine under gone ring-opening polymerization in the presence of catalytic amounts of acetic acid to form hyperbranched aminopolymers that were covalently bound to the SBA-15 support. Jones reported an HAS sample to have an amine loading of 7.0 mmol N/g with a pore volume of 0.25 cc/g[162].

Fauth et al.[163] prepared the CO_2 adsorbent by functionalization of commercially available porous silica with APTES and PEI. They displayed the sorption capacity ranges of 2.7 − 3.5 mmol CO_2/g sorbent at 40 °C under different CO_2 partial pressures. Dao et al.[117] improved the sorption capacity of MSU-F, Al-MSU-F, MCM-41 and MSU-H mesoporous silica by mixed amine impregnation namely, TEPA, PZ, DBU, MEA, DEA, TEA, DEAP and PEG. The maximum sorption capacity 5.9 mmol CO_2/g adsorbent was observed with 40 wt% TEPA and 30 wt% DEA impregnated MSU-F silica.

Recently, Olah group found that fumed silica and precipitated silica were better supports for impregnation of PEI than silica gel, aluminium oxide, poly(4-vinylpyridine), and other ones [164, 165]. Moreover, they also reported that mesoporous silica (MCM-41, SBA-15) was not necessary to achieve good CO_2 adsorption and that precipitated or fumed silica yielded better results. Further, nanostructured fumed silica was functionalized with various organoamine,

namely MEA, DEA, TEA, TEPA, PEHA, PEI (mw = 423, 800, 25000), as well as 2-amino-2-methyl-1,3-propanediol (AMP), 2-(2-aminoethylamino)-ethanol (AEAE), diisopro-panolamine (DIPA) and imidazole by wet impregnation[164]. They observed that the samples impregnated with MEA, DEA, AEDA and TEA were not suitable for CO_2 separation because of amine leaching problem at higher temperature. Li et al. [166] functionalized the nano-silica by different molecular weight PEI. The sorption capacity decreased with increasing molecular weight from 800 to 25000 Da of PEI and maximum for 800 Da (4.59 mmol CO_2/g) at 105°C and 1 bar. Additionally, linear PEI functionalized nano-silica showed lower.

Wang et al. [167] decorated the surface of hierarchical porous silica (HPS) by PEI and TEPA in presence of wide variety of surfactants namely, cetyltrimethylammonium bromide (CTAB), dodecyltrimethyl ammonium bromide (DTAB), octadecyltrimethyl ammonium bromide (OTAB), pluronic P123 (P123), Pluronic F127 (F127), sodium dodecylbenzene- sulfonate (SDBS), sodium dodecyl sulfate (SDS), sorbitanmonooleate (Span80) and phosphatidylcholine. They concluded that the presence surfactant increased the utilization of amine groups of polyethyleneimine during CO_2 adsorption and sharply improved the sorption performance of the adsorbent.

2.4 Objectives of the Present Study

Pure and functionalized AC, zeolites and MOFs have been extensively studied for CO_2 adsorption. But, the sharp reduction in CO_2 sorption capacity of ACs, zeolites and MOFs with increase in temperature makes them less favorable for practical application. The presence of metal oxides and amines in the carbon based adsorbent does not improve the CO_2 adsorption capacity. Surface modification of zeolites with different cations improves the CO_2/N_2 selective

separation. However, complete regeneration of zeolite requires high thermal energy which strongly influences the CO_2 sorption capacity as well as its cyclic performance. Most of the MOFs are highly sensitive towards moisture. Hence, further research is needed to improve its CO_2 sorption performance in moist conditions at high temperature and low partial pressure.

Mesoporous silica with high specific surface area, large pore size, high pore volume and high thermal stability look more promising for CO_2 capture. The presence of surface silanol groups in mesoporous silica promotes the grafting of aminosilane. Tunable pore size facilitates functionalization of the wide variety of polyethyleneimine inside the pore and large pore volume is able to accumulate a large amount of polyethyleneimine during impregnation. In the presence of moisture, the enhancement of CO_2 adsorption capacity makes it superior over AC, zeolites and MOFs. However, 3D structure provides an easy pathway for host and guest molecules during its performance. Therefore, amine-functionalized mesoporous silica based carbon capture technology can become an alternative in future.

The 3D KIT-6 consisting of larger interconnected pore with large pore space could result in fast adsorption kinetics. Therefore, the present work is undertaken to investigate the adsorption potential of large 3D porous material for CO_2.

Hence, the major objectives of the present work **Development of Amine Functionalized Mesoporous Silica (KIT-6) for Carbon Dioxide Capture**are summarized in terms of the **following measurable objectives.**

- Synthesis of three dimensional mesoporous silica with large interconnected pore (KIT-6) and study the hydrothermal, thermal, hydrolytic, mechanical stability as well as its CO_2 adsorption performance.

- Synthesis, grafting mechanism and CO_2 sorption performance of monoaminosilane (APTES) grafted KIT-6
- Synthesis and CO_2 sorption performance of higher order (di-, tri- and poly-) aminosilane grafted KIT-6
- Synthesis and CO_2 sorption performance of KIT-6 impregnated with polyethyleneimine

2.5 Conclusions

The foregoing sections have described the recent progress made in the investigation of adsorption performance over the wide variety of AC, zeolites, MOFs and mesoporous silica for CO_2 capture application at low pressure and wide range of temperature. Research on functionalizing solid supports with amine functional groups for CO_2 capture has reached various stages of development. With regard to the prospects of creating new materials suitable for real-world applications, the present work has tested the stability of different mesoporous materials. The 3D KIT-6 with large pore size shows the better stability than other mesoporous silica. Further, this work has formulated the road map for the development of amine functionalized mesoporous silica (KIT-6) for CO_2 capture at wide range of temperature and pressure.

References

[1] S. Choi, J.H. Drese, C.W. Jones, Adsorbent materials for carbon dioxide capture from large anthropogenic point sources, ChemSusChem 2 (2009) 796−854.

[2] A. Samanta, A. Zhao, G.K.H. Shimizu, P. Sarkar, R. Gupta, Post-combustion CO_2 capture using solid sorbents: A review, Ind. Eng. Chem. Res. 51 (2012) 1438−1463.

[3] J.-R. Li, J. Sculley, H.-C. Zhou, Metal–organic frameworks for separations, Chem. Rev. 112 (2012) 869−932.

[4] S.-Y. Ding, W. Wang, Covalent organic frameworks (COFs): from design to applications, Chem. Soc. Rev. 42 (2013) 548−568.

[5] R. Sanz, G. Calleja, A. Arencibia, E.S. Sanz-Pérez, CO_2 capture with pore-expanded MCM-41 silica modified with amino groups by double functionalization, Microporous Mesoporous Mater. 209 (2015) 165−171.

[6] D. Wang, X. Wang, X. Ma, E. Fillerup, C. Song, Three-dimensional molecular basket sorbents for CO_2 capture: Effects of pore structure of supports and loading level of polyethylenimine, Catal. Today 233 (2014) 100−107.

[7] M. Kruk, M. Jaroniec, Gas adsorption characterization of ordered organic-inorganic nanocomposite materials, Chem. Mater. 13 (2001) 3169-3183.

[8] M. Nakashima, S. Shimada, M. Inagaki, T.A. Centeno, On the adsorption of CO_2 by molecular sieve carbons−volumetric and gravimetric studies, Carbon 33 (1995) 1301−1306.

[9] M. Molina-Sabio, A.M.A. Muñecas, F. Rodríguez-Reinoso, B. McEnaney, Adsorption of CO_2 and SO_2 on activated carbons with a wide range of micropore size distribution, Carbon 33 (1995) 1777−1782.

[10] S. Sircar, Sorption of carbon dioxide on activated carbons: Effect of the heat of sorption during kinetic measurements, Carbon 19 (1981) 153−160.

[11] G. Knopp, C. Prasse, T.A. Ternes, P. Cornel, Elimination of micropollutants and transformation products from a wastewater treatment plant effluent through pilot scale ozonation followed by various activated carbon and biological filters, Water Res. 100 (2016) 580−592.

[12] T.L. Silva, A. Ronix, O. Pezoti, L.S. Souza, P.K.T. Leandro, K.C. Bedin, K.K. Beltrame, A.L. Cazetta, V.C. Almeida, Mesoporous activated carbon from industrial laundry sewage sludge: Adsorption studies of reactive dye Remazol Brilliant Blue R, Chem. Eng. J. 303 (2016) 467−476.

[13] A. Kongnoo, P. Intharapat, P. Worathanakul, C. Phalakornkule, Diethanolamine impregnated palm shell activated carbon for CO_2 adsorption at elevated temperatures, J. Environ. Chem. Eng. 4 (2016) 73−81.

[14] Y.-J. Wu, Y. Yang, X.-M. Kong, P. Li, J.-G. Yu, A.M. Ribeiro, A.E. Rodrigues, Adsorption of pure and binary CO_2, CH_4, and N_2gas components on activated carbon beads, J. Chem. Eng. Data 60 (2015) 2684−2693.

[15] C.A. Grande, R. Blom, A. Möller, J. Möllmer, High-pressure separation of CH_4/CO_2 using activated carbon, Chem. Eng. Sci. 89 (2013) 10−20.

[16] R.V. Siriwardane, M.-S. Shen, E.P. Fisher, J.A. Poston, Adsorption of CO_2 on molecular sieves and activated carbon, Energy Fuels 15 (2001) 279−284.

[17] M. Sevilla, P. Valle-Vigón, A.B. Fuertes, N-doped polypyrrole-based porous carbons for CO_2 capture, Adv. Funct. Mater. 21 (2011) 2781−2787.

[18] Y.N. Prajapati, B. Bhaduri, H.C. Joshi, A. Srivastava, N. Verma, Aqueous phase adsorption of different sized molecules on activated carbon fibers: Effect of textural properties, Chemosphere 155 (2016) 62−69.

[19] D. Cazorla-Amorós, J. Alcañiz-Monge, A. Linares-Solano, Characterization of activated carbon fibers by CO_2 adsorption, Langmuir 12 (1996) 2820−2824.

[20] L. Wang, R.T. Yang, Significantly Increased CO_2 Adsorption performance of nanostructured templated carbon by tuning surface area and nitrogen doping, J. Phys. Chem. C 116 (2011) 1099−1106.

[21] M.G. Plaza, I. Durán, N. Querejeta, F. Rubiera, C. Pevida, Experimental and simulation study of adsorption in postcombustion conditions using a microporous biochar. 1. CO_2 and N_2 adsorption, Ind. Eng. Chem. Res. 55 (2016) 3097−3112.

[22] A. Garcia-Gallastegui, D. Iruretagoyena, V. Gouvea, M. Mokhtar, A.M. Asiri, S.N. Basahel, S.A. Al-Thabaiti, A.O. Alyoubi, D. Chadwick, M.S.P. Shaffer, Graphene oxide as support for layered double hydroxides: Enhancing the CO_2 adsorption capacity, Chem. Mater. 24 (2012) 4531−4539.

[23] H. An, B. Feng, S. Su, CO_2 capture capacities of activated carbon fibre-phenolic resin composites, Carbon 47 (2009) 2396−2405.

[24] D. Iruretagoyena, X. Huang, M.S.P. Shaffer, D. Chadwick, Influence of alkali metals (Na, K, and Cs) on CO_2 adsorption by layered double oxides supported on graphene oxide, Ind. Eng. Chem. Res. 54 (2015) 11610−11618.

[25] D. Menard, X. Py, N. Mazet, Activated carbon monolith of high thermal conductivity for adsorption processes improvement: Part A: Adsorption step, Chem. Eng. Process. Process Intensif. 44 (2005) 1029−1038.

[26] M. Bhagiyalakshmi, P. Hemalatha, M. Palanichamy, H.T. Jang, Adsorption, regeneration and interaction of CO_2 with a polythiophene–carbon mesocomposite, Colloids Surf., A 374 (2011) 48-53.

[27] S. Shahkarami, A.K. Dalai, J. Soltan, Enhanced CO_2 adsorption using MgO-impregnated activated carbon: Impact of preparation techniques, Ind. Eng. Chem. Res. 55 (2016) 5955−5964.

[28] D.P. Vargas, M. Balsamo, L. Giraldo, A. Erto, A. Lancia, J.C. Moreno-Piraján, Equilibrium and dynamic CO_2 adsorption on activated carbon honeycomb monoliths, Ind. Eng. Chem. Res. 55(2016)7898–7905.

[29] M.G. Plaza, A.S. González, C. Pevida, F. Rubiera, Influence of water vapor on CO_2 adsorption using a biomass-based carbon, Ind. Eng. Chem. Res. 53 (2014) 15488−15499.

[30] N.P. Wickramaratne, M. Jaroniec, Activated carbon spheres for CO_2 adsorption, ACS Appl. Mater. Interfaces 5 (2013) 1849-1855.

[31] H. Yi, Z. Wang, H. Liu, X. Tang, D. Ma, S. Zhao, B. Zhang, F. Gao, Y. Zuo, Adsorption of SO_2, NO, and CO_2 on activated carbons: Equilibrium and thermodynamics, J. Chem. Eng. Data 59 (2014) 1556−1563.

[32] B. Yuan, X. Wu, Y. Chen, J. Huang, H. Luo, S. Deng, Adsorption of CO_2, CH_4, and N_2 on ordered mesoporous carbon: Approach for greenhouse gases capture and biogas upgrading, Environ. Sci. Technol. 47 (2013) 5474−5480.

[33] F. Su, C. Lu, H.-S. Chen, Adsorption, desorption, and thermodynamic studies of CO_2 with high-amine-loaded multiwalled carbon nanotubes, Langmuir 27 (2011) 8090−8098.

[34] Q. Liu, J. Shi, S. Zheng, M. Tao, Y. He, Y. Shi, Kinetics studies of CO_2 adsorption/desorption on amine-functionalized multiwalled carbon nanotubes, Ind. Eng. Chem. Res. 53 (2014) 11677−11683.

[35] D. Iruretagoyena, M.S.P. Shaffer, D. Chadwick, Layered double oxides supported on graphene oxide for CO_2 adsorption: Effect of support and residual sodium, Ind. Eng. Chem. Res. 54 (2015) 6781−6792.

[36] P. Cabrera-Sanfelix, Adsorption and reactivity of CO_2 on defective graphene sheets, J. Phys. Chem. A 113 (2009) 493−498.

[37] Y. Park, Y. Ju, D. Park, C.-H. Lee, Adsorption equilibria and kinetics of six pure gases on pelletized zeolite 13X up to 1.0 MPa: CO_2, CO, N_2, CH_4, Ar and H_2, Chem. Eng. J. 292 (2016) 348−365.

[38] B. Yang, Y. Liu, M. Li, Separation of CO_2–N_2 using zeolite NaKA with high selectivity, Chin. Chem. Lett. 27 (2016) 933−937.

[39] J. Zhao, G. Wang, L. Qin, H. Li, Y. Chen, B. Liu, Synthesis and catalytic cracking performance of mesoporous zeolite Y, Catal. Commun. 73 (2016) 98−102.

[40] X. Hu, J. Bai, C. Li, H. Liang, W. Sun, Silver-based 4A zeolite composite catalyst for styrene epoxidation by one-pot hydrothermal synthesis, Eur. J. Inorg. Chem. (2015) 3758−3763.

[41] B. Hosseini, A.A. Nourbakhsh, K.J.D. MacKenzie, Magnesiothermal synthesis of nanostructured SiC from natural zeolite (clinoptilolite) and mesoporous carbon CMK-1, Ceram. Int. 41 (2015) 8809−8813.

[42] O. Cheung, Z. Bacsik, P. Krokidas, A. Mace, A. Laaksonen, N. Hedin, K^+ Exchanged zeolite ZK-4 as a highly selective sorbent for CO_2, Langmuir 30 (2014) 9682−9690.

[43] T.-H. Bae, M.R. Hudson, J.A. Mason, W.L. Queen, J.J. Dutton, K. Sumida, K.J. Micklash, S.S. Kaye, C.M. Brown, J.R. Long, Evaluation of cation-exchanged zeolite adsorbents for post-combustion carbon dioxide capture, Energy Environ. Sci. 6 (2013) 128−138.

[44] R.V. Siriwardane, M.-S. Shen, E.P. Fisher, Adsorption of CO_2, N_2, and O_2 on natural zeolites, Energy Fuels 17 (2003) 571−576.

[45] S. Cavenati, C.A. Grande, A.E. Rodrigues, Adsorption equilibrium of methane, carbon dioxide, and nitrogen on zeolite 13X at high pressures, J. Chem. Eng. Data 49 (2004) 1095−1101.

[46] Z.-M. Wang, T. Arai, M. Kumagai, Adsorption separation of low concentrations of CO_2 and NO_2 by synthetic zeolites, Energy Fuels 12 (1998) 1055−1060.

[47] S.-T. Yang, J. Kim, W.-S. Ahn, CO_2 adsorption over ion-exchanged zeolite beta with alkali and alkaline earth metal ions, Microporous Mesoporous Mater. 135 (2010) 90−94.

[48] Z. Bacsik, O. Cheung, P. Vasiliev, N. Hedin, Selective separation of CO_2 and CH_4 for biogas upgrading on zeolite NaKA and SAPO-56, Appl. Energy 162 (2016) 613−621.

[49] Y.D. Li, H.H. Yi, X.L. Tang, F.R. Li, Q. Yuan, Adsorption separation of CO_2/CH_4 gas mixture on the commercial zeolites at atmospheric pressure, Chem. Eng. J. 229 (2013) 50−56.

[50] R. Arletti, L. Gigli, F. di Renzo, S. Quartieri, Evidence for the formation of stable CO_2 hydrates in zeolite Na-Y: Structural characterization by synchrotron X-ray powder diffraction, Microporous Mesoporous Mater. 228 (2016) 248−255.

[51] T.D. Pham, R. Xiong, S.I. Sandler, R.F. Lobo, Experimental and computational studies on the adsorption of CO_2 and N_2 on pure silica zeolites, Microporous Mesoporous Mater. 185 (2014) 157−166.

[52] T.-H. Pham, B.-K. Lee, J. Kim, C.-H. Lee, Enhancement of CO_2 capture by using synthesized nano-zeolite, . Taiwan Inst. Chem. Eng. 64 (2016) 220−226.

[53] S.E. Siporin, B.C. McClaine, R.J. Davis, Adsorption of N_2 and CO_2 on zeolite X exchanged with potassium, barium, or lanthanum, Langmuir 19 (2003) 4707−4713.

[54] J.-Y. Kim, J. Kim, S.-T. Yang, W.-S. Ahn, Mesoporous SAPO-34 with amine-grafting for CO_2 capture, Fuel 108 (2013) 515−520.

[55] A. Zukal, I. Dominguez, J. Mayerova, J. Cejka, Functionalization of delaminated zeolite ITQ-6 for the adsorption of carbon dioxide, Langmuir 25 (2009) 10314−10321.

[56] D. Madden, T. Curtin, Carbon dioxide capture with amino-functionalised zeolite-β: A temperature programmed desorption study under dry and humid conditions, Microporous Mesoporous Mater. 228 (2016) 310−317.

[57] F. Su, C. Lu, S.-C. Kuo, W. Zeng, Adsorption of CO_2 on amine-functionalized Y-type zeolites, Energy Fuels 24 (2010) 1441−1448.

[58] C.H. Lee, D.H. Hyeon, H. Jung, W. Chung, D.H. Jo, D.K. Shin, S.H. Kim, Effects of pore structure and PEI impregnation on carbon dioxide adsorption by ZSM-5 zeolites, J. Ind. Eng. Chem. 23 (2015) 251−256.

[59] X.W. Liu, F. Gao, J. Xu, L.H. Zhou, H.L. Liu, J. Hu, Zeolite@Mesoporous silica-supported-amine hybrids for the capture of CO_2 in the presence of water, Microporous Mesoporous Mater. 222 (2016) 113−119.

[60] J.-R. Li, R.J. Kuppler, H.-C. Zhou, Selective gas adsorption and separation in metal-organic frameworks, Chem. Soc. Rev. 38 (2009) 1477−1504.

[61] J.L.C. Rowsell, O.M. Yaghi, Effects of functionalization, catenation, and variation of the metal oxide and organic linking units on the low-pressure hydrogen adsorption properties of metal−organic frameworks, J. Am. Chem. Soc. 128 (2006) 1304−1315.

[62] G. Férey, C. Mellot-Draznieks, C. Serre, F. Millange, J. Dutour, S. Surblé, I. Margiolaki, A chromium terephthalate-based solid with unusually large pore volumes and surface area, Science 309 (2005) 2040−2042.

[63] D. Saha, Z. Bao, F. Jia, S. Deng, Adsorption of CO_2, CH_4, N_2O, and N_2 on MOF-5, MOF-177, and Zeolite 5A, Environ. Sci. Technol. 44 (2010) 1820−1826.

[64] J.W. Liu, L.F. Chen, H. Cui, J.Y. Zhang, L. Zhang, C.Y. Su, Applications of metal-organic frameworks in heterogeneous supramolecular catalysis, Chem. Soc. Rev. 43 (2014) 6011-6061.

[65] J.A. Mason, K. Sumida, Z.R. Herm, R. Krishna, J.R. Long, Evaluating metal-organic frameworks for post-combustion carbon dioxide capture via temperature swing adsorption, Energy Environ. Sci. 4 (2011) 3030−3040.

[66] M.T. Kapelewski, S.J. Geier, M.R. Hudson, D. Stück, J.A. Mason, J.N. Nelson, D.J. Xiao, Z. Hulvey, E. Gilmour, S.A. FitzGerald, M. Head-Gordon, C.M. Brown, J.R. Long, M_2(m-dobdc) (M = Mg, Mn, Fe, Co, Ni) Metal–organic frameworks exhibiting increased charge density and enhanced H_2 binding at the open metal sites, J. Am. Chem. Soc. 136 (2014) 12119-12129.

[67] W. Huang, X. Zhou, Q. Xia, J. Peng, H. Wang, Z. Li, Preparation and adsorption performance of GrO@Cu-BTC for separation of CO_2/CH_4, Ind. Eng. Chem. Res. 53 (2014) 11176−11184.

[68] Y. Liu, J. Hu, X. Ma, J. Liu, Y.S. Lin, Mechanism of CO_2 adsorption on Mg/DOBDC with elevated CO_2 loading, Fuel 181 (2016) 340−346.

[69] Z. Zhao, Z. Li, Y.S. Lin, Adsorption and diffusion of carbon dioxide on metal−organic framework (MOF-5), Ind. Eng. Chem. Res. 48 (2009) 10015−10020.

[70] J. Liu, Y. Wang, A.I. Benin, P. Jakubczak, R.R. Willis, M.D. LeVan, CO_2/H_2O Adsorption equilibrium and rates on metal-organic frameworks: HKUST-1 and Ni/DOBDC, Langmuir 26 (2010) 14301−14307.

[71] J.H. Cavka, C.A. Grande, G. Mondino, R. Blom, High pressure adsorption of CO_2 and CH_4 on Zr-MOFs, Ind. Eng. Chem. Res. 53 (2014) 15500−15507.

[72] H. Jasuja, K.S. Walton, Experimental study of CO_2, CH_4, and water vapor adsorption on a dimethyl-functionalized Ui0-66 framework, J. Phys. Chem. C 117 (2013) 7062−7068.

[73] Y. Zhang, W. Su, Y. Sun, J. Liu, X. Liu, X. Wang, Adsorption equilibrium of N_2, CH_4, and CO_2 on MIL-101, J. Chem. Eng. Data 60 (2015) 2951−2957.

[74] Z.J. Zhang, S.S. Huang, S.K. Xian, H.X. Xi, Z. Li, Adsorption equilibrium and kinetics of CO_2 on chromium terephthalate MIL-101, Energy Fuels 25 (2011) 835−842.

[75] P.L. Llewellyn, M. Garcia-Rates, L. Gaberova, S.R. Miller, T. Devic, J.C. Lavalley, S. Bourrelly, E. Bloch, Y. Filinchuk, P.A. Wright, C. Serre, A. Vimont, G. Maurin, Structural origin of unusual CO_2 adsorption behavior of a small-pore aluminum bisphosphonate MOF, J. Phys. Chem. C 119 (2015) 4208−4216.

[76] X. Wang, H. Li, X.-J. Hou, Amine-functionalized metal organic framework as a highly selective adsorbent for CO_2 over CO, J. Phys. Chem. C 116 (2012) 19814-19821.

[77] S. Couck, J.F.M. Denayer, G.V. Baron, T. Rémy, J. Gascon, F. Kapteijn, An amine-functionalized MIL-53 metal−organic framework with large separation power for CO_2 and CH_4, J. Am. Chem. Soc. 131 (2009) 6326−6327.

[78] S. Xian, Y. Wu, J. Wu, X. Wang, J. Xiao, Enhanced dynamic CO_2 adsorption capacity and CO_2/CH_4 selectivity on polyethylenimine-impregnated UiO-66, Ind. Eng. Chem. Res. 54 (2015) 11151−11158.

[79] F. Martínez, R. Sanz, G. Orcajo, D. Briones, V. Yángüez, Amino-impregnated MOF materials for CO_2 capture at post-combustion conditions, Chem. Eng. Sci. 142 (2016) 55−61.

[80] D.K. Maity, A. Halder, B. Bhattacharya, A. Das, D. Ghoshal, Selective CO_2 adsorption by nitro functionalized metal organic frameworks, Cryst. Growth Des. 16 (2016) 1162−1167.

[81] P.M. Schoenecker, C.G. Carson, H. Jasuja, C.J.J. Flemming, K.S. Walton, Effect of water adsorption on retention of structure and surface area of metal-organic frameworks, Ind. Eng. Chem. Res. 51 (2012) 6513−6519.

[82] P. Küsgens, M. Rose, I. Senkovska, H. Fröde, A. Henschel, S. Siegle, S. Kaskel, Characterization of metal-organic frameworks by water adsorption, Microporous Mesoporous Mater. 120 (2009) 325−330.

[83] J. Liu, A.I. Benin, A.M.B. Furtado, P. Jakubczak, R.R. Willis, M.D. LeVan, Stability effects on CO_2 adsorption for the DOBDC series of metal–organic frameworks, Langmuir 27 (2011) 11451−11456.

[84] J.A. Mason, T.M. McDonald, T.-H. Bae, J.E. Bachman, K. Sumida, J.J. Dutton, S.S. Kaye, J.R. Long, Application of a High-Throughput analyzer in evaluating solid adsorbents for post-combustion carbon capture via multicomponent adsorption of CO_2, N_2 and H_2O, J. Am. Chem. Soc. 137 (2015) 4787-4803.

[85] T. Graham, XXXV.-On the properties of silicic acid and other analogous colloidal substances, J. Am. Chem. Soc. 17 (1864) 318-327.

[86] R. Aelion, A. Loebel, F. Eirich, Hydrolysis of ethyl silicate*, J. Am. Chem. Soc. 72 (1950) 5705-5712.

[87] C. Vincent, R. Joseph E, V.Clarence D, Process for producing low-bulk density silica, US3556725 A, 1971.

[88] W. Stöber, A. Fink, E. Bohn, Controlled growth of monodisperse silica spheres in the micron size range, J. Colloid Interface Sci. 26 (1968) 62−69.

[89] G. Kallrath, H. Biegler, Process for producing silica in the form of hollow spheres, US 3383172 A, 1968.

[90] T. Yanagisawa, T. Shimizu, K. Kuroda, C. Kato, The preparation of alkyltrimethylammonium-kanemite complexes and their conversion to microporous materials, Bull. Chem. Soc. Jpn. 63 (1990) 988−992.

[91] C.T. Kresge, M.E. Leonowicz, W.J. Roth, J.C. Vartuli, J.S. Beck, Ordered mesoporous molecular sieves synthesized by a liquid-crystal template mechanism, Nature 359 (1992) 710-712.

[92] J.S. Beck, J.C. Vartuli, W.J. Roth, M.E. Leonowicz, C.T. Kresge, K.D. Schmitt, C.T.W. Chu, D.H. Olson, E.W. Sheppard, S.B. McCullen, J.B. Higgins, J.L. Schlenker, A new family of mesoporous molecular-sieves prepared with liquid-crystal templates, J. Am. Chem. Soc. 114 (1992) 10834−10843.

[93] C.T. Kresge, W.J. Roth, The discovery of mesoporous molecular sieves from the twenty year perspective, Chem. Soc. Rev. 42 (2013) 3663-3670.

[94] F. Hoffmann, M. Cornelius, J. Morell, M. Froba, Silica-based mesoporous organic-inorganic hybrid materials, Angew. Chem.-Int. Edit. 45 (2006) 3216-3251.

[95] M. Kruk, M. Jaroniec, R. Ryoo, S.H. Joo, Characterization of MCM-48 silicas with tailored pore sizes synthesized via a highly efficient procedure, Chem. Mater. 12 (2000) 1414-1421.

[96] M. Kruk, M. Jaroniec, J.H. Kim, R. Ryoo, Characterization of highly ordered MCM-41 silicas using X-ray diffraction and nitrogen adsorption, Langmuir 15 (1999) 5279−5284.

[97] A. Sayari, Novel synthesis of high-quality MCM-48 silica, J. Am. Chem. Soc. 122 (2000) 6504−6505.

[98] J.C. Vartuli, C.T. Kresge, M.E. Leonowicz, A.S. Chu, S.B. McCullen, I.D. Johnsen, E.W. Sheppard, Synthesis of mesoporous materials - liquid-crystal templating versus intercalation of layered silicates, Chem. Mater. 6 (1994) 2070−2077.

[99] Q. Huo, D.I. Margolese, U. Ciesla, P. Feng, T.E. Gier, P. Sieger, R. Leon, P.M. Petroff, F. Schuth, G.D. Stucky, Generalized synthesis of periodic surfactant/inorganic composite materials, Nature 368 (1994) 317-321.

[100] J.S. Beck, J.C. Vartuli, G.J. Kennedy, C.T. Kresge, W.J. Roth, S.E. Schramm, Molecular or supramolecular templating: Defining the role of surfactant chemistry in the formation of microporous and mesoporous molecular sieves, Chem. Mater. 6 (1994) 1816−1821.

[101] A. Corma, Q.B. Kan, M.T. Navarro, J. PerezPariente, F. Rey, Synthesis of MCM-41 with different pore diameters without addition of auxiliary organics, Chem. Mater. 9 (1997) 2123−2126.

[102] A. Sayari, P. Liu, M. Kruk, M. Jaroniec, Characterization of large-pore MCM-41 molecular sieves obtained via hydrothermal restructuring, Chem. Mater. 9 (1997) 2499−2506.

[103] R. Serna-Guerrero, A. Sayari, Applications of pore-expanded mesoporous silica. 7. Adsorption of volatile organic compounds, Environ. Sci. Technol. 41 (2007) 4761−4766.

[104] M. Hartmann, C. Bischof, Mechanical stability of mesoporous molecular sieve MCM-48 studied by adsorption of benzene, n-heptane, and cyclohexane, J. Phys. Chem. B 103 (1999) 6230−6235.

[105] Z.Y. Liu, Y.X. Wei, Y. Qi, S.G. Zhang, Y. Zhang, Z.M. Liu, Synthesis of MCM-41 type materials with remarkable hydrothermal stability from UTM-1, Microporous Mesoporous Mater. 93 (2006) 205−211.

[106] J.M. Kim, R. Ryoo, Disintegration of mesoporous structures of MCM-41 and MCM-48 in water, Bull. Korean Chem. Soc. 17 (1996) 66−68.

[107] R. Mokaya, W. Jones, Efficient post-synthesis alumination of MCM-41 using aluminium chlorohydrate containing Al polycations, J. Mater. Chem. 9 (1999) 555−561.

[108] S. Jun, J.M. Kim, R. Ryoo, Y.-S. Ahn, M.-H. Han, Hydrothermal stability of MCM-48 improved by post-synthesis restructuring in salt solution, Microporous Mesoporous Mater. 41 (2000) 119−127.

[109] R. Ryoo, S. Jun, Improvement of hydrothermal stability of MCM-41 using salt effects during the crystallization process, J. Phys. Chem. B 101 (1997) 317−320.

[110] J.M. Kim, S. Jun, R. Ryoo, Improvement of hydrothermal stability of mesoporous silica using salts: Reinvestigation for time-dependent effects, J. Phys. Chem. B 103 (1999) 6200−6205.

[111] J. Yu, J.L. Shi, H.R. Chen, J.N. Yan, D.S. Yan, Effect of inorganic salt addition during synthesis on pore structure and hydrothermal stability of mesoporous silica, Microporous Mesoporous Mater. 46 (2001) 153−162.

[112] D.Y. Zhao, J.L. Feng, Q.S. Huo, N. Melosh, G.H. Fredrickson, B.F. Chmelka, G.D. Stucky, Triblock copolymer syntheses of mesoporous silica with periodic 50 to 300 angstrom pores, Science 279 (1998) 548−552.

[113] D. Zhao, Q. Huo, J. Feng, B.F. Chmelka, G.D. Stucky, Nonionic triblock and star diblock copolymer and oligomeric surfactant syntheses of highly ordered, hydrothermally stable, mesoporous silica structures, J. Am. Chem. Soc. 120 (1998) 6024−6036.

[114] V. Zelenak, D. Halamova, L. Gaberova, E. Bloch, P. Llewellyn, Amine-modified SBA-12 mesoporous silica for carbon dioxide capture: Effect of amine basicity on sorption properties, Microporous Mesoporous Mater. 116 (2008) 358−364.

[115] J. Wei, J. Shi, H. Pan, W. Zhao, Q. Ye, Y. Shi, Adsorption of carbon dioxide on organically functionalized SBA-16, Microporous Mesoporous Mater. 116 (2008) 394−399.

[116] F. Zheng, D.N. Tran, B.J. Busche, G.E. Fryxell, R.S. Addleman, T.S. Zemanian, C.L. Aardahl, Ethylenediamine-modified SBA-15 as regenerable CO_2 sorbent, Ind. Eng. Chem. Res. 44 (2005) 3099−3105.

[117] D.S. Dao, H. Yamada, K. Yogo, Large-Pore Mesostructured silica impregnated with blended amines for CO_2 capture, Ind. Eng. Chem. Res. 52 (2013) 13810−13817.

[118] P. Selvam, S.K. Bhatia, C.G. Sonwane, Recent advances in processing and characterization of periodic mesoporous MCM-41 silicate molecular sieves, Ind. Eng. Chem. Res. 40 (2001) 3237−3261.

[119] W. Yan, J. Tang, Z. Bian, J. Hu, H. Liu, Carbon dioxide capture by amine-impregnated mesocellular-foam-containing template, , Ind. Eng. Chem. Res. 51 (2012) 3653−3662.

[120] W.-J. Son, J.-S. Choi, W.-S. Ahn, Adsorptive removal of carbon dioxide using polyethyleneimine-loaded mesoporous silica materials, Microporous Mesoporous Mater. 113 (2008) 31-40.

[121] C. Pirez, J.-M. Caderon, J.-P. Dacquin, A.F. Lee, K. Wilson, Tunable KIT-6 mesoporous sulfonic acid catalysts for fatty acid esterification, ACS Catal. 2 (2012) 1607−1614.

[122] R. Serna-Guerrero, Y. Belmabkhout, A. Sayari, Modeling CO_2 adsorption on amine-functionalized mesoporous silica: 1. A semi-empirical equilibrium model, Chem. Eng. J. 161 (2010) 173−181.

[123] S. Loganathan, M. Tikmani, A.K. Ghoshal, Novel pore-expanded MCM-41 for CO_2 capture: Synthesis and characterization, Langmuir 29 (2013) 3491−3499.

[124] Y.G. Ko, S.S. Shin, U.S. Choi, Primary, secondary, and tertiary amines for CO_2 capture: Designing for mesoporous CO_2 adsorbents, J. Colloid Interface Sci. 361 (2011) 594−602.

[125] M. Caplow, Kinetics of carbamate formation and breakdown, J. Am. Chem. Soc. 90 (1968) 6795-6803.

[126] T. Tsuda, T. Fujiwara, Polyethyleneimine and macrocyclic polyamine silica gels acting as carbon dioxide absorbents, Journal of the Chemical Society, Chem. Commun. (1992) 1659−1661.

[127] O. Leal, C. Bolivar, C. Ovalles, J.J. Garcia, Y. Espidel, Reversible adsorption of carbon dioxide on amine surface-bonded silica gel, Inorg. Chim. Acta 240 (1995) 183−189.

[128] X. Xu, C. Song, J.M. Andresen, B.G. Miller, A.W. Scaroni, Novel polyethylenimine-modified mesoporous molecular sieve of MCM-41 type as high-capacity adsorbent for CO_2 capture, Energy Fuels 16 (2002) 1463−1469.

[129] S. Loganathan, M. Tikmani, A. Mishra, A.K. Ghoshal, Amine tethered pore-expanded MCM-41 for CO2 capture: Experimental, isotherm and kinetic modeling studies, Chem. Eng. J. 303 (2016) 89-99.

[130] T.C. dos Santos, S. Bourrelly, P.L. Llewellyn, J.W. de M. Carneiro, C. M. Ronconi, Adsorption of CO_2 on amine-functionalised MCM-41: Experimental and theoretical studies, Phys. Chem. Chem. Phys. 17 (2015) 11095−11102.

[131] L. Zhou, J. Fan, G. Cui, X. Shang, Q. Tang, J. Wang, M. Fan, Highly efficient and reversible CO_2 adsorption by amine-grafted platelet SBA-15 with expanded pore diameters and short mesochannels, Green Chem. 16 (2014) 4009−4016.

[132] N.N. Linneen, R. Pfeffer, Y.S. Lin, CO2 adsorption performance for amine grafted particulate silica aerogels, Chem. Eng. J. 254 (2014) 190−197.

[133] R. Sanz, G. Calleja, A. Arencibia, E.S. Sanz-Perez, Development of high efficiency adsorbents for CO_2 capture based on a double-functionalization method of grafting and impregnation, J. Mater. Chem. A 1 (2013) 1956−1962.

[134] Y.G. Ko, H.J. Lee, H.C. Oh, U.S. Choi, Amines immobilized double-walled silica nanotubes for CO2 capture, J. Hazard. Mater. 250–251 (2013) 53−60.

[135] U. Patil, A. Fihri, A.-H. Emwas, V. Polshettiwar, Silicon oxynitrides of KCC-1, SBA-15 and MCM-41 for CO_2 capture with excellent stability and regenerability, Chem. Sci. 3 (2012) 2224−2229.

[136] L. Wang, R.T. Yang, Increasing Selective CO_2 Adsorption on Amine-Grafted SBA-15 by Increasing Silanol Density, J. Phys. Chem. C 115 (2011) 21264−21272.

[137] M.R. Mello, D. Phanon, G.Q. Silveira, P.L. Llewellyn, C.M. Ronconi, Amine-modified MCM-41 mesoporous silica for carbon dioxide capture, Microporous Mesoporous Mater. 143 (2011) 174−179.

[138] M. Gil, I. Tiscornia, Ó. de la Iglesia, R. Mallada, J. Santamaría, Monoamine-grafted MCM-48: An efficient material for CO_2 removal at low partial pressures, Chem. Eng. J. 175 (2011) 291−297.

[139] S. Cui, W. Cheng, X. Shen, M. Fan, A. Russell, Z. Wu, X. Yi, Mesoporous amine-modified SiO_2 aerogel: a potential CO_2 sorbent, Energy Environ. Sci. 4 (2011) 2070−2074.

[140] Y. Belmabkhout, N. Heymans, G. De Weireld, A. Sayari, Simultaneous adsorption of H_2S and CO_2 on triamine-grafted pore-expanded mesoporous MCM-41 silica, Energy Fuels 25 (2011) 1310−1315.

[141] A. Sayari, Y. Belmabkhout, Stabilization of amine-containing CO_2 adsorbents: Dramatic effect of water vapor, J. Am. Chem. Soc. 132 (2010) 6312−6314.

[142] V. Zeleňák, M. Badaničová, D. Halamová, J. Čejka, A. Zukal, N. Murafa, G. Goerigk, Amine-modified ordered mesoporous silica: Effect of pore size on carbon dioxide capture, Chem. Eng. J. 144 (2008) 336-342.

[143] C. Knöfel, J. Descarpentries, A. Benzaouia, V. Zeleňák, S. Mornet, P.L. Llewellyn, V. Hornebecq, Functionalised micro-/mesoporous silica for the adsorption of carbon dioxide, Microporous Mesoporous Mater. 99 (2007) 79−85.

[144] G.P. Knowles, J.V. Graham, S.W. Delaney, A.L. Chaffee, Aminopropyl-functionalized mesoporous silicas as CO_2 adsorbents, Fuel Process. Technol. 86 (2005) 1435−1448.

[145] S. Kim, J. Ida, V.V. Guliants, Y.S. Lin, Tailoring pore properties of MCM-48 silica for selective adsorption of CO_2, J. Phy. Chem. B 109 (2005) 6287−6293.

[146] N. Hiyoshi, K. Yogo, T. Yashima, Adsorption characteristics of carbon dioxide on organically functionalized SBA-15, Microporous Mesoporous Mater. 84 (2005) 357−365.

[147] H.Y. Huang, R.T. Yang, D. Chinn, C.L. Munson, Amine-grafted MCM-48 and silica xerogel as superior sorbents for acidic gas removal from natural gas, Ind. Eng. Chem. Res. 42 (2003) 2427−2433.

[148] M.E. McGovern, K.M.R. Kallury, M. Thompson, Role of solvent on the silanization of glass with octadecyltrichlorosilane, Langmuir 10 (1994) 3607−3614.

[149] N. Gartmann, C. Schütze, H. Ritter, D. Brühwiler, The Effect of water on the functionalization of mesoporous silica with 3-aminopropyltriethoxysilane, J. Phys. Chem. Lett. 1 (2010) 379−382.

[150] A.S. Maria Chong, X.S. Zhao, Functionalization of SBA-15 with APTES and characterization of functionalized materials, J. Phys. Chem. B 107 (2003) 12650−12657.

[151] N.A. Brunelli, S.A. Didas, K. Venkatasubbaiah, C.W. Jones, Tuning cooperativity by controlling the linker length of silica-supported amines in catalysis and CO_2 capture,J. Am. Chem. Soc. 134 (2012) 13950−13953.

[152] K.O. Moura, H.O. Pastore, Comparative Adsorption of CO_2 by Mono-, Di-, and Triamino-organofunctionalized magnesium phyllosilicates, Environ. Sci. Technol. 47 (2013) 12201−12210.

[153] K. Sim, N. Lee, J. Kim, E.-B. Cho, C. Gunathilake, M. Jaroniec, CO_2 adsorption on amine-functionalized periodic mesoporous benzenesilicas, ACS Appl. Mater. Interfaces 7 (2015) 6792−6802.

[154] X. Xu, C. Song, B.G. Miller, A.W. Scaroni, Influence of moisture on CO_2 separation from gas mixture by a nanoporous adsorbent based on polyethylenimine-modified molecular sieve MCM-41, Ind. Eng. Chem. Res. 44 (2005) 8113−8119.

[155] X. Wang, X. Ma, C. Song, D.R. Locke, S. Siefert, R.E. Winans, J. Möllmer, M. Lange, A. Möller, R. Gläser, Molecular basket sorbents polyethylenimine–SBA-15 for CO_2 capture from flue gas: Characterization and sorption properties, Microporous Mesoporous Mater. 169 (2013) 103−111.

[156] K. Li, J. Jiang, S. Tian, F. Yan, X. Chen, Polyethyleneimine-nano silica composites: a low-cost and promising adsorbent for CO_2 capture, J. Mater. Chem. A 3 (2015) 2166−2175.

[157] M.J. Al-Marri, M.M. Khader, M. Tawfik, G. Qi, E.P. Giannelis, CO_2 sorption kinetics of scaled-up polyethylenimine-functionalized mesoporous silica sorbent, Langmuir 31 (2015) 3569−3576.

[158] R. Sanz, G. Calleja, A. Arencibia, E.S. Sanz-Pérez, CO_2 adsorption on branched polyethyleneimine-impregnated mesoporous silica SBA-15, Appl. Surf. Sci. 256 (2010) 5323−5328.

[159] Y. Liu, J. Shi, J. Chen, Q. Ye, H. Pan, Z. Shao, Y. Shi, Dynamic performance of CO_2 adsorption with tetraethylenepentamine-loaded KIT-6, Microporous Mesoporous Mater. 134 (2010) 16−21.

[160] L. Wei, Z. Gao, Y. Jing, Y. Wang, Adsorption of CO_2 from simulated flue gas on pentaethylenehexamine-loaded mesoporous silica support adsorbentInd. Eng. Chem. Res. 52 (2013) 14965−14974.

[161] J.C. Hicks, J.H. Drese, D.J. Fauth, M.L. Gray, G. Qi, C.W. Jones, Designing adsorbents for CO_2 capture from flue gas-hyperbranched aminosilicas capable of capturing CO_2 reversibly, J. Am. Chem. Soc. 130 (2008) 2902−2903.

[162] J.H. Drese, S. Choi, R.P. Lively, W.J. Koros, D.J. Fauth, M.L. Gray, C.W. Jones, Synthesis–structure–property relationships for hyperbranched aminosilica CO_2 adsorbents, Adv. Funct. Mater. 19 (2009) 3821−3832.

[163] D.J. Fauth, M.L. Gray, H.W. Pennline, H.M. Krutka, S. Sjostrom, A.M. Ault, Investigation of porous silica supported mixed-amine sorbents for post-combustion CO_2 capture, Energy Fuels 26 (2012) 2483−2496.

[164] A. Goeppert, S. Meth, G.K.S. Prakash, G.A. Olah, Nanostructured silica as a support for regenerable high-capacity organoamine-based CO_2 sorbents, Energy Environ. Sci. 3 (2010) 1949−1960.

[165] G.A. Olah, A. Goepert, S. Meth, G.K.S. Prakash, Nano-structure supported solid regenerative polyamine and polyamine polyol absorbents for the separation of carbon dioxide from gas mixtures including the air, U.S Patents, US7795175 B2 (2008).

[166] J. Wang, D. Long, H. Zhou, Q. Chen, X. Liu, L. Ling, Surfactant promoted solid aminesorbents for CO_2 capture, Energy Environ. Sci. 5 (2012) 5742-5749.

[167] K. Li, J. Jiang, F. Yan, S. Tian, X. Chen, The influence of polyethyleneimine type and molecular weight on the CO_2 capture performance of PEI-nano silica adsorbents, Applied Energy 136 (2014) 750-755.

CHAPTER 3

EXPERIMENTAL

CHAPTER 3

This chapter presents the synthesis procedure of different ordered mesoporous silica used in this study. Various characterization techniques including physical, structural, thermal and gas adsorption are discussed.

3.1 Experimental

3.1.1 *Materials*

The chemicals pluronic P123 (EO_{20}-PO_{70}-EO_{20}, mw ~ 5800 Da, Sigma-Aldrich), a triblock copolymer and cetrimide (CTAB, Merck), a structure directing agent were purchased. Tetraethyl orthosilicate (TEOS, ≥ 99%, Sigma-Aldrich) were used as a silica source during synthesis of MCM-41, SBA-15 and KIT-6. The (3-aminopropyle)triethoxysilane (APTES, Himedia) and N^1-(3-trimethoxysilylpropyle)diethylenetriamine (TMPTA, Aldrich) and other amines such as,diethylenetriamine (DETA, Merck), tetraethylenepentamine (TEPA, Aldrich), pentaethylenehexamine (PEHA, Aldrich) and polyethyleneimine (PEI, mw = 800, 1200 and 25K, Aldrich) were purchased. Other chemicals such as hydrochloric acid (HCl, 35%), n-butanol (≥ 99%), ethanol (≥ 99%), ammonia solution (NH_3, 25%) and anhydrous toluene (≥ 99%) were purchased from Merck. All the chemicals were used without any further treatment. All the solutions were prepared with Millipore purified water.

3.1.2 *Synthesis of ordered mesoporous silica*

Ordered mesoporous KIT-6 was synthesized following the earlier reported procedure present in the literature [1]. In a typical synthesis process, pluronic (4.0 g) was dissolved in HCl (7.9 g, 35 wt%) and Millipore purified water (144.0 g) using magnetic stirrer. After the solution became homogeneous, BuOH (4.0 g) was added and mixed for an hour. The silica source TEOS (8.6 g) was added in the solution and stirred for 24 h. During synthesis, the temperature of the mixture was maintained at 313 K. The molar gel composition is TEOS (1.0): pluronic (0.017): HCl (1.83): H_2O (195): BuOH (1.31). The resulting solution was then transferred to a teflon autoclave and aged for 24 h at 373 K in the static condition. The white solid product was filtered. Half of the solid product (KIT-6) was washed with distilled water and another half (KIT-6/D) was kept without washing. The resulting solid product was dried overnight at 373 K in hot air oven. Surfactant free KIT-6 was obtained after calcination at 550 K for 5 h. The structure of the ordered KIT-6 was controlled by changing the alcohol in the synthesis solution.

Highly ordered MCM-41 was synthesized by the following procedure [2]: 2.0 g CTAB was dissolved in 120 mL Millipore purified water. After complete dissolution, 9.0 mL of NH_3 was added. The 10 mL of TEOS was added drop wise in solution and stirred for another 12 h at room temperature. The white solid product was filtered, washed with distilled water and dried at 100 °C for 24 h. Surfactant free MCM-41 was obtained after calcination at 550 °C for 5 h. MCM-41 with high pore volume was synthesized by changing the concentration of NH_3 from 9 to 1 mL in the synthesis solution [2]. Other synthesis steps were similar as explained for hexagonal MCM-41. Ammonia presents in the solution control the rate of TEOS hydrolysis during MCM-41 formation.

SBA-15 was synthesized by the following procedure [3]: 4.0 g of P123 was dissolved in 144 mL of 1.7 N HCl at 40 °C. After itbecame homogeneous, 8.0 g TEOS was added in the solution and stirred for another 24 h at 40 °C. The resulting mixture was transferred to teflon lined autoclave and aged at 100 °C for 24 h. The white solid product was obtained by filtration and dried at 100 °C for 24 h. Surfactant free SBA-15 was obtained after calcination at 550 °C for 5 h.

3.1.3 *Adsorbent synthesis*

3.1.3.1 *Screening of amine*

Varieties of aminosilanes are commercially available for different applications. They consist of alkyl group, silane and functional group. The typical aminosilane consist of alkyl group (methyl/ethyl) connected with silica amine groups in the form of organic chain (Figure 3.1). The alkyl groups (R−) of aminosilane reacted with the silanol groups present on mesoporous silica surface by condensation reaction and grafted over the surface as shown in Figure 3.2.

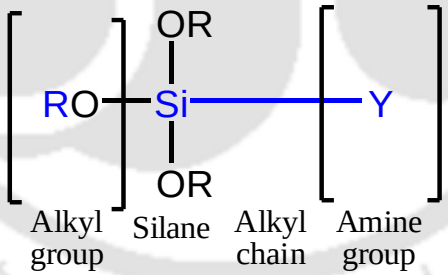

Figure 3.1 Schematic of organosilane used in grafting in mesoporous silica

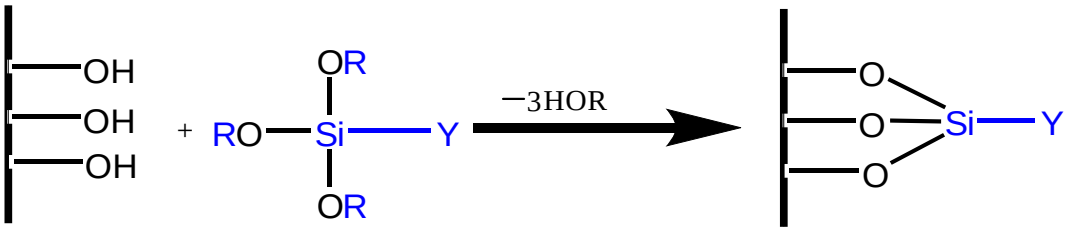

Figure 3.2 Schematic of organosilane grafting in mesoporous silica

From the literature study, it is seen that primary amine is a major choice for CO_2 adsorption [2-5]. It has the highest amine efficiency during CO_2 adsorption as well as oxidative, thermal stability during regeneration [5]. Additionally, C_3 linker length based aminosilane gives the highest separation during CO_2 adsorption as well as activity during catalytic reaction. Therefore, as per literature serve (3-aminopropyl)triethoxysilane is a desirable candidate for designing the CO_2 adsorbent [2–5].

Amine concentration in adsorbent is reflected by the CO_2 sorption capacity of the adsorbent [2,3,6−8]. Amine concentration can be improved by grafting of triaminosilane i.e. TMPTA in KIT-6. Further (higher than 3 molecules per aminosilane) amine grafting sharply reduced the CO_2 adsorption capacity of the adsorbent. Again, the sorption capacity of adsorbent is improved by impregnation of wide varieties of aliphatic polyethyleneimines in KIT-6.

3.1.3.2 *Aminosilane grafting*

Pure KIT-6 was functionalized by post grafting method, both in dry and aqueous solution. Before grafting, 1.0 g of KIT-6 was dried at 120 ºC in vacuum to remove the pre-adsorbed moisture. In a typical dry grafting process, 1.0 g of KIT-6 was dispersed in 50 mL of dry toluene taken in a flask. In the resulting solution ‘x’ mmol of APTES was added and refluxed at 80°C for 24 h. The treated sample was filtered, washed with copious amount of toluene and ethanol.Solid product was dried at 80°C in vacuum for 16 h. The functionalized KIT-6 was stored for further analysis and denoted as KIT’x’AP (where ‘x’ represents the concentration of APTES in mmol/g). In aqueous grafting, ‘y’ ml of water was added in the dispersed KIT-6 solution and stirred for 2 h at room temperature. The optimized concentration of APTES from dry grafting process was added

in the solution and refluxed at 80°C for 24 h. Other steps were similar as explained above and the functionalized material was denoted as 'y'KIT'x'AP.

In TMPTA grafting, 1.0 g of KIT-6 was dispersed in 150 mL toluene and stirred for 1 h to make homogeneous. Then, 'x' mmol of TMPTA was added in the solution and refluxed at 85 ºC in stirring condition for 24 h. The TMPTA grafted KIT-6 was filtered and repeatedly washed with toluene and ethanol. The solid product was dried at 80 ºC in high vacuum for 16 h and stored for further analysis. The obtained samples were designated as KIT'x'TA, where 'x' was the concentration of TMPTA. In aqueous grafting, after complete dispersion of KIT-6 in toluene, 'y' mL Millipore purified water was added and stirred for 3 h to modify the silica surface. The further steps were similar as discussed in dry grafting. The resulting samples were denoted as 'y'KIT'x'TA. Similar procedure was followed for the MCM-41 and SBA-15 functionalization with TMPTA. Functionalized MCM-41 and SBA-15 was denoted as 'y'MCM'x'TA and 'y'SBA'x'TA, respectively.

3.1.3.3 *Impregnation of Polyethyleneimine*

Polyethylenimine was incorporated in KIT-6 by wet impregnation method [6,7]. Initially, 1.0 g of KIT-6 was dried in vacuum oven at 120 ºC for 3 h. During this stage, the pre-adsorbed moisture was removed from the adsorbent. The concentration of polyethyleneimine in KIT-6 was calculated using the equation 'x' (wt%) = (wt of polyethyleneimine ×100)/ (wt of polyethyleneimine + wt of KIT-6). Initially, 1.0 g TEPA was stirred for 30 min in 50 mL ethanol. After it turned homogeneous, 1.0 g of dry KIT-6 was added and refluxed at 80 ºC for 6 h. Solid product was obtained after evaporation of ethanol and subsequent drying at 70 ºC in vacuum for 6 h. The resulting adsorbent was stored for further analysis after drying for an hour in hot air oven at 100 ºC.

Similar procedure was followed for DETA, PEHA impregnation in KIT-6. The functionalized adsorbents were denoted as ‘x’ DETA/KIT, ‘x’ TEPA/KIT, ‘x’ PEHA/KIT, ‘x’ PEI-800/KIT, ‘x’ PEI-1.2K/KIT and ‘x’ PEI-2.5K/KIT for DETA, TEPA, PEHA, PEI-800, PEI-1200 and PEI-25000, respectively The other mesoporous silica MCM-41, SBA-15, and high pore volume MCM-41 was functionalized with PEHA by the above reported procedure. Functionalized adsorbents were denoted as ‘x’ PEHA/MCM, ‘x’ PEHA/SBA and ‘x’ PEHA/HV for MCM-41, SBA-15 and high pore volume MCM-41.

KIT-6 was functionalized with high molecular weight polyethyleneimine (PEI-800, PEI-1200 and PEI-25K) by wet impregnation method as discussed above. 1.0 g PEI was stirred for 30 min in 50 mL methanol. After it turned homogeneous, 1.0 g of dry KIT-6 was added in the solution and stirred for 6 h. The solid product was obtained after evaporation of methanol and subsequent drying at 70 ºC in vacuum for 6 h. The resulting adsorbent was stored for further analysis after drying for an hour in hot air oven at 100 ºC.

Surfactant occluded as-synthesized KIT-6 was functionalized with DETA, PEHA, TEPA, PEI-800 and PEI-25K by wet impregnation method as discussed above. The resulting adsorbent was denoted as ‘x’ DETA/ASK, ‘x’ TEPA/ASK, ‘x’ PEHA/ASK, ‘x’ PEI-800/ASK and ‘x’ PEI-2.5K/ASK.

3.2 Characterization of Adsorbent

The textural properties of the adsorbents were analyzed by automated volumetric gas sorption analyzer (Quantachrome Autosorb iQ). A difinite amount (~ 100 mg) of sample was taken in the sample holder and fitted with the outgas port in sorption analyzer. Before analysis, the as-synthesized KIT-6 was out-gassed under vacuum for 3 h at 120 ºC and calcined at 150 ºC. Aminosilane grafted KIT-6 was degassed in vacuum for 3 h at 120 ºC and polyethyleneimine

impregnated at 100 ºC. After degassing, sample holder was filled with the helium. Further, N_2 adsorption/desorption isotherms of the adsorbents were recorded at −196 ºC. The Brunauer-Emmett-Teller (BET) equation was used to calculate the specific surface area in relative pressure (P/P_0) range 0.05 – 0.3 and total pore volume (V_t) as 0.99. The pore size distribution was calculated by N_2 desorption branch of equilibrium isotherm using Barret-Joyner-Halenda (BJH) method. The micropore volume (Vmic) was calculated by t-plot using de Boer method. Non-local density functional theory (NLDFT) analyses were also used to evaluate the pore sizes. The NLDFT analysis was performed based on equilibrium model with cylindrical pore.

Powder X-ray diffraction spectra was recorded using Bruker D8 advance diffractometer using CuKα (λ = 0.154250 nm) radiation operating at 40 kV and 40 mA, using 0.01° step size with 1.0 scan speed over range 0.5 – 5°. The inter-plane spacing (d_{211}) was calculated by Bragg's law ($n\lambda = 2d_{211}Sin\theta$; where θ is the diffraction angle at (211) plane position). The unit cell parameter (a_0) was calculated from the relation $a_0 = (d211) \times \sqrt{(h^2 + k^2 + l^2)}$. The wall thickness of KIT-6 was calculated as $a_0/\xi_0 = \langle h \rangle + W_h/2$; where ξ_0 is 3.092 for the dimensionless area of the minimal gyroid surface, <h> is pore wall thickness, and W_h is hydraulic pore diameter [9,10]. The W_h was analysed by NLDFT method as reported by Schumacher [10].

Surface morphology were collected from the field emission scanning electron microscope (FESEM, Zeiss, Sigma). Before analysis, samples were coated with Au by sputtering for 180 sec. Transmission electron microscopy (TEM) images were viewed with JEOL JEM 2100 at the maximum accelerating voltage of 200 kV. During sample preparation, KIT-6 was dispersed in ethanol and a small drop was put on carbon coated copper grid.

Thermal properties of the adsorbent were performed in thermogravimetric (TG, NETZSCH TG 209F1 Libra) analyzer in the temperature range 30 – 800 ºC with 10 ºC/min heating rate in N_2 atmosphere.

Molecular composition of the adsorbent was identified by Fourier transform infrared (FTIR, PerkinElmer) spectrometer in attenuated total reflection (ATR) and diffuse reflectance infrared Fourier transform (DRIFT) mode in the wavenumber range 4000 – 400 cm^{-1}.

3.3 Adsorption/Desorption Measurement

Adsorption and desorption measurements for CO_2 on pure and organosilane functionalized adsorbents were performed using a Rubotherm gravimetric magnetic suspension balance (Figure 3.3) at different temperatures. A definite amount of adsorbent was placed in a sample holder, suspended with a magnetic balance. The sample was closed by external fitting. Initially, adsorbent was outgassed at 120 °C at low pressure in helium atmosphere to remove the unwanted gas and moisture present. Weight loss in the sample was recorded in the computer. Subsequently, the sample was cooled to 30°C. Before starting the analysis, buoyancy correction was performed using He till 20 bar. The temperature was maintained during analysis by external circulator bath. CO_2 was inserted in the sample chamber at a desired pressure, and the system was on hold for 20 minutes till thermodynamic equilibrium was reached. The change in weight, pressure and temperature were measured continuously for every pressure point and the adsorption capacity was evaluated at different temperatures 30, 45, 60 and 75 °C. In a typical kinetic measurement, CO_2 was purged into the sample chamber with a step input at 1 bar pressure. Cyclic adsorption/desorption capacities of the materials were analyzed at 30 °C and regeneration at 120 °C in helium atmosphere.

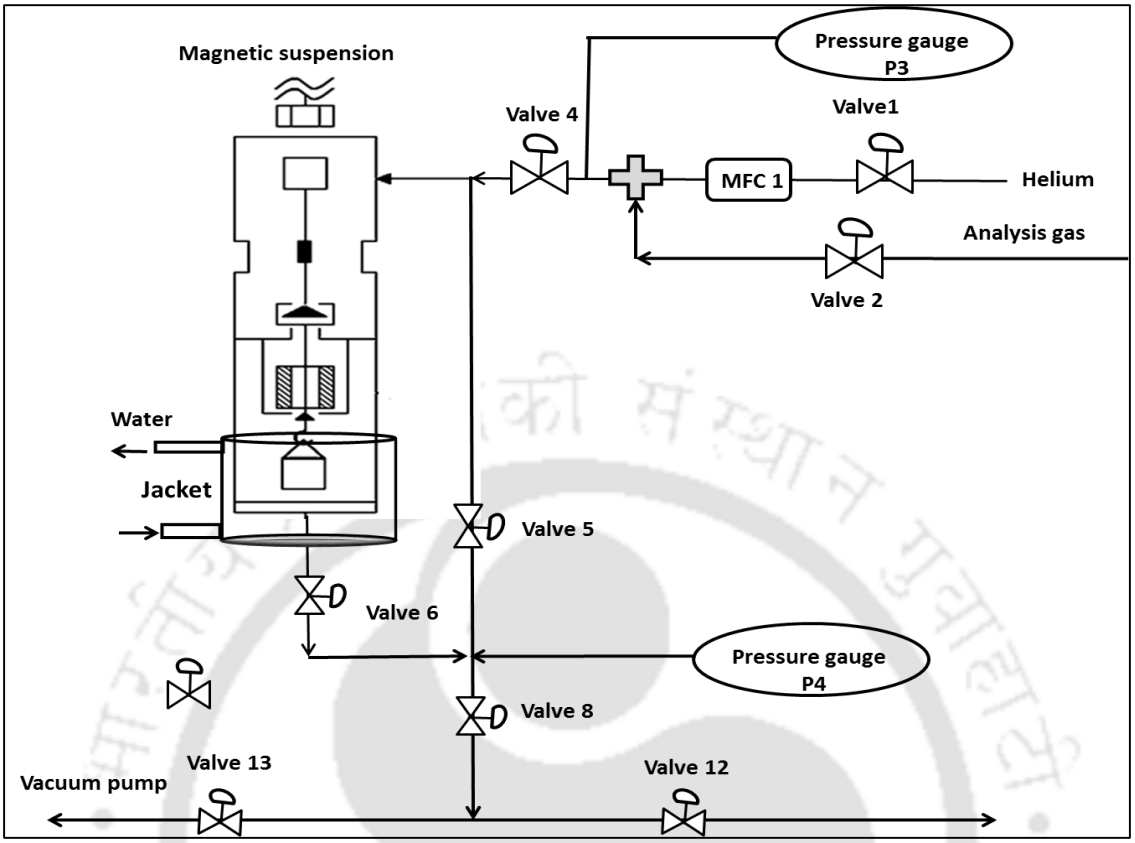

Figure 3.3 Flow diagram of gravimetric adsorption apparatus

Adsorption/desorption isotherms for CO_2 (20 bar), N_2 (20 bar) and H_2 (30 bar) were also measured using volumetric adsorption apparatus (Quantachrome iSorbHP1-XKRLSPN100). The CO_2/N_2 adsorption isotherms were measured at different temperatures and pressures. However, H_2 uptakes were measured at −196 ºC, −10 ºC, 0 ºC and 20 ºC. In adsorption analysis, ~ 0.5 g mesoporous KIT-6 was placed in a sample holder, fitted with adsorption apparatus. Before analysis, sample was degassed at 150 ºC for 3 h and filled with the He gas. Before starting the real gas adsorption, void volume at analysis temperature was calculated using He gas. During analysis, temperatures were maintained using external polyScience thermostatic circulating bath.

Adsorption temperature −196 ºC was maintained by liquid nitrogen and that from 60 ºC to 120 ºC was maintained using external furnace. Ultra-high purity (> 99.99%) grade gases were used during analysis and then physical properties summarized in Table 3.1.

Table 3.1 Physical properties of CO_2, N_2 and H_2

Adsorbate	CO_2	N_2	H_2
Kinetic diameter (Å)	3.30	3.64	2.89
Polarizability (10^{-25} cm^{-3})	29.1	17.4	8.04
Dipole moment (10^{-19} esu^{-1} cm^{-1})	0	0	0
Quadrupole moment (10^{-27} esu^{-1} cm^{-1})	6.62	15.2	43.0

References

[1] T.-W. Kim, F. Kleitz, B. Paul, R. Ryoo, MCM-48-like large mesoporous silicas with tailored pore structure facile synthesis domain in a ternary triblock copolymer-butanol-water system, J. Am. Chem. Soc. 127 (2005) 7601-7610.

[2] S. Loganathan, M. Tikmani, A. K. Ghoshal, Novel pore-expanded MCM-41 for CO_2 capture: synthesis and characterization, Langmuir 29 (2013) 3491–3499.

[3] L. Wang, R. T. Yang, Increasing selective CO_2 adsorption on amine-grafted SBA-15 by increasing silanol density, J. Phys. Chem. C 115 (2011) 21264–21272.

[4] Y. G. Ko, S. S. Shin, U. S. Choi, Primary, secondary, and tertiary amines for CO_2 capture: designing for mesoporous CO_2 adsorbents, J. Colloid Interface Sci.361 (2011) 594–602.

[5] N.A. Brunelli, S.A. Didas, K. Venkatasubbaiah, C.W. Jones, Tuning cooperativity by controlling the linker length of silica-supported amines in catalysis and CO_2 capture, J. Am. Chem. Soc. 134 (2012) 13950-13953

[6] X. Xu, C. Song, B.G. Miller, A.W. Scaroni, Influence of moisture on CO_2 separation from gas mixture by a nanoporous adsorbent based on polyethylenimine-modified molecular sieve MCM-41, Ind. Eng. Chem. Res. 44 (2005) 8113-8119.

[7] X. Wang, X. Ma, C. Song, D.R. Locke, S. Siefert, R.E. Winans, J. Möllmer, M. Lange, A. Möller, R. Gläser, Molecular basket sorbents polyethylenimine–SBA-15 for CO_2 capture from flue gas: characterization and sorption properties, Microporous Mesoporous Mater. 169 (2013) 103-111.

[8] K.O. Moura, H.O. Pastore, Comparative adsorption of CO_2 by mono-, di-, and triamino-organofunctionalized magnesium phyllosilicates, Environ. Sci. Technol. 47 (2013) 12201-12210.

[9] P. I. Ravikovitch, A. V. Neimark, Relations between structural parameters and adsorption characterization of templated nanoporous materials with cubic symmetry, Langmuir 16 (2000) 2419-2423.

[10] K. Schumacher, P. I. Ravikovitch, A. D. Chesne, A. V. Neimark, K. K. Unger, Characterization of MCM-48 materials, Langmuir 16 (2000) 4648-4654.

CHAPTER 4

HYDROTHERMAL, THERMAL, MECHANICAL AND HYDROLYTIC STABILITY OF MESOPOROUS KIT-6

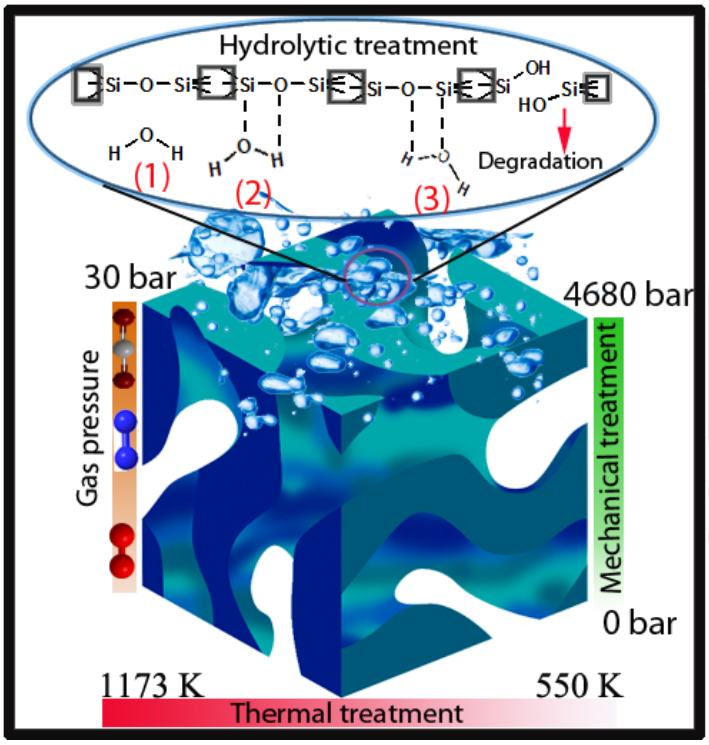

CHAPTER 4

This chapter contains the comprehensive study of hydrothermal, mechanical, thermal and hydrolytic stability of KIT-6 in wide range of temperature and pressure. In hydrothermal study samples are aged at four different temperatures viz. 60, 80, 100 and 120 °C. Thermal stability of KIT-6 is performed between 400 to 900 °C. Mechanical stability is investigated between 0 to 4680 bar. Hydrolytic stability of KIT-6 is investigated in atmospheric condition, water and boiling water. Stability of internal porous structure of the KIT-6 is analysed by high pressure gas adsorption. This part of work has been published inMicroporous and Mesoporous Materials242 (2017)127-135.

4.1 Introduction

In early 1990, the discovery of mesoporous molecular sieves (M41S) with uniform structure by researchers of the Mobil oil corporation using quaternary ammonium ($C_nH_{2n+1}(CH_3)_3NX$, X = Cl or Br) ionic template was a great embodiment in material science [1]. It has attracted great attention in wide applications like host-guest chemistry, size-selective separation, nano-material synthesis and enzyme immobilization due to its aloof intrinsic properties such as high specific surface area (> 600 m^2/g), pore volume (> 0.5 cc/g) and narrow distribution of pore size (2–30 nm) [2−7]. Furthermore, covalently grafted organosilane with silanol groups present on the silica surface shows improved performance during catalysis and gas separation applications [4,6,7].

The physiochemical properties of mesoporous materials strongly affect the performance of process used for industrial applications. However, the pore characteristics (pore diameter, specific surface area, pore volume, etc.) of the materials are strongly dependent on the synthesis procedures as well as post-synthesis treatments (calcination, pelletization, etc.). O'Brien et al. [8]

and Hartmann et al. [9] focused on the mechanical stabilities of both MCM-41 and MCM-48, whereas the thermal stabilities of MCM-41 and FSM were tested by Inagaki et al.[8−10]. Traditional MCM-41(hexagonal), MCM-48 (cubical) and FSM got their architecture collapsed and physicochemical properties destroyed in high pelletization pressure and moist conditions due to thinner pore wall.

A major breakthrough in the synthesis of mesoporous silica with large pores namely SBA-15 was achieved using low cost, nontoxic and biodegradable, non-ionic triblock copolymer (Pluronic, PEO_x–PPO_y–PEO_x) as a structure directing agent [11]. The synthesized silica with pluronic remarkably improved the pore size (4 – 30 nm), wall thickness (up to 6 nm), thermal and hydrothermal stability. Subsequently, Ryoo et al. [12] modified the 2-D hexagonal structure (SBA-15) to 3D cubical (KIT-6) by incorporation of additional co-structure directing agent (n-butanol) in the synthesis solution. The 3D structure with large inter-connected pores shows better performance during application in catalysis and gas adsorption/purification compared to 1D and 2D mesoporous silica. Application of the mesoporous silica in areas such as industrial catalysis, nano material synthesis and commercial adsorption has been carried out by surface modification as well as specific structure formation through post synthesis treatment in extreme external conditions such as high temperature, high pressure and moist condition. Therefore, it is essential to understand the behaviour of mesoporous KIT-6 in extreme external conditions like high pressure, high temperature and high moisture content.

In this chapter, we have synthesized the highly ordered 3D KIT-6 in mild acidic condition and thereafter comprehensively studied the hydrothermal, thermal, mechanical and hydrolytic stability in extreme external conditions by N_2 adsorption/desorption, small angle X-ray scattering and electron micrograph. Further, highly stable KIT-6 has been exposed to high gas pressure and

the obtained results have been analysed to explore the use in CO_2/N_2, CO_2/H_2 selective separation and H_2 storage without any structural destruction.

4.2 Materialsand Methods

4.2.1 Synthesis of KIT-6

Highly ordered mesoporous KIT-6 was synthesized as earlier reported procedure [12]. The detailed synthesis procedure of KIT-6/D (without water wash) and KIT-6 (with water wash) was discussed in Chapter 3.

In hydrothermal study, after transferring the solution into Teflon autoclave, it was aged at four different temperatures viz. 60, 80, 100 and 120 ºC and corresponding samples are denoted as K-60, K-80, K-100 and K-120, respectively. Further, three different KIT-6 namely K-80, K-100 and K-120 were thermally treated (calcined) at five different temperatures viz. 400, 550, 700, 800 and 900 ºC for 5 h with 1.5 ºC/min heating rate. Mechanical stability was investigated as follows: calcined KIT-6 powder was compressed in a stainless steel die of 13 mm diameter for 10 min by hydraulic press. External pressure was calculated from the applied load and the die diameter. Hydrolytic stability at room temperature was investigated by the following procedure: KIT-6 (0.5 g) was dispersed in 25 mL Millipore purified water in four different flasks and kept static for 5, 10, 15 and 30 days. Resulting material was filtered, dried at 100 ºC for 24 h in hot air oven and stored for further analysis. Moreover, hydrolytic stability of KIT-6 was also studied after boiling in water. Stability of internal porous structure of the KIT-6 was analysed by high pressure gas adsorption. Additionally, high gas adsorption/storage capacity makes it a promising candidate for CO_2 separation and H_2 storage.

4.2.2 Characterization of materials

All the synthesized KIT-6 was characterized by various analytical techniques as discussed in chapter 3. X-ray diffraction (XRD) spectra was used to identify the phase present in the KIT-6 and also to calculate the unit cell dimensions (a_0). The specific surface area (S_{BET}), pore volume (V_t) and pore diameter (W) were determined from the N_2 adsorption/desorption analyser. Surface composition of KIT-6 was analysed from diffusive reflectance infrared Fourier transform (DRIFT) spectra. DRIFT spectra were collected using vibrational spectroscopy between wavenumber 600 – 1500 cm^{-1}.Surface morphology was collected from field emission scanning electron microscope (FESEM) and transmission electron microscopy (TEM). Adsorption/desorption isotherm of CO_2 (20 bar), N_2 (20 bar) and H_2 (30 bar) were measured using volumetric adsorption apparatus.

4.3 Results and Discussion

4.3.1 *Effect of water wash on porosity*

The N_2 adsorption/desorption isotherms (at −196 ºC) of KIT-6 are shown in Figure 4.1. Both the samples (KIT-6/D and KIT-6) exhibit type IV isotherm as per IUPAC classification with a sharp hysteresis loop [13]. The sharp increase in volume adsorbed is observed in the relative pressure interval from 0.66 to 0.8, indicating the presence of uniform mesopores. The N_2 uptake capacity at respective elative pressure is substantially higher for KIT-6 compared to KIT-6/D. It confirms that the textural properties of KIT-6 are significantly changed on microscopic level after washing with water and the values are summarized in Table 4.1. Afterwashing, the S_{BET} of KIT-6/D is increased from 720 to 857 m^2/g. However, V_t is increased from 1.10 to 1.25 cc/g. The W_{BJH} pore size distribution is centered at 6.6 nm for KIT-6/D and it remains unchanged even after washing

with water. The S_{micro} is increased from 203 m^2/g (KIT-6/D) to 259 m^2/g (KIT-6) after washing and correspondingly V_{micro} is also increased from 0.09 to 0.13 cc/g. The water washing appears to suppress the shrinkage accompanying the calcination, and this is likely to contribute to the increased S_{BET} and V_t of KIT-6. However, just after washing with water similar cubical mesoporous structure SBA-1 collapses [9].

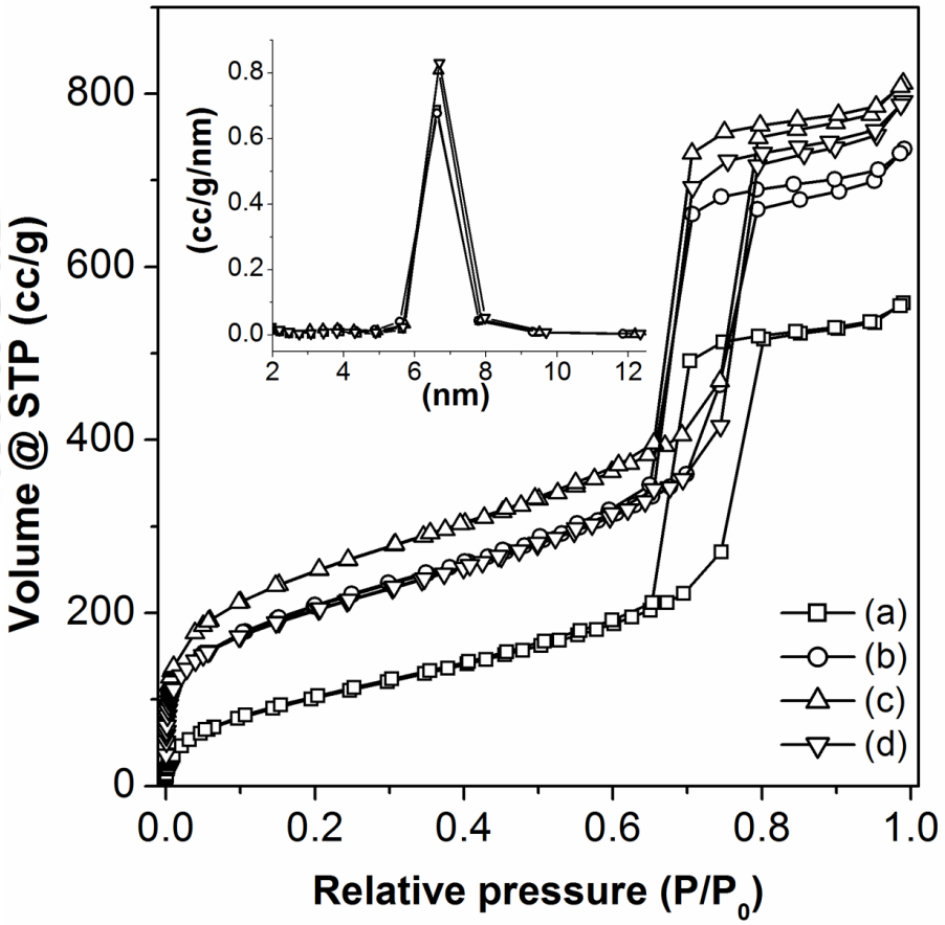

Figure 4.1 N_2 adsorption/desorption isotherm (−196 ºC) of (a) as-synthesized KIT-6(□) (b) KIT-6/D (Δ), (c) KIT-6 (○) and (d) KIT-6/6M (■)

Table 4.1 Structural parameters of mesoporous KIT-6

Sample	d_{211} (nm)	a_0 (nm)	S_{BET} (m^2/g)	V_t (cc/g)	W_{BJH} (nm)	W_{DFT} (nm)	S_{micro} (m^2/g)	V_{micro} (cc/g)
ASK	10.14	24.83	394	0.86	6.6	8.1	0	0
KIT-6/D	9.2	22.53	720	1.10	6.6	8.1	203	0.09
KIT-6	9.59	23.49	857	1.25	6.6	8.1	259	0.13
KIT-6/6M	ND	ND	710	1.22	6.6	8.1	145	0.06

$d_{211:}$ Interplanar space; a_0: unit cell parameter; S_{BET}: specific surface area; V_t: pore volume; W_{BJH}: pore size by BJH method; W_{DFT}: pore size by NLDFT method; ASK: as synthesized KIT-6; KIT-6/6M: KIT-6 after ageing for 6 months at normal temperature and pressure; ND: not determined,

XRD spectra of KIT-6 and KIT-6/D are shown in Figure 4.2. The three major peaks correspond to d_{211}, d_{220} and d_{420} reflections in the range $2\theta = 0.5 – 5.0°$ in both the spectra. However, the peak position does not shift considerably even after washing. It indicates that the synthesized material is 3D cubical structure with Ia3d space group [12,14] and it preserves the original cubical structure even after washing with water. The XRD peak intensity of KIT-6 is comparable in both the cases. The width of the d_{211} peak is similar for both the samples, suggesting a comparable degree of structural ordering. The unit-cell parameter (a_0) changes significantly from 22.53 to 23.49 nm after washing (Table 4.1), which is similar to the value reported by Wilson et al. (a_0 = 23.2 nm) [4].

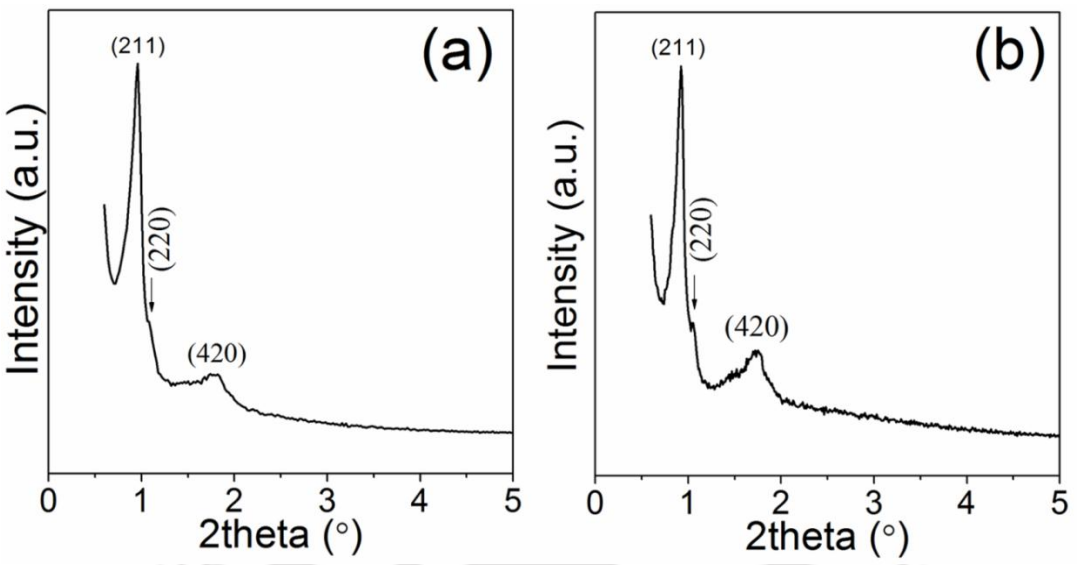

Figure 4.2 X-ray diffraction spectra of (a) KIT-6/D and (b) KIT-6

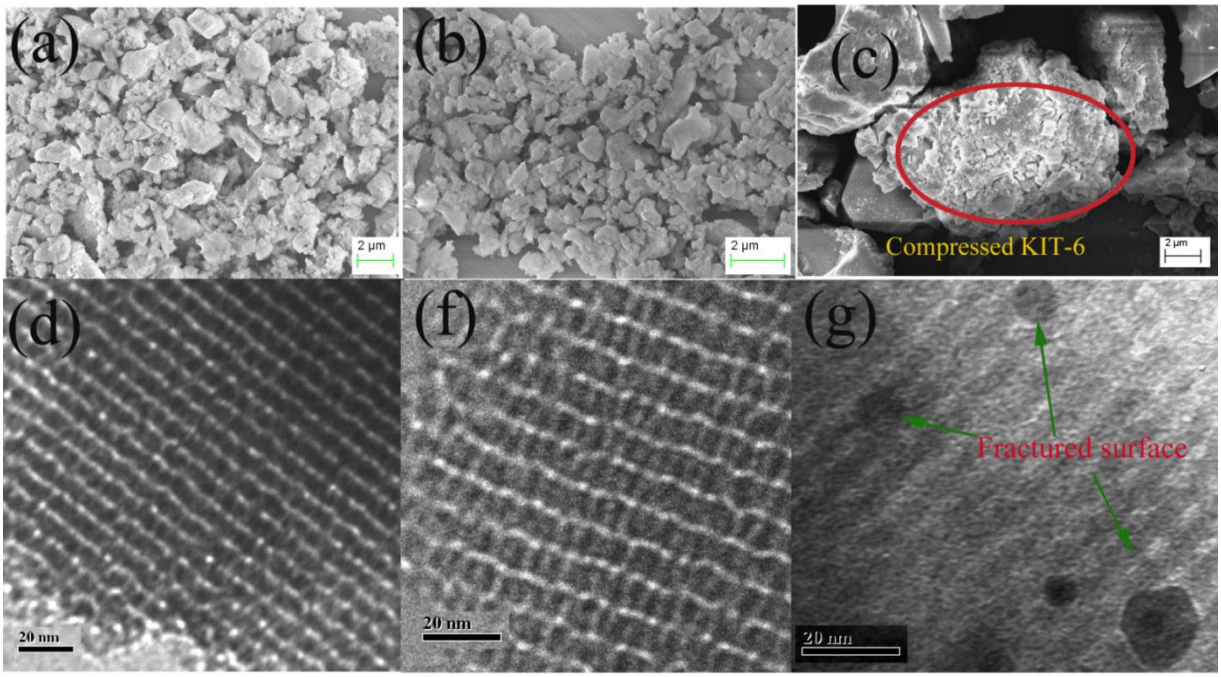

Figure 4.3 FESEM micrograph (a) without washing (KIT-6/D) (b) with washing (KIT-6), (c) mechanically compressed to 4680 bar KIT-6 and TEM micrograph of (d) KIT-6/D (e) KIT-6 and (f) mechanically compressed to 4680 bar KIT-6

The surface morphology of KIT-6 and KIT-6/D is shown in Figure 4.3. The FESEM micrographs of KIT-6/D and KIT-6 are alike 3D particle with ~1 to 2 µm size [15]. TEM micrographs of KIT-6/D and KIT-6 show highly ordered cubical mesoporous channels (Figure 4.3d, e) present in the material and the results are consistent with well-defined XRD data [14]. The above results confirm that KIT-6 has preserved its structure even after washing. The average pore size of both KIT-6/D and KIT-6 is ~ 6.6 nm, which is in well agreement with N_2 adsorption/desorption.

4.3.2 *Hydrothermal ageing*

The XRD patterns and structural properties of the hydrothermally aged KIT-6 at different temperatures are shown in Figure 4.4 and Table 4.2, respectively. All the samples exhibit a sharp resolved peak corresponding to d_{211} plane, confirming that no structure distortion occurs during synthesis. The reflection peak position is shifted towards lower angle with increase in hydrothermal temperature. However, widths of the d_{211} peak are similar for all the synthesized samples. The reflection peak intensity of KIT-6 increases with increasing the hydrothermal temperature during synthesis [16−19]. It is interesting to note that, a_0 increases with increase in temperature [4,16]. It is possibly due to higher degree of TEOS silanization with increase in hydrothermal temperature [20].

Table 4.2 Textural properties of hydrothermally treated KIT-6 at different temperatures

Sample	d_{211} (nm)	a_0 (nm)	S_{BET} (m^2/g)	V_t (cc/g)	W_{BJH} (nm)	W_{DFT} (nm)	<h> (nm)	S_{micro} (m^2/g)	V_{micro} (cc/g)	Yield* (gm)
K-60	8.4	20.57	733	0.77	4.9	6.2	3.55	274	0.13	2.44
K-80	9	22.04	871	1.13	5.7	7.0	3.62	302	0.14	2.36
K-100	9.59	23.49	857	1.25	6.6	8.1	3.54	260	0.13	2.27
K-120	9.8	24	822	1.51	8	9.4	3.06	170	0.07	2.14

<h>: pore wall thickness; *: Yield of product analyzed after calcination at 550 °C

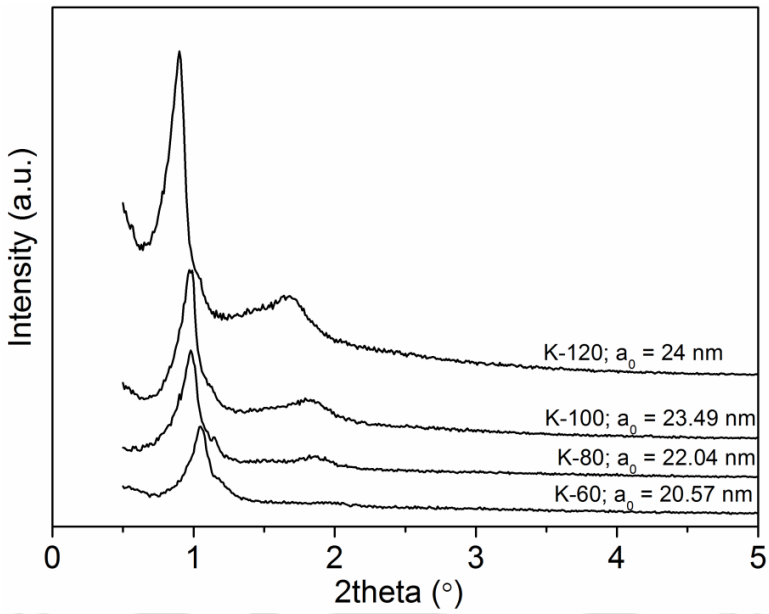

Figure 4.4 X-ray diffraction pattern of KIT-6 after ageing at different temperatures

The N_2 adsorption/desorption isotherms of all the hydrothermally treated samples at different temperatures show typical type IVwith H1 hysteresis (Figure 4.5). The N_2 volume adsorbed is increased significantly with increase in hydrothermal temperature. The appearance of the H1 hysteresis loop indicates that the synthesized porous materials have high pore uniformity with facile pore connectivity [13]. As can be seen, with increasing hydrothermal temperature, the hysteresis loop shifts towards higher relative pressure. Thus, it can be concluded that the mesopores size of material substantially increases with temperature (Table 4.2). However, Kruk et al. improved the pore size of SBA-15 by addition of organic solvent (hexane, 1,3,5-triisopropylbenzene) in the synthesis solution [19,21]. It is interesting to observe that wall thickness of mesopores is decreased remarkably with increase in hydrothermal temperature (Table 4.2). The increment in pore volume and reduction in wall thickness are interrelated. Higher hydrothermal temperature leads to some structural degradation of porous material and it is conclusive based on the yield obtained after synthesis (Table 4.2). Additionally, structural degradation can lead to interconnectivity between the porous channels and

improves the V_t and W_{BJH} of KIT-6. However, more traditional MCM-41completely loses its ordered structure after increase of pore size up to 6.6 nm by hydrothermal treatment [16].

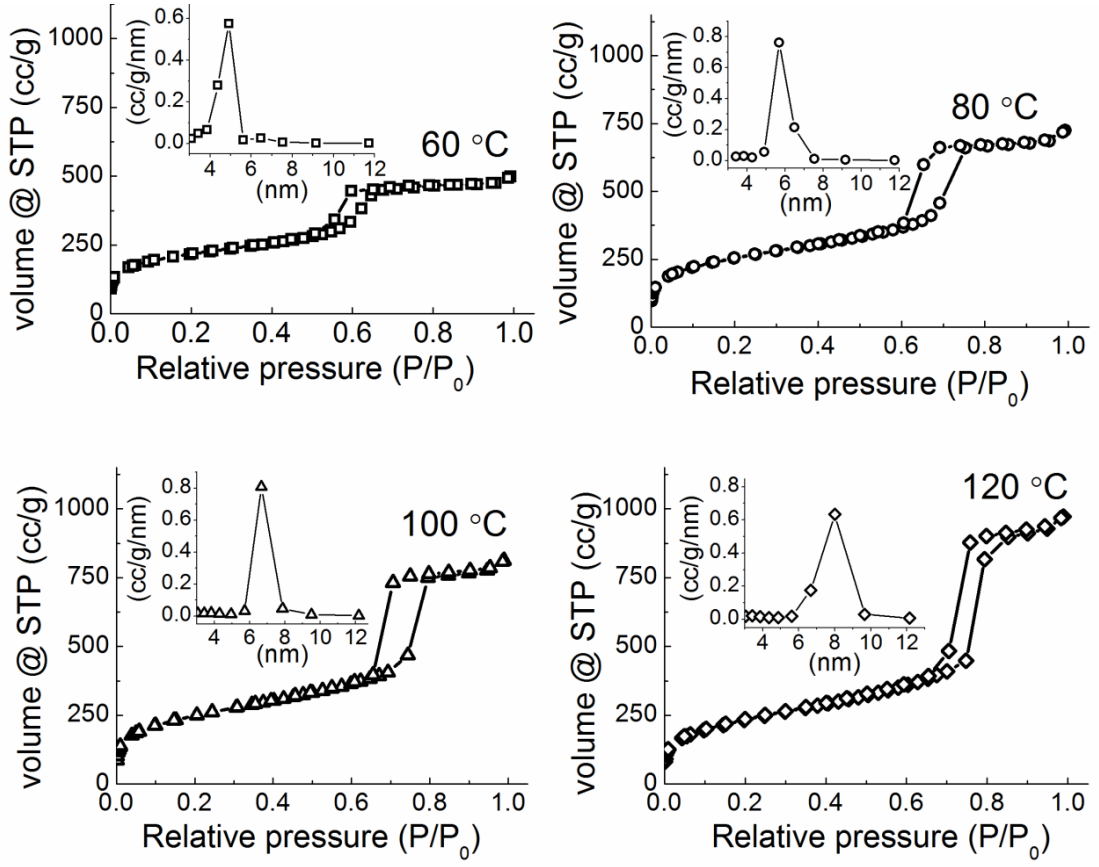

Figure 4.5 N_2 adsorption/desorption isotherm (−196 °C) with BJH pore size distribution of KIT-6 silica synthesized at different hydrothermal temperature

4.3.3 *Mechanical performance*

The powder XRD spectra of original and compressed KIT-6 (under 780, 1560, 2340 and 4680 bar) are shown in Figure 4.6. The prominent peak d_{211} intensity decreases gradually, whereas the a_0 is not changed significantlywith increase in pressure intensity (Table 4.3). The similar diffraction effect is observed with the other mesoporous silica such as MCM-41,

MCM-48, SBA-1 and SBA-15 reported in the literature [8−10,22]. Higher pressure may reduce the SAXS intensity towards silica pore wall due to agglomeration of KIT-6. The above statement is confirmed from the FESEM micrograph of mechanically compressed KIT-6 under 4680 bar (Figure 4.3c). Additionally, the crystallinity of the material is also reduced by surface fracture of ordered mesoporous silica [10,22,23]. TEM micrograph of mechanically pressed KIT-6 (under 4680 bar) is shown in Figure 4.3f. Under high pressure, some defects are created on the surface and the order of structure as well as crystallinity of KIT-6 is reduced. However, the KIT-6 patterns are still detectable even if the material is exposed for ultra-high pressure, confirming that mesoporous structure is partially preserved.

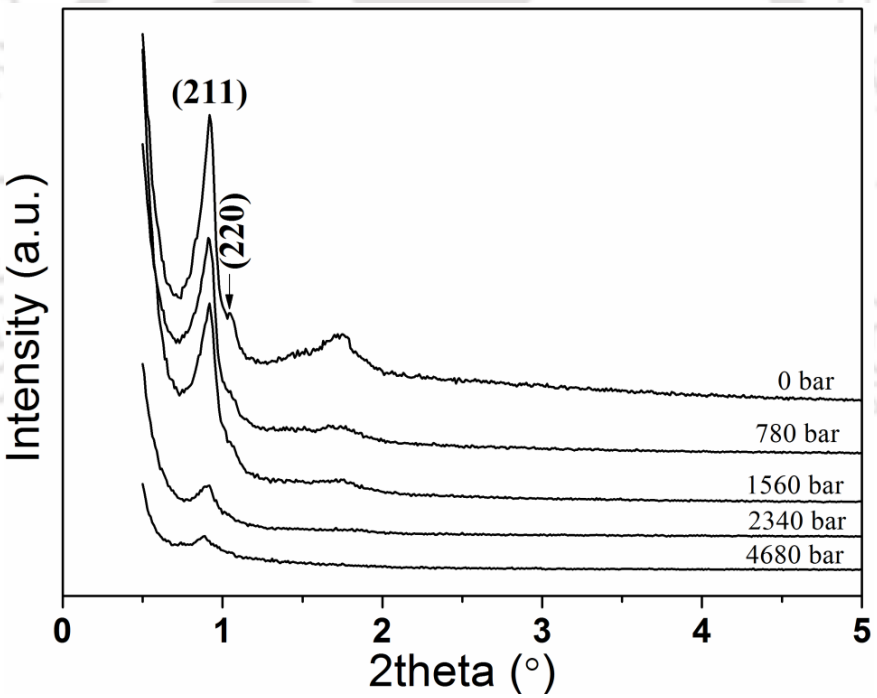

Figure 4.6 X-ray scattering of mechanically compressed KIT-6 silica at different pressure

Table 4.3 Textural properties of mechanically pressed KIT-6

Load (bar)	d_{211} (nm)	a_0 (nm)	S_{BET} (m^2/g)	V_t (cc/g)	W_{BJH} (nm)	W_{DFT} (nm)	S_{micro} (m^2/g)	V_{micro} (cc/g)
0	9.59	23.49	857	1.25	6.6	8.14	259	0.13
780	9.59	23.49	827	1.2	6.6	8.14	235	0.11
1560	9.59	23.49	806	1.14	6.6	8.14	223	0.1
2340	9.38	22.97	756	0.98	6.6	8.14	197	0.09
4680	9.38	22.97	651	0.77	3.86	5.08	7	0.03

The N_2 adsorption/desorption isotherm of mechanically pressed KIT-6 is shown in Figure 4.7 and its textural properties are summarized in Table 4.3. The N_2 adsorption isotherm indicates that the textural property of KIT-6 does not change significantly till 1560 bar compression pressure. The reduction in S_{BET} (~ 5.8 %) and V_t (~ 8%) of the KIT-6 is less compared to other mesoporous silica MCM-41, MCM-48, SBA-15, FSM-16 and KCC-1 for similar pressure [8−10,20,22,23]. With further increase in pressure (up to 4680 bar), N_2 adsorption capacity is decreased and correspondingly S_{BET} (~24%) and V_t (~38%) are also decreased. The micropore area (S_{micro}) gradually decreases with increasing pressure and becomes negligible at 4680 bar but it preserves the mesoporous area. It is due to collapse of thinner pore wall (Si–O–Si) structure present in the material. Tatsumi et al.[22] showed that the $S_{BET}$and V_t of MCM-41 and MCM-48 completely vanish due to destruction of its structure under 1730 bar. However, SBA-15 lost its S_{BET} (25% of initial) and V_t (40% of initial) under 1910 bar [24]. The pore size distribution does not change significantly with pressure up to 2340 bar. However, further increase in pressure (4680 bar) broadens the pore and shifts the bi-nodal pore size distribution of KIT-6 (Figure 6b). It may be due to additional pore formation in the material. Under ultra-high pressure (4680 bar), some new pores are formed within the particles by wall collapse as well as due to agglomeration of KIT-6 particles as shown in Figure 4.3c. However, some pores are blocked by fracture of Si–O–Si bridge.

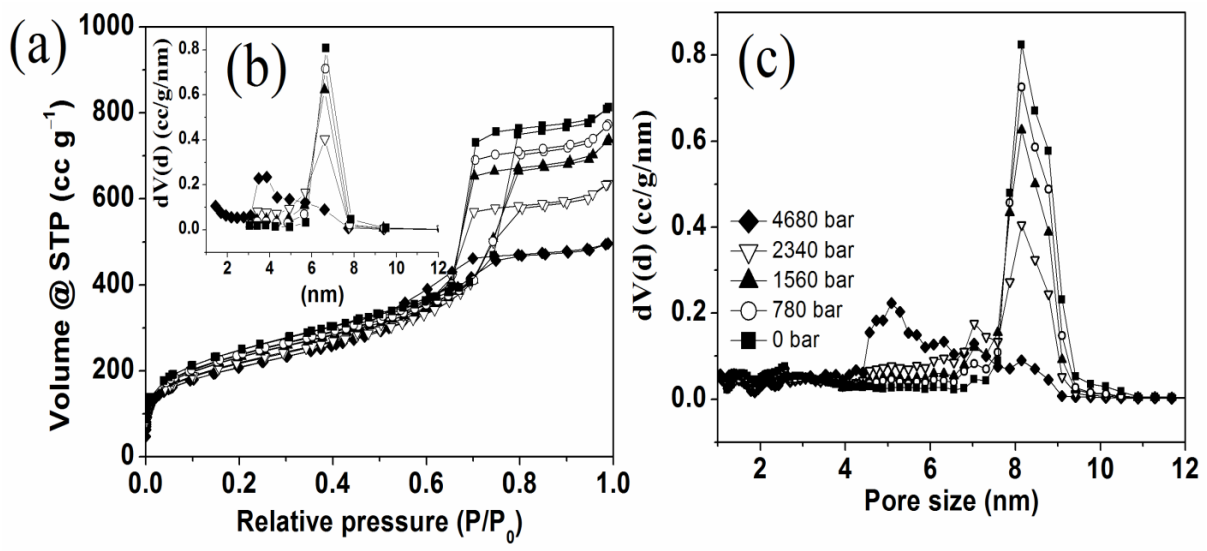

Figure 4.7 Effect of the load on (a) N_2 adsorption/desorption at −196 ºC (b) BJH pore size distribution and (c) NLDFT pore size distribution of KIT-6

The overall hydrolysis of TEOS and subsequent dehydration reaction forms siloxane (Si−O−Si) network during mesoporous silica formation. Its destruction with applied pressure is analyzed by DRIFT spectra of samples (Figure 4.8). The peak corresponding to 960 cm^{-1} represents the Si−OH stretching vibration of free surface silanols present in mesoporous silica [25]. The broad peaks corresponding to 1250 – 1040 cm^{-1} and ~799 cm^{-1} assign the asymmetric and symmetric stretching vibrations of siloxan bridge (Si–O–Si) present in the material [25,26]. The peak intensity corresponding to 1250 – 1040 cm^{-1} and ~799 cm^{-1} gradually decreases with increase in pressure due to collapsing of Si–O–Si bridge present in KIT-6 mesoporous silica.

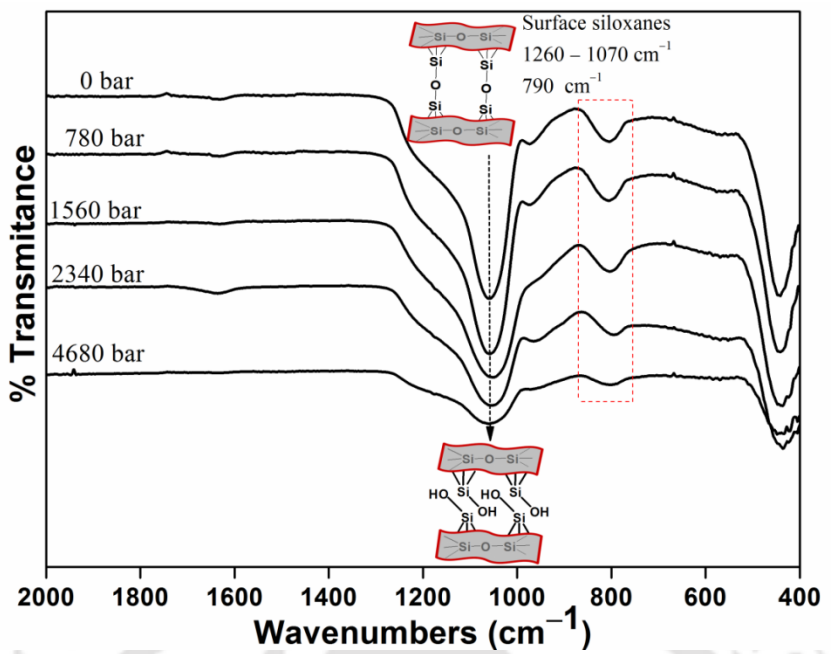

Figure 4.8 DRIFT spectra of mechanically compressed KIT-6 at different pressure

4.3.4 *Thermal performance*

The as-synthesized K-80, K-100 and K-120 mesoporous samples with different textural properties were calcined at 400 ºC, 550 ºC, 700 ºC, 800 ºC and 900 ºC for 5 h with 1.5 ºC/min heating rate. The N_2 adsorption/desorption isotherm (at −196 °C) of all the calcined samples are shown in Figure 4.9 and their textural properties are summarized in Figure 4.10. Before calcination, the S_{BET} of K-100 is 394 m^2/g. However, S_{BET} is improved to 977 m^2/g after calcination at 400 °C. The enhancement in S_{BET} after calcination is mainly due to template removal from the porous channels [7]. After calcination at 400 °C, the S_{BET} of K-80 and K-120 is 1088 m^2/g and 803 m^2/g, respectively.

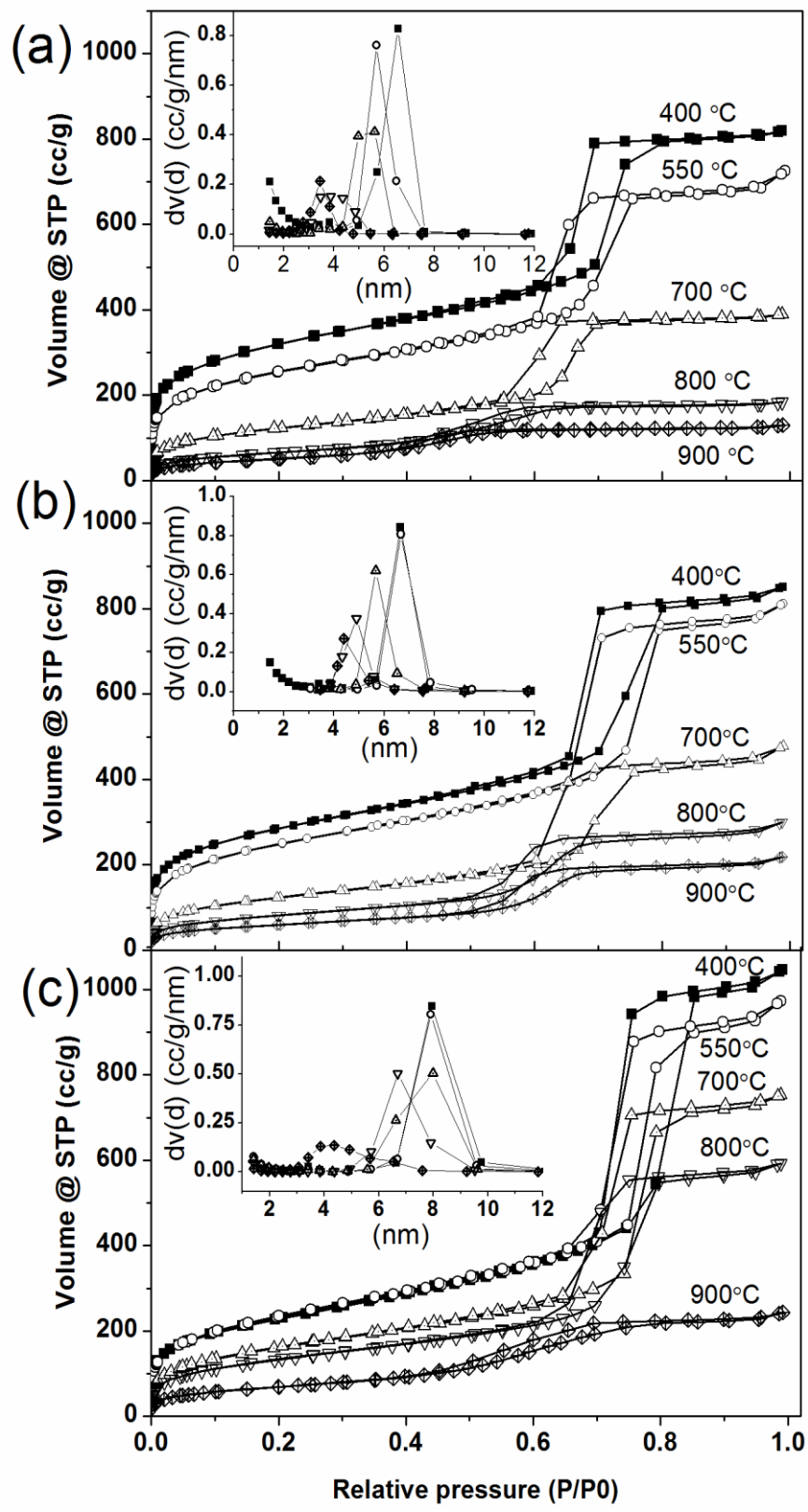

Figure 4.9 N_2 adsorption/desorption isotherm (at −196 ºC) of calcined KIT-6 at different temperatures (a) K-80 (b) K-100 and (c) K-120

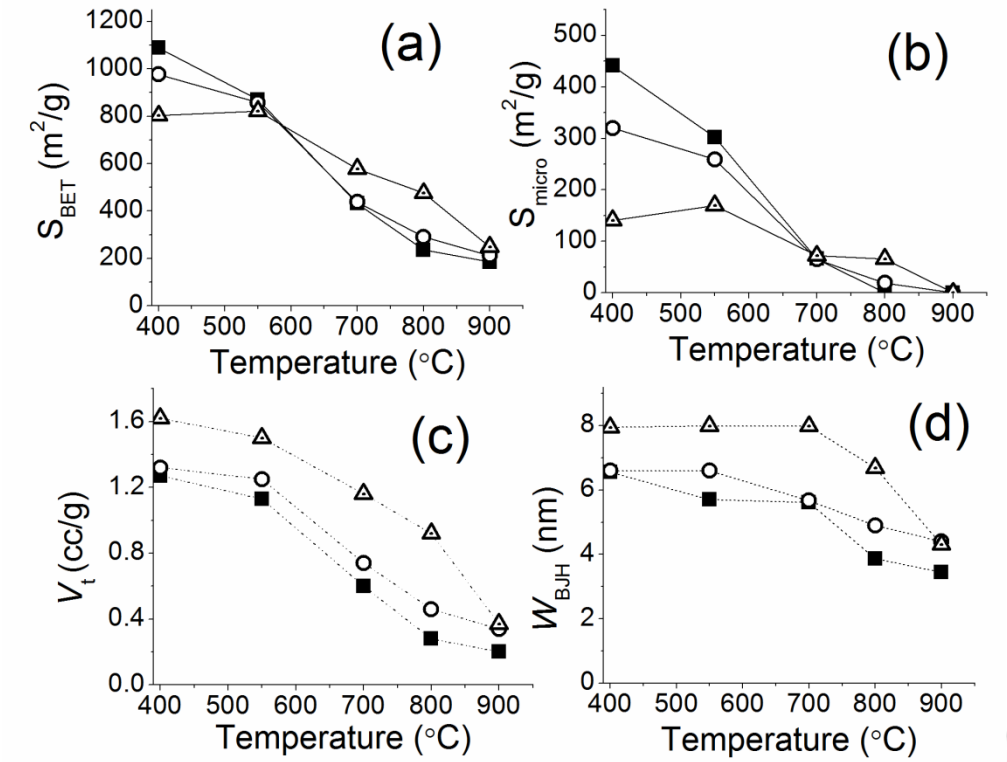

Figure 4.10 (a) specific surface area (b) micropore surface area from t-plot method (c) specific pore volume (V_t) (d) BJH pore size of calcined sample at different temperatures (■: K-80, ○: K-100 and Δ: K-120)

It is observed that N_2 adsorption capacity gradually decreases with increase in calcination temperature from 400 °C to 900 °C in all the three samples as shown in Figure 4.9. The size of the hysteresis loop also reduces with increases in temperature and is gradually shifted towards lower relative pressure. It indicates that the S_{BET}, S_{micro}, W_{BJH} and $V_t$decrease with increase in calcination temperature as shown in Figure 4.10a – d. Moreover, XRD intensity of KIT-6 (K-80) decreases with increase in temperature from 400 °C to 900 °C ($2\theta = 0.5 - 5^{o}$; Figure 4.11). It indicates that the a_0 value also decreases with increase in hydrothermal temperature (Figure 4.11). The above results suggest that the pore present in KIT-6 gradually shrinkes with increase in calcination temperature up to 900 °C [20,27,28]. However, MCM-41 completely loses its hexagonal structure at 800 °C as reported earlier by Broyer et al. [29].

After calcination at 900 °C, the S_{BET} of K-80, K-100 and K-120 are reduced by 83%, 78.3% and 69% of their initial surface area. The major loss in S_{BET}, W_{BJH}, V_t and S_{micro} is for the sintering of pore wall of KIT-6 with temperature. Cassiers et al. studied the thermal behaviour of wide varieties of mesoporous silica; in particular, MCM-41, MCM-48, HMS, FSM- 16, KIT-1, PCH, and SBA-15 [20]. They revealed that MCM-41, MCM-48, KIT-1, HMS and SBA-15 completely lost their textural properties at 850 °C. The higher thermal stability of KIT-6 is possibly due to thicker pore wall compared to MCM-41, MCM-48, SBA-15 and SBA-16 [20,28-30].

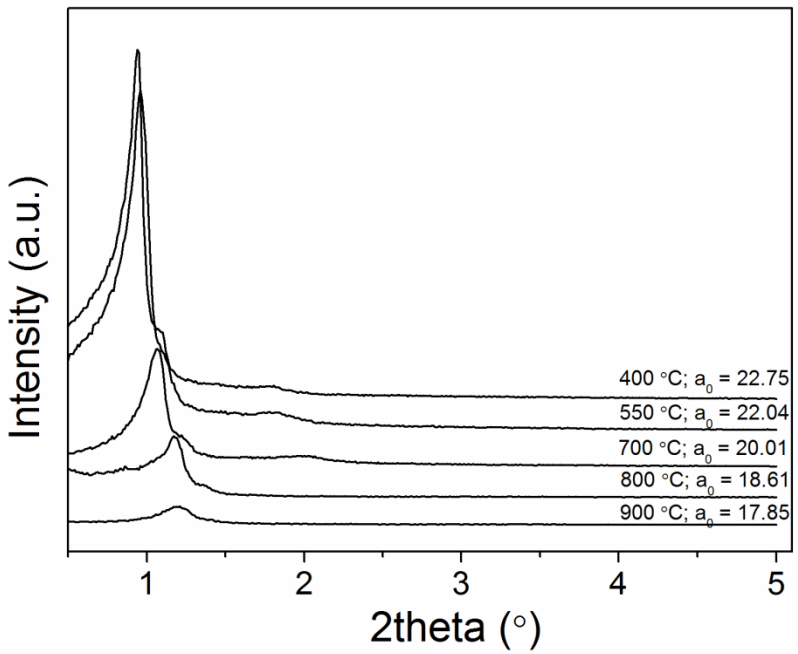

Figure 4.11 X-ray diffraction spectra of calined KIT-6 (K-80) at different temperatures

4.3.5 *Hydrolytic performance*

Stability of the mesoporous silica under atmospheric and extreme moist conditions decides the working limitation and life span of the material. In most of the catalytic reactions water is used as a primary solvent. Hence, it is essential to understand the different ageing conditions (such as ambient conditions, water at room temperature and boiling temperature) on the

physical properties of KIT-6. The physical properties of hydrolytically treated KIT-6 are analyzed by N_2 adsorption/ desorption isotherm. The N_2 adsorption isotherm of KIT-6/6M (aged for 6 months in ambient condition) is shown in Figure 4.1d and is compared with KIT-6. The N_2 uptake capacity of KIT-6/6M is drastically decreased in lower relative pressure (P/P_0 below 0.6). However, the maximum uptake capacity at relative pressure ~ 0.99 is nearly constant. It indicates that V_t and W_{BJH} is nearly constant in mesoporous KIT-6/6M. The reduction in S_{BET} from 857 to 710 m^2/g is mainly due to slow hydrolysis of exposed silica skeleton (Si–O–Si) in presence of atmospheric moisture [31]. However, most promising mesoporous MCM-41 lost its half of structural properties within 3 months [29].

In further study, KIT-6 (30D CW) was gradually aged for 30 days in cold water. It is observed that N_2 adsorption capacity slowly decreases with time (Figure 4.12) and even after 30 days, 30 D CW preserved the S_{BET} (614 m^2/g) and V_t (1.03 cc/g) (Table 4.4). Under further extreme condition, KIT-6 is boiled in Millipore purified water for 72 h. The X-ray peak intensity does not change significantly with time as shown in Figure 4.13. It confirms that the parent material preserves its original structure even after boiling for 72 h. It is interesting to observe that the capillary condensation in porous channel during N_2 adsorption is shifted towards the higher relative pressure (Figure 4.14). It indicates that pore size of KIT-6 becomes wider with increased ageing in boiling water (BW). The W_{BJH} increases from 6.6 to 7.95 nm. However, S_{BET} is decreased from 857 m^2/g to 492 m^2/g after 72 h ageing in boiling water (Table 4.4). The pore wall thickness is reduced from ~ 3.54 nm (fresh KIT-6) to 3.14 nm (72h BW). The above results suggest that KIT-6 surface is gradually degraded in layer form with water as reported in Figure 4.15. During hydrolytic treatment, water is adsorbed on the incipient silaxone tip (Si–O–Si) present on the silica surface by formation of pentacoordinated silicon intermediate. It produces strain by the reaction mechanism presented in Figure 4.15 and raptures the pore wall of mesoporous silica [31,32]. Resulting phenomena

reduce the S_{BET} and V_t of KIT-6. In boiling conditions, rate of hydrolysis of Si–O–Si is significantly increased compared to atmospheric temperature. The same can be understood from S_{BET} of 30D CW and 72h BW sample (Table 4.4). Further, after boiling for 13 days, KIT-6 completely losses its morphology as confirmed by N_2 adsorption/desorption and X-ray spectra. The stable structural performance of 3D KIT-6 in extreme moist condition is possibly due to thicker pore wall compared to MCM-41, MCM-48, SBA-15 and SBA-1 [9,20,23,33].

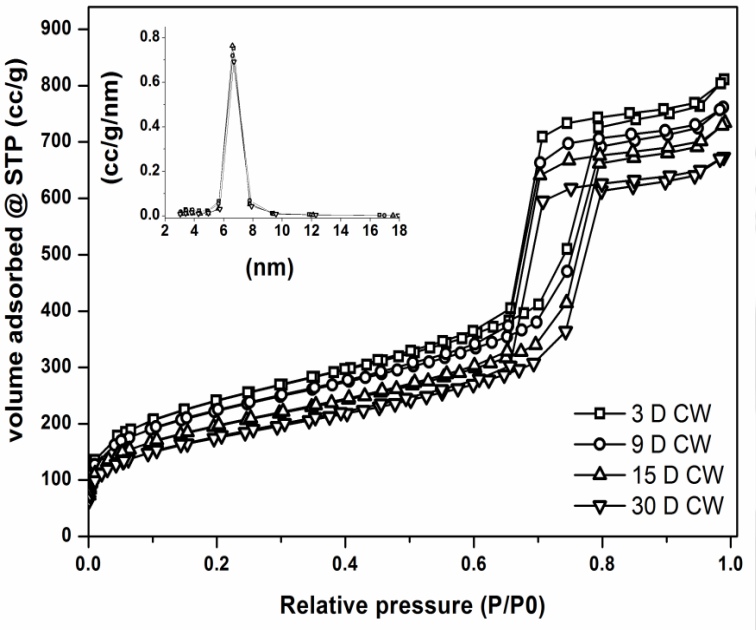

Figure 4.12 N_2 adsorption/desorption (−196 ºC) of KIT-6 after aging for 30 days in cold water

Table 4.4 Effect of ageing on textural properties of KIT-6

Time	S_{BET} m^2/g	V_t (cc/g)	W_{BJH} (nm)	S_{micro} (m^2/g)
0	857	1.25	6.6	259
3 D CW	838	1.25	6.6	231
9 D CW	776	1.17	6.6	208
15 D CW	683	1.13	6.6	159
30 D CW	614	1.04	6.7	128
24 h BW	613	1.23	6.7	104
48 h BW	513	1.23	7.9	79
72 h BW	492	1.37	7.95	75

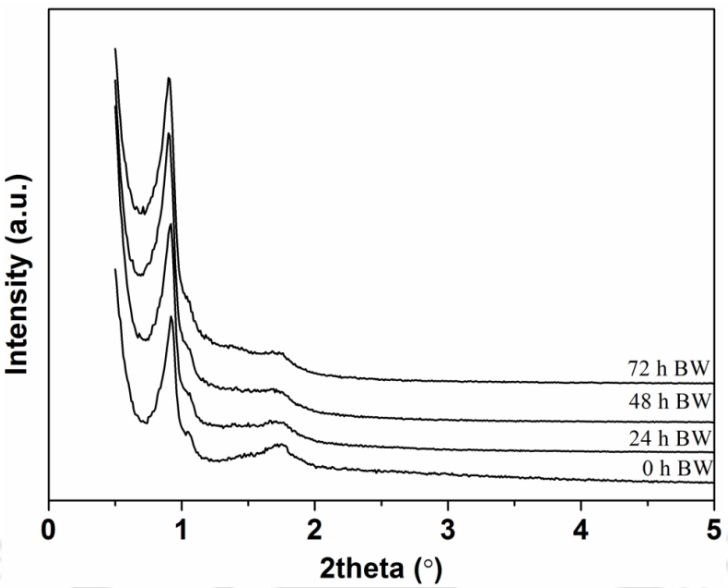

Figure 4.13 X-ray spectra of KIT-6 after aging in boiling water (100 ºC) for 3 days

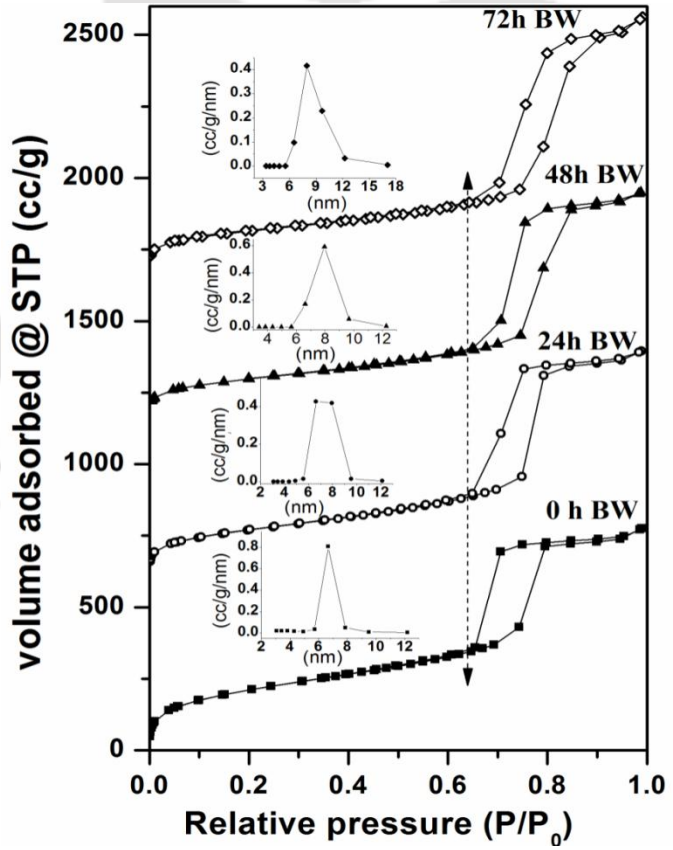

Figure 4.14 N_2 adsorption/desorption (−196 ºC) and corresponding BJH pore size distribution of hydrolytically treated KIT-6 in boiling water (100 ºC)

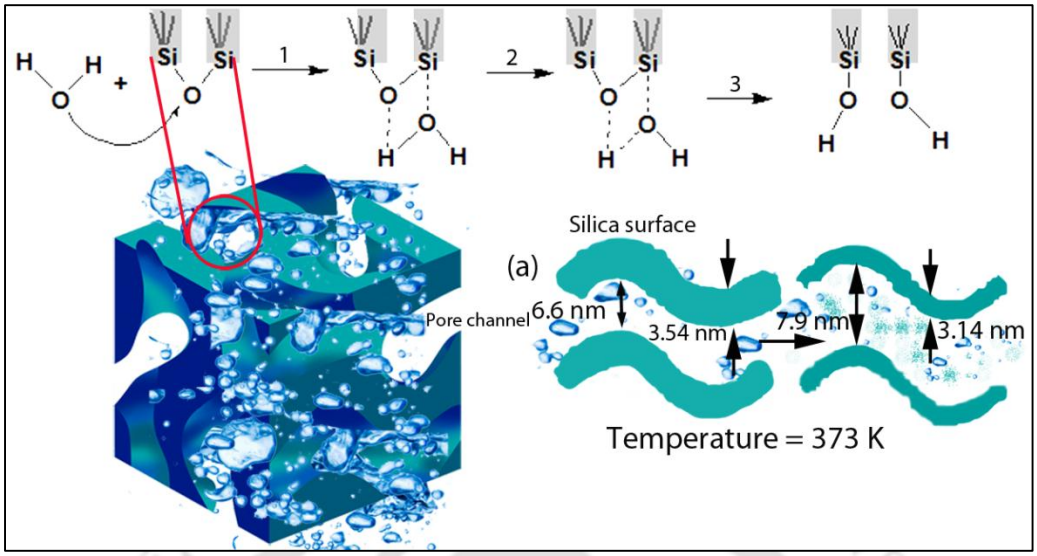

Figure 4.15 Dissociation of KIT-6 surface with water

4.3.6 *CO_2/N_2/H_2adsorption isotherm for* KIT-*6*

Gas separation and storage is a major unit operation in chemical industries. Structural stability and its performance during practical application is an essential parameter of any material. Performance of the porous material during practical application is proportional to the textural properties such as surface area, pore diameter and pore volume. The CO_2, N_2 and H_2 adsorption performance of KIT-6 (washed with water) up to 30 bar are shown in Figure 4.16. The $CO_2/N_2/H_2$ adsorption isotherm over KIT-6 is highly reversible with pressure. As expected, adsorption capacity of all the gases increases with pressure and shows the maximum adsorption capacity of 10.1 mmol CO_2/g, 1.24 mmol N_2/g , and 0.33 mmol H_2/g of KIT-6 at 0 ºC and 20 bar (Figure 4.16). The adsorption capacity of all the gases decreases with increasing temperature like other physisorbents [34−38]. It is mainly due to increase in kinetic energy of sorbent molecule with increase in temperature [36]. The CO_2 adsorption capacity is much higher than N_2 and H_2 for any pressure and temperature. The difference in adsorption capacity can be understood on the

basis of polarizability and quadrupole moment of the sorbent molecules. The higher polarizability (H_2, 8.04 × 10^{25} cm^{-3}< N_2, 17.4 × 10^{25} cm–3 < CO_2, 29.1× 10^{25} cm^{-3}) and quadrupole moment (H_2, 6.62 × 10^{27} esu^{-1} cm^{-1}< N_2, 15.2 × 10^{27} esu^{-1} cm^{-1}< CO_2, 43.0 × 10^{27} esu^{-1} cm^{-1}) of sorbent molecules show higher adsorption capacity [35]. The sorption capacity ratio at 0 ºC for CO_2/ N_2 and CO_2/$H_2$are 17.7 and 142, respectively at 1 bar. However the ratio becomes 8.2 and 31, respectively at 20 bar. Higher CO_2/N_2 and CO_2/H_2 adsorption ratio indicates that KIT-6 is a good adsorbent for CO_2 separation and H_2 purification [36−38].

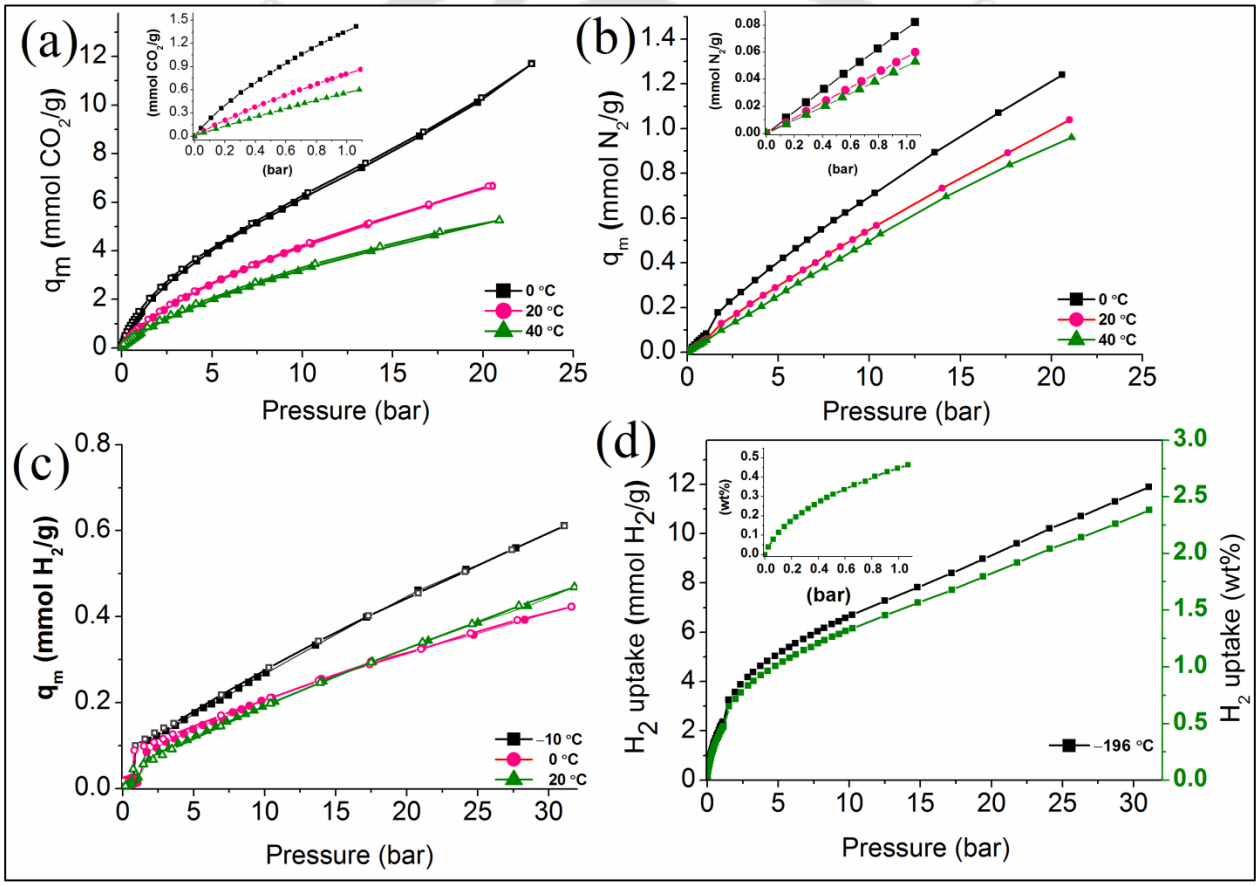

Figure 4.16 (a) CO_2 adsorption isotherm (■ – 0 ºC, ●– 20 ºC, ▲ – 40 ºC) (b) N_2 adsorption isotherm (■ – 0 ºC, ●– 20 ºC, ▲ – 40 ºC) (c) H_2 adsorption isotherm (■ – −10 ºC, ●– 0 ºC, ▲–20 ºC) and (d) H_2 adsorption isotherm at −196 ºC

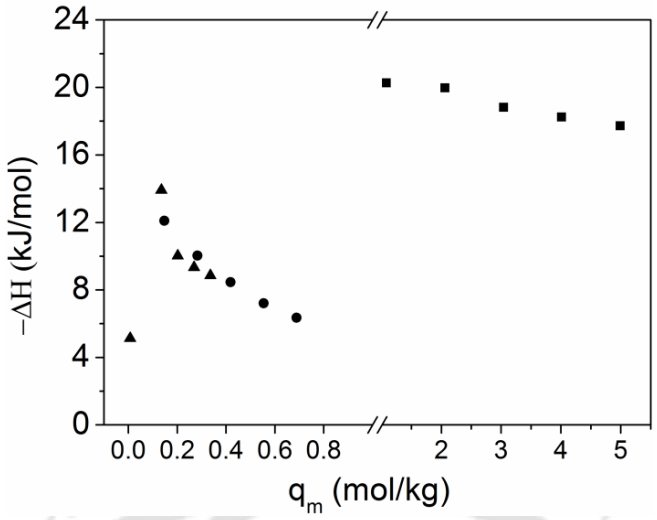

Figure 4.17 Isosteric heat of adsorption (■ – CO_2; ● – N_2; ▲– H_2)

Hydrogen storage in porous material is an emerging field and numerous efforts have been taken up in their development by a large community of researchers. However, high thermally and mechanically stable mesoporous silica did not receive much attention in hydrogen storage by researchers [35−38]. Figure 4.16d, shows the hydrogen storage performance in KIT-6 at −196 ºC and till 30 bars. The maximum H_2 uptake capacity is 2.3 mmol/g (0.46 wt%) and 11.9 mmol/g (2.38 wt%) at 1 and 30 bar (−196 °C), respectively. The H_2 storage capacity of KIT-6 is comparable with other available porous materials reported in literatures carbon (0.29 wt% at −100°C and 1 bar) and MIL-53 (3.1 wt% at 20 bar and -196 °C) [36−38].

The isosteric heats of adsorption ($-\Delta H_{ads}$) of CO_2, N_2 and H_2 were evaluated using the Clausius−Clapeyron equation ($-\Delta H = R[(\partial \ln(P)/\partial(1/T)]$ and compared in Figure 4.17 [55]. It was evaluated from the slope of the plot of ln(P) vs 1/T at the same adsorption capacity. The $-\Delta H_{ads}$ on KIT-6 at zero coverage is as follows: CO_2 (21 kJ/mol) > N_2 (12 kJ/mol) > H_2 (8.6 kJ/mol); which is similar to other reported adsorbents [7,36−38]. The lower value of $-\Delta H_{ads}$ for N_2 and H_2 is mainly for the low surface interaction than CO_2 [35].

4.4 Conclusions

In this chapter, hydrothermal, thermal, mechanical and hydrolytic stability of the 3D cubical KIT-6 on microscopic level have been analysed by N_2 adsorption/desorption isotherm, XRD spectra and high pressure $CO_2/N_2/H_2$ adsorption. The incipient as-synthesized KIT-6 shows stable structural property with improved surface area after washing with water. The hydrothermal ageing of KIT-6 during synthesis significantly improves the pore size up to 8 nm without any structural disturbance. The S_{BET} and V_t of KIT-6 (~ 5%) change slightly for the destruction of pore wall in presence of high load pressure (1560 bar). With further increase in pressure up to 4680 bar, the S_{BET} is reduced by ~ 24% for the substantial loss in porosity and increases the amorphous phase in KIT-6. However, there is also a substrincial loss in pore volume. Thermal analysis indicates that the KIT-6 is more stable than other mesoporous silica MCM-41, MCM-48, SBA-1 and SBA-15, for its thicker pore wall. The surface of KIT-6 is corroded by hydrolysis of siloxane bridge of KIT-6 in presence of moisture and increases with increasing water concentration and temperature. KIT-6 shows the adsorption capacities 1.42 mmol CO_2/g (1 bar) and 10.1 mmol CO_2/g (20 bar) at 0 ºC with high reversibility. In case of H_2, maximum storage capacity obtained is 2.38 wt% at −196 ºC and 30 bar without any structural destruction. Among the other mesoporous silica such as MCM-41, MCM-48, SBA-1 KIT-1, HMS and SBA-15, KIT-6 shows the highest mechanical stability for the thicker pore wall and 3D cubical structure. This study suggests that 3D KIT-6 with interconnected pores can be an ideal material for industrial applications as catalysis, support of nanomaterial architecture, CO_2 selective separation/purification and H_2 storage.

References

[1] J. S. Beck, J. C. Vartuli, W. J. Roth, M. E. Leonowicz, C. T. Kresge, K. D. Schmitt, C. T. W. Chu, D. H. Olson, E. W. Sheppard, A new family of mesoporous molecular sieves prepared with liquid crystal templates, J. Am. Chem. Soc. 114 (1992) 10834–10843.

[2] S. Minakata, T. Nagamachi, K. Nakayama, T. Suzuki, T. Tanakab, The Diels–Alder reaction of C_{60} and Cyclopentadiene in mesoporous silica as a reaction medium, Chem. Commun.47 (2011) 6338–6340.

[3] H. Shintaku, K. Nakajima, M. Kitano, N. Ichikuni, M. Hara, Lewis acid catalysis of TiO_4 tetrahedra on mesoporous silica in water, ACS Catal. 4 (2014) 1198−1204.

[4] C. Pirez, J.-M. Caderon, J.–P. Dacquin, A. F. Lee, K. Wilson, Tunable KIT-6 mesoporous sulfonic acid catalysts for fatty acid Esterification, ACS Catal. 2 (2012) 1607−1614.

[5] A. Galarneau, D. Desplantier-Giscard, F. D. Renzo, F. Fajula, Thermal and mechanical stability of micelle-templated silica supports for catalysis, Catal. Today 68 (2001) 191–200.

[6] J. E. Lee, N. Lee, T. Kim, J. Kim, T. Hyeon, Multifunctional mesoporous silica nanocomposite nanoparticles for theranostic applications, Acc. Chem. Res. 44 (2011) 893–902.

[7] L. Wang, R. T. Yang, Increasing selective CO_2 adsorption on amine-grafted SBA-15 by increasing silanol density, J. Phys. Chem. C 115 (2011) 21264–21272.

[8] V. Y. Gusev, X. Feng, Z. Bu, G. L. Haller, J. A. O'Brien, Mechanical stability of pure silica mesoporous MCM-41 by nitrogen adsorption and small-angle X-ray diffraction measurements, J. Phys. Chem., 100 (1996) 1985–1988.

[9] A. Vinu, V. Murugesan, M. Hartmann, Pore size engineering and mechanical stability of the Cubic mesoporous molecular sieve SBA-1, Chem. Mater. 15 (2003) 1385–1393.

[10] T. Ishikawa, M. Matsuda, A. Yasukawa, K. Kandori, S. Inagaki, T. Fukushima, S. Kondo, Surface silanol groups of mesoporous silica FSM-16,J. Chem. Soc., Faraday Trans. 92 (1996) 1985–1989.

[11] D. Zhao, J. Feng, Q. Huo, N. Melosh, G. H. Fredrickson, B. F. Chmelka, G. D. Stucky, Triblock copolymer syntheses of mesoporous silica with periodic 50 to 300 angstrom pores, Science 279 (1998) 548–552.

[12] F. Kleitz, S. H. Choi, R. Ryoo, Cubic Ia3d large mesoporous silica: Synthesis and replication to platinum nanowires, carbon nanorods and carbon nanotubes, Chem. Commun. (2003)2136–2137.

[13] M. Kruk, M. Jaroniec, Gas adsorption characterization of ordered organic-inorganic nanocomposite materials, Chem. Mater. 13 (2001) 3169–3183.

[14] T. W. Kim, F. Kleitz, B. Paul, R. Ryoo, MCM-48-like large mesoporous silicas with tailored pore structure: Facile synthesis domain in a ternary triblock copolymer-butanol-water system, J. Am. Chem. Soc. 127 (2005) 7601–7610.

[15] W.-J. Son, J.-S. Choi, W.-S. Ahn, Adsorptive removal of carbon dioxide using polyethyleneimine-loaded mesoporous silica materials, Microporous Mesoporous Mater. 113 (2008) 31–40.

[16] A. Sayari, P. Liu, M. Kruk, M. Jaroniec, Characterization of large-pore MCM-41 molecular sieves obtained via hydrothermal restructuring, Chem. Mater. 9 (1997) 2499 − 2506.

[17] M. J. Kim, R. Ryoo, Synthesis and pore size control of cubic mesoporous silica SBA-1, Chem. Mater. 11 (1999) 487–491.

[18] J. Fan, C. Yu, L. Wang, B. Tu, D. Zhao, Y. Sakamoto, O. Terasaki, Mesotunnels on the silica wall of ordered SBA-15 to generate three-dimensional large-pore mesoporous networks, J. Am. Chem. Soc. 123 (2001) 12113–12114.

[19] M. Kruk, L. Cao, Pore size tailoring in large-pore SBA-15 silica synthesized in the presence of Hexane, Langmuir 23 (2007) 7247-7254.

[20] K. Cassiers, T. Linssen, M. Mathieu, M. Benjelloun, K. Schrijnemakers, P.V.D. Voort, P. Cool, E. F. Vansant, A detailed study of thermal, hydrothermal, and mechanical stabilities of a wide range of surfactant assembled mesoporous silicas, Chem. Mater. 14 (2002) 2317 – 2324.

[21] L. Cao, M. Kruk, Short synthesis of ordered silicas with very large mesopores, RSC Adv., 4 (2014) 331−339.

[22] T. Tatsumi, K. A. Koyano, Y. Tanaka, S. Nakata, Mechanical Stability of Mesoporous Materials, MCM-48 and MCM-41, J. Porous Mat. 6 (1999) 13–17.

[23] V. Polshettiwar, D. Cha, X. Zhang, J. M. Basset, High-surface-area silica nanospheres (KCC-1) with a fibrous morphology, Angew. Chem. Int. Ed. 49 (2010) 9652 – 9656.

[24] S. Chytil, L. Haugland, E. A. Blekkan, On the mechanical stability of mesoporous silica SBA-15, Micropor. Mesopor. Mater.111 (2008) 134–142.

[25] X. S. Zhao, G. Q. Lu, A. K. Whittaker, G. J. Millar, H. Y. Zhu,Comprehensive study of surface chemistry of MCM-41 using ^{29}Si CP/MAS NMR, FTIR, pyridine-TPD, and TGA, J. Phys. Chem. B 101 (1997) 6525−6531.

[26] R. M. Pasternack, S. R. Amy, Y. J. Chabal Attachment of 3-(Aminopropyl) triethoxysilane on silicon oxide surfaces: dependence on solution temperature, Langmuir 24 (2008) 12963–12971.

[27] I.-M. Hung, D.-T. Hung, K.-Z. Fung, M.-H. Hon, Effect of calcination temperature on morphology of mesoporous YSZ, J. Eur. Ceramic Soc. 26 (2006) 2627–2632.

[28] R. M. Grudzien, B. E. Grabicka, M. Jaroniec, Adsorption studies of thermal stability of SBA-16 mesoporous silicas, Appl. Surf. Sci. 253 (2007) 5660–5665

[29] M. Broyer, S. Valange, J. P. Bellat, O. Bertrand, G. Weber, Z. Gabelica, Influence of ageing, thermal, hydrothermal, and mechanical treatments on the porosity of MCM-41 mesoporous silica, Langmuir 18 (2002) 5083–5091.

[30] F. Kleitz, W. Schmidt, F. Schüth, Calcination behavior of different surfactant-templated mesostructured silica materials, Micropor. Mesopor. Mater. 65 (2003) 1–29.

[31] T. S. Mahadevan, S. H. Garofalini, Dissociative chemisorption of water onto silica surfaces and formation of hydronium ions, J. Phys. Chem. C 112 (2008) 1507–1515.

[32] T. A. Michalske, S. W. Freiman, A molecular interpretation of stress corrosion in silica. Nature 295 (1982) 511–512.

[33] M. Hartmann, C. Bischof, Mechanical stability of mesoporous molecular sieve MCM-48 studied by adsorption of Benzene, n-Heptane, and Cyclohexane, J. Phys. Chem. B 103 (1999) 6230–6235.

[34] Y. Park, Y. Ju, D. Park, C. H. Lee, Adsorption equilibria and kinetics of six pure gases on pelletized Zeolite 13X up to 1.0 MPa: CO_2, CO, N_2, CH_4, Ar and H_2, Chem. Eng. J. 292 (2016) 348–365.

[35] K. Sumida, D. L. Rogow, J. A. Mason, T. M. McDonald, E. D. Bloch, Z. R. Herm, T.-H. Bae, J. R. Long, Carbon dioxide capture in metal–organic frameworks, Chem. Rev. 112 (2012) 724–781.

[36] B. Schmitz, U. Müller, N. Trukhan, M. Schubert, G. Férey, M. Hirscher, Heat of adsorption for hydrogen in microporous high-surface-area materials, Chem Phys Chem. 9 (2008) 2181–2184.

[37] D. Sahu, P. Mishra, S. Edubilli, A. Verma, S. Gumma, Hydrogen adsorption on Zn-BDC, Cr-BDC, Ni-DABCO, and Mg- DOBDC metal−organic frameworks, J. Chem. Eng. Data 58 (2013) 3096−3101.

[38] R. J. Konwar, M. De, Effects of synthesis parameters on zeolite templated carbon for hydrogen storage application, Micropor. Mesopor. Mater. 175 (2013) 16–24.

CHAPTER 5

(3-AMINOPROPYL)TRIETHOXYSILANE GRAFTED ORDERED MESOPOROUS SILICA KIT-6 FOR CO_2 ADSORPTION

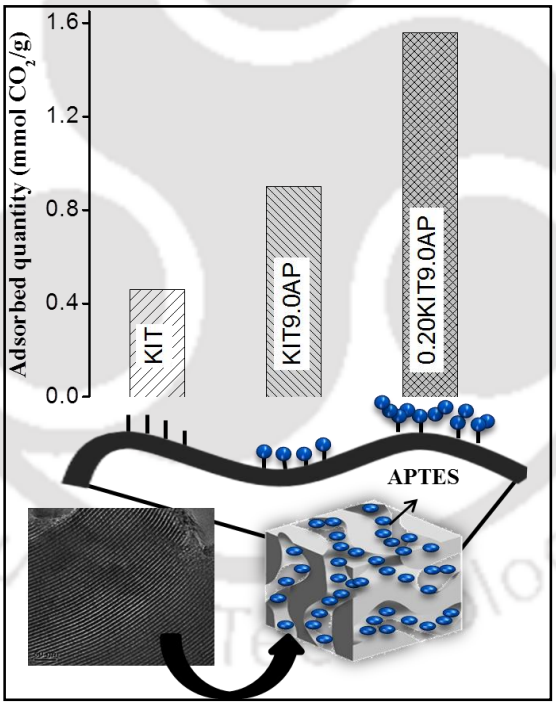

CHAPTER 5

In this chapter, grafting of (3-aminopropyl)triethoxysilane on mesoporous KIT-6 in dry and aqueous grafting solvent is presented. The grafting mechanism of aminosilane on mesoporous silica is illustrated by several analytical techniques. The grafting capacity of aminosilane is enhanced in aqueous solution. The CO_2 adsorption performance of aminosilane grafted KIT-6 in wide range of temperature and pressure is discussed. This part of work has been published in ***Chem. Eng. J., 262 (2015) 882–890****.*

5.1 Introduction

Coal, oil and natural gas are the major sources of energy and these provide 80% of world energy demand. These energy sectors are the major anthropogenic sources of CO_2 [1]. According to earlier studies of paleoclimate data and CO_2 concentration in atmosphere, the rapid increase of global warming is mainly due to CO_2 and other greenhouse gases [2]. By observation of "Mauna Loa Observatory" Hawaii, CO_2 atmospheric concentration has already reached ~406 ppm in 2016 and it will reach 450 ppm in next few years, which is sufficient to increase global surface temperature above 2 °C of the maximum limit range [3].

Carbon capture and storage (CCS) is important to mitigate the global warming and its consequences by capture of CO_2 from large anthropogenic sources. Adsorption is an attractive and cost effective CO_2 capture process [4−6]. There have been numerous literatures reported on CO_2 adsorption in amine grafted MCM and SBA series. But only few of them concentrate on the CO_2 adsorption behavior in KIT-6. MCM-41 and SBA-15 have 2D hexagonal structure with parallel cylindrical pore whereas KIT-6 has 3D cubical structure with large interconnecting pores

and may provide a better grafting surface for amine and easy transport for the CO_2 molecules. As far as we know, there is no report available on APTES modified KIT-6. In this work KIT-6 was synthesized and functionalized with various concentrations of APTES in dry and aqueous solution. The resulting materials were characterized through various techniques and it was observed that the presence of water in the grafting solution influences the amine loading on KIT-6. The CO_2 adsorption capacity measurements were performed in a gravimetric Rubotherm measurement set-up at various temperatures. Cyclic adsorption/desorption capacity of the adsorbents were analyzed at 30 °C.

5.2 Materials and Methods

5.2.1 *Synthesis of adsorbents*

Traditional 3D cubical KIT-6 was synthesized by following the procedure of Kim et al. [7] and explained in section 3.2. Pure mesoporous silica was functionalized by post grafting method, both in dry and aqueous solution. Before grafting, 1.0 g of KIT-6/D was dried at 120 ºC in vacuum to remove the pre adsorbed moisture. In a typical dry grafting process, 1.0 g of KIT-6/D was dispersed in a 50 ml of dry toluene taken in a flask. In the resulting solution 'x' mmole of APTES was added and refluxed at 80°C for 24 h. The treated sample was filtered, washed with toluene and dried at 80°C in vacuum for 16 h. The functionalized KIT-6 was stored for further analysis and denoted as KIT'x'AP (where 'x' represents the concentration of APTES in mmol/g). In aqueous grafting, 'y' ml of water was added in the dispersed KIT-6 (1.0 g) solution and stirred for 2 h at room temperature. Optimized concentration of APTES from dry grafting process was added in the solution and refluxed at 80°C for 24 h. Other steps were similar as explained above and the functionalized material was denoted as 'y'KIT'x'AP.

5.2.2 *Characterizationof adsorbent*

Mesoporous material structure of KIT-6, dry solution grafted KIT'x'AP and aqueous solution grafted 'y'KIT'x'AP adsorbents were characterized by powder X-ray diffractometer (XRD, Bruker, D8 Advance) with Cu Kα radition (power 40 kV, 40 mA). Surface morphology was measured by TEM (JEOL JEM-2100 at 200 kV). Physical properties of the adsorbent were measured by nitrogen adsorption/desorption isotherm (Quantachrome autosorb iQ) at –196 °C. The Brunauer-Emmett-Teller surface area (S_{BET}) was calculated over relative pressure range (P/P_0) 0.05-0.30 and pore volume at 0.99. Pore size distributions were determined by Barrett-Joyner-Halenda (BJH) method of nitrogen adsorption curve. Functional groups present in the adsorbent were analyzed by diffuse reflectance infrared Fourier transform (DRIFT) spectra (IR-Affinity, Shimadzu) and amount of APTES grafted was examined by thermo gravimetric(TG) analyzer (Netzsch Sat) in the temperature range of 25−800 °C with a heating rate 10°C/min.

Adsorption and desorption measurements ofCO_2 on KIT, KIT'x'AP and 'y'KIT'x'AP adsorbents were performed using a Rubotherm gravimetric magnetic suspension balance at different temperatures for pressure till 5 bar as explained in Chapter 3. In a typical kinetic measurement, CO_2 was purged in to the sample chamber with a step input at 1 bar pressure. Cyclic adsorption/desorption capacities of the materials were analysed at 30 °C and regeneration was done at 120 °C in helium atmosphere.

5.3 Results and Discussion

5.3.1 *X-ray diffraction analysis*

The XRD pattern of KIT-6 confirms the gyroidal cubic Ia3d structure with d_{211} and d_{220} plane of the material [7,8]. In dry and aqueous solution grafted adsorbents KIT'x'AP and 'y'KIT'x'AP

show nearly the same Bragg's diffraction peak d_{211} position but intensities are sparsely reduced with increase in the APTES concentration as shown in Figure 5.1. In addition, for 'y'KIT'x'AP, peak intensity was drastically decreased. This indicates that the regularity of the silica materials is preserved after APTES loading both in dry and aqueous solution grafting processes but internal surface of the pore and external surface of the adsorbent are more occupied during aqueous grafting by amine.

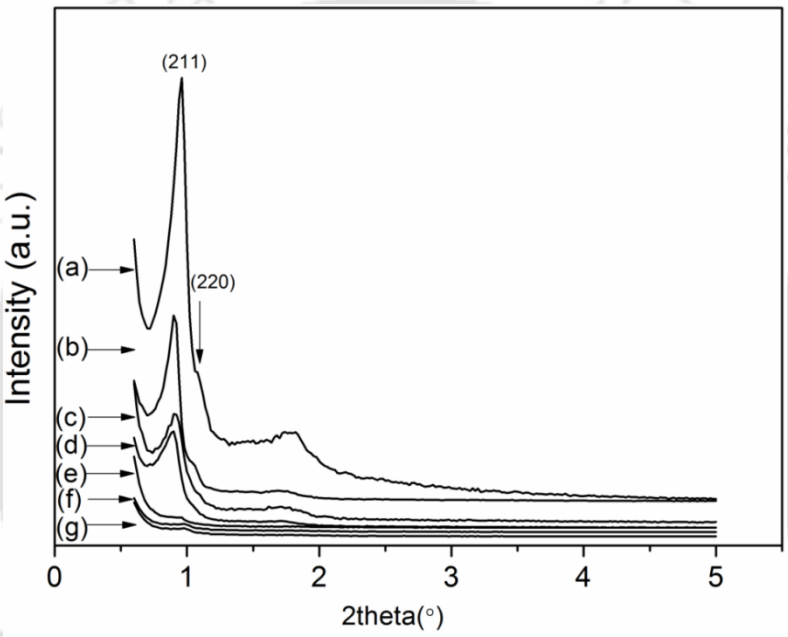

Figure 5.1 X-ray diffraction pattern of (a) KIT-6, (b) KIT 7.0AP, (c) KIT 9.0AP, (d) KIT 11.0AP, (e) 0.15KIT 9.0AP, (f) 0.2KIT 9.0AP and (g) 0.25KIT 9.0AP adsorbents

5.3.2 *N_2 adsorption/desorption isotherm*

Nitrogen adsorption/desorption isotherm and BJH pore size distribution of pure and APTES grafted (dry and aqueous) adsorbents are depicted in Figure 5.2. The nitrogen adsorption isotherms for KIT-6, KIT'x'AP and 'y'KIT'x'AP are of type IV according to the IUPAC classification with a hysteresis loop, which is the characteristic of mesoporous materials [9].

Physical properties like specific surface area (S_{BET}), pore volume (V_t) and pore diameter (W_{BJH}) of the materials are summarized in Table 5.1. With increase in the APTES concentration in solution from 7.0 to 11.0 mmol/g, S_{BET} and V_t of KIT-6 are decreased drastically from 711 to 285 m^2/gand from 1.05 to 0.59 cm^3/g respectively [4−6,9,10]. This indicates that some pore volume and area are still available for amine loading. Further, with increase in the volume of water from 0.15 to 0.25 mL in optimum APTES grafted adsorbent, specific surface area and pore volume of the adsorbent decrease sharply from 297 to 12 m^2/gand from 0.62 to 0.05 cm^3/g,respectively due to higher amount of APTES loading.

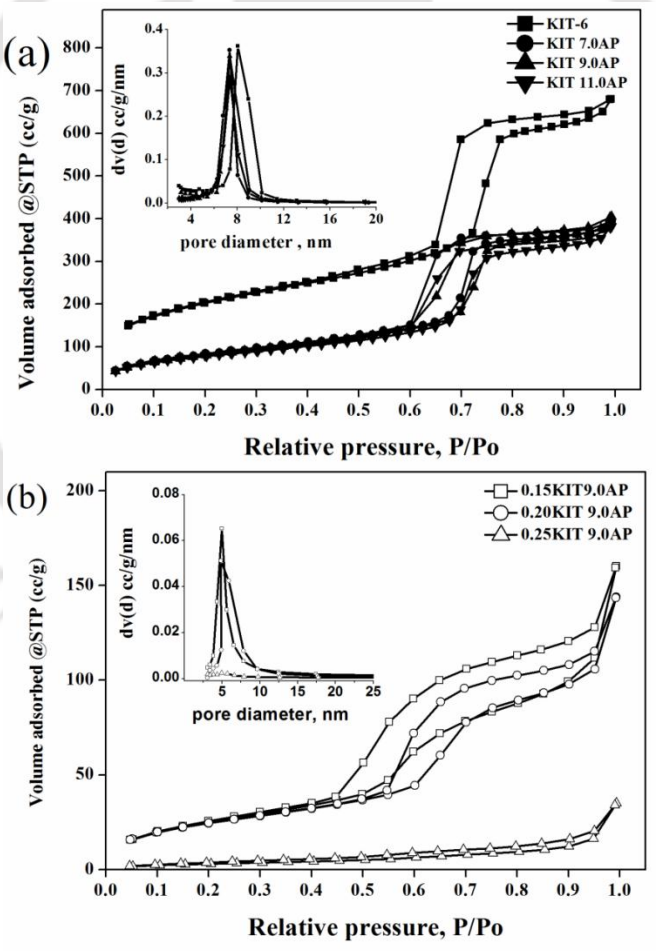

Figure 5.2 N_2 adsorption/desorption isotherm of (a) KIT-6 and dry grafted KIT'x'AP and (b) aqueous grafted 'y'KIT'x'AP adsorbents

Table 5.1. Structural properties of materials.

Sample	S_{BET} (m^2/g)	V_t (cm^3/g)	W_{BJH} (nm)
KIT-6	711	1.05	8.04
KIT 7.0AP	304	0.68	7.35
KIT 9.0AP	297	0.62	7.34
KIT 11.0AP	285	0.59	7.34
0.15KIT 9.0AP	95	0.26	4.97
0.20KIT 9.0AP	90	0.22	4.83
0.25KIT 9.0AP	12	0.05	4.80

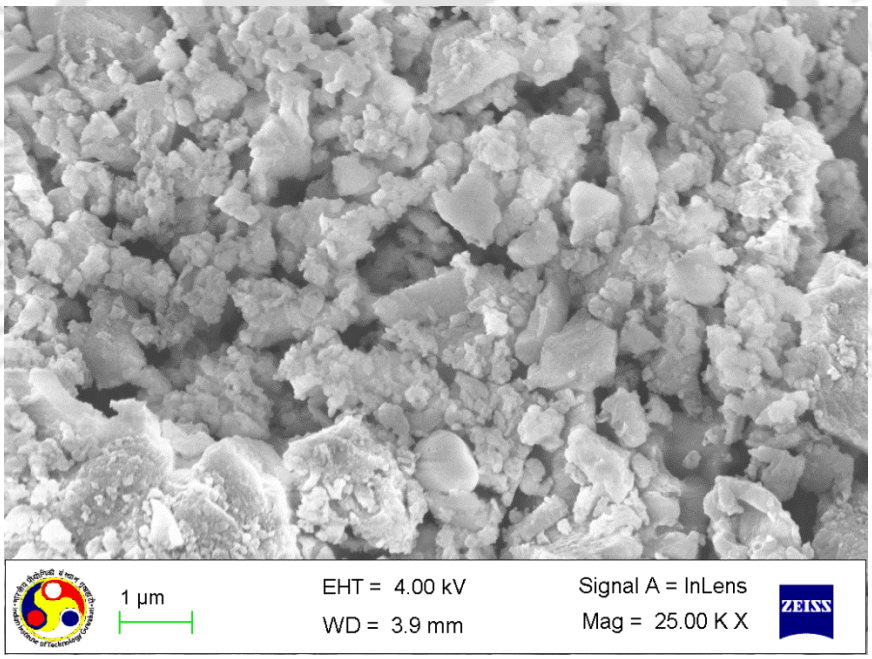

Figure 5.3 FESEM micrograph of KIT-6

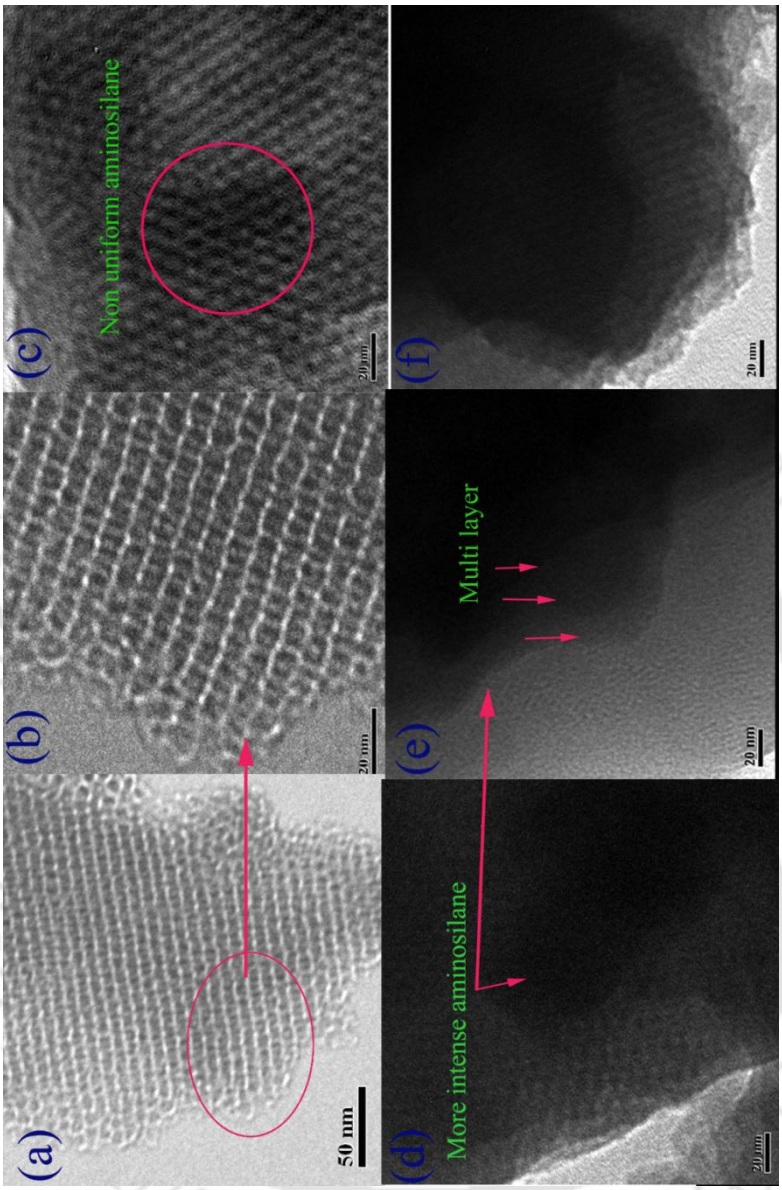

Figure 5.4 TEM micrograph of (a, b) KIT-6, (c) KIT 9.0AP (d) 0.15KIT 9.0AP (e) 0.20KIT 9.0AP and (f) 0.25KIT 9.0AP adsorbents

5.3.3 *Electron micrograph*

KIT-6 is highly ordered three dimensional mesoporous silica as can be seen from FESEM (Figure 5.3) and TEM (Figure 5.4) micrograph. KIT-6 exhibits a well-defined three dimensional structure (ca. 1.0 – 2.0 μm size) with interconnected pore (ca. 6.6 nm) [7]. TEM micrograph of KIT-6 clearly shows that the synthesized mesoporous silica is highly ordered with cubical structure. Molecular apportionment of aminosilane on KIT-6 is analyzed by TEM micrograph. It conspicuously shows the APTES non-uniformly distributed over KIT 9.0AP (Figure 5.4C) [11,12]. In aqueous grafting, APTES density gradually increases with increasing water concentration in the grafting solvent (Figure 5.4D−F). TEM micrograph of 0.20KIT 9.0AP and 0.25KIT 9.0AP, it clearly shows that the APTES forms a layer during grafting. It is mainly due to formation of polymer over the surface [12,13]. In aqueous amine solution grafting, maximum pore volume was utilized and no damage of the structure is observed after grafting.

Table 5.2 CO_2 adsorption capacities of amine functionalized adsorbents at 30 °C

Sample	APTES loading (mmol N/g)	Adsorption capacity at 1bar (mmol CO_2/g)	Adsorption efficiency (mmol CO_2/mmol N)
KIT-6	---	0.48	---
KIT 7.0AP	1.43	0.76	0.53
KIT 9.0AP	1.50	0.90	0.60
KIT 11.0AP	1.72	0.83	0.48
0.15KIT 9.0AP	2.15	1.26	0.58
0.20KIT 9.0AP	2.44	1.56	0.64
0.25KIT 9.0AP	2.67	0.32	0.12

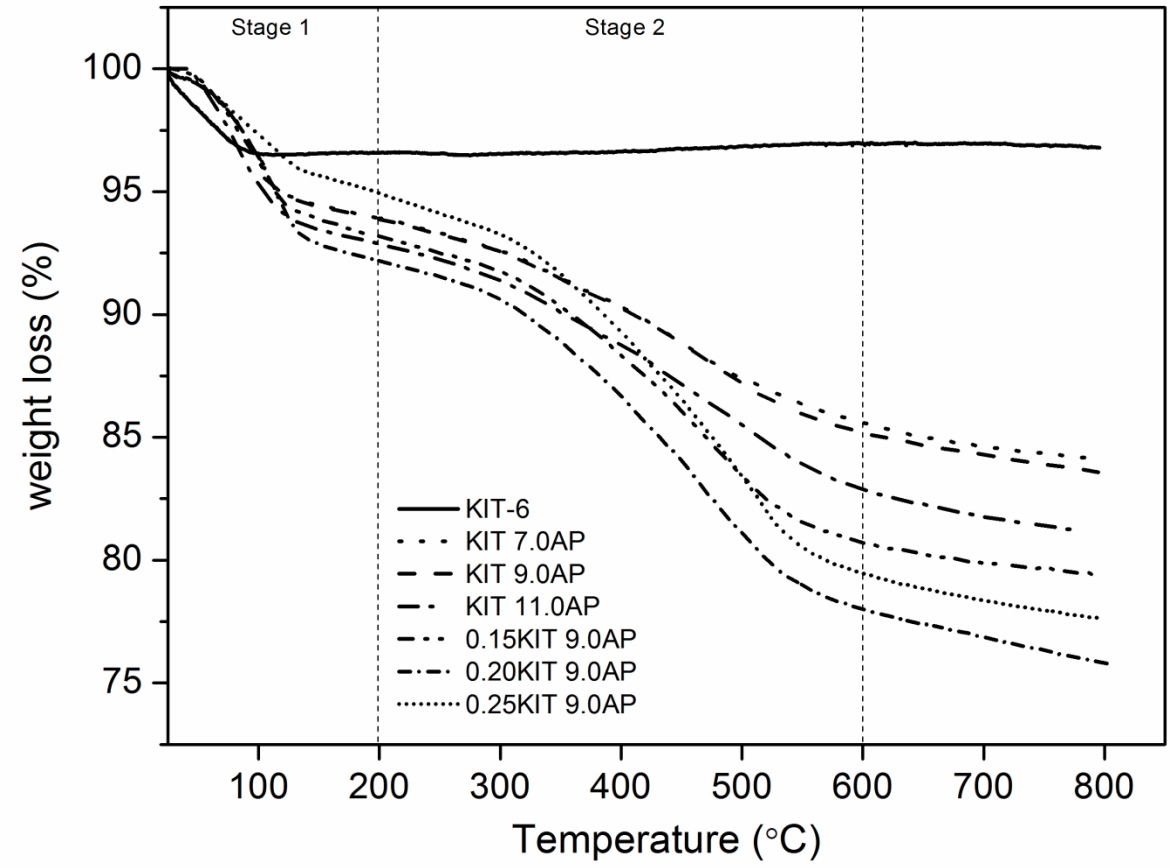

Figure 5.5 TGA curves of pure KIT-6, KIT 'x'AP and 'y'KIT '9.0'AP adsorbents

5.3.4 *Thermal analysis*

Amount of APTES and thermal stability of KIT'x'AP and 'y'KIT'x'AP were analysed by TG analyzer and the results are shown in Figure 5.5. The total mass loss in the adsorbents is grossly occurred in two steps. The mass loss in the first stage, (temperature range 25–200 °C) is due to liberation of moisture, adsorbed gases and isolated APTES molecules. The mass loss in second stage (200–600 °C), corresponds to the degradation of grafted amine as discussed in section A1 [13,14]. The total mass loss in this temperature range is 8.31% for KIT 7.0AP, 8.68% for KIT 9.0AP, 9.98% for KIT 11.0AP, 12.48% for 0.15KIT 9.0AP, 14.17 % for 0.20KIT 9.0AP, and

15.48 % for 0.25KIT 9.0AP which correspond to APTES content of 1.43, 1.50, 1.72, 2.15, 2.44 and 2.67 mmol N/g of adsorbent (Table 5.2).With increasing the concentration of APTES in the dry grafting process from 7.0 to 11.0 mmol/g adsorbent, loading of amine is increased in the following order KIT 7.0AP < KIT 9.0AP < KIT 11.0AP. In case of aqueous grafting, with increasing the water content from 0.15 to 0.25 mL in the mixture, the amine loading is increased in the following order 0.15KIT 9.0AP < 0.20KIT 9.0AP < 0.25KIT 9.0AP.

5.3.5 *Diffuse reflectance infrared Fourier transform spectra*

The DRIFT spectra were recorded in the range 500 – 4000 cm^{-1} to confirm the APTES in the adsorbents as shown in the Figure 5.6. The band across ~1040 to ~1250 cm^{-1} and peak across ~800 cm^{-1} are attributed to the asymmetric and symmetric stretch of siloxane groups, respectively, and the peak at 960 cm^{-1} corresponds to the free silanol group of mesoporous silica[15,16]. The broad peak at 3200 – 3600 cm^{-1} represents the hydrogen bonded surface silanol groups, and at 3740 cm^{-1} for single and geminal silanol groups of KIT-6. The other peaks at 1620 cm^{-1} and 2360 cm^{-1} represent the physically adsorbed water and CO_2 respectively [17]. In APTES grafted adsorbents, the peaks around ~1485 cm^{-1} and ~1567 cm^{-1} represent the $–NH_2$ and –NH– groups associated with the surface [18]. The peak intensity is found higher in case of aqueous grafted adsorbents when compared to dry grafted adsorbents which confirm the higher APTES loading in aqueous grafting. The bands around ~2876 cm^{-1} and ~2930 cm^{-1} correspond to the symmetric and asymmetric deformation of the CH_2 groups of propyl chain present in APTES [19].

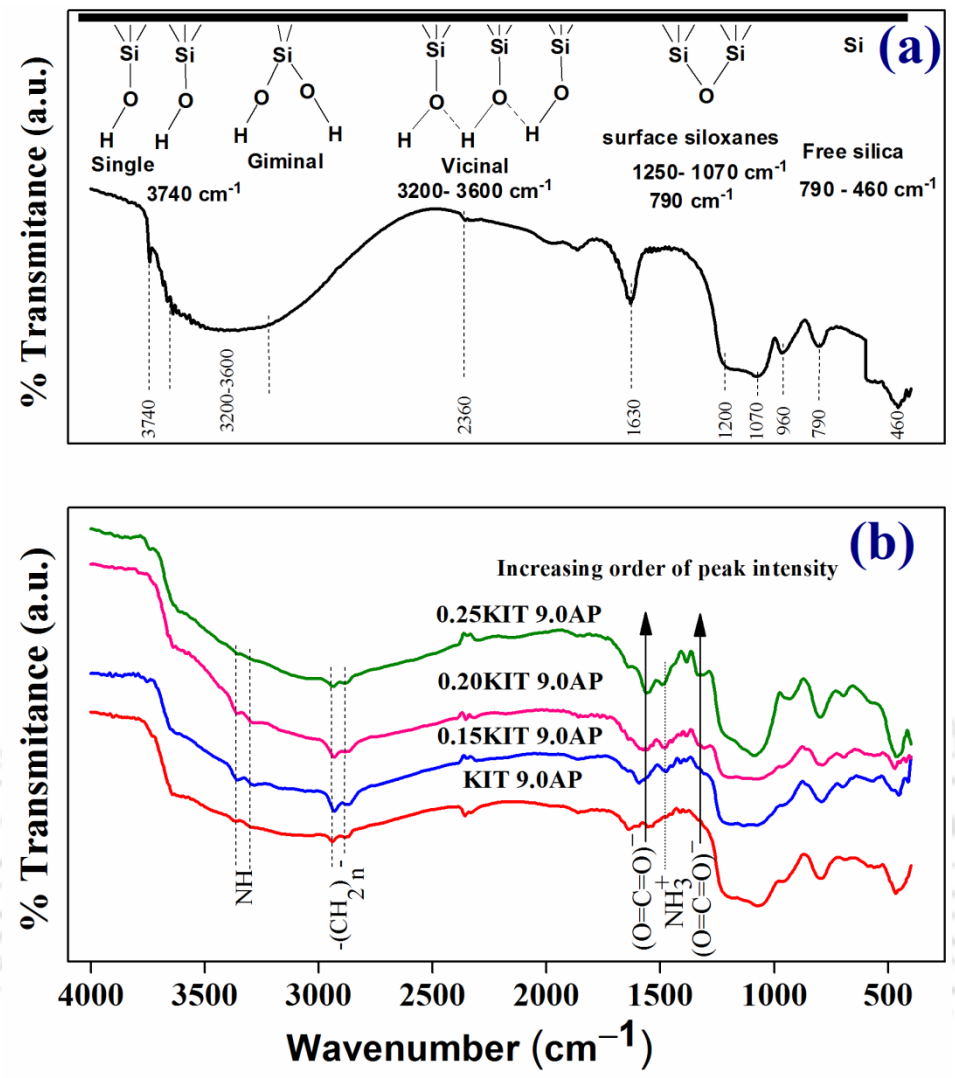

Figure 5.6 DRIFT spectra of KIT-6 and 'y'KIT 'x'AP adsorbents

5.3.6 *CO_2 adsorption on APTES grafted adsorbents*

Adsorbent with different APTES loading ranging from 1.60 to 1.92 mmol/g were synthesized in dry toluene and tested for the CO_2 adsorption. The adsorption isotherms at 30°C are shown in Figure 5.7. All isotherms clearly indicate the increase in CO_2 adsorption capacity with increasing pressure. In the low pressure region (< 0.20 bar), a sharp increase in adsorption capacity

observed is attributed to the chemisorption between CO_2 and amine functional group present on the surface in both dry and aqueous grafted adsorbents. The equilibrium adsorption capacities at 1 bar follow the order KIT-6 < KIT 7.0AP < KIT 11.0AP < KIT 9.0AP at 30 °C (Table 5.2). The maximum adsorption capacity of 0.90 mmol CO_2/g is observed in KIT 9.0AP at 1 bar. Although, APTES loading is maximum (1.92 mmol N/g) on KIT 11.0AP adsorbent, adsorption capacity is less compared to KIT 9.0AP. It clearly indicates that adsorption capacity is not increased even at higher amine loading. This suggests that in higher APTES concentration amine groups are overlapped with each other and reduce the accessible amine groups for CO_2 surface area of the adsorbent [20].

Presence of water in the grafting solution shows dramatic change in the attachment of APTES on the adsorbents and CO_2 adsorption capacity. The adsorbents synthesized in presence of water (y = 0.15 – 0.25) show higher adsorption capacity in following order 0.25KIT 9.0AP (0.32 mmol CO_2/g) < 0.15KIT 9.0AP (1.26 mmol CO_2/g) < 0.20KIT 9.0AP (1.56 mmol CO_2/g) at 1bar and 30 °C (Table 5.2). The adsorption capacities of 0.15KIT 9.0AP and 0.20KIT 9.0AP are increased with the maximum at 0.20 mL water. Any further increase in the water content i.e. 0.25KIT 9.0AP decreases the adsorption capacity significantly even with higher amine loading. This suggests that when grafting is done in presence of higher water concentration, less amine groups are accessible in the adsorbent for CO_2.This is possibly because APTES has oligomerized in the solution and even closed the pore of the adsorbent during grafting [11]. At low water concentration, the APTES oligomer might not grow enough inside the pores and thus results in more CO_2 adsorption.

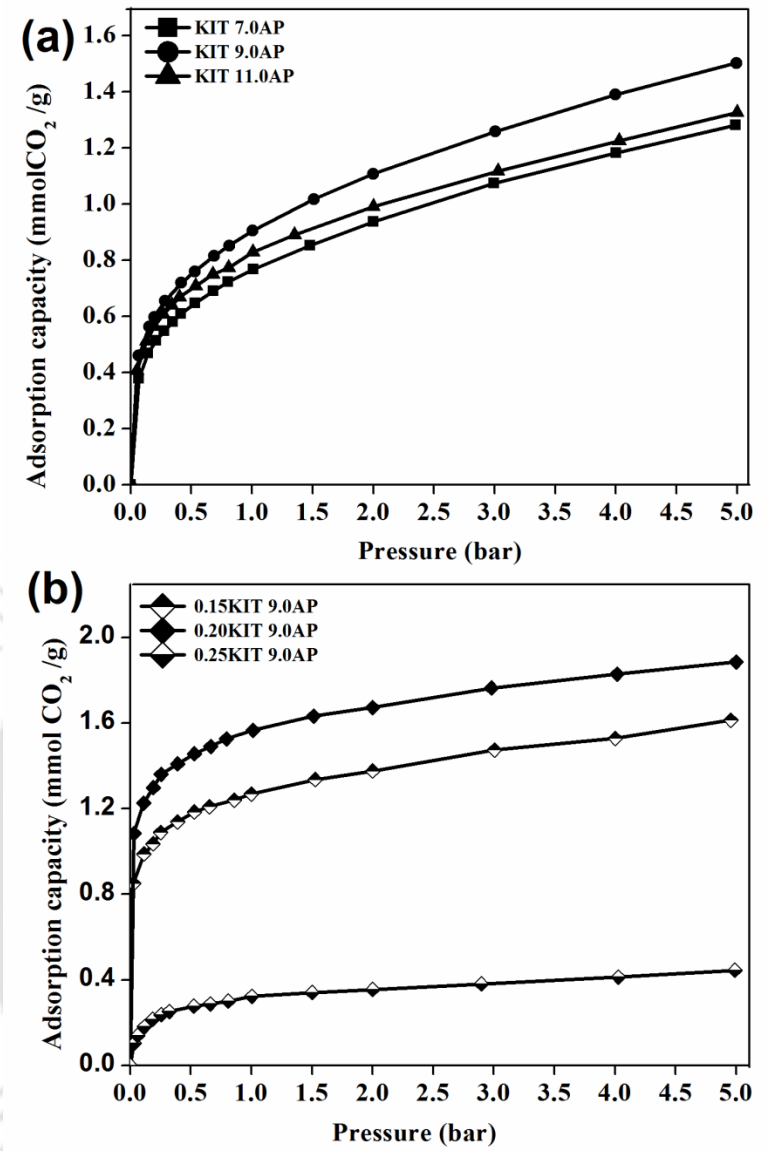

Figure 5.7 CO_2 adsorption capacities at 30°C for different APTES functionalized adsorbents (a) KIT 'x'AP and (b) 'y'KIT 9.0AP till 5 bar

5.3.7 *Grafting mechanism of APTES and CO_2 interaction*

Optimum amine concentration onto adsorbent minimizes the capex and opex of CO_2 capture process. CO_2 adsorption capacity of pure KIT-6 is 0.48 mmol/g at 1 bar and 30 °C attributed to the physisorption of CO_2 on the silica surface. The effect of amine concentration on

CO_2adsorption is shown in Figure 5.7. CO_2 adsorption is less in case of dry solution grafted adsorbents when compared to the aqueous solution grafted one. Thus, the optimum amine loading and CO_2 adsorption depend on the kind of grafting process. The amine loading is found to have increased with increase in APTES concentration (Table 5.2) in dry solution grafting because, ethoxy group of silane directly reacts with surface silanol groups (single, hydrogen-bonded and geminal silanol group) via condensation reaction (Figure 5.8b) and non-uniformly distributed over the surface [20]. On the other side, aqueous grafting is more complex than dry grafting over silica as the reaction mechanism proceeds via hydrolysis followed by double condensation reaction (Figure 5.8c) [11,13,20]. In case of aqueous grafting, the exposed Si–O–Si (surface siloxanes) tip reacts with water and generates two single silanol groups on the surface [22,23]. Initially, hydrogen atom of water gets bonded with oxygen of surface siloxane by electrostatic force of attraction and forms intermediate penta–coordinated silane by SN^2 reaction mechanism. After breakage of siloxane bridge, new single silanol groups are formed. In this step, single silanol group concentration is significantly increased on the surface. Finally, aminosilane hydrolysis in presence of water and subsequent condensation get them grafted on the surface as shown in the Figure 5.8C. Free aminosilane present in solution is further grafted by condensation with grafted aminosilane and forms multilayer onto the surface (Figure 5.8) [11]. It can be understood by N_2 adsorption/desorption isotherm (Table 5.1) and TEM micrograph (Figure 5.4). During aqueous grafting, amine loading follows the order 0.15KIT 9.0AP < 0.20KIT 9.0AP < 0.25KIT 9.0AP with increasing the concentration of water from 0.15 to 0.25 mL.

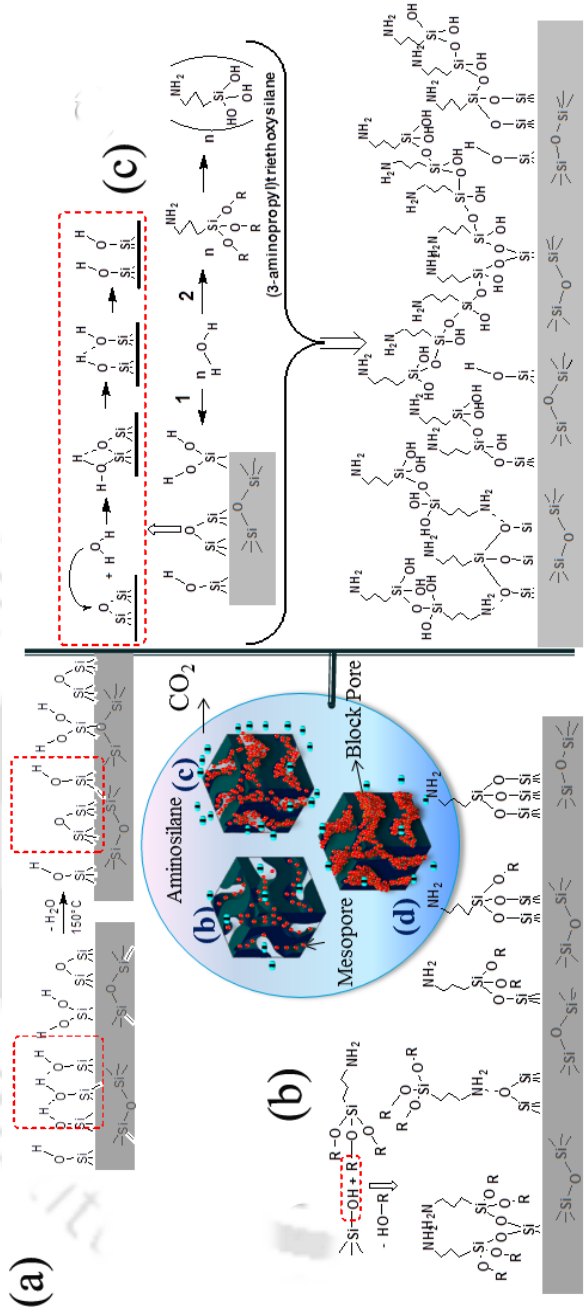

Figure 5.8. Grafting mechanisam of APTES (a) reaction of silica surface with water (b) anhydrous grafting and (c) aqueous grafting

Thus, on the basis of above results, we summarize the mechanism of APTES grafting and distribution onto adsorbents as follows. In dry grafting, APTES molecules diffuse into mesopore (> 2nm) of pure KIT-6 and get uniformly grafted (Figure 5.8). In aqueous grafting APTES oligomers diffuse in the pore and get grafted over surface. For longer time periods in aqueous solution, it forms multilayers of aminosilane. In contrast, with higher water concentration higher molecular weight oligomers are formed in the solution which blocks the pores as shown in Figure 5.8 [11].

At low pressure, the interaction between CO_2 with grafted amine by chemisorption could be explained by Caplow mechanism [24,25]. Dry CO_2 (Lewis acid) directly reacts with basic amine groups present on the surface of adsorbent via zwitterion intermediate and produces carbamate as shown in reaction 1.

$$CO_2 + -NH_2 \rightarrow -NH_2^+COO^- ; \quad -NH_2^+COO^- + -NH_2 \rightarrow -NHCOO^- + -NH_3^+ \quad 5.1.$$

Adsorption efficiency for monoamine is the ratio of number of mmol of CO_2 adsorbed per mmol of amine [10]. In overall adsorption reaction 5.1, each mmol CO_2 requires two mmol amine with maximum possible efficiency is 0.5. The adsorption efficiency of the adsorbents KIT 'x'AP and 'y'KIT 9.0AP lies between 0.48 – 0.60 mmol CO_2 $mmol^{-1}$ N and 0.12 – 0.64 mmol CO_2/mmol N respectively (Table 5.2). The efficiency of amine grafted adsorbents is higher at higher pressure, which might be possible due to the combined effects of chemisorption and physisorption between adsorbate and adsorbent. The adsorption efficiency of 0.25KIT9.0AP is quite low (0.12 mmol CO_2/mmol N) as compared to others which may be due to the blockage of the pores as mentioned earlier.

5.3.8 *CO_2 adsorption kinetics*

Dynamic CO_2 adsorption isotherm of the optimum amine grafted adsorbents (in dry and aqueous conditions) is shown in Figure 5.9. It is observed that the CO_2 adsorption capacity of KIT-6, KIT 9.0AP and 0.20KIT 9.0AP are 0.48, 0.90 and 1.56 mmol/grespectivelyat 1 bar and 30 °C. It may be noted that in first few minutes adsorption isotherm is sharply increased due to chemisorption between CO_2 and amine. About 90.0 % of the ultimate adsorption capacity is reached within initial 10 minutes and the equilibrium is reached after 20 minutes.

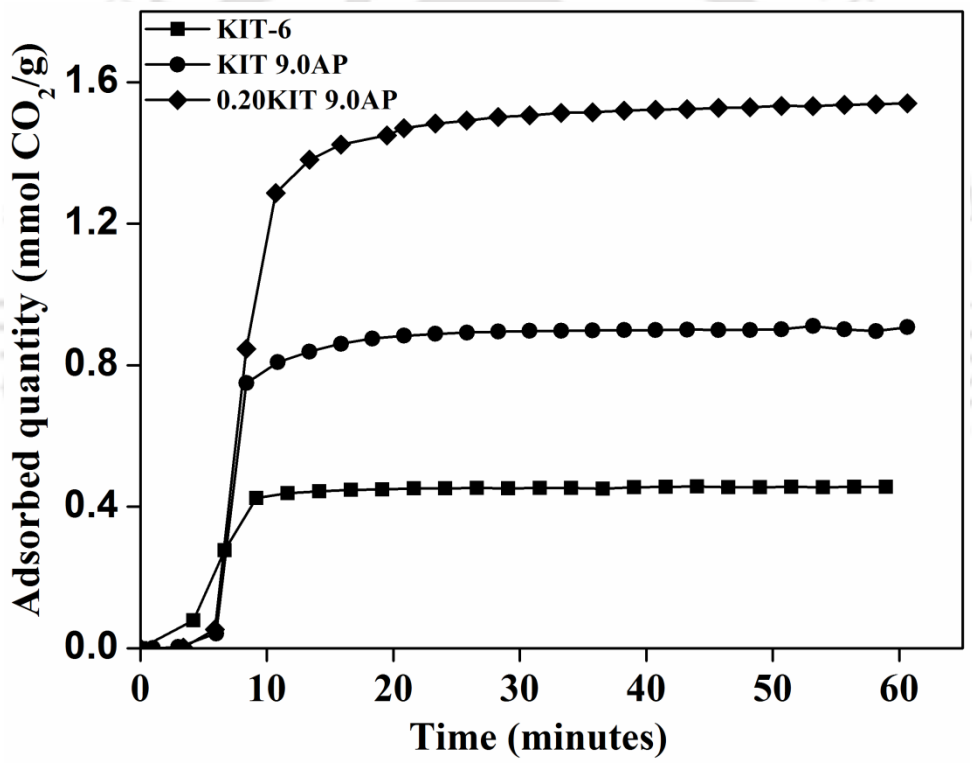

Figure 5.9 Dynamic adsorption performance of KIT-6, optimum amine loaded KIT 9.0AP and 0.20KIT 9.0AP adsorbents.

5.3.9 *Effect of the temperature on CO_2 adsorption*

The adsorption capacities of KIT-6, KIT 9.0AP and 0.20KIT 9.0AP at various temperatures (30, 45, 60 and 75 °C) are depicted in Figure 5.10. The adsorption capacities at 1 bar of KIT-6, KIT 9.0AP and 0.20KIT 9.0AP were found to be 0.48, 0.33, 0.24, 0.19 mmol CO_2/g, 0.90, 0.73, 0.63, 0.55 mmol CO_2/g, and 1.56, 1.50, 1.44, 1.31 mmol CO_2/g at 30, 45, 60 and 75 °C respectively. It is observed that the adsorption capacity decreases with increasing the temperature and is related to the exothermic interaction between CO_2 and adsorbent [9]. The amount of heat that is evolved in CO_2 adsorption process is estimated by Clausius-Clapeyronequation in the form of isosteric heat of adsorption ($-\Delta H°$) [26]. It is calculated from the slope of the ln(P) vs (1/T) curve (Figure 5.11) for the same adsorbed amount, where P and T represent the applied CO_2 pressure and temperature of the adsorption process, respectively. The values of $\Delta H°$ for KIT-6, KIT 9.0AP and 0.20KIT 9.0AP are –20.21, –33.18 and –31.26 kJ/mol respectively. The $-\Delta H°$ value is low in pure KIT-6 due to physisorption between CO_2 and silica surface and well comparable with earlier reported value (22 – 23 kJ/mol) [27]. The $\Delta H°$ value of amine grafted adsorbent is significantly higher due to strong interaction (chemisorption) between CO_2 and amine sites. The calculated values of $\Delta H°$ for amine grafted adsorbents KIT 9.0AP and 0.20KIT 9.0AP are ~ –33.21 and –31.26 kJ/mol which is comparable to other APTES functionalized mesoporous silica (–34.3 kJ/mol) [10].

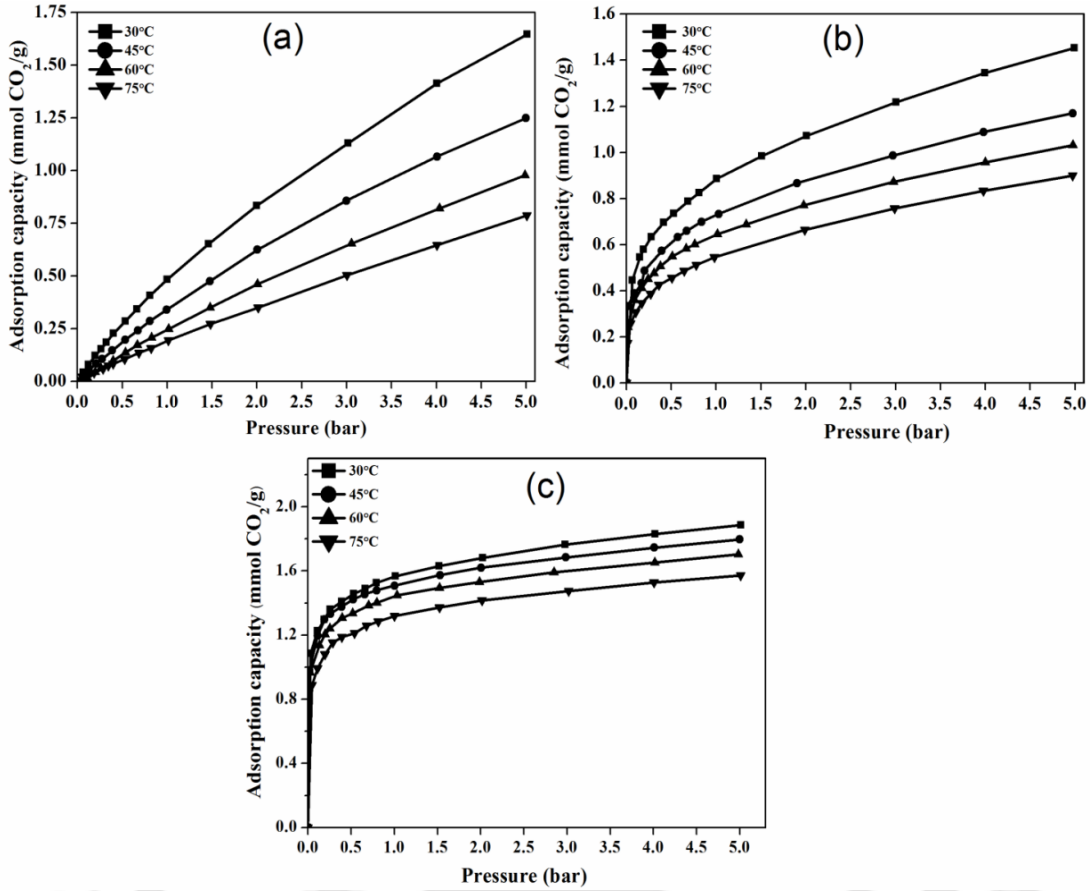

Figure 5.10 Adsorption isotherms of (a) KIT-6 (b) KIT 9.0AP and (c) 0.20KIT9.0AP at different temperatures

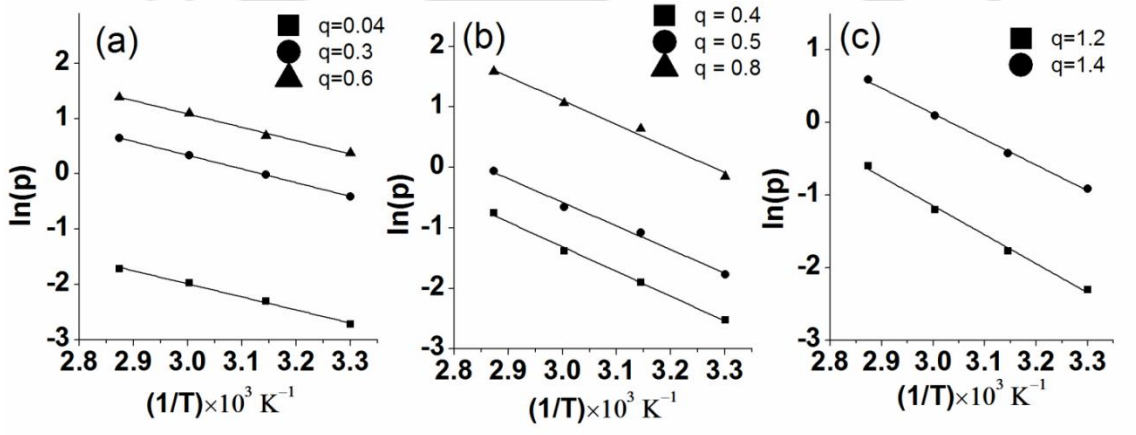

Figure 5.11 Typical plot of ln(P) versus (1/T) of different adsorbents (a) KIT-6 (b) KIT 9.0AP and (c) 0.20KIT 9.0AP for calculation of isosteric heat of adsorption

5.3.10 *Cyclic adsorption/desorption performance of adsorbent*

High adsorption capacity and stable cyclic adsorption/desorption performance of an adsorbent is desired parameter for any practical adsorptive separation process. Cyclic performance of the optimum adsorbents (KIT-6, KIT 9.0AP and 0.20KIT 9.0AP) for CO_2separationare shown in Figure 5.12 for 10 cycles. Regenerated adsorbent was exposed to CO_2 environment for 30 minutes for adsorption at 30 °C and again regenerated in 30 minutes at 120 °C under helium atmosphere. The adsorption capacities of KIT-6, KIT 9.0AP and 0.20KIT 9.0AP are found to be constant at 0.48, 0.90, and 1.56 mmol/g and stable till the 10^{th} cycle.

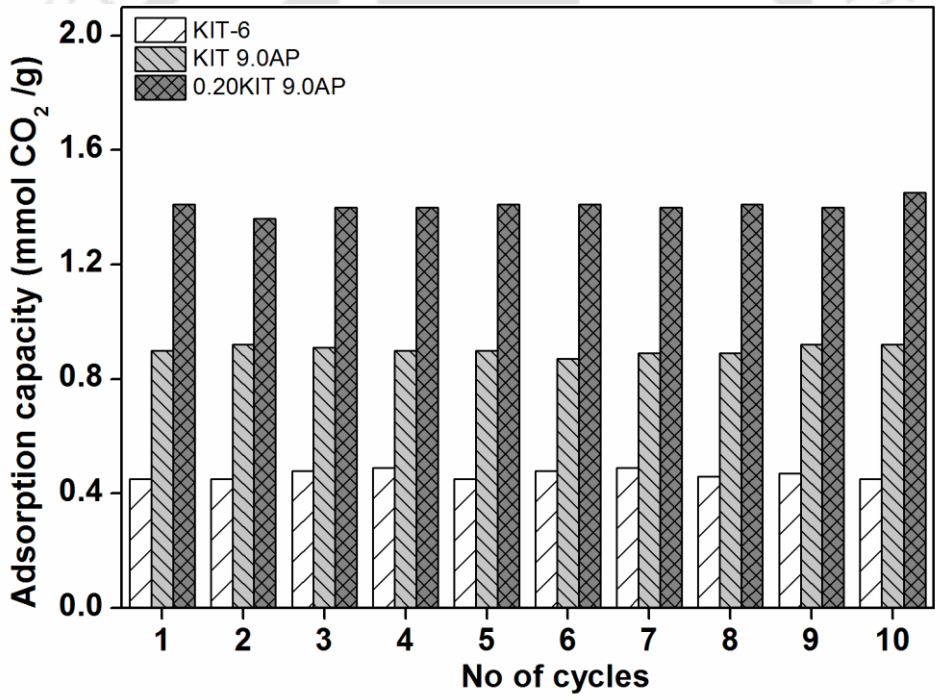

Figure 5.12 Cyclic CO_2 adsorption/desorption performance of KIT-6, KIT 9.0AP and 0.20KIT 9.0AP

5.4 Conclusions

In this study, APTES functionalized KIT-6 in both dry and aqueous solution were synthesized and tested as sorbent for CO_2 separation. The amine loading on KIT-6 is found to be maximum in case of aqueous grafting. It utilizes the maximum surface area, pore volume and amine present in the solution. The grafting mechanism of APTES on KIT-6 is explained in both dry and aqueous conditions. Notably, the sorption capacity is found to be dependent on the accessible amine site for CO_2 interaction and is the maximum for aqueous solution grafted adsorbent (0.20KIT 9.0AP) with adsorption capacity of 1.56 mmol/g at 1 bar and 30 °C. In addition, KIT 9.0AP and 0.20KIT 9.0AP show stable performance in cyclic study. Aqueous amine solution grafted adsorbent (0.20KIT 9.0AP) shows the best CO_2 adsorption capacity compared to the most of the mesoporous silica reported in literature.

References

[1] Key world energy statistics, The international energy agency (IEA) 2013. <http://www.iea.org/publications/freepublications/publication/KeyWorld2013.pdf>.

[2] S.L. Thompson, S.H. Schneider, Carbon dioxide and climate: ice and ocean, Nature 290 (1981) 9–10.

[3] M. Steinacher, F. Joos, T.F. Stocker, Allowable carbon emissions lowered by multiple climate targets, Nature 499 (2013) 197–201.

[4] V. Zeleňák, M. Badaničová, D. Halamová, J. Čejka, A. Zukal, N. Murafa, G. Goerigk, Amine-modified ordered mesoporous silica: effect of pore size on carbon dioxide capture, Chem. Eng. J. 144 (2008) 336–342.

[5] X. Yan, L. Zhang, Y. Zhang, K. Qiao, Z. Yan, S. Komarneni, Amine-modified mesocellular silica foams for CO2 capture, Chem. Eng. J. 168 (2011) 918–924.

[6] S. Loganathan, M. Tikmani, A.K. Ghoshal, Novel pore-expanded MCM-41 for CO2 capture: synthesis and characterization, Langmuir 29 (2013) 3491–3499.

[7] T.-W. Kim, F. Kleitz, B. Paul, R. Ryoo, MCM-48-like large mesoporous silicas with tailored pore structure: facile synthesis domain in a ternary triblock copolymer-butanol-water system, J. Am. Chem. Soc. 127 (2005) 7601–7610.

[8] L. Qian, Y. Ren, T. Liu, D. Pan, H. Wang, G. Chen, Influence of KIT-6's pore structure on its surface properties evaluated by inverse gas chromatography, Chem. Eng. J. 213 (2012) 186–194.

[9] L. Wang, R.T. Yang, Increasing selective CO_2 adsorption on amine-grafted SBA-15 by increasing silanol density, J. Phys. Chem. C 115 (2011) 21264–21272.

[10] Y.G. Ko, S.S. Shin, U.S. Choi, Primary, secondary, and tertiary amines for CO_2 capture: designing for mesoporous CO_2 adsorbents, J. Colloid Interface Sci. 361 (2011) 594–602.

[11] N. Gartmann, C. Schütze, H. Ritter, and D. Brühwiler,The effect of water on the functionalization of mesoporous silica with 3-aminopropyltriethoxysilane J. Phys. Chem. Lett. 1 (2010) 379–382.

[12] M. Etienne, A. Walcarius, Analytical investigation of the chemical reactivity and stability of aminopropyl-grafted silica in aqueous medium, Talanta 59 (2003) 1173–1188.

[13] P.J.E. Harlick, A. Sayari, Applications of pore-expanded mesoporous silica. 5. Triamine grafted material with exceptional CO_2 dynamic and equilibrium adsorption performance, Ind. Eng. Chem. Res. 46 (2006) 446–458.

[14] V. Zelenak, D. Halamova, L. Gaberova, E. Bloch, P. Llewellyn, Amine-modified SBA-12 mesoporous silica for carbon dioxide capture: effect of amine basicity on sorption properties, Microporous Mesoporous Mater. 116 (2008) 358–364.

[15] Y. Borodko, J.W. Ager, G.E. Marti, H. Song, K. Niesz, G.A. Somorjai, Structure sensitivity of vibrational spectra of mesoporous silica SBA-15 and Pt/SBA-15, J. Phys. Chem. B 109 (2005) 17386–17390.

[16] X.S. Zhao, G.Q. Lu, A.K. Whittaker, G.J. Millar, H.Y. Zhu, Comprehensive study of surface chemistry of MCM-41 using 29Si CP/MAS NMR, FTIR, pyridine-TPD, and TGA, J. Phys. Chem. B 101 (1997) 6525–6531.

[17] C.S. Srikanth, S.S.C. Chuang, Infrared study of strongly and weakly adsorbed CO2 on fresh and oxidatively degraded amine sorbents, J. Phys. Chem. C 117 (2013) 9196–9205.

[18] Y. Liu, J. Liu, W. Yao, W. Cen, H. Wang, X. Weng, Z. Wu, The effects of surface acidity on CO2 adsorption over amine functionalized protonated titanate nanotubes, RSC Adv. 3 (2013) 18803–18810.

[19] F. Goethals, B. Meeus, A. Verberckmoes, P.V.D. Voort, I.V. Driessche, Hydrophobic high quality ring PMOs with an extremely high stability, J. Mater. Chem. 20 (2010) 1709–1716.

[20] Z. Chen, S. Deng, H. Wei, B. Wang, J. Huang, G. Yu, Polyethylenimineimpregnated resin for high CO_2 adsorption: An efficient adsorbent for CO_2 capture from simulated flue gas and ambient air, Appl. Mater. Interfaces 5 (2013) 6937–6945.

[21] A. Simon, T. Cohen-Bouhacina, M.C. Porté, J.P. Aimé, C. Baquey, Study of two grafting methods for obtaining a 3-aminopropyltriethoxysilane monolayer on silica surface, J. Colloid Interface Sci. 251 (2002) 278–283.

[22] T. A. Michalske, S. W. Freiman, A molecular interpretation of stress corrosion in silica. Nature 295 (1982) 511–512.

[23] T. S. Mahadevan, S. H. Garofalini, Dissociative chemisorption of water onto silica surfaces and formation of hydronium ions, J. Phys. Chem. C 112 (2008) 1507–1515.

[24] M. Caplow, Kinetics of carbamate formation and breakdown, J. Am. Chem. Soc. 90 (1968) 6795–6803.

[25] M. Gil, I. Tiscornia, Ó. Lglesia, R. Mallada, J. Santamaría, Monoamine-grafted MCM-48: an efficient material for CO_2 removal at low partial pressures, Chem. Eng. J. 175 (2011) 291–297.

[26] J.A. Dunne, R. Mariwala, M. Rao, S. Sircar, R.J. Gorte, A.L. Myers, Calorimetric heats of adsorption and adsorption isotherms. 1. O_2, N_2, Ar, CO_2, CH_4, C_2H_6, and SF_6 on silicalite, Langmuir 12 (1996) 5888–5895.

[27] C. Knöfel, J. Descarpentries, A. Benzaouia, V. Zeleňák, S. Mornet, P.L. Llewellyn, V. Hornebecq, Functionalised micro-/mesoporous silica for the adsorption of carbon dioxide, Microporous Mesoporous Mater. 99 (2007) 79–85.

CHAPTER 6

N-(3-TRIMETHOXYSILYLPROPYL)DIETHYLENETRIAMINE GRAFTED KIT-6 FOR CO_2/N_2 SELECTIVE SEPARATION

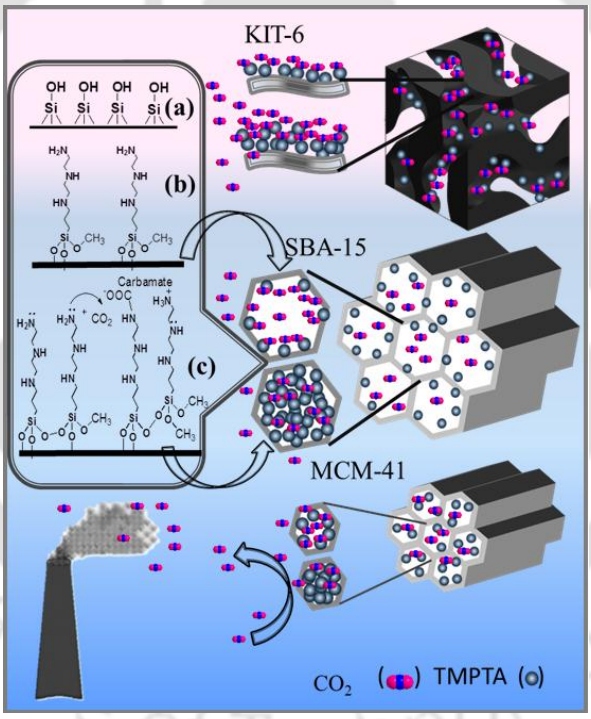

CHAPTER 6

This chapter highlights the importance for selection of suitable support for aminosilane grafting as well as amine concentration. N^1-(3-trimethoxysilylpropyl)diethylenetriamine is grafted on various ordered and commonly used mesoporous silica namely MCM-41, SBA-15 and KIT-6 in both anhydrous and aqueous conditions for CO_2/N_2 adsorption. The functionalized adsorbents are characterized by different analytical techniques. The change in adsorption performance is comprehensively illustrated based on the morphology of mesoporous silica. This part of work has been published in ***RSC Adv. 6 (2016) 898–909****.*

6.1 Introduction

Increasing trends of CO_2 concentration in the atmosphere is creating alarming conditions in the form of global warming across the globe. Especially in last few decades, the rate of CO_2 emission in the form of flue gas is drastically increased from large anthropogenic source, particularly a coal based thermal power plant. This is possibly for industrialization and growth in energy demand across the globe [1,2]. Higher CO_2 concentrations is leading to several environmental issues and therefore, reducing CO_2 emissions from the large anthropogenic source is urgently required.

In order to control the CO_2 concentration in the atmosphere, carbon capture and utilization (CCU)is a promising technology and is becoming indispensable to develop an efficient and cost effective separation process [3]. Amine functionalized ordered mesoporous silica (OMSs) received an attention of a large community in CO_2 capture application [4−8]. The physical

properties of the support and method of grafting play important roles in the performance of the adsorbent. The CO_2sorption capacity of APTES functionalized KIT-6 is directly proportional to the accessible amine sitesas discussed in Chapter 5. Amine intensity in adsorbent can be tailored by increasing the amine chain length present in the aminosilane. Additionally, aqueous solution grafting was more significant for aminosilane loading as well as CO_2 adsorption over anhydrous one.

This Chapter focuses on in-depth understanding in designing the highly CO_2/N_2 selective aminosilane grafted adsorbent. In view of exploiting the presence of more amino nitrogen for capturing more CO_2, this study attempts selection of the best one from the group of commonly used mesoporous adsorbents. In the process of investigation, the traditional MCM-41, SBA-15 and KIT-6 mesoporous silica are synthesized. Thereafter, they are functionalized with N^1-(3-Trimethoxysilylpropyl)-diethylenetriamine by post grafting method in aqueous solution. The adsorbents are characterized by various analytical and spectroscopic techniques and also by CO_2/N_2 uptake measurements under different conditions. The adsorption capacity is compared to decide upon the best support for CO_2 adsorption. The variations in adsorption capacities are also elucidated by grafting mechanism and structural properties of the adsorbents.

6.2 Materials and Methods

6.2.1 *Synthesis of adsorbent*

Traditional mesoporous silica MCM-41 (Small pore hexagonal), SBA-15 (Large pore hexagonal) and KIT-6 (3D cubical) are synthesized by following the earlier reported procedure of Loganathan et al. [9], Wang et al. [10] and Kim et al.[11] respectively. The comprehensive synthesis procedure is explained in Chapter 3, section 3.2.

Ordered mesoporous silica is functionalized by post grafting method, both in dry and aqueous solution. Before grafting, 1.0 g KIT-6 is dried at 120 ºC in vacuum to remove the pre-adsorbed moisture. In a typical dry grafting process, 1.0 g of KIT-6 is dispersed in a 150 ml of dry toluene in a flask. In the resulting solution 'x' mmol of TEMPTA is added and refluxed at 80°C for 24 h. The treated sample is filtered, washed with toluene and ethanol and dried at 80°C in vacuum for 16 h.Similar, synthesis procedure is followed for MCM-41 and SBA-15. The obtained samples are designated as M'x'T, S'x'T and K'x'T of MCM-41, SBA-15 and KIT-6, respectively of base material. In aqueous grafting, after complete dispersion of mesoporous silica in toluene, 0.10 mL Millipore purified water was added and stirred for 3 h to modify the silica surface. The further steps were similar as discussed in dry grafting. The resulting samples are denoted as WM20T, WS20T and WK30T.

6.2.2 *Characterization of adsorbent*

High resolution X-ray powder diffraction spectra are recorded by Bruker D8 advance diffractometer using CuKα radiation operating at 40 kV and 40 mA. Surface micrographs of synthesized OMSs are recorded by field emission scanning electron microscope (FESEM) (Zeiss, Sigma). Transmission electron micrograph (TEM) is recorded using a Jeol (JEM 2100, 200 keV) instrument. Nitrogen adsorption/desorption isotherm is recorded on Quantachrome automated volumetric gas sorption analyzer (autosorb iQ) at –196 ºC. Pore size distribution was analysed by Barrett-Joyner-Halenda (W_{BJH}) method from the N_2 desorption branch. Thermal analysis and aminosilane present in the adsorbents are analyzed by thermogravimetry (TG,Netzsch) analyzer.

CO_2/N_2 adsorption measurements are performed in high pressure volumetric gas adsorption apparatus (iSorbHP1-XKRLSPN100). A sample weight of ~500 mg is loaded into a sample

holder and fitted with instrument. Before analysis, pre-adsorbed moisture and gases are removed by degassing the adsorbent at 110 ºC for 3 h in ultra-high vacuum and the actual weight of adsorbent is measured. CO_2/N_2 adsorption measurement is conducted at 30, 45, and 60 ºC.

6.3 Results and Discussion

6.3.1 *X-ray diffraction analysis*

The small angle X-ray diffraction patterns before and after TMPTA grafted MCM-41, SBA-15 and KIT-6 are shown in Figure 6.1. In diffraction spectra, peaks observed at 2.6º (100), 0.90º (100) and 0.93º (211) for MCM-41, SBA-15 and KIT-6 mesoporous silica, receptively clearly indicates that the synthesized OMSs are highly ordered in nature with corresponding hexagonal, hexagonal and la3d bicontinuous cubic lattice structure [9−12]. After grafting of TMPTA, peak intensity is significantly reduced in MCM-41 and sparsely reduced in SBA-15 and KIT-6 (Figure 6.1). This is possibly due to complete pore filling in MCM-41 and partial pore filling in SBA-15 and KIT-6 [13]. In addition, the peaks (110, 200), (110, 200) and (211) are diminishing after grafting of TMPTA in MCM-41, SBA-15 and KIT-6, respectively. Thus, with increasing amine concentration in the solution, peak intensity is decreased in all the adsorbents. In case of aqueous grafted adsorbent (Figure 6.1), intensity of the major peak is drastically reduced due to higher aminosilane loading.

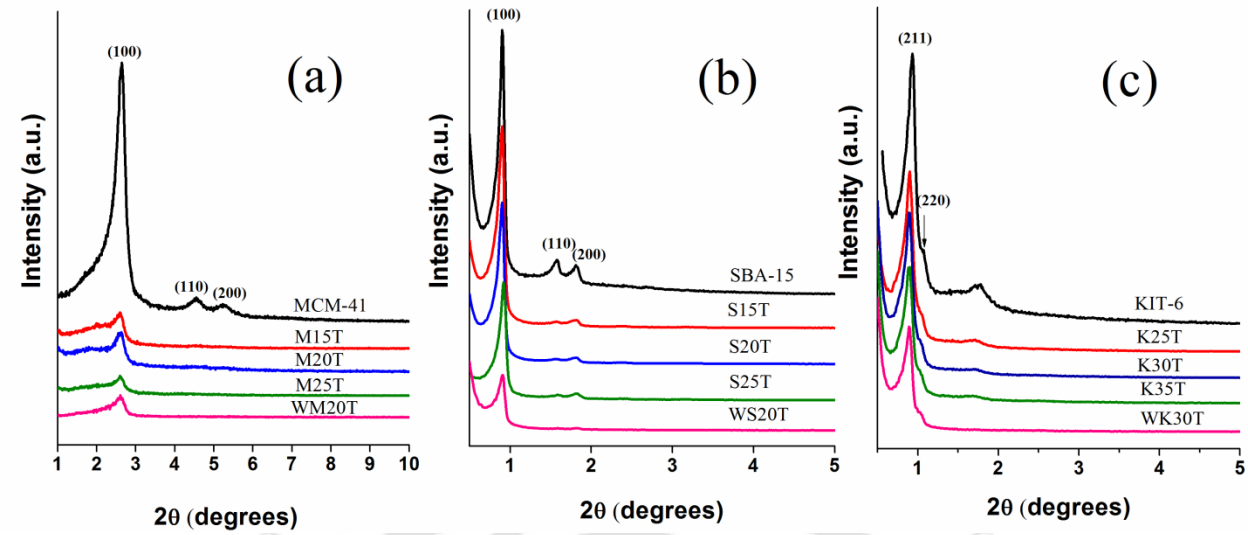

Figure 6.1 X-ray diffraction pattern of TMPTA grafted (a) MCM-41 (b) SBA-15 and (c) KIT-6

6.3.2 *Electron micrograph*

Figure 6.2 shows the corresponding FESEM and TEM micrograph of pure MCM-41, SBA-15 and KIT-6. As seen in Figure 6.2(a), MCM-41 exhibits monodispersed thin platelets with average particle size ~ 0.6 – 1.0 μm [9]. Figure 6.2b shows that synthesized SBA-15 is a rod shaped particle structure in the form of a highly ordered bundle [12]. KIT-6 is seen as a particle with average size ~1 − 2 μm as shown in Figure 6.2c [13]. TEM micrographs of MCM-41, SBA-15 and KIT-6 clearly show the highly ordered structure of the synthesized material as reported in literature.The average pore size of MCM-41, SBA-15 and KIT-6 from the TEM micrograph is ca. 2 nm, 6.6 nm and 6.6 nm, respectively.

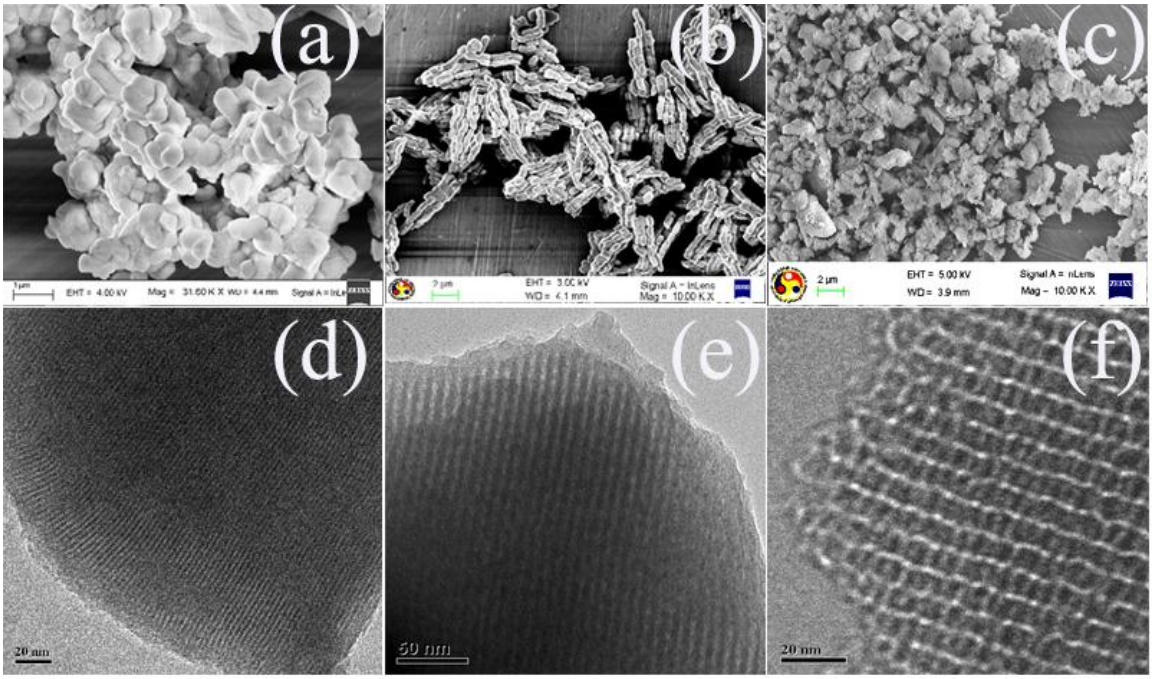

Figure 6.2 FESEM micrograph of (a) MCM-41 (b) SBA-15, (c) KIT-6 and TEM micrograph of (d) MCM-41 (e) SBA-15 and (f) KIT-6 mesoporous silica

6.3.3 *N_2 adsorption/desorption*

The nitrogen adsorption/desorption isotherm and pore size distribution of pure and TMPTA grafted OMSs are shown in Figure 6.3 and physical properties are summarized in Table 6.1. All the OMSs demonstrate the type IV isotherm which is the general characteristic of mesoporous (2–50 nm) material [9,10,13,14]. SBA-15 and KIT-6 show the type H1 hysteresis loop, which is characteristic of material with interconnected large cylindrical pore geometry and high degree of pore size uniformity [15]. However, MCM-41 does not show any hysteresis, which is mainly due to the presence of narrow slit like pores in the material with pore size close to micropore range [15]. The specific surface area (S_{BET}) of mesoporous MCM-41 (2.2 nm), SBA-15 (6.6 nm) and KIT-6 (6.6 nm) are 1492, 857 and 860 m^2/g, respectively. After anhydrous aminosilane grafting

on MCM-41, S_{BET} and pore volume are sharply reduced whereas S_{BET} of SBA-15 and KIT-6 approximately become 2/5th of the original. This is obviously caused by the aminosilane grafting in the channels and internal mesoporous surface [10]. But, approximately 50% of the pore volume of SBA-15 and KIT-6 remain empty. The surface area and pore volume of MCM-41, SBA-15 and KIT-6 are sharply reduced after aqueous aminosilane grafting (Table 6.1) due to higher amount of aminosilane grafting in presence of water [6]. It may be noticed that pore diameters of hexagonal MCM-41 and SBA-15 are highly reduced after aqueous aminosilane grafting whereas that of KIT-6 is not much affected. This is because of the presence of inter-connected porous channels in KIT-6.

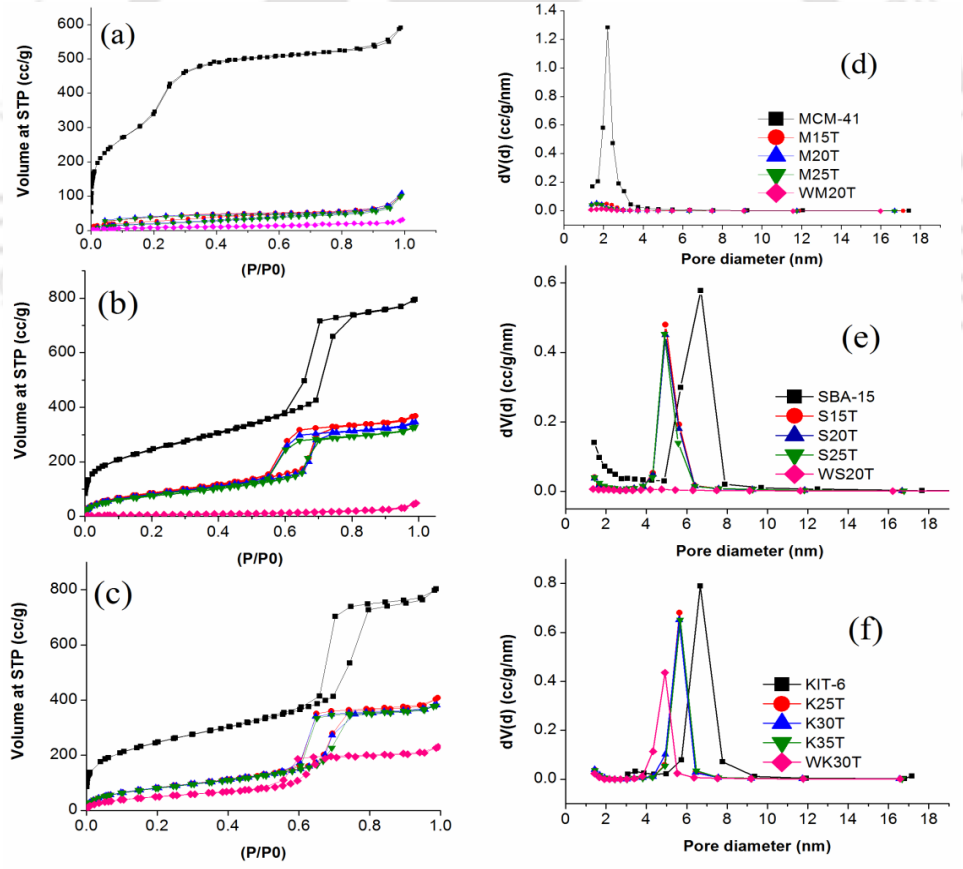

Figure 6.3 N_2 adsorption/desorption before and after TMPTA grafting of (a) MCM-41 (b) SBA-15, (c) KIT-6 at −196 ºC and BJH pore size distribution of (d) MCM-41 (e) SBA-15 and (f) KIT-6 adsorbents

Table 6.1 Textural properties of the TMPTA grafted OMSs

OMSs	Specific surface area S_{BET} (m^2/g)	Pore volume V_t (cc/g)	Pore diameter W_{BJH} (nm)
MCM-41	1492	0.91	2.2
M15T	107	0.16	2.1
M20T	82	0.16	1.6
M25T	77	0.16	1.6
WM20T	31	0.005	1.6
SBA-15	857	1.23	6.6
S15T	321	0.57	4.9
S20T	301	0.53	4.9
S25T	281	0.50	4.9
WS20T	24	0.007	1.35
KIT-6	860	1.24	6.6
K20T	316	0.61	5.6
K25T	312	0.61	5.6
K30T	310	0.59	5.6
K35T	305	0.59	5.6
WK30T	190	0.36	4.9
WK30T	55	0.12	4.3

6.3.4 *FTIR analysis*

The mechanism of aminosilane grafting over OMSs and CO_2 interaction with functionalized adsorbent is discussed through the IR–spectra as shown in Figure 6.4. Surface properties of MCM-41, SBA-15 and KIT-6 before grafting are compared using IR- spectra. In all the OMSs, a peak with a wide shoulder 3750 – 3400 cm^{-1} ascribes the presence of hydrogen-bonded silanol group (Si–OH) present on the surface [16]. Other peaks at 1250 – 1040 cm^{-1}, and ~ 799 cm^{-1} assign the asymmetric and symmetric stretching vibration of Si–O–Si silanol bridge [16]. The peaks at 960 cm^{-1} and ~1620 cm^{-1} represent the free silanol groups and adsorbed water present on the silica surface [17,18]. After TMPTA grafting in OMSs, some new peaks are evolved and some peaks are disappeared in the spectra. The peak corresponding to 960 cm^{-1} is completely disappeared in the aminosilane grafted adsorbents because of grafting of aminosilane with the

free silanol group present on the surface. The bands at 2940 – 2880 cm^{-1} and 1410 cm^{-1} are attributed to C–H and C–N stretching of aminosilane, respectively [14,18]. The peaks at 1630, 1580 and 1309 cm^{-1} are associated with chemical reaction between CO_2 and amine and formation of ammonium ions (NH_3^+), carbamate $(C{=}O{=}C)^-$ and $NCOO^-$ skeletal vibration, respectively [19].

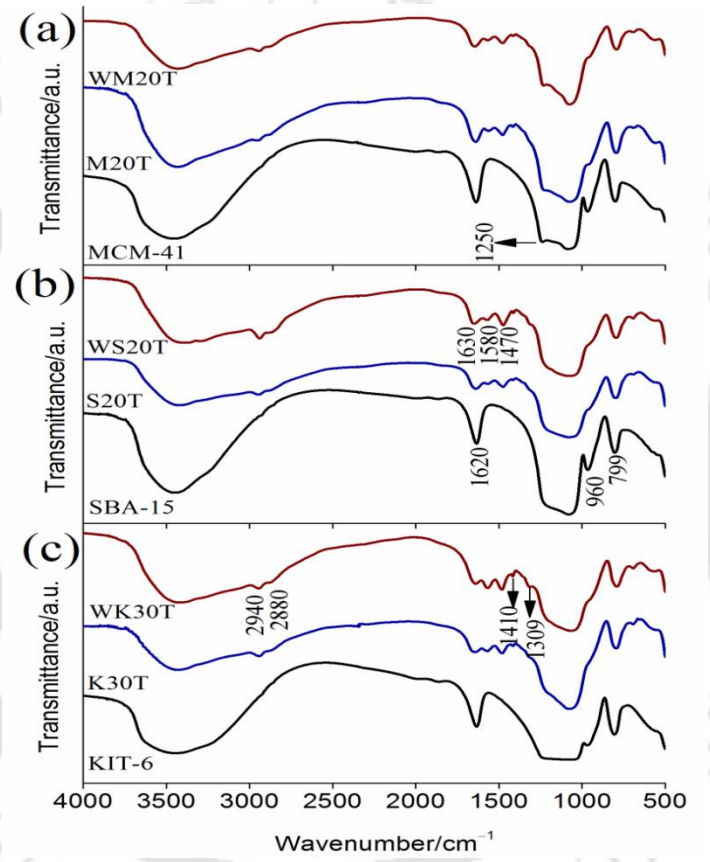

Figure 6.4 IR-spectra of pure and TMPTA grafted (a) MCM-41 (b) SBA-15 and (c) KIT-6

6.3.5*CO_2/N_2 adsorption on MCM-41, SBA-15 and KIT-6*

The selection of appropriate mesostructured support can substantially reduce the size of the capture equipment and the operational cost. The CO_2 sorption capacity of sorbent is a primary objective in designing the separation process. Thus, initially CO_2 adsorption is performed on

pure OMSs at different temperatures to understand the effect of aminosilane loading. Before adsorption experiment, OMSs are degassed at 150 ºC for 3 h in ultra-high vacuum to remove the pre-adsorbed moisture and CO_2. The CO_2 adsorption isotherms on MCM-41, SBA-15 and KIT-6 at different temperatures 30, 45 and 60 ºC under pressure range up to 1 bar are shown in Figure 6.5. The equilibrium adsorption capacity (q_e) almost linearly increases with increasing the pressure over all the OMSs. The following trend of q_e is observed for different OMSs: SBA-15(0.74 mmol CO_2/g) > KIT-6 (0.64 mmol CO_2/g) > MCM-41 (0.56 mmol CO_2/g) at 30ºC and 1 bar. The lowest q_e of MCM-41 even after the highest S_{BET} compared to SBA-15 and KIT-6 is possibly for different surface properties. SBA-15 (3.4 – 8.5 OH/nm^2) [10] contains more surface silanol than MCM-41 (2.5 – 3.0 OH/nm^2) [16] that resulted in the highest q_e. KIT-6 possibly contains intermediate number of silanol groups on the surface. The adsorption capacity is strongly influenced by temperature. The amount of CO_2 adsorbed on MCM-41 is decreased with increase in temperature and similar trends are observed with SBA-15 and KIT-6 as shown in Figure 6.5 [9,20].

The N_2 adsorption isotherm on MCM-41, SBA-15 and KIT-6 under pressure range 1 bar is shown in Figure 6.5. The q_e is linearly increases with pressure as per the following order MCM-41 (0.04 mmol N_2/g) ~ SBA-15 (0.04 mmol N_2/g) < KIT-6 (0.05 mmol N_2/g) at 30 °C and 1 bar.

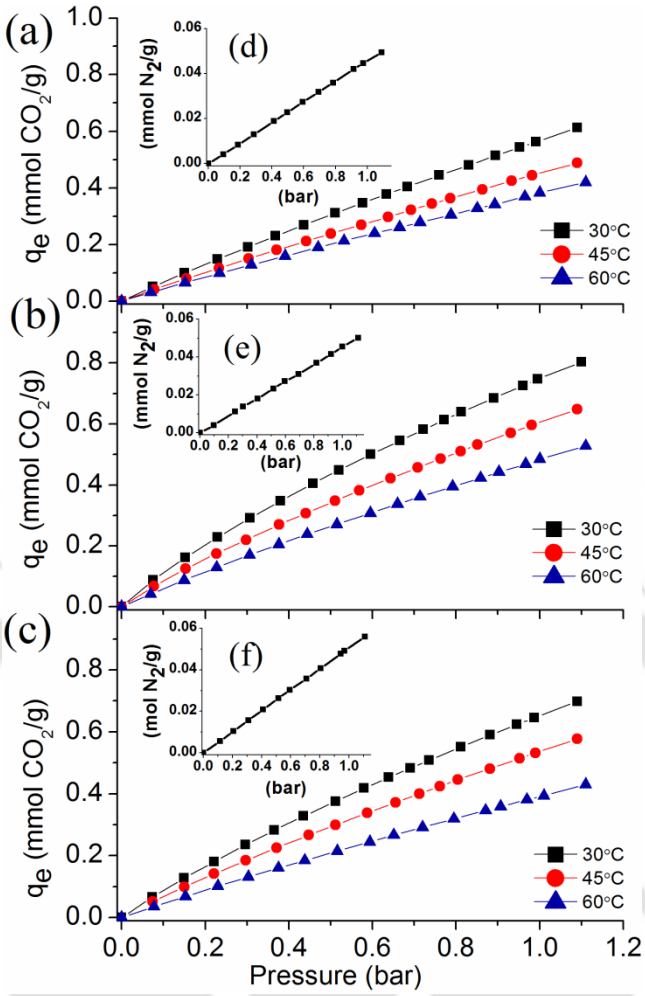

Figure 6.5 CO_2 adsorption on (a) MCM-41, (b) SBA-15, and (c) KIT-6 and corresponding N_2 adsorption in (d), (e) and (f), respectively at 30ºC

6.3.6*Effect of aminosilane concentration*

In order to understand the effect of aminosilane concentration in the solvent on grafting capacity as well as on q_e, a series of experiments are performed by varying the TMPTA to OMSs ratio and the results are summarized in Figure 6.6. The hexagonal structured MCM-41 and SBA-15 show maximum CO_2 q_e for 2:1 (TMPTA: OMS) ratio. But, in case of three dimensional KIT-6,

3:1 (TMPTA: OMS) ratio gives the maximum adsorption capacity. This q_e is reduced marginally with higher concentration. The TMPTA intensity at the internal surface is increased but the active site is reduced due to overlapping with each other [4,21,22]. The degree of grafting on OMS is in the following order KIT-6 > SBA-15 > MCM-41. Diffusional resistance and pore blocking can control the movement of amine into the interior of the pore. Presence of interconnected pores in KIT-6 reduces the diffusional resistance and thereby reduces the hindrance of the movement of amine for grafting [7]. This in turn reduces the pore blocking also.

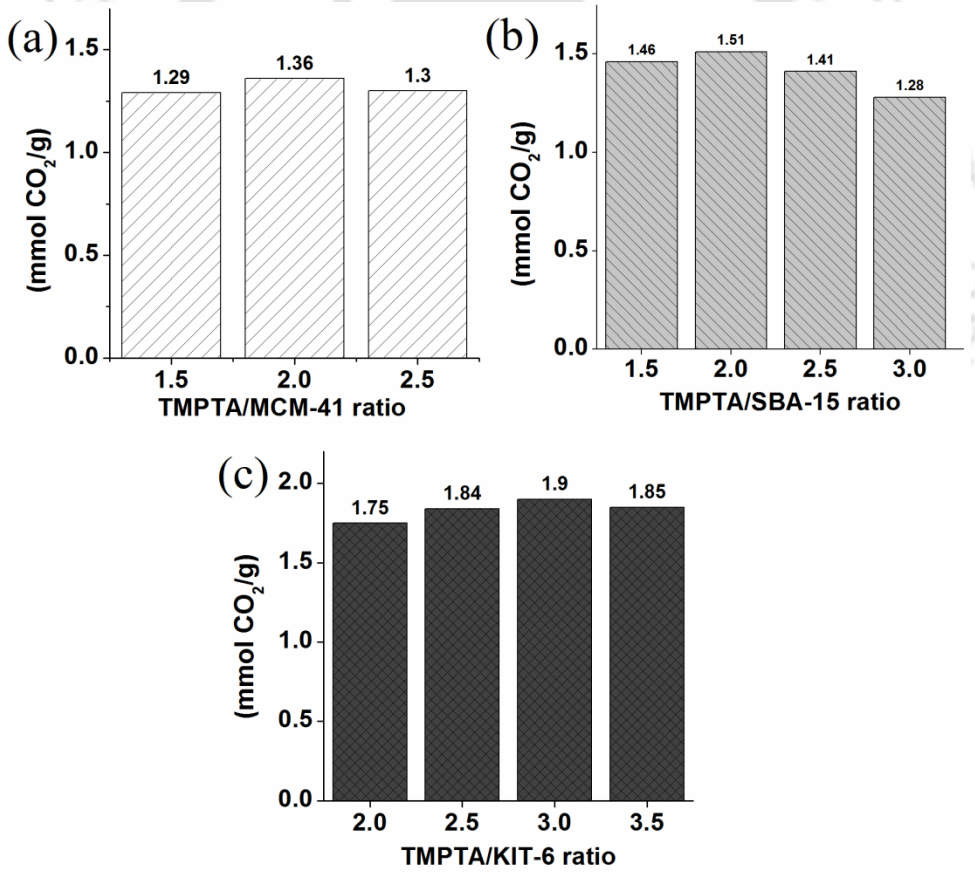

Figure 6.6 Effect of aminosilane (TMPTA) to OMSs ratio on CO_2 adsorption

Extracted information from anhydrous grafting is used further for aqueous grafting as the latter is a more efficient way to graft the aminosilane in OMSs. In the present study, water to OMSs ratio (0.1) in solution is maintained during grafting of aminosilane. The q_e of aqueous grafted adsorbent (WM20T and WS20T) is reduced to 0.66 and 0.64 mmol CO_2/g from 1.36 (M20T) and 1.54 (S20T) mmol CO_2/g of adsorbent as shown in Figure 6.7. Whereas, the q_e of WK30T is increased from 1.89 mmol CO_2/gg to 2.59 mmol CO_2/g at 30 ºC and 1 bar. This suggests that the surface architecture and mesopore size of OMS affects the degree of silylation and q_e. However, aminosilane loading is higher during aqueous grafting than anhydrous as explained in the section below [4,6]. The reduction in q_e of aqueous grafted adsorbents WM20T and WS20T is possibly due to plugging the pores of MCM-41 and SBA-15 through inter aminosilane condensation reaction.

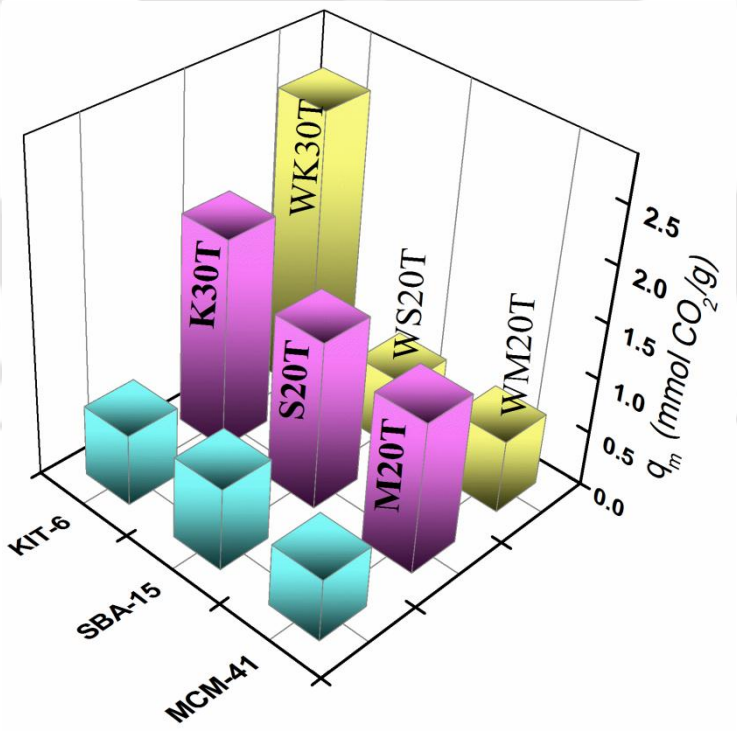

Figure 6.7 Effect of water used in aminosilane grafting and CO_2 adsorption capacity

Table. 6.2 Summary of TMPTA grafted OMSs as adsorbent

OMSs	q_e (mmol CO_2/g) **30 ºC**	**60 ºC**	(mmol N/g)	% amine efficiency mmol(CO_2)/mmol(N)	Selectivity at 30 ºC	ΔH_{ads} (kJ/mol)
MCM-41	0.56	0.39	—	—	14	18
SBA-15	0.74	0.48	—	—	23	20
KIT-6	0.64	0.40	—	—	15	20
M20T	1.36	1.14	3.72	36.6	491	31
WM20T	0.67	—	4.70	14.2	—	—
S20T	1.54	1.18	3.98	38.7	635	67
WS20T	0.63	—	5.46	8.7	—	—
K30T	1.89	1.73	4.25	44.8	793	42
WK30T	2.59	2.38	5.73	45.1	873	33

q_e: Equilibrium adsorption capacity at 1 bar; Selectivity: Calculated at 0.15:0.85 partial pressure ratio, ΔH_{ads}: Enthalpy of adsorption

6.3.7 *Effect of temperature on CO_2/N_2 adsorption*

Sorption temperature as well as capacity of adsorbent are the essential parameters in designing the adsorption process. In the present section, CO_2/N_2 adsorption isotherm on M20T, S20T and K30T at (30, 45, and 60) ºC in the pressure range of 0 – 1.0 bar are performed and the results are depicted in Figure 6.8. The CO_2 q_e of all the aminosilane grafted adsorbents progressively decreases with increasing temperature. The maximum q_e is obtained at 30 ºC as per the following order K30T (1.89 mmol CO_2/g) > S20T (1.54 mmol CO_2/g) > M20T (1.36 mmol CO_2/g). When the temperature is increased to 60 ºC, q_e becomes 1.63, 1.04, 1.01 mmol CO_2/g of K30T, S20T and M20T respectively at 1 bar.

The similar trends of CO_2 adsorption isotherm over aqueous grafted adsorbent (WK30T) are observed at different temperatures. However, reduction in CO_2 adsorption capacity of WK30T with temperature is much less as shown in Figure 6.9. The q_e is 2.59, 2.47 and 2.38

mmol CO_2/g at 30, 45 and 60 ºC, respectively. The values are much higher than M20T and S20T. Table 6.2, summarizes the maximum q_e and compares with other TMPTA grafted mesoporous silica. As can be seen from the table, WK30T is better performing with respect to other adsorbents. It is further observed that larger pore containing mesoporous silica gives better q_e after TMPTA aqueous grafting compared to smaller size mesoporous silica [5,23−25].

Dual-site Langmuir (DSL) model provides excellent agreement between experimental and predicated adsorption capacity [26,27]. In present study, multi temperature DSL model (equation 6.1) is used to fit the experimental data of TMPTA grafted mesoporous silica for CO_2. Where, q_e^1 and q_e^2 are the saturation capacities (mmol CO_2/g adsorbent) at sites 1 and 2 respectively. In DSL equation *b* and *P* are the Langmuir parameter (bar^{-1}) and pressure (bar), respectively.

$$q_e = \frac{(q_e^1 b_1 P)}{(1+ b_1 P)} + \frac{(q_e^2 b_2 P)}{(1+ b_2 P)} \quad (6.1)$$

The Langmuir parameters follow the temperature dependence as per equation 2:

$$b_1 = b_o \exp\left(b_1^{(1)}/T\right); \qquad b_2 = b_o \exp\left(b_2^{(2)}/T\right) \quad (6.2)$$

Where T is the temperature in Kelvin.

Enthalpy of adsorption (ΔH_{ads}) is calculated at different adsorption capacities (mmol CO_2/g adsorbent) by Clausius–Clapeyron equation as follows:

$$-\Delta H_{ads} = R\frac{\partial(lnP)}{\partial(1/T)}\Big|_q = R\left(\frac{b_1^{(1)} q_e^1 b_1 (1+b_2)^2 + b_1^{(1)} q_e^2 b_2 (1+b_1)^2}{q_e^1 b_1 (1+b_2)^2 + q_e^2 b_2 (1+b_1)^2}\right) \quad (3)$$

The DSL model (continuous line) (Figure 6.8 and 6.9) show excellent agreement with the experimental data (solid points) at different temperatures.

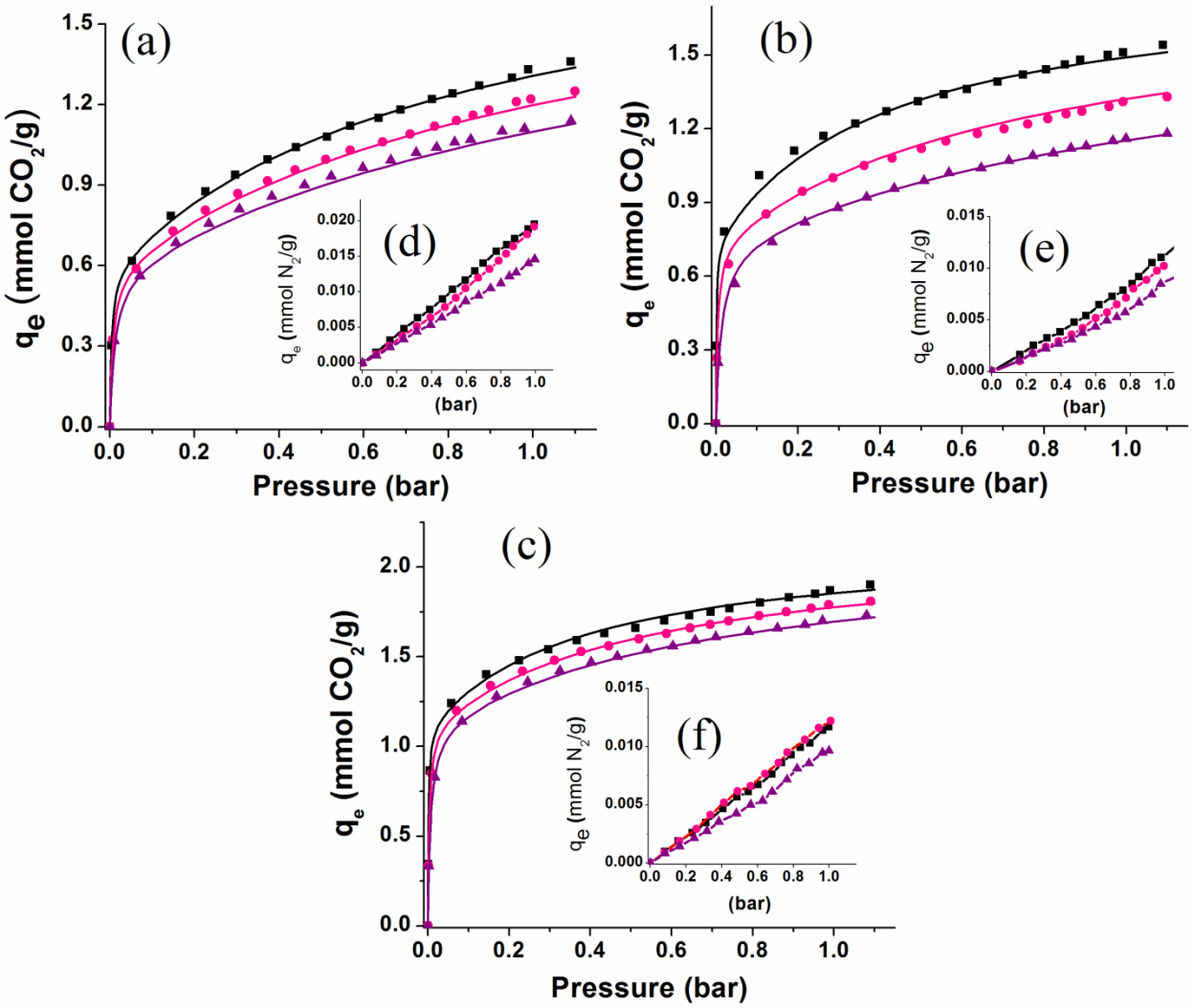

Figure 6.8 CO_2 adsorption isotherms of (a) M20T (b) S20T and (c) K30T and N_2 adsorption isotherm of (d) M20T, (e) S20T and (f) K30T at different temperatures (■-30 ºC) (●-45 ºC) and (▲-60 ºC)

The reduction in CO_2 adsorption capacity over amine grafted adsorbents can be explained by the classical adsorption mechanism. The CO_2 adsorption on amine grafted OMSs is an exothermic process and it becomes more favourable at lower temperature. Compared to some other aminosilane functionalized adsorbent, similar behaviour is observed in this section [12,14,25]. However, Sayari et al.[28] showed that the q_e of TMPTA grafted PE-MCM-41 was somewhat increased with increasing the temperature. Higher temperature facilitates the diffusion of CO_2 in aminosilane layer and exposed more active amine sites for interaction.

The similar adsorption behaviour is also observed in polyamine impregnated mesoporous silica [13,21,29]. But in the present case, CO_2 diffusion in aminosilane layer with temperature is dominated by the desorption process and reduces the capacity at higher temperature.

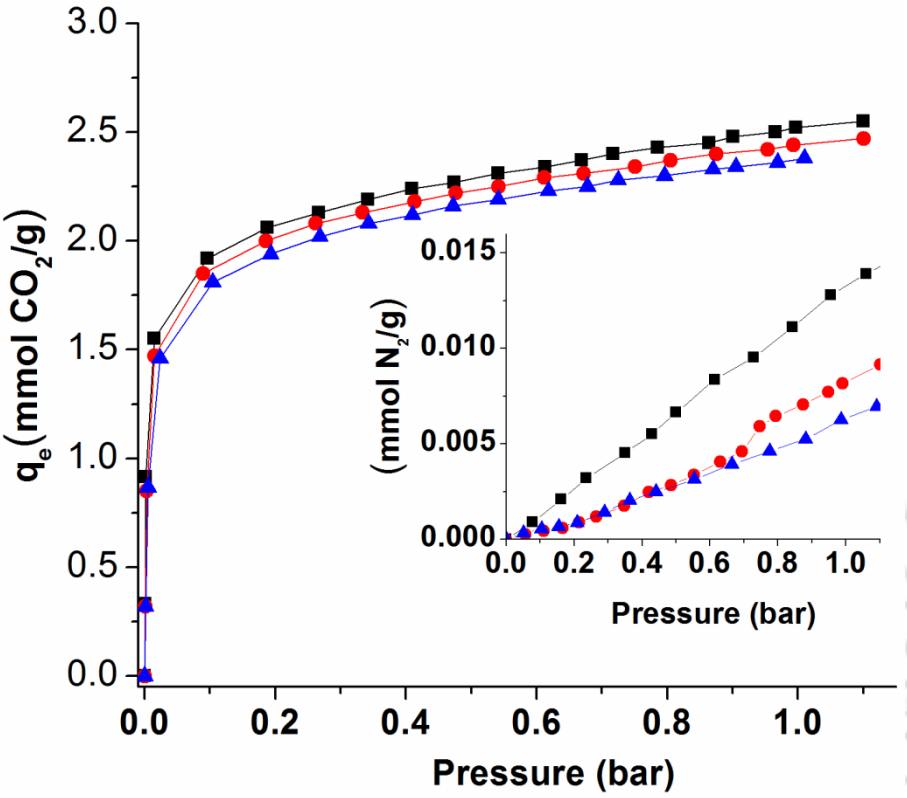

Figure 6.9 CO_2/N_2 adsorption isotherms for WK30T at different temperatures (■-30 ºC) (●-45 ºC) and (▲-60 ºC)

During grafting, aminosilane covers a small fraction of the surface [23]. Sorption capacity of amine functionalized adsorbent is the combined effect of chemical and physical adsorption [28]. At low CO_2 partial pressure (~ till 0.15 bar), the sorption capacity of M20T, S20T and K30T is increased sharply which is mainly for chemical interaction between CO_2 and grafted aminosilane [13,29]. Moreover, at higher CO_2 partial pressure sorption capacity gradually increases with pressure and it is probably for physical adsorption with the surface [28].

Low q_e of N_2 indirectly indicates the high CO_2/N_2 selectivity of the adsorbent. Figures 6.8d, 6.8e and 6.8f show the effect of temperature (30, 45 and 60 ºC) on N_2 adsorption performance

over M20T, S20T and K30T. Nitrogen q_e at 30 ºC and 1 bar is 0.019, 0.012 and 0.011 mmol N_2/g of M20T, S20T and K30T adsorbent, respectively. There is no major difference in q_e of all the adsorbents and moreover not much affected with adsorption temperature. In case of aqueous grafted WK30T, q_e is 0.013, 0.008 and 0.007 mmol N_2/g adsorbent at 30, 45 and 60 ºC at 1 bar, respectively as shown in Figure 6.9b. The adsorption capacity of N_2 in amine grafted mesoporous silica is much lower than other adsorbents like MOF and polymeric adsorbent [26,30,31] which makes amine functionalized mesoporous silica a lucrative option over other adsorbents. Additionally, the q_e of CO_2 is much higher than that of N_2 at all temperatures in all the adsorbents because of the greater quadrupole moment and polarizability of CO_2 (4.30×10^{-26} esu cm^2 and 29.11×10^{-25} cm^3, respectively) than N_2 (1.52×10^{-26} esu cm^2 and 17.403×10^{-25} cm^3, respectively) [32].

The important parameter before selection of any adsorbent is the selectivity. It is defined by $S_{x/y} = (q_{ei}/q_{ej})/ (p_i/p_j)$; Where q_{ei}, q_{ej} and p_i, p_j are the amounts adsorbed and corresponding partial pressure for component *i* and *j*, respectively [33]. CO_2 and N_2 (~ 15: 85) are the major components of flue gas emitted from coal based thermal power plant. On the basis of this composition, the selectivity at 30 ºC is 14, 23 and 15 of MCM-41, SBA-15 and KIT-6, respectively as shown in Table 6.2. After TMPTA grafting, selectivity is improved to 491, 635, 793 and 873 of M20T, S20T, K30T and WK30T, respectively.

6.3.8 *Enthalpy of adsorption*

Enthalpy of adsorption (ΔH_{ads}) is calculated by Clausius–Clapeyron relation. The ΔH_{ads} values for CO_2 on pure MCM-41, SBA-15 and KIT-6 are ca. 18 kJ/mol, 20 kJ/mol and 18 kJ/mol and constant with loading. At zero coverage of CO_2 adsorption over TMPTA grafted adsorbents; $-\Delta H_{ads}$ value is much higher than that of pure OMSs (Figure 6.10) [5,10]. This is due to the chemical interactions between CO_2 and amine present on the surface as earlier is

confirmed by several authors [10,14,25,28]. The $-\Delta H_{ads}$ values are summarized in the Table. 6.2. A sharp reduction in enthalpy is observed with increase in loading at higher pressure. It confirms the fact that the amine functionalized silica contains two different types of sites for CO_2 adsorption as earlier was explained by Sayari et al.[34] which are namely amine and bare silica surface. In the initial phase, higher enthalpy value is for major contribution from chemisorption with amine and later the lower value is because of the major contribution from physical interaction with the surface due to exhaustion of amine.

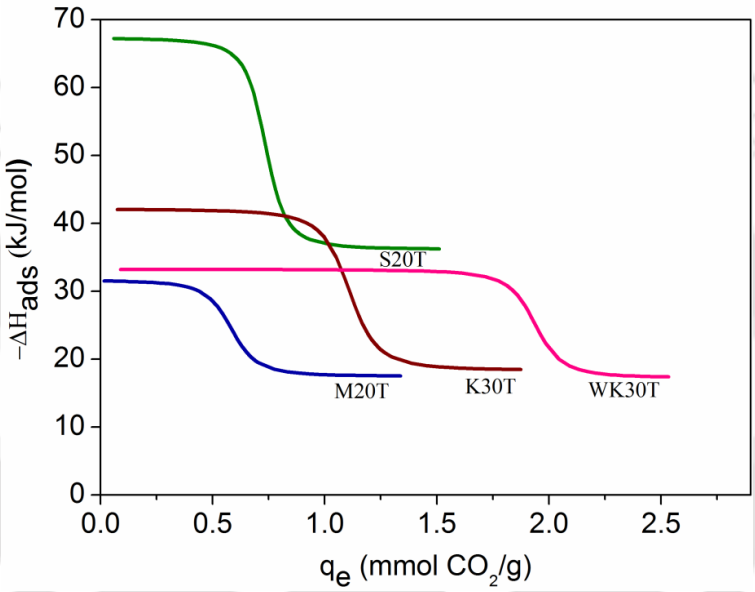

Figure 6.10 Enthalpy curve of CO_2 adsorption over M20T, S20T, K30T and WK30T adsorbents

6.3.9*TGA analysis*

The amount of TMPTA present in the adsorbents is analyzed by TG analysis [17,35]. Figure 6.11 shows the TGA curves of aminosilane grafted MCM-41, SBA-15 and KIT-6 and the corresponding differential thermal gravimetric (DTG) curves. TGA curves clearly show that the organic aminosilane is completely degraded within 750 ºC. A sharp weight loss in all the

adsorbents is observed in the initial temperature range 30 – 150 ºC, which is attributed to the loss of moisture and adsorbed gases. The three peaks observed in Figure 6.11 in the ranges (150 – 250), (250 – 500) and (500 –750) ºC are due to decomposition of grafted aminosilane [6,10,25,35]. The corresponding amine group numbers (mmol N/g-adsorbent) are summarized in Table 6.2. The amine groups available for CO_2 during adsorption is the highest in KIT-6 and the least in MCM-41 for both dry and anhydrous grafted adsorbents. During grafting in MCM-41 and SBA-15 the cylindrical pore mouth gets easily plugged by TMPTA. But in KIT-6, interconnected channel provides better surface accessability for grafting of guest molecule and accommodates higher amount of amine. The similar phenomenon was also reported by Zeleňák et al.[7] with aminopropyl grafting over different porous structures.

Amine efficiency is the ratio of CO_2 adsorbed (mmol CO_2/g) to amine group number (mmol N/ g) present in the adsorbent [12,24,25]. Hence, theoretical maximum possible amine efficiency is 0.5. TMPTA consists of one primary amine and two secondary amines. Primary and secondary amine of TMPTA reacts with CO_2 and form carbamate with zwitterion intermediate where two amines react with one molecule of CO_2 under dry condition [12]. Efficiency of grafted aminosilane in CO_2 adsorption increases with increase in the pore diameter of OMSs and it follows the order K30T > S20T > M20T. In case of hexagonal aqueous grafted adsorbents (WM20T and WS20T), efficiency is decreased sharply even after higher amine loading. This indicates that the hexagonal pore has a diffusional limitation for CO_2 adsorption possibly due to pore blocking by condensation reactions between aminosilanes during grafting (Figure 6.12). The similar trends were observed by several authors in recent study over amine functionalized adsorbent [13,20]. In case with WK30T, amine group number and CO_2 adsorption capacity are proportionally increased. It is due to the mesoporous inter connected channels present in KIT-6, thus reducing the said limitation.

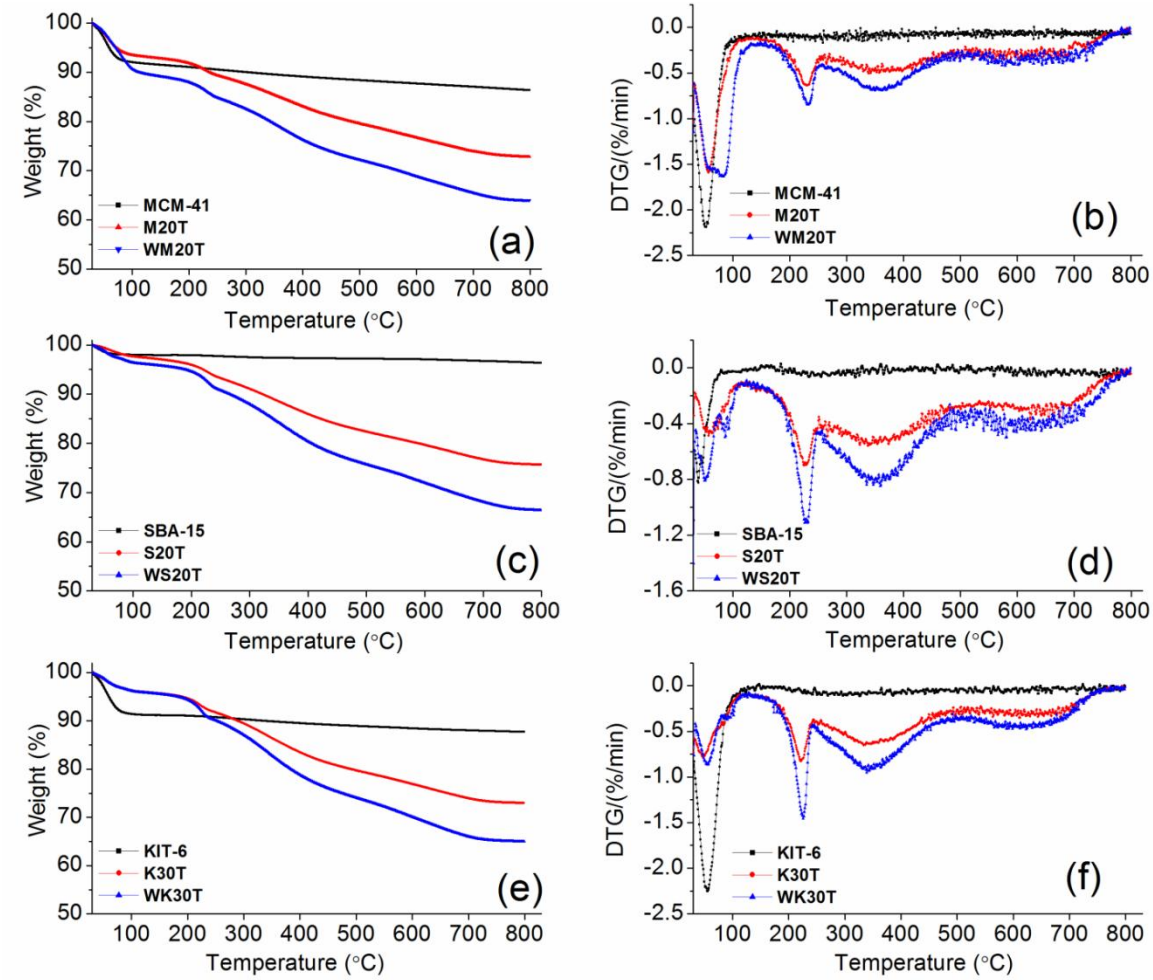

Figure 6.11 Thermogravimetric (TG) analysis curves of pure and TMPTA grafted (a) MCM-41, (c) SBA-15 and (e) KIT-6 and corresponding differential thermal gravimetric (DTG) analysis in (b) MCM-41, (d) SBA-15 and KIT-6.

6.3.10 *Grafting mechanism*

The main prerequisite in developing an efficient amine functionalized adsorbent is the selection of base mesoporous silica. The aminosilane is grafted on high surface area OMSs with different structure (hexagonal, cubical), pore size and pore volume. The q_e of amine functionalized adsorbent is directly associated with accessible amine groups for CO_2 during adsorption.A schematic of grafting procedure is shown in Figure 6.12. Figure 3 shows the

synthesized support MCM-41 (2.2 nm), SBA-15 (6.6 nm) and KIT-6 (6.6 nm) have different pore sizes. All the mesoporous silica are enriched with surface silanol groups and participate in grafting reaction. In anhydrous grafting, aminosilane directly reacts with surface silanol groups by condensation reaction (Figure 6.12b) and is grafted over the surface. However, lower adsorption capacity of M20T is possibly for lower amine loading due to smaller pore size of MCM-41 as is reflected from Table 1.

TMPTA is highly sensitive to moisture. In the presence of water, TMPTA forms a cluster *via*. hydrolysis reaction [36]. However, water also gets adsorbed on the negatively charged siloxane bridge of mesoporous silica and raptures the surface as explained in Chapter 5, section 5.3. In this process, it creates new surface silanol groups on the surface, which also promotes the aminosilane grafting capacity. The q_e of the aqueous grafted adsorbents are summarized in Table 6.2 and the grafting mechanism is shown in Figure 6.12. The higher accumulation of aminosilane in WM20T, WS20T and WK10T is the result of the combined effect of increment in surface silanol groups and hydrolysis reaction between aminosilanes. During grafting, aminosilane forms a cluster in internal surface of the adsorbents [36]. The q_e of WM20T and WS20T is reduced but the same is increased in WK10T, even if the aminosilane loading is increased in all the adsorbents as analyzed by TGA analysis. The increments in aminosilane loading are also understood by reduction in surface area and pore volume (Table 6.1).

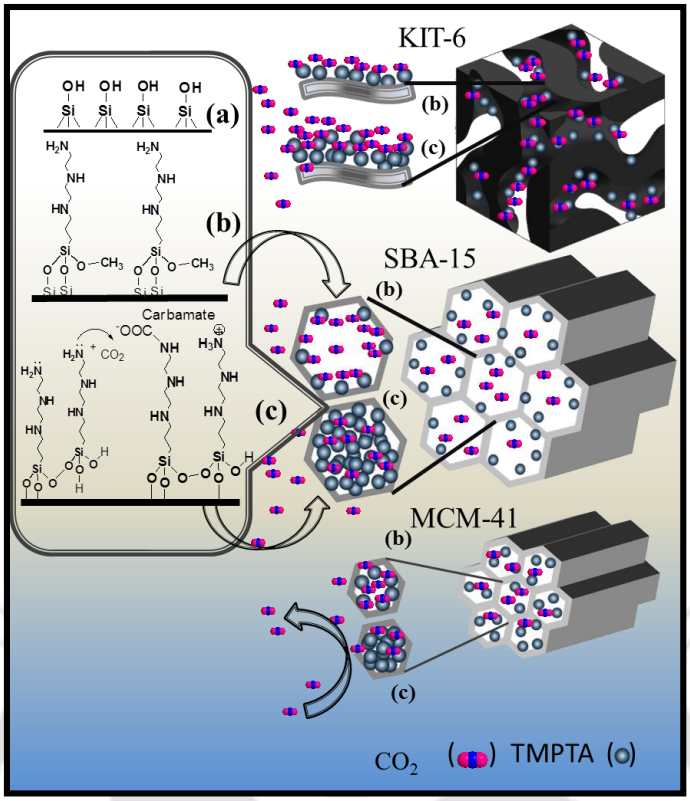

Figure 6.12 Grafting mechanism of aminosilane in different mesoporous silica MCM-41, SBA-15 and KIT-6

The structure and pore size of the support play important roles in the performance of adsorbent. The reduction in adsorption capacity can be correlated with the support structure and pore opening. During aqueous aminosilane grafting, pores of the hexagonal mesoporous silica MCM-41 and SBA-15 are blocked by aminosilane condensation reaction as shown in Figure 6.12 and become a nonporous adsorbent as is also observed by N_2 adsorption/desorption analysis (pore volume becomes zero). The approximately same q_e of WM20T (0.64 mmol CO_2/g) and WS20T (0.62 mmol CO_2/g) corroborate the above statement. During grafting in KIT-6, TMPTA forms a cluster in the channels by condensation and enhances the aminosilane loading. But it does not block the channels during grafting and enhances CO_2 adsorption capacity by increasing the active amine sites. The enhancement in q_e of WK10T is the consequence of the above fact.

6.3.11 *Reusability performance of adsorbents*

In order to have practical applicability, stable sorption capacity in cyclic use is a primary criterion of a good adsorbent. In the present study, 20 adsorption/desorption cycles are studied for M20T, S20T, K30T and WK30T at 30 ºC. After each cycle of adsorption, samples are degassed at 95 ºC for an hour. All the adsorbents showed the stable sorption capacity till 20 cycles (Figure 6.13) as earlier observed with APTES grafted KIT-6. This indicates the stable attachment of aminosilane with the silica surface and no amine loss to the environment [4].

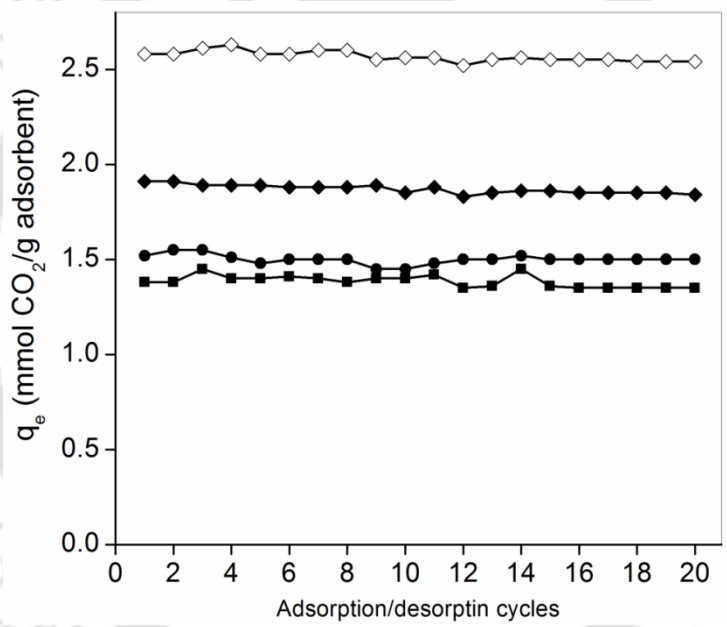

Figure 6.13 Cyclic performance of TMPTA grafted M20T (■), S20T (●), K30T (♦) and WK30T (◊) adsorbents

6.4 Conclusions

In this chapter, a series of ordered mesoporous silica samples namely MCM-41, SBA-15 and KIT-6 are synthesized and functionalized with TMPTA in both anhydrous and aqueous solution. The adsorption capacity of anhydrous grafted adsorbents follows the order as K30T

(1.89 mmol CO_2/g) > S20M (1.54 mmol CO_2/g) > M20T (1.36 mmol CO_2/g) at 30 ºC and 1 bar. Adsorption capacity is increased to 2.59 mmol CO_2/g after aqueous grafting over KIT-6, although that for MCM-41 and SBA-15 is sharply reduced. Intermolecular condensation of aminosilane during aqueous grafting blocks the pores and thereby reduces the CO_2 sorption capacity of TMPTA grafted MCM-41 and SBA-15. The CO_2/N_2 selectivity of the KIT-6 based adsorbent is much higher than that of MCM-41 and SBA-15. The lower adsorption capacity as well as selectivity of TMPTA grafted MCM-41 and SBA-15 makes them less favourable during particle application. In addition to CO_2 adsorption, WK30T is easily regenerable at moderate temperature and show good stability for several adsorption/adsorption cycles. However, presence of interconnected channels in KIT-6 eliminates the possibility of pore blocking and illuminates the TMPTA grafted KIT-6 with high CO_2 adsorption capacity and excellent CO_2/N_2 selectivity.

References

[1] Annual energy outlook 2015 with projections to 2040. (http://www.eia.gov/forecasts/aeo/)

[2] F. M. Orr, Jr., CO_2 capture and storage: are we ready? Energy Environ. Sci., 2009, **2**, 449–458.

[3] P. Markewitz, W. Kuckshinrichs, W. Leitner, J. Linssen, P. Zapp, R. Bongartz, A. Schreibera, T. E. Müller, Worldwide innovations in the development of carbon capture technologies and the utilization of CO_2, Energy Environ. Sci., 5 (2012) 7281–7305.

[4] N. N. Linneen, R. Pfeffer, Y. S. Lin, CO_2 adsorption performance for amine grafted particulate silica aerogels, Chem. Eng. J., 254 (2014) 190–197.

[5] T. C. Santos, S. Bourrelly, P. L. Llewellyn, J. W. M. Carneiro, C. M. Ronconi, Adsorption of CO_2 on amine-functionalised MCM-41: experimental and theoretical studies, Phys. Chem. Chem. Phys., 17 (2015) 11095–11102.

[6] P. J. E. Harlick, A. Sayari, Applications of pore-expanded mesoporous silica. 5. triamine grafted material with exceptional CO_2 dynamic and equilibrium adsorption performance, Ind. Eng. Chem. Res., 46 (2007) 446–458.

[7] V. Zeleňák, M. Badaničová, D. Halamová, J. Čejka, A. Zukal, N. Murafa, G. Goerigk, Amine-modified ordered mesoporous silica: Effect of pore size on carbon dioxide capture, Chem. Eng. J., 144 (2008) 336–342.

[8] N. Hiyoshi, K. Yogo, T. Yashima, Adsorption characteristics of carbon dioxide on organically functionalized SBA-15, Microporous Mesoporous Mater., 84 (2005) 357–365.

[9] S. Loganathan, M. Tikmani, A. K. Ghoshal,Novel pore-expanded MCM-41 for CO_2 capture: synthesis and characterization, Langmuir, 29 (2013) 3491–3499.

[10] L. Wang, R. T. Yang, Increasing selective CO_2 adsorption on amine-grafted SBA-15 by increasing silanol density, J. Phys. Chem. C, 115 (2011) 21264–21272.

[11] T.-W. Kim, F. Kleitz, B. Paul, R. Ryoo, MCM-48-like large mesoporous silicas with tailored pore structure: Facile synthesis domain in a ternary triblock copolymer-butanol-water system, J. Am. Chem. Soc., 127 (2005) 7601–7610.

[12] Y. G. Ko, S. S. Shin, U. S. Choi, Primary, secondary, and tertiary amines for CO_2 capture: Designing for mesoporous CO_2 adsorbents, J. Colloid Interface Sci., 361 (2011) 594–602.

[13] W.-J. Son, J.-S. Choi, W.-S. Ahn, Adsorptive removal of carbon dioxide using polyethyleneimine-loaded mesoporous silica materials, Micropor. Mesopor. Mater., 113 (2008) 31−40.

[14] M. R. Mello, D. Phanon, G. Q. Silveira, P. L. Llewellyn, C. M. Ronconi, Amine-modified MCM-41 mesoporous silica for carbon dioxide capture, Microporous Mesoporous Mater., 143 (2011) 174–179.

[15] M. Kruk, M. Jaroniec, Characterization of ordered organic-inorganic nanocomposite materials, Chem. Mater. 13 (2001) 3169−3183.

[16] X. S. Zhao, G. Q. Lu, A. K. Whittaker, G. J. Millar, H. Y. Zhu,Comprehensive study of surface chemistry of MCM-41 using ^{29}Si CP/MAS NMR, FTIR, Pyridine-TPD, and TGA, J. Phys. Chem. B, 101 (1997) 6525–6531.

[17] V. Zelenak, D. Halamova, L. Gaberova, E. Bloch, P. Llewellyn,Amine-modified SBA-12 mesoporous silica for carbon dioxide capture: Effect of amine basicity on sorption properties, Microporous Mesoporous Mater., 116 (2008) 358–364.

[18] C. K. P. Neeli, S. Ganji, V. S. P. Ganjala, S. R. R. Kamaraju D. R. Burri,Effects of template removal on both morphology of mesoporous silica-coated gold nanorod and its biomedical application, RSC Adv., 4 (2014) 14128–14135.

[19] C.S. Srikanth, S.S.C. Chuang, Infrared study of strongly and weakly adsorbed CO_2 on fresh and oxidatively degraded amine sorbents, J. Phys. Chem. C 117 (2013) 9196–9205.

[20] X. Yan, S. Komarneni, Z. Yan, CO_2 adsorption on Santa Barbara Amorphous-15 (SBA-15) and amine-modified Santa Barbara Amorphous-15 (SBA-15) with and without controlled microporosity, J. Colloid Interface Sci., 390 (2013) 217–224.

[21] Q. Wu, S. Chen, H. Liub,Effect of surface chemistry of polyethyleneimine grafted polypropylene fiber on its CO_2 adsorption, RSC Adv., 4 (2014) 27176–27183.

[22] R. Kishor, and A. K. Ghoshal, APTES grafted ordered mesoporous silica KIT-6 for CO_2 adsorption, Chem. Eng. J., 262 (2015) 882–890.

[23] R. Sanz, G. Calleja, A. Arencibia, and E. S. Sanz-Pérez, Amino functionalized mesostructured SBA-15 silica for CO_2 capture: Exploring the relation between the adsorption capacity and the distribution of amino groups by TEM, Microporous Mesoporous Mater., 158 (2012) 309–317.

[24] G. P. Knowles, S. W. Delaney, A. L. Chaffee,Diethylenetriamine[propyl(silyl)]-functionalized (DT) mesoporous silicas as CO_2 adsorbents, Ind. Eng. Chem. Res., 45 (2006) 2626–2633.

[25] L. Zhou, J. Fan, G. Cui, X. Shang, Q. Tang, J. Wang, M. Fan,Highly efficient and reversible CO_2 adsorption by amine-grafted platelet SBA-15 with expanded pore diameters and short mesochannels, Green Chem., 16 (2014) 4009–4016.

[26] P. Mishra, S. Edubilli, B. Mandal, S. Gumma, Adsorption characteristics of metal−organic frameworks containing coordinatively unsaturated metal sites: Effect of metal cations and adsorbate properties, J. Phys. Chem. C 118 (2014) 6847− 6855.

[27] S. García, J. J. Pis, F. Rubiera, C. Pevida Predicting mixed-gas adsorption equilibria on activated carbon for precombustion CO_2 capture, Langmuir, 29 (2013) 6042−6052.

[28] Y. Belmabkhout, A. Sayari, Isothermal versus non-isothermal adsorption-desorption cycling of triamine-grafted pore-expanded MCM-41 mesoporous silica for CO_2 capture from flue gas, Energy Fuels, 24 (2010) 5273–5280.

[29] D. S. Dao, H. Yamada, K. Yogo,Large-pore mesostructured silica impregnated with blended amines for CO_2 capture, Ind. Eng. Chem. Res., 52 (2013) 13810−13817.

[30] M. G. Rabbani, T. E. Reich, R. M. Kassab, K. T. Jackson, H. M. El-Kaderi, High CO_2 uptake and selectivity by triptycene-derived benzimidazole-linked polymers, Chem. Commun., 48 (2012) 1141–1143.

[31] J. Wang, J. Huang, X. Wu, B. Yuan, Y. Sun, Z. Zeng, S. Deng,Effect of nitrogen group on selective separation of CO_2/N_2 in porous polystyrene, Chem. Eng. J., 256 (2014) 390–397.

[32] J.–R. Li, R. J. Kuppler, H.–C. Zhou, Selective gas adsorption and separation in metal–organic frameworks, Chem. Soc. Rev., 38 (2009) 1477–1504.

[33] J.–X. Hu, H. Shang, J.–G. Wang, L. Luo, Q. Xiao, Y.–J. Zhong, W.–D. Zhu,Highly enhanced selectivity and easy regeneration for the separation of CO_2 over N_2 on melamine-based microporous organic polymers, Ind. Eng. Chem. Res., 53 (2014) 11828−11837.

[34] Y. Belmabkhout, G. D. Weireld, A. Sayari, Amine-bearing mesoporous silica for CO_2 and H_2S removal from natural gas and biogas, Langmuir 25 (2009) 13275–13278.

[35] M. Gil, I. Tiscornia, Ó. Iglesia, R. Mallada, J. Santamaría, Monoamine-grafted MCM-48: An efficient material for CO_2 removal at low partial pressures, Chem. Eng. J., 175 (2011) 291–297.

[36] C.–H. Chiang, N.–I Liu, J. L. Koenig, Magic-angle cross-polarization carbon 13NMR study of aminosilane coupling agents on silica surfaces, J. Colloid Interface Sci., 86 (1982) 26–34.

CHAPTER 7

POLYETHYLENIMINE FUNCTIONALIZED ORDERED MESOPOROUS SILICA FOR CO_2 SEPARATION

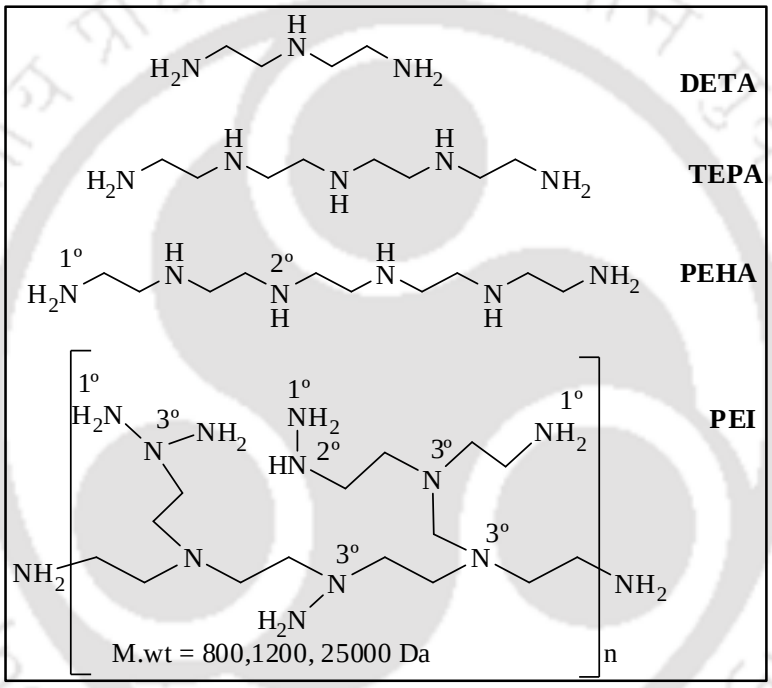

CHAPTER 7

The chapter elucidates the CO_2/N_2 adsorption behaviour of polyethylenimine impregnated mesoporous KIT-6 adsorbent in wide range of temperature and pressure. The effect of molecular weight of polyethylenimine on thermal stability as well as CO_2 adsorption performance is explained by different characterized techniques. In addition, the CO_2 adsorption performance of PEHA impregnated KIT-6 is compared with that of the functionalized MCM-41, SBA-15 and HV MCM-41. Stability of the absorbent during particle application is explained by cyclic performance of the adsorbent.

7.1 Introduction

Release of greenhouse gases to environment results in increased average temperature of earth, which is tending towards alarming limit of 2ºC [1,2]. In the last few decades, the atmospheric CO_2 concentration has been increased from ~320 to ~400 ppm, and it influenced the global surface temperature, reduced the pH of ocean surface water and disturbed the ecosystem [1–6]. Majority of the greenhouse gases are released from thermal power plant, cement industries, solid wastes and chemical industries where carbon dioxide (CO_2) shares 80–85% of it [4,5]. Emission of greenhouse gases to the atmosphere is required to be controlled in order to reduce its adverse effect on ecosystem and environment. To that end, carbon capture and utilization (CCU) is a one of the possible option [5−7].

The major component of flue gas from a thermal power plant is N_2 with ~0.10 – 0.15 bar partial pressure of CO_2 at moderate temperature (> 75 °C) [6]. Solid supported amine functionalized mesoporous silica has very high selectivity towards CO_2 at low partial pressure and wide range of temperature [8−12]. Mesoporous silica is functionalized by both

aminosilane grafting and wet impregnation methods. The sorption capacity of aminosilane grafted ordered mesoporous silica is higher at room temperature and gradually decreases with increases in temperature as shown in Chapter 5 and 6.Although, Wang et al. [9] studied the CO_2 adsorption at different temperatures on PEI functionalized three dimensional molecular sorbents (MCF, MSU and HMS) and compared with MCM-41, SBA-15 and carbon-black. It was found that the pore size, pore volume and support dimension play a critical role in the sorption performance of adsorbent. Additionally, sorption capacity of adsorbents increases with increase in adsorption temperature to some extent.

With these premises in mind, this Chapter was undertaken keeping in view of design of adsorbent with high adsorption capacity at moderate temperature and low CO_2 partial pressure with high selectivity. Incidentally, three dimensional cubical KIT-6 possess the required attractive properties like large interconnected channels (> 6.6 nm), which facilitate the movement of host and guest molecules and higher pore volume helps in accommodating large amount of polyethylenimine. In this chapter, three dimensional KIT-6 is functionalized with DETA, TEPA, PEHA and branched PEI of different M_w (800, 1200 and 25000 Da) by wet impregnation method.The surface morphology of adsorbent is studied by various analytical techniques. Additionally, its effect on CO_2/N_2 adsorption capacity and selectivity is investigated for wide temperature ranges. Further, the sorption capacity is compared with more traditional MCM-41, SBA-15 and high pore volume MCM-41 (HV MCM-41). Thus, this study possibly provides a deeper insight in designing of polyethylenimine functionalized CO_2 selective adsorbent.

7.2 Materialsand Methods

7.2.1 *Synthesis of adsorbent*

Traditional 3D cubical KIT-6 is synthesized by following the procedure of Kim et al. [13] and explained in Chapter 3.Other mesoporous silica namely MCM-41 [14], SBA-15 [15] and HV MCM-41 [14] are synthesized as earlier reported procedure and also explained in Chapter 3. Polyethylenimine functionalized KIT-6 is prepared by wet impregnation method and comprehensively discussed in Chapter 3. The resulting products are denoted K/'x' DETA, K/'x' TEPA, K/'x' PEHA, K/'x' 8PEI, K/'x' 12PEI and K/'x' 250PEI and stored for further analysis, where 'x' is wt% of polyethylenimine in KIT-6. Other PEHA impregnated mesoporous silica MCM-41, SBA-15 and HV MCM-41 are denoted as M/60 PEHA, S/ 60PEHA and HVM/ 60 PEHA, respectively.

7.2.2 *Characterization of adsorbent*

Synthesized adsorbents are characterized by various analytical techniques, electron microscope (field emission scanning electron microscope (FESEM, Zeiss-Sigma) and transmission electron microscope (TEM, JEOL, JEM-2100 at 200 kV)), X-ray diffraction (XRD, Bruker, D8 Advance), nitrogen adsorption/desorption (–196 ºC), diffusive reflectance infrared Fourier transform (DRIFT) spectrometer (PerkinElmer Spectrum, Version 10.4.3) and thermo gravimetric analyzer (TGA, NETZSCH TG 209F1 Libra). CO_2 and N_2 adsorption/desorption analysis are performed in high pressure adsorption setup (iSorbHP1-XKRLSPN100) by volumetric method. Ultra-pure CO_2 (99.99%) and N_2 (99.99%) are used in adsorption measurement. The above characterization techniques are comprehensively discussed in Chapter 3.

7.3 Results and Discussion

7.3.1 *Electron micrograph*

The structure and morphology of pure mesoporous silica is investigated by electron micrograph as shown in the Figure 7.1 and 7.2. FESEM micrograph of KIT-6, SBA-15,

MCM-41 and HV MCM-41 (Figure 7.1) clearly shows the synthesized mesoporous silica exhibiting as a particle of ~ 1−2 μm [16], bundle of rope [17], plate type and uniform ~ 2 – 3 μm particles [14], respectively. TEM micrograph (Figure 7.2) indicates that the KIT-6 and SBA-15 consist of highly ordered uniform mesoporous channels with ~ 6.5 nm. However, MCM-41 is highly ordered mesoporous silica with ~2.0 nm pore size and HV MCM-41 is disordered in nature like mesoporous silica foam [18].

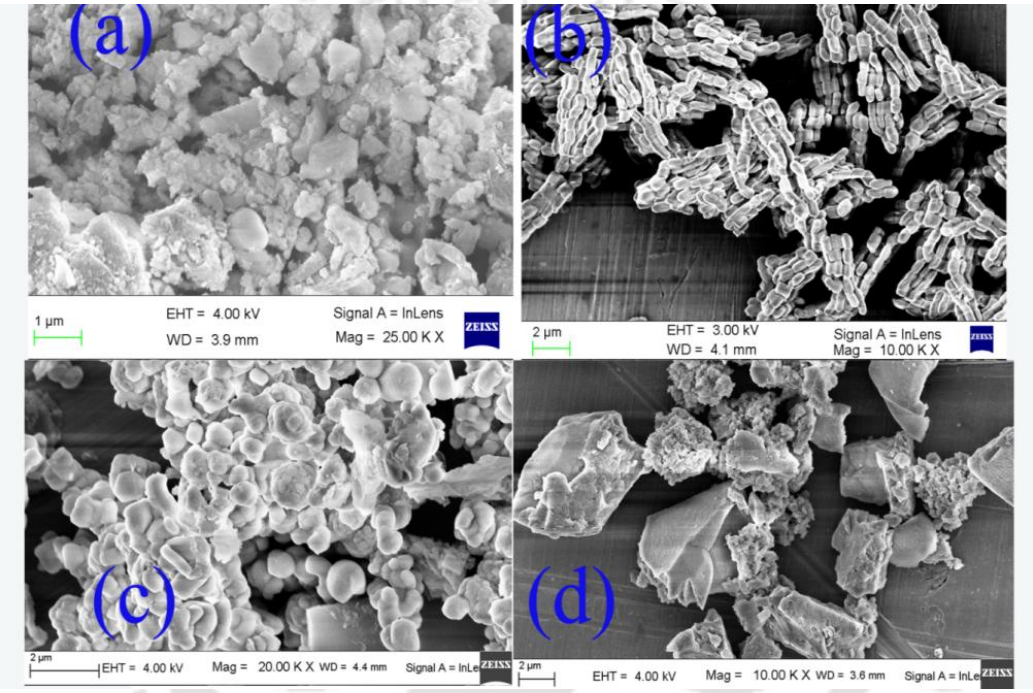

Figure 7.1 FESEM micrograph of (a) KIT-6 (b) SBA-15, (c) MCM-41 and (d) HV MCM-41

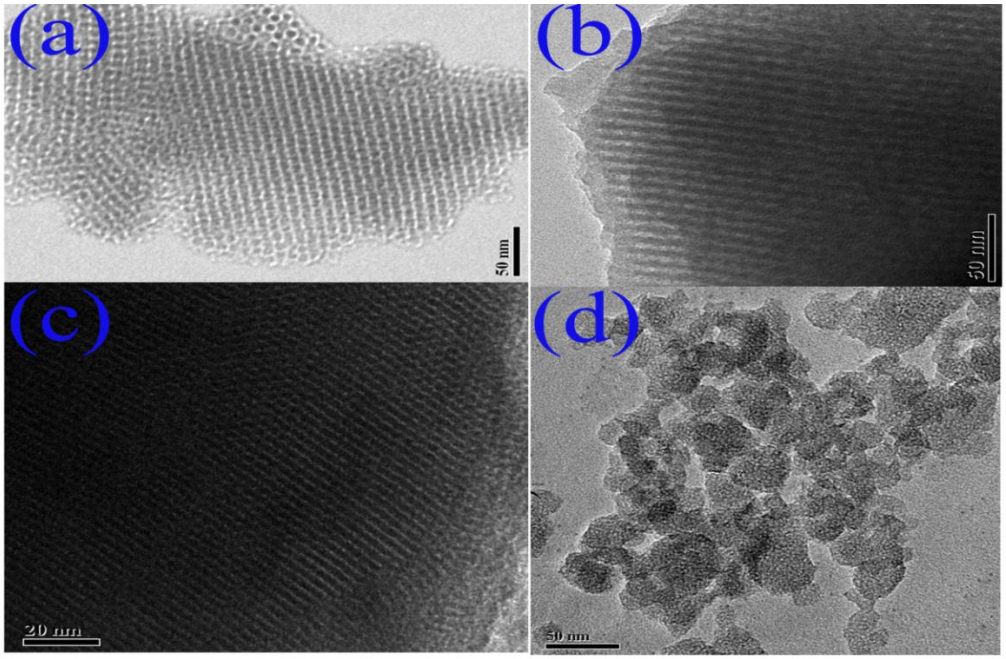

Figure 7.2 TEM micrograph of (a) KIT-6 (b) SBA-15, (c) MCM-41 and (d) HV MCM-41.

Surface morphology of polyethylenimine impregnated KIT-6 is investigated by FESEM spectra as shown in **Figure 7.3**. After impregnation, surface texture of all the mesoporous silica becomes denser following the order K/ 60 TEPA < K/60 PEHA < K/50 PEI-800 < K/ 50 PEI-25K. This intensity of agglomeration can be understood by the degree of surface coverage of silica with polyethylenimine [19]. Almost no agglomeration is observed in K/60 TEPA, K/60 PEHA and K/60 PEI-800, indicating that almost all the polyethylenimine got inserted into the pores. However with K/50PEI-25K, some of the PEI exists on the external surface of KIT-6 as shown in Figure 7.3e. Similar phenomena were also observed by Qi et al. and Snaz et al. during PEI impregnation in mesoporous silica capsules and SBA-15 [20,21]. Intensity of surface coverage on KIT-6 is increased with increasing the M_w of PEI (Figure 7.3). It indicates that PEI with ultra-high M_w (25000 Da) is partially inserted in pore and partially covers the surface, which results in the partial agglomeration of the adsorbent [19].

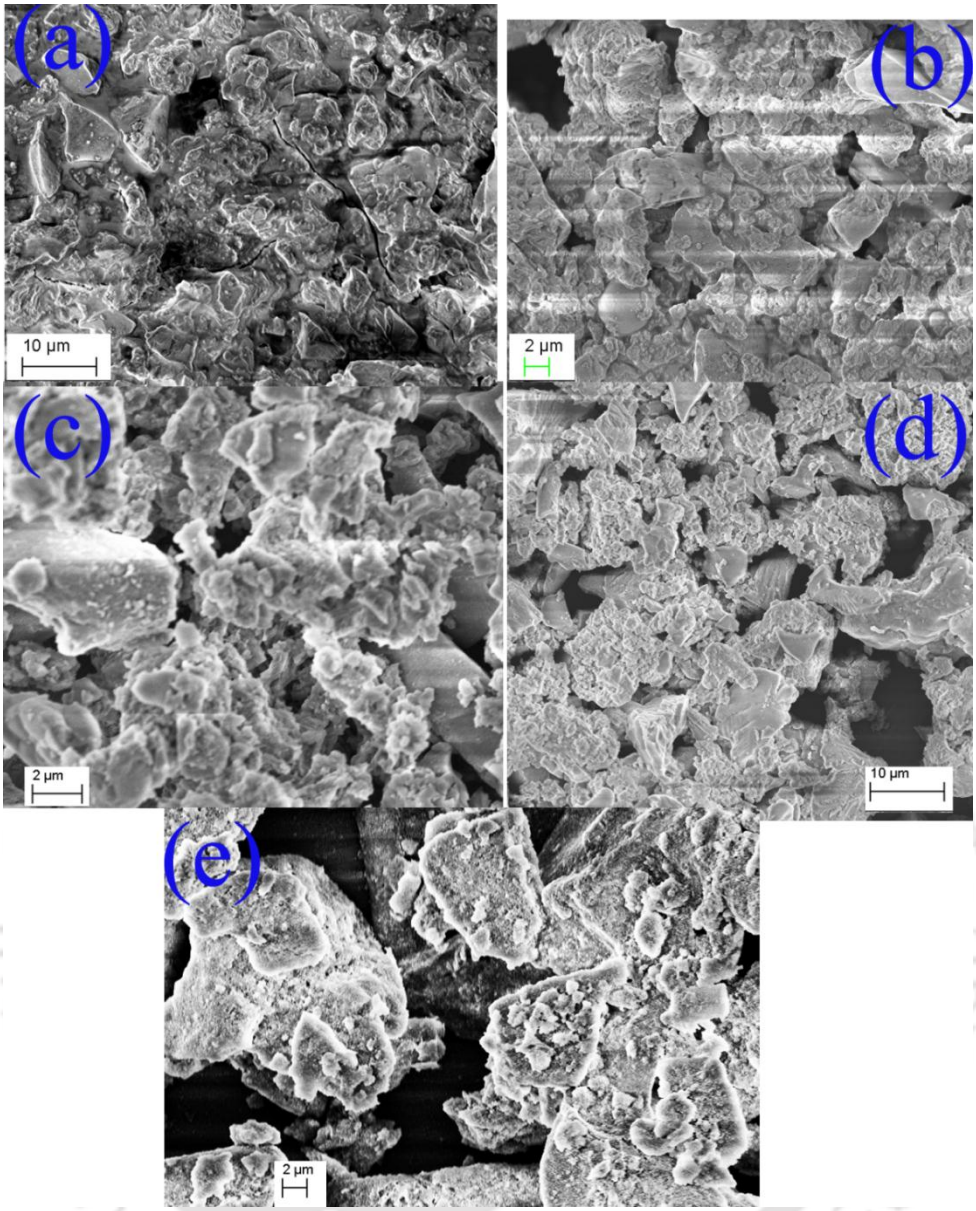

Figure 7.3 FESEM micrograph of (a) K/ 60 TEPA (b) K/ 60 PEHA, (c) K/ 50 PEI-800 (d) K/ 50 PEI-1200 and (e) K/ 50 PEI-25K adsorbents.

7.3.2 *N_2 adsorption/desorption isotherm*

The N_2 adsorption/desorption isotherm at –196 ºC and the pore size distribution of pure adsorbents are shown in Figure 7.4. The extracted physical properties are summarized in Table 7.1. The isotherms observed for the different mesoporous silica (KIT-6, SBA-15, MCM-41and HV MCM-41) samples depict a typical type IV adsorption/desorption isotherm

and exhibit remarkably sharp capillary condensation steps, which is the characteristic feature of the mesoporous material [22]. The S_{BET} of KIT-6, SBA-15, MCM-41 and HV MCM-41 is 860 m^2/g, 857 m^2/g, 1492 m^2/g and 986 m^2/g, respectively.

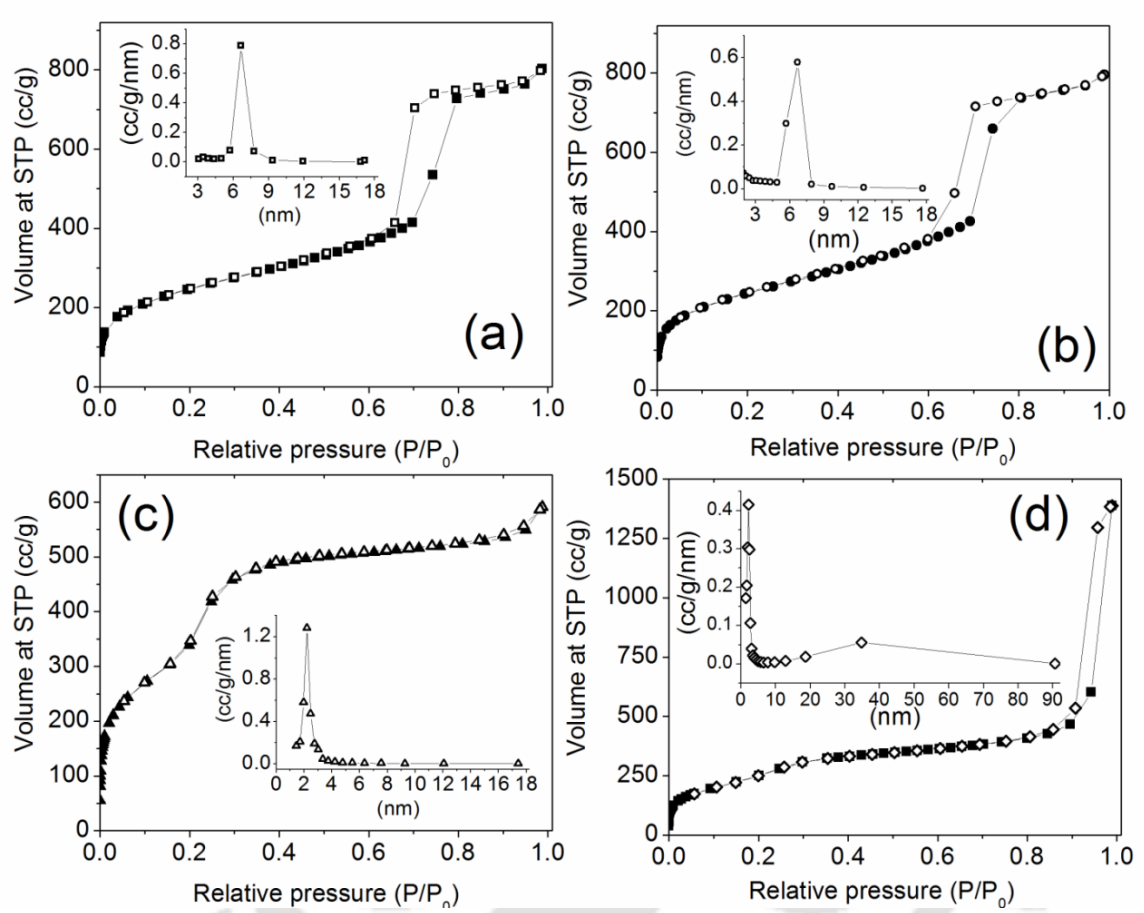

Figure 7.4 N_2 adsorption/desorption (−196 ºC) isotherm (a) KIT-6, (b) SBA-15, (c) MCM-41 and (d) HV MCM-41and the corresponding BJH pore size distribution from desorption branch

Table 7.1 Physical properties of different mesoporous silica

Sample	**S_{BET} (m^2/g)**	**V_t (cc/g)**	**P_d (nm)**
KIT-6	860	1.24	6.6
SBA-15	857	1.23	6.6
MCM-41	1492	0.91	2.2
HV MCM-41	986	2.15	2.2

7.3.3 *X-ray diffraction spectra*

X-ray diffraction spectra for all the different mesoporous silica KIT-6, SBA-15, MCM-41 and HV MCM-41 samples are reported in Figure 7.5. All three mesoporous silicas show well resolved sharp peak in low angle corresponding to $d_{(211)}$ (KIT-6, cubical), $d_{(100)}$ (SBA-15, hexagonal) and $d_{(100)}$ (MCM-41, hexagonal) plain, indicates the synthesized material as highly crystalline and ordered in nature [14−17]. It is also confirmed by the TEM micrograph (Figure 7.2). In case of HV MCM-41, low-angle peak intensity for the $d_{(100)}$ plane is sharply reduced compared to ordered MCM-41. It is mainly for the reduction in its ordered structure and it might be due to the fact that large pore volume MCM-41 materials are not crystalline on the atomic level compared to ordered one. TEM micrograph of large pore volume MCM-41 (Figure 7.2d) corroborates the X-ray spectra and above statement.

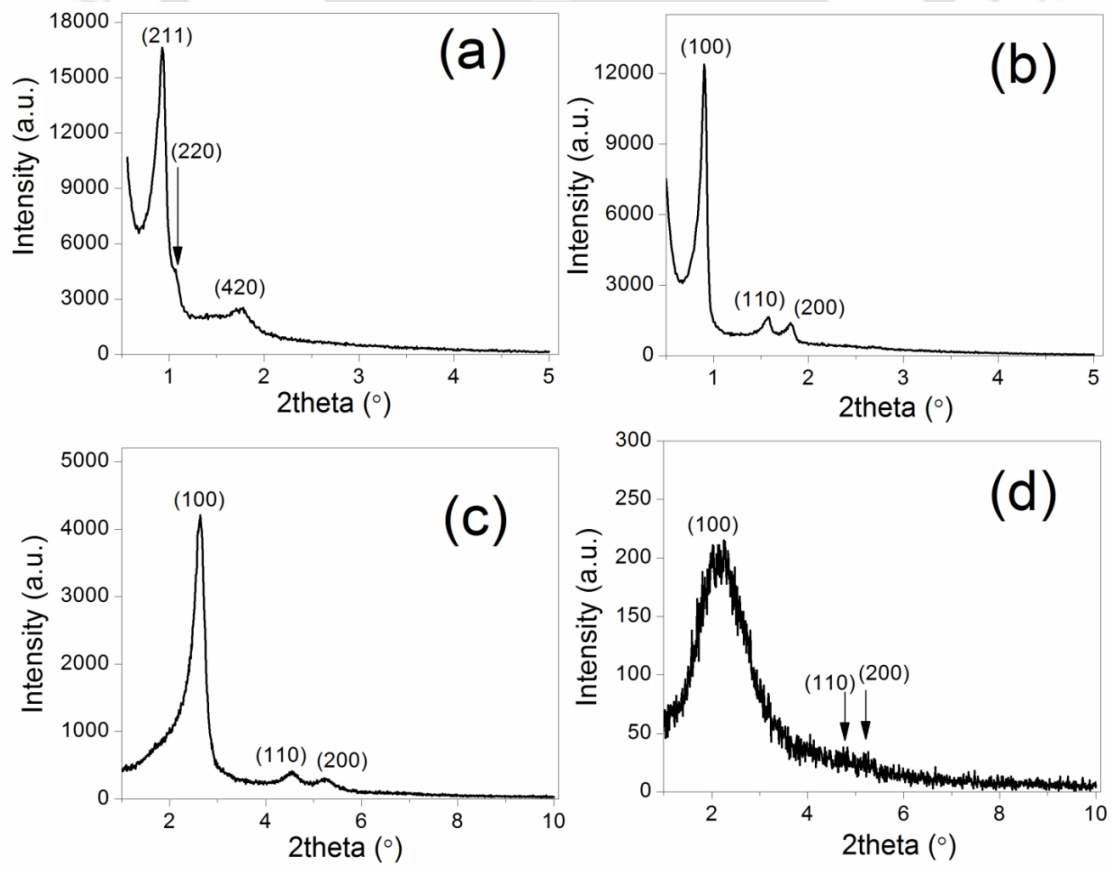

Figure 7.5 X-ray diffraction spectra of (a) KIT-6, (b) SBA-15, (c) MCM-41 and (d) HV MCM-41

In order to understand the effect of polyethylenimine concentration on structure of mesoporous silica, X-ray diffraction analysis of PEHA impregnated KIT-6 is performed. Figure 7.6 clearly shows that the peak intensity gradually decreases with increasing the PEHA concentration in the KIT-6. This trend suggests that loaded PEHA is mainly filled inside porous channels and the structure of KIT-6 is stuffed. Simultaneously, it also reduces the scattering intensity towards the silica wall. Further increasing the PEHA amount to 60 wt.%, the peak deviation becomes larger suggesting an increase in the PEHA loading that covers the silica surface completely. It implies that the overloaded PEHA may coat over the external surface of particles and cause the agglomeration, which is evidenced by FESEM images shown in Figure 7.3.

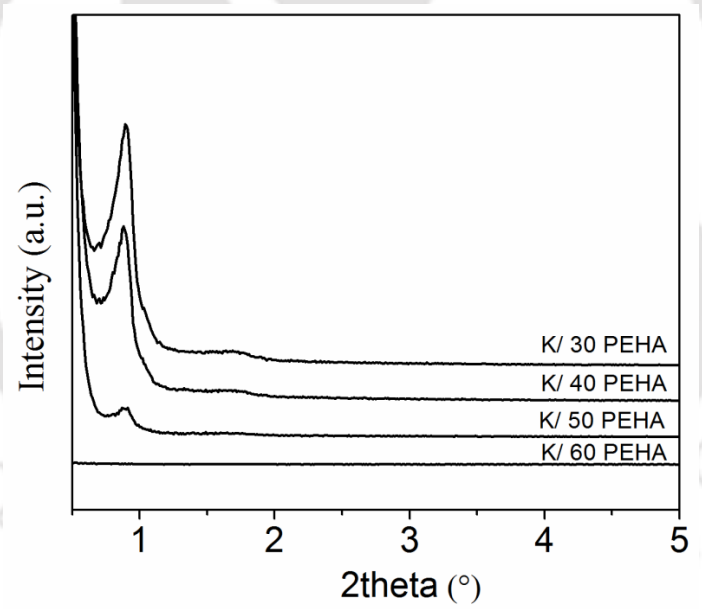

Figure 7.6 X-ray diffraction spectra of PEHA impregnated KIT-6

7.3.4 *TGA analysis*

Figure 7.7 shows the TGA of the KIT-6 samples loaded with different polyethylenimine. As shown in figure, pure KIT-6 loses ca. 5 wt% near 100 °C due to desorption of CO_2 and moisture and similar phenomenon is also observed for polyethylenimine impregnated KIT-6.

The TGA analysis revealed a rapid weight loss event at a temperature range of 150–500 °C (Figure 7.7). In this temperature range, weight loss can be attributed mostly to the volatilization and decomposition of polyethylenimine molecules [23,24]. It is interesting to observe that, thermal stability of adsorbents increases with increase in molecular weight of polyethylenimine as follows K/60 TEPA < K/60 PEHA < K/50 PEI-800 < K/50 PEI1200 < K/50 PEI-2.5K. The similar phenomenon was reported by Goeppert et al. [12].

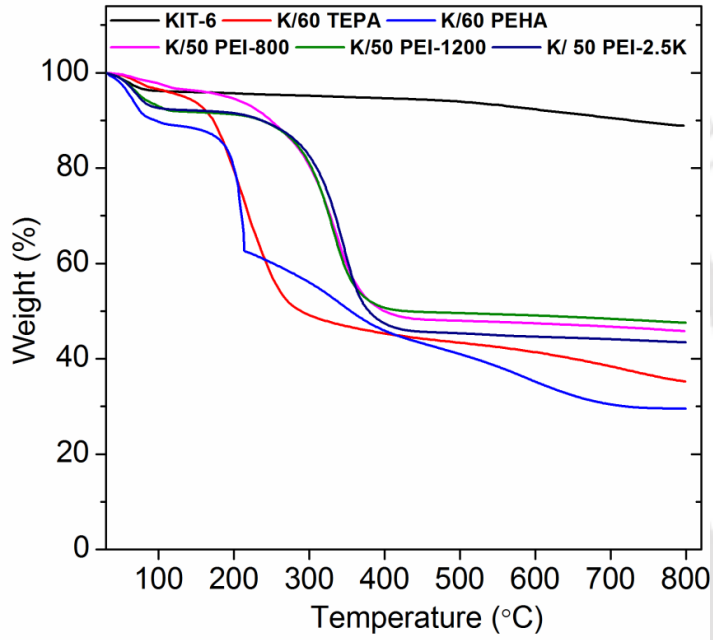

Figure 7.7 TGA analysis of polyethylenimine impregnated KIT-6 between 30 to 800 °C with 10 °C heating rate in N_2 atmosphere

7.3.5 *DRIFT analysis*

DRIFT analysis is employed to evaluate the functional groups present in the adsorbent and depicted in Figure 7.8. The peaks corresponding to 3750 – 3400 cm^{-1}, 1642 cm^{-1}, 1250 – 1020 cm^{-1}, 960 cm^{-1}, and ~799 cm^{-1} in the DRIFT spectra (Figure 7.8a) respectively represent the hydrogen bonded silanol group, physically adsorbed water, asymmetric vibration of silanol group, free surface silanol group and symmetric stretching vibration of silanol group present in the KIT-6 [25]. After impregnation, some new peaks are evolved in

1650 – 1300 cm^{-1} which confirms the presence of polyethylenimine in the adsorbent as well as chemical interaction between atmospheric CO_2 and amine. The peaks corresponding to ~1650 cm^{-1} and 1580 cm^{-1} represent the NH deformation of NH_2^+ and NH_3^+ formation by CO_2 adsorption with amine present in polyethylenimine chain [20]. The other peaks corresponding to ~1316 and ~ 1400 cm^{-1} are for skeletal vibration of carbamate ($NCOO^-$) and stretching vibration of –NC group of carbamate [26]. The stretching vibration of C–H and bending vibration of CH_2 present in polyethylenimine chain are ascribed to the peaks at 2950 – 2860 cm^{-1} and 1460 cm^{-1}, respectively [19,25,26].

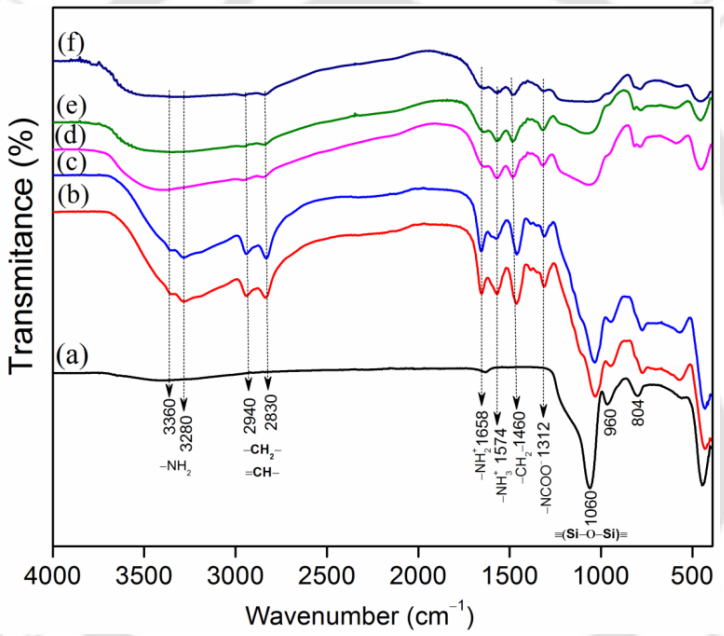

Figure 7.8 DRIFT spectra of (a) KIT-6, (b) K/60 TEPA, (c) K/60 PEHA, (d) K/50 PEI-800, (e) K/50 PEI-1200 and (f) K/50 PEI-25K adsorbents

7.3.6 CO_2adsorption performance

7.3.6.1 *Effect of polyethylenimine concentration*

Several functionalized mesoporous KIT-6 based adsorbent are synthesized to evaluate the influence of polyethylenimine concentration on CO_2 adsorption capacity and the results are shown in Figure 7.9. It is clearly shown that the adsorption capacity gradually increases with

increases in case of TEPA and PEHA loading at 75°C and 1 bar. In 60 wt% impregnated KIT-6 shows the maximum adsorption capacity of 3.12 mmol CO_2/g and 3.41 mmol CO_2/g for TEPA and PEHA, respectively. However, 50 wt%PEI-800 and PEI-1200 impregnated KIT-6 shows the maximum adsorption capacity of 2.4 mmol CO_2/g and 1.67 mmol CO_2/g, respectively, and further increase in concentration reduces the sorption capacity of the adsorbent. In case of low thermally stable DETA impregnated KIT-6, the adsorption capacity is evaluated at 30 °C. The adsorption capacity of DETA impregnated KIT-6 decreases with increases in concentration. High adsorption capacity in low concentration is mainly for the well dispersion of DETA in the internal pore volume of KIT-6. Further reduction in sorption capacity is probably for the reduction in internal pore volume of adsorbent.

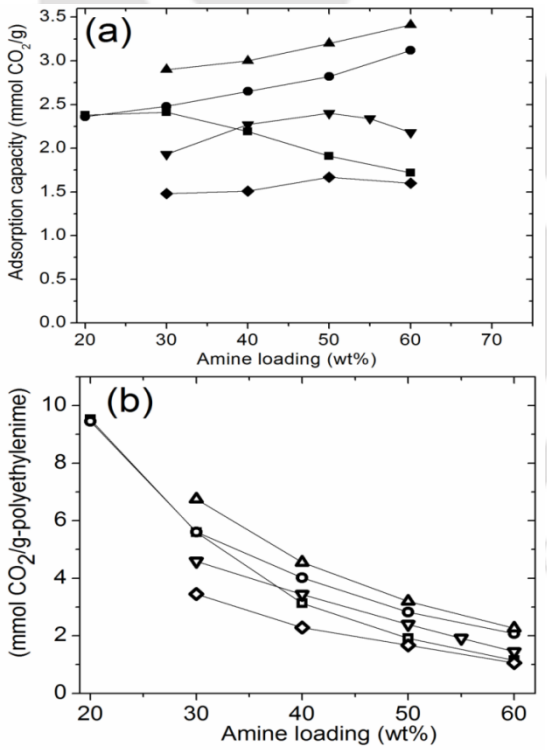

Figure 7.9 CO_2 adsorption capacities of polyethylenimine impregnated sorbents versus (a) amine concentration and (b) amine efficiency of the adsorbent. (■- K/'x'DETA at 30°C; ●- K/'x'TEPA at 75°C; ▲- K/'x'PEHA at 75°C; ▼- K/'x'PEI-800 at 75°C; ♦- K/'x'PEI-1200 at 75°C)

Polyethylenimine efficiency of an adsorbent is the ratio of amount of CO_2 adsorbed to amine (mmol CO_2/g polyethylenimine) present in the adsorbent. The amine efficiency gradually decreases with increases in polyethylenimine concentration in the adsorbent as shown in Figure 7.9b. Though a higher concentration of impregnated polyethylenimine can supply more active sites, it can also block the pores. Therefore, the reduction in amine efficiency might be because of the partially reduction in accessibility of the adsorption amine sites [16,23].

7.3.6.2*Effect of adsorption temperature on polyethylenimine impregnated KIT-6*

The equilibrium CO_2 adsorption isotherms of K/60 TEPA, K/60 PEHA, K/50 PEI-800, K/50 PEI-1200 and K/50 PEI-25K at different temperatures with an interval of 15ºC between (30 – 120) ºC for pressure upto1.0 bar are shown in Figure 7.10. When the partial pressure of CO_2 is lower than 0.10 bar, adsorption capacity increases sharply with pressure in all the adsorbents and then approaches to saturation. The sharp increase in adsorption capacity at low partial pressure is mainly for chemical reaction between CO_2 and amine group present in polyethylenimine as shown in Figure 7.11 [27]. The tested adsorbents get saturated till ~0.15 bar and adsorption capacity does not change significantly with further increase in CO_2 partial pressure [11]. It is possibly due to insignificant reactive amine site for reaction as well as free volume present for physisorption.

The sorption capacity of the optimized adsorbent increases with temperature from 30 – 120 ºC as shown in Figure 7.10. The capacity increased is from 2.27, 1.90, 1.34, 0.93, 0.88 mmol CO_2/g to 3.95, 4.45, 3.0, 2.44, 2.40 mmol CO_2/g for K/60 TEPA, K/60 PEHA, K/50 PEI-800, K/50 PEI-1200 and K/50 PEI-25K, respectively by increasing the temperature from 30 ºC to 105 ºC at 1.0 bar [9,11,28]. At lower temperature, CO_2 adsorption is kinetically controlled. Later, rate of adsorption increases with temperature without any structural changes in the adsorbent. With increase in temperature, kinetic energy of CO_2 is increased. However, the

viscosity of polyethylenimine and diffusional resistance of CO_2 in the inner layer is decreased and thus, more amine sites are exposed for CO_2 interaction during adsorption process [19].

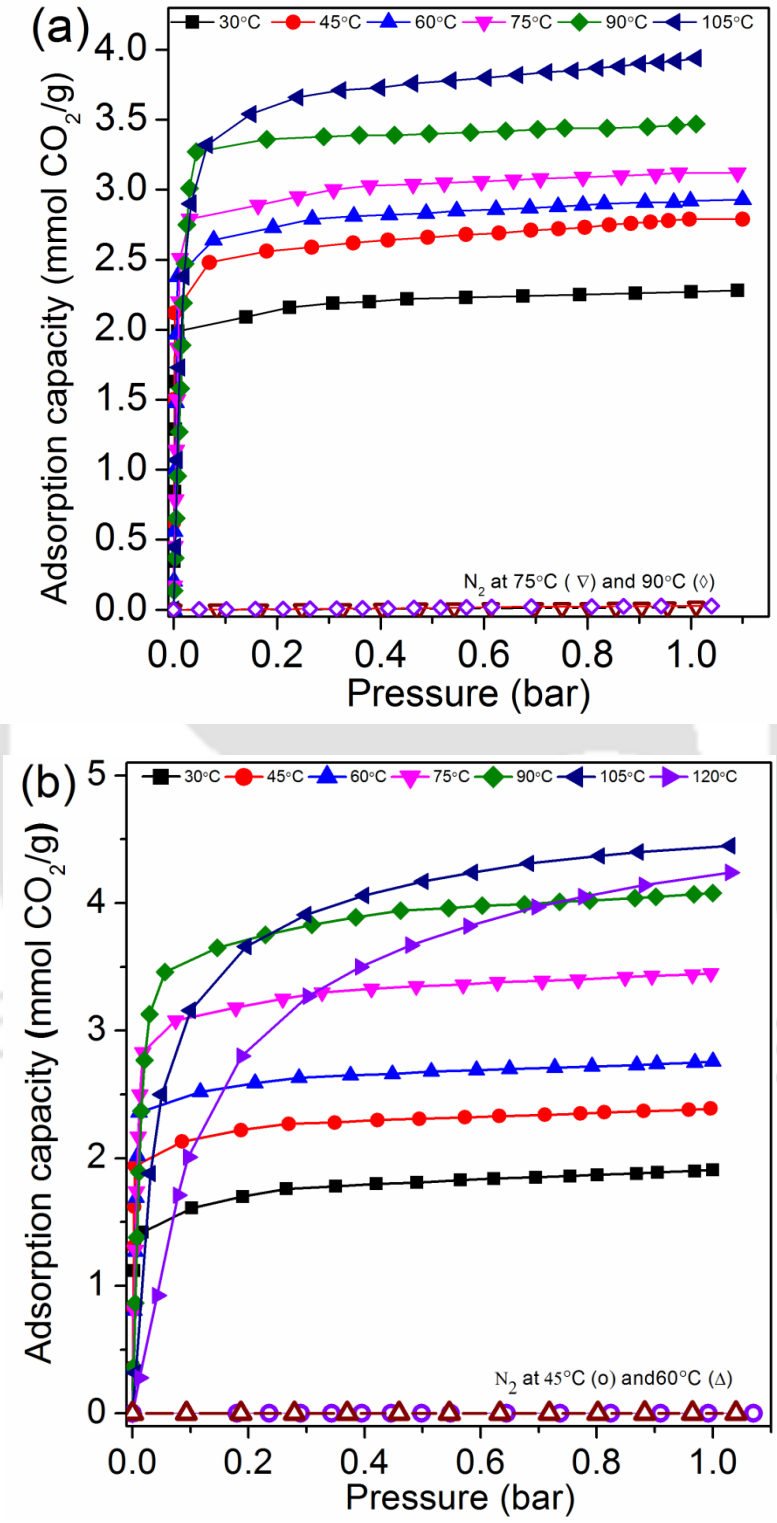

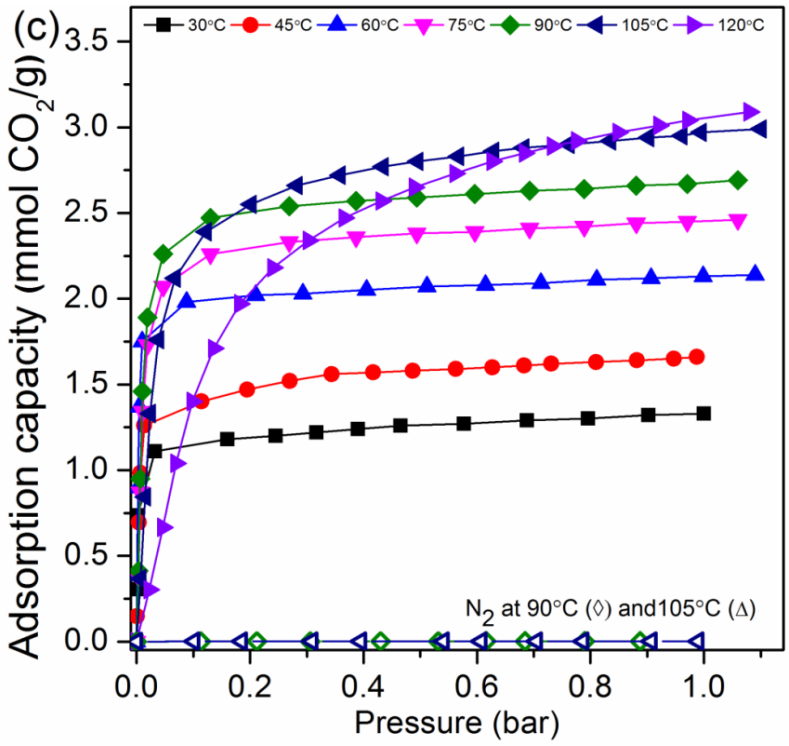

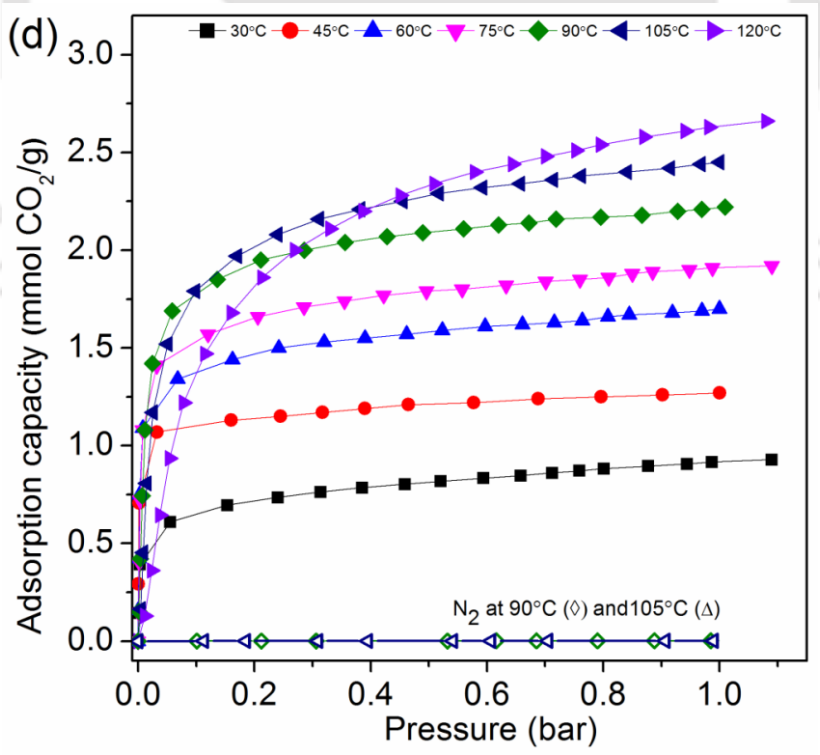

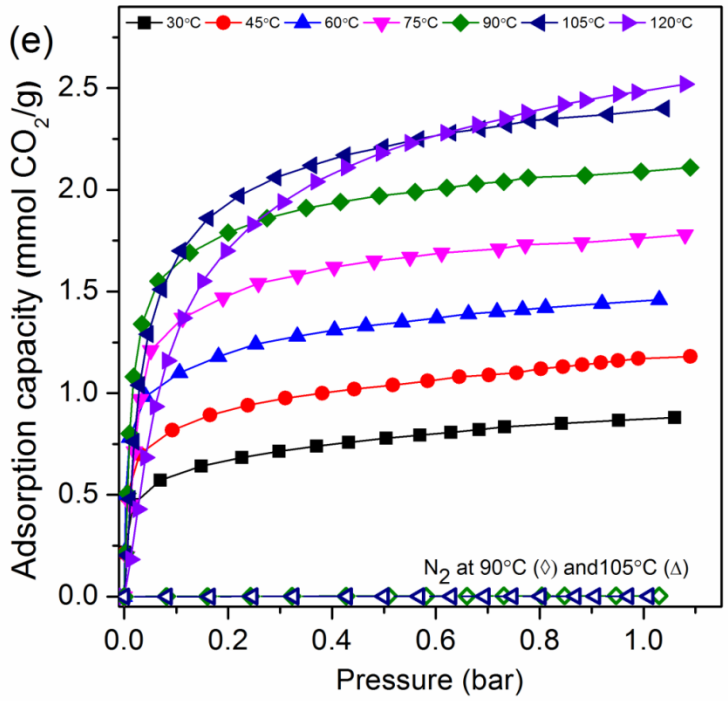

Figure 7.10 CO_2 sorption capacity as a function of temperature for (a) K/60 TEPA, (b) K/60 PEHA, (c) K/50 PEI-800, (d) K/50 PEI-1200 and (e) K/50 PEI-25K

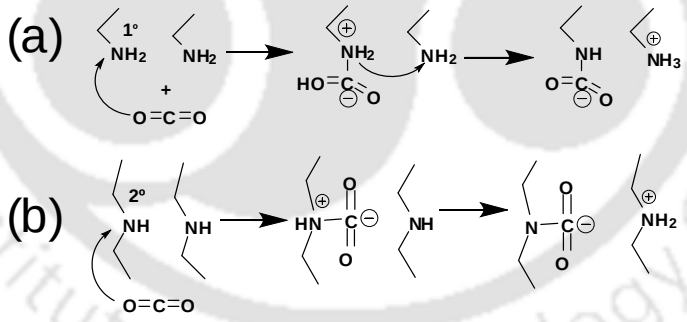

Figure 7.11 CO_2 reaction with (a) primary amine and (b) secondary amine present in the polyethylenimine.

The effect of temperature on sorption performance of adsorbent can be understood from the nature of the CO_2 equilibrium adsorption isotherm (Figure 7.10) and is schematically explained in Figure 7.12. The overall CO_2 adsorption on amine grafted mesoporous silica is a

combined effect of chemical interaction with amine and physical interaction with the surface as reported by Sayari et al. [29] and Kishor et al. [30]. During impregnation, polyethylenimine is filled in the mesoporous channel of KIT-6 as is observed from electron micrograph (Figure 7.3). During adsorption, initially a sharp increase in adsorption capacity (Figure 7.10) is observed for chemisorption between CO_2 and amine sties [31]. At low temperature (30 ºC), polyethylenimine is available in the form of a layer during adsorption and CO_2 readily reacts with the exposed amine of upper layer (Figure 7.12). In order to understand the rate of CO_2 uptake at lower temperature, CO_2 (at 1 bar) is inserted in the manifold of volumetric adsorption apparatus and exposed in the adsorbent. The rate of CO_2 uptake is prohibitively slow and sorbent does not show complete saturation even under a day of exposure in CO_2 environment. With increase in temperature, the flexibility of polyethylenimine chain molecule and inter molecular distance between molecules are increased [23,32]. It reduces the diffusion resistance to pass CO_2 molecules deeper and deeper in polyethylenimine during adsorption as shown in Figure 7.12. It is important to notice that the nature of CO_2 adsorption isotherm in the temperature range 45 – 105 ºC is as similar as that at 30 ºC. All the adsorbents get saturated with CO_2 during adsorption at ~ 0.15 bar in (45 – 105) ºC as shown in Figure 7.10 and capacity gradually increases with temperature. Additionally, higher temperature also promotes desorption of CO_2 with amine. It indicates that the thermodynamic equilibrium adsorption of CO_2 with amine is more dominant than desorption between 30 − 105 ºC. This is concluded from the enhancement in the sorption capacity form (2.27 to 3.95), (1.90 to 4.45), (1.34 to 3.0), (0.92 to 2.44) and (0.88 to 2.4) mmol CO_2/g of K/60 TEPA, K/60 PEHA, K/ 50 PEI-800, K/50 PEI-1200 and K/50 PEI-25K, respectively from 30 to 105 ºC at 1.0 bar. At high temperature (120 ºC) and low pressure, the adsorption capacity of adsorbent sharply reduced and the shape of the isotherm becomes like an arc (Figure 7.10). It indicates, desorption is more dominant at high

temperature (120 ºC) and low partial pressure. However, slightly increase in adsorption capacity at 1.0 bar is probably for the combined effect of physisorption with the surface as well as further interaction of CO_2 with amine. At higher than 120 ºC, PEI molecules start degrading and adsorbent becomes brown in colour. A similar phenomenon is also observed during TGA analysis.

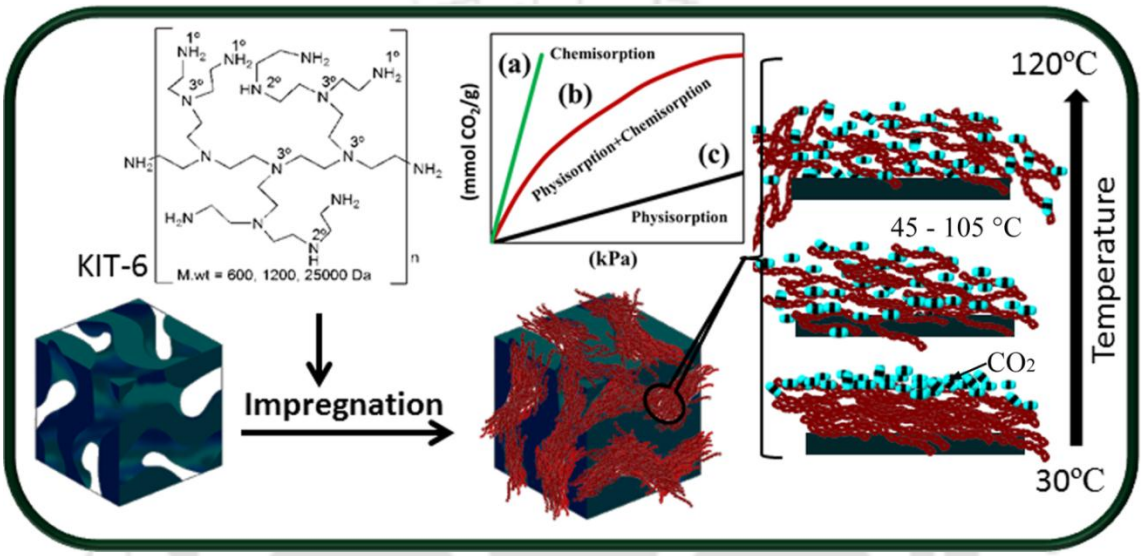

Figure 7.12 Systematic illustration of CO_2 adsorption on polyethylenimine impregnated mesoporous silica.

Major components in the flue gas of a coal based thermal power plant are CO_2 (~10 – 15 vol%) and N_2 [6]. For practical application, adsorbent should have high adsorption capacity as well as high selectivity at low CO_2 partial pressure and moderate temperature. The adsorption capacity of K/60 TEPA, K/60 PEHA, K/ 50 PEI-800, K/50 PEI-1200 and K/50 PEI-25K is 3.36, 3.36, 2.50, 1.90, 1.7 mmol CO_2/g at 90 °C and 0.15 bar respectively. With increased temperature i.e. at 105 ºC, adsorption capacity of K/60 TEPA, K/60 PEHA, K/ 50 PEI-800, K/50 PEI-1200 and K/50 PEI-25K is 3.54, 3.66, 2.50, 1.90 and 1.86 mmol CO_2/g, respectively. It is worth noting that the adsorption capacity at low partial pressure is increased

with temperature from 90 °C to 105 °C. K/60 PEHA shows the highest adsorption capacity than other polyethylenimine impregnated KIT-6. This indicates that the increment in adsorption capacity at higher pressure and temperature is presumably for deep diffusion in polyethylenimine film (Figure 7.12).

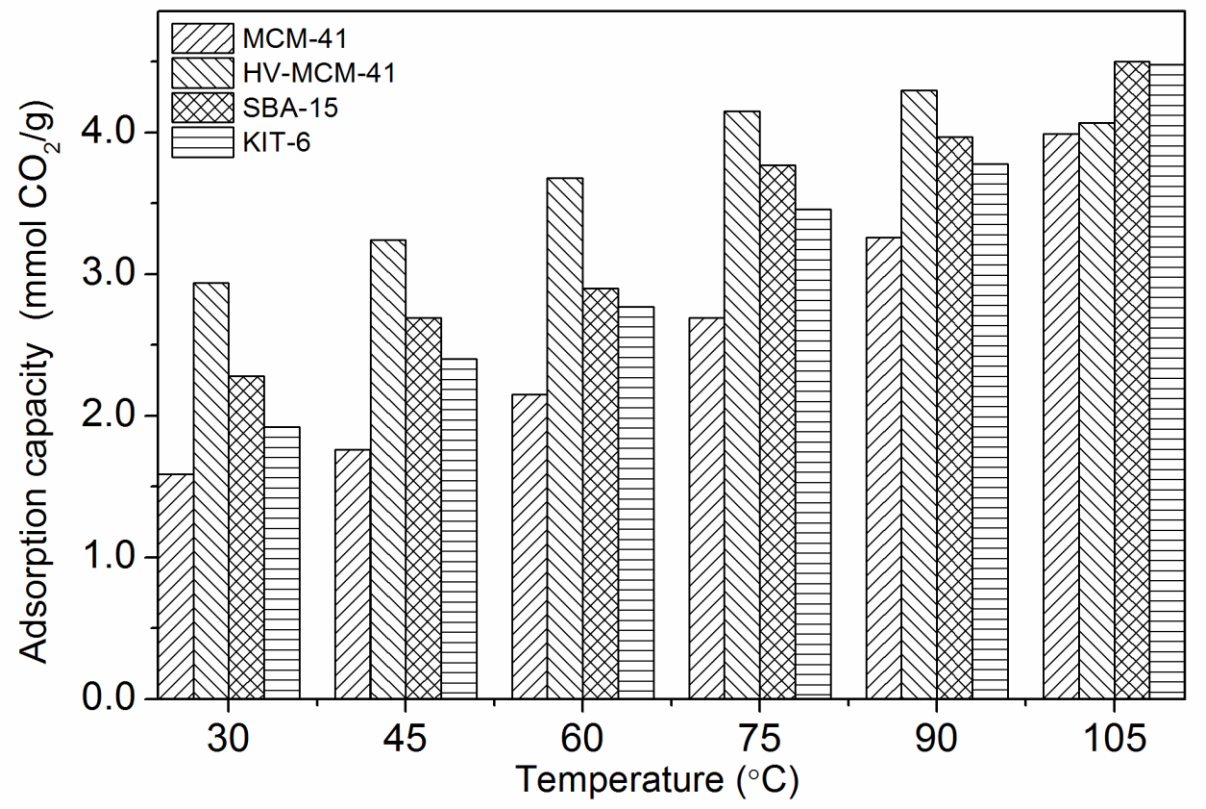

Figure 7.13 CO_2 adsorption capacities of various mesoporous silica materials after 60 wt% PEHA loading

CO_2 adsorption capacities of 60 wt% PEHA impregnated MCM-41, SBA-15 and HV MCM-41 are compared with K/60 PEHA in Figure 7.13. The CO_2 adsorption capacities of the PEHA-loaded mesoporous silica adsorbents fall within a range of 1.59 – 4.0 mmol/g, 2.94 − 4.30 mmol/g and 2.28− 4.4 mmol/g of MCM-41 (2.2 nm), HV MCM-41(2.2 nm) and SBA-15 (6.6 nm), respectively. As shown in the parentheses in the above sequence, the adsorption

capacity depends on both average pore diameter and pore volume of the mesoporous silica. It is believed that PEHA can be introduced to the pore interior more easily as the pore diameter of the mesoporous silica increases and high pore volume accommodates more and more amine. The sorption capacity of KIT-6 and SBA-15 shows the nearly same adsorption capacity. It is possibly for similar physical properties. However, smaller pore size of MCM-41 and HV MCM-41 inhibits the CO_2 diffusion inside the pore during adsorption.

The N_2 adsorption isotherms of K/60 TEPA, K/60 PEHA, K/ 50 PEI-800, K/50 PEI-1200 and K/50 PEI-25K are shown in Figure 7.10. In order to ensure the accuracy, nitrogen adsorption measurements are repeated three times. The adsorption capacity is not much affected with polyethylenimine molecular weight. The mean adsorption capacity is very low (~2 x 10^{-3}) mmol N_2/g of all the adsorbent as shown in Figure 7.10. Lin et al.[33] tested the breakthrough performance of polyethylenimine impregnated MIL-101 in equimolar CO_2/N_2 mixture. N_2 eluted rapidly from the column whereas CO_2 eluted after some time. It suggests that CO_2 has very strong interaction towards amine sites compared to N_2. Whereas, Yan et al.[34] showed that the CO_2 adsorption capacity was not influenced by presence of N_2 over polyethylenimine impregnated MCF. Ultra low N_2 adsorption capacity at 1 bar for all the amine functionalized KIT-6 (K/60 TEPA, K/60 PEHA, K/ 50 PEI-800, K/50 PEI-1200 and K/50 PEI-25K) indicates that the polyethylenimine impregnated adsorbent can become a suitable adsorbent for practical application to capture CO_2 from the large anthropogenic source at moderate temperature.

7.3.6.3*Cyclic performance*

High CO_2 sorption capacity at low partial pressure, high selectivity, low regeneration temperature and fast adsorption/desorption kinetics are important criteria of a good adsorbent for practical application. On the other hand, stability of adsorbent in wide range of

temperature and pressure during application is equally important. The stability of the adsorbent during practical application fixes the working boundary and frequency of adsorbent replacement after adsorption (A)/desorption (D) cycles. The flue gas temperature of thermal power plant is much higher than atmospheric temperature and it varies with feed composition. Thus, it is important to define the best working temperature range for a specific application.

In the present section, the cyclic performance of synthesized adsorbent is studied over wide range of temperature and pressure in dry CO_2 to know the best working conditions. After each cycle, sample is degased at 100 ºC for 30 min in high vacuum. The adsorption capacity of K/60 PEHA lies between 4 and 4.5 mmol CO_2/g for temperature between 90 °C and 105 °C at 1 bar. After 20 adsorption/desorption cycle, sorption capacity is decreased to ~2.0 % to ~3.0 % of the initial adsorption capacity at 90A/100D and 105A/100D, respectively (Figure 7.14). Adsorption capacity of K/60 PEHA gradually decreases after desorption at 120 °C as shown in Figure 7.14. After 10^{th} cycle, adsorption capacity of K/60 PEHA reduced to ~8.0 % of the initial adsorption capacity (Figure 7.14). The reduction in adsorption capacity at 120 ºC degassing temperature is due to leaching of PEHA form the porous channel of KIT-6. However, the CO_2 sorption capacity of low molecular weight amine like DETA and TEPA impregnated adsorbents sharply reduces with each cycles. Therefore, PEHA impregnated KIT-6 is more effective for CO_2 adsorption from a large anthropogenic source at moderate temperature and low pressure. Among these above adsorbents, K/60 PEHA appears to be the most suited one for practical application, as it provides considerably stable adsorption capacity with good thermal stability. In addition, K/60 PEHA also takes care of the environmental issues by eliminating the amine loss in atmosphere during regeneration.

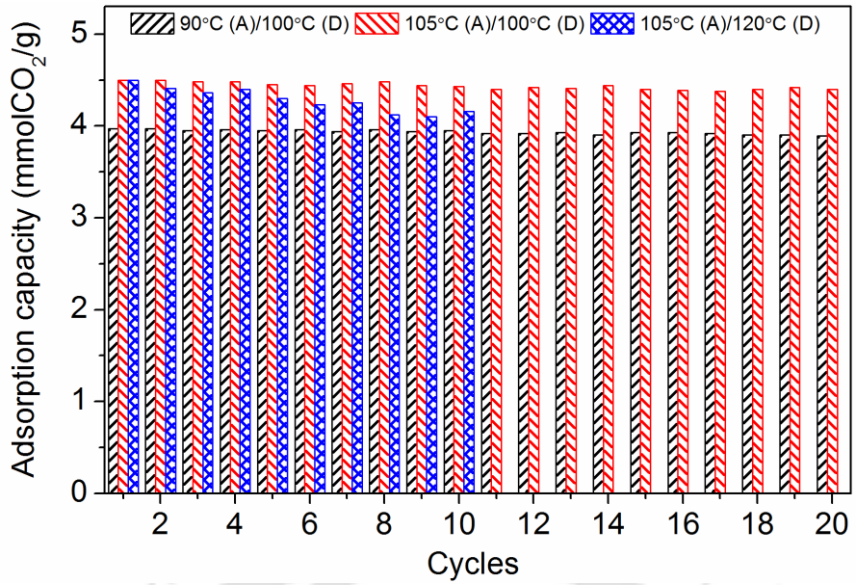

Figure 7.14 Cyclic performance of K/60 PEHA adsorbent

7.4 Conclusions

In this study, the large variety of polyethylenimine functionalized KIT-6 based adsorbent is synthesized by wet impregnation method and deployed for CO_2 adsorption at moderate temperature and low pressure. Further, optimum adsorbent was compared with M/60 PEHA, S/60 PEHA and HVM/ 60 PEHA. Polyethylenimine forms a layer in the porous channels of KIT-6 during impregnation. The results show that the CO_2 adsorption capacity is increased with increasing in temperature for all the amine functionalized adsorbent and the maximum sorption capacity 4.0 to 4.5 mmol CO_2/g (K/60 PEHA) at 90 to 105°C and 1 bar. S/60 PEHA shows the same adsorption capacity as K/60 PEHA at 105 °C and 1 bar. The adsorption capacity is increased by chemisorption between CO_2 and amine site as well as by reduced in diffusion resistance between layered polyethylenimine while temperature is raised from 30 to 105 °C. Among the above tested adsorbents, adsorption capacity follows the order K/60 PEHA (4.5 mmol/g) ~ S/60 PEHA (4.5 mmol/g) < HV M/60 PEHA (4.07 mmol/g) < M/60 PEHA (3.99mmol/g), respectively. As the concern is to research for a long term practical application of highly CO_2/N_2 selective adsorbent as well as to eliminate the amine loss in

atmosphere, the tested adsorbent K/60 PEHA shows stable performance during (90–105) °C adsorption/100 °C desorption and thus the most preferred one amongst the above adsorbents studied.

References

[1] M. Meinshausen, N. Meinshausen, W. Hare, S. C. B. Raper, K. Frieler, R. Knutti, D. J. Frame, M. R. Allen, Greenhouse–gas emission targets for limiting global warming to 2°c, Nature, 458 (2009) 1158–1162.

[2] L. B. Firth, N. Mieszkowska, R. C. Thompson, S. J. Hawkins, Climate change and adaptational impacts in coastal systems: The case of sea defences, Environ. Sci.: Processes Impacts, 15 (2013) 1665-1670.

[3] A human health perspective on climate change published by environmental health perspectives and the national institute of environmental health sciences, 2010.

[4] CO_2 emissions from fuel combustion highlights, International Energy Agency Statistics, 2012.

[5] A.B. Rao, E.S. Rubin, A technical, economic, and environmental assessment of amine-based CO_2 capture technology for power plant greenhouse gas control, Environ. Sci. Technol., 36 (2002) 4467–4475.

[6] K. A. Mumford, K. H. Smith, C. J. Anderson, S. Shen, W. Tao, Y. A. Suryaputradinata, A. Qader, B. Hooper, R. A. Innocenzi, S. E. Kentish, G. W. Stevens, Post-combustion capture of CO_2: results from the solvent absorption capture plant at Hazelwood power station using potassium carbonate solvent, Energy Fuels, 26 (2012) 6449–6449

[7] P. Markewitz, W. Kuckshinrichs, W. Leitner, J. Linssen, P. Zapp, R. Bongartz, A. Schreiber, T. E. Müller, Worldwide innovations in the development of carbon capture technologies and the utilization of CO_2, Energy Environ. Sci., 5 (2012) 7281–7305.

[8] A. Sayari, Y. Belmabkhout, Stabilization of amine-containing CO_2 adsorbents: Dramatic effect of water vapor, J. Am. Chem. Soc., 132 (2010) 6312–6314.

[9] D. Wang, X. Wang, X. Ma, E. Fillerup, C. Song, Three-dimensional molecular basket sorbents for CO_2 capture: Effects of pore structure of supports and loading level of polyethylenimine, Catalysis Today, 233 (2014) 100–107.

[10] Y. Kuwahara, D.Y. Kang, J. R. Copeland, P. Bollini, C. Sievers, T. Kamegawa, H. Yamashita, C. W. Jones, Enhanced CO_2 adsorption over polymeric amines supported on heteroatom-incorporated SBA-15 silica: Impact of heteroatom type and loading on sorbent structure and adsorption performance, Chem. Eur. J., 18 (2012)16649 – 16664.

[11] N. Gargiulo, A. Peluso, P. Aprea, F. Pepe, D. Caputo, CO_2 adsorption on polyethylenimine-functionalized SBA-15 mesoporous silica: Isotherms and modeling, J. Chem. Eng. Data 59 (2014) 896−902.

[12] A. Goeppert, S. Meth, G. K. S. Prakash, G. A. Olah, Nanostructured silica as a support for regenerable high-capacity organoamine-based CO_2 sorbents, Energy Environ. Sci., 3, (2010) 1949–1960.

[13] T.-W. Kim, F. Kleitz, B. Paul, R. Ryoo, MCM-48-like large mesoporous silicas with tailored pore structure: Facile synthesis domain in a ternary triblock copolymer-butanol-water system, J. Am. Chem. Soc., 127 (2005) 7601–7610.

[14] S. Loganathan, M. Tikmani, A. K. Ghoshal, Novel pore-expanded MCM-41 for CO_2 capture: Synthesis and characterization, Langmuir, 29 (2013) 3491–3499.

[15] X. Wang, X. Ma, C. Song, D. R. Locke, S. Siefert, R. E. Winans, J. Möllmer, M. Lange, A. Möller, R. Gläser, Molecular basket sorbents polyethylenimine-SBA-15 for CO_2 capture from flue gas: Characterization and sorption properties, Micropor. Mesopor. Mater. 169 (2013) 103–111.

[16] W.-J. Son, J.-S. Choi, W.-S. Ahn, Adsorptive removal of carbon dioxide using polyethyleneimine-loaded mesoporous silica materials, Micropor. Mesopor. Mater., 113 (2008) 31−40.

[17] X. Yan, S. Komarneni, Z. Yan CO_2 adsorption on Santa Barbara Amorphous-15 (SBA-15) and amine-modified Santa Barbara Amorphous-15 (SBA-15) with and without controlled microporosity, J. Colloid Interface Sci., 390 (2013) 217–224.

[18] J. Zhao, F. Simeon, Y. Wang, G. Luob and T. A. Hatton, Polyethylenimine-impregnated siliceous mesocellular foam particles as high capacity CO_2 adsorbents, *RSC Adv*., 2 (2012) 6509–6519.

[19] M. J. Al-Marri, M. M. Khader, M. Tawfik, G. Qi, E. P. Giannelis, CO_2 sorption kinetics of scaled-up polyethylenimine-functionalized mesoporous silica sorbent, Langmuir, 31 (2015) 3569−3576.

[20] G. Qi, Y. Wang, L. Estevez, X. Duan, N. Anako, A. A. Park,W. Li, C. W. Jones, E. P. Giannelis, High efficiency nanocomposite sorbents for CO_2 capture based on amine-functionalized mesoporous capsules, Energy Environ. Sci. 4 (2011) 444–452.

[21] R. Sanz, G. Calleja, A. Arencibia, E. S. Sanz-Pérez, Amino functionalized mesostructured SBA-15 silica for CO_2 capture: Exploring the relation between the adsorption capacity and the distribution of amino groups by TEM, Micropor. Mesopor. Mater.158 (2012) 309–317.

[22] M. Kruk, M. Jaroniec, Characterization of ordered organic-inorganic nanocomposite materials, Chem. Mater. 13 (2001) 3169−3183.

[23] X. Xu, C. Song, J. M. Andresen, B. G. Miller, A. W. Scaroni, Novel polyethylenimine-modified mesoporous molecular sieve of MCM-41 type as high-capacity adsorbent for CO_2 capture, Energy Fuels, 16 (2002) 1463–1469

[24] X. Zhang, X. Zheng, S. Zhang, B. Zhao, W. Wu, AM-TEPA Impregnated disordered mesoporous silica as CO_2 capture adsorbent for balanced adsorption−desorption properties, Ind. Eng. Chem. Res. 51 (2012) 15163−15169.

[25] V. Zelenak, D. Halamova, L. Gaberova, E. Bloch, P. Llewellyn, Amine-modified SBA-12 mesoporous silica for carbon dioxide capture: effect of amine basicity on sorption properties, Microporous Mesoporous Mater. 116 (2008) 358–364.

[26] C.S. Srikanth, S.S.C. Chuang, Infrared study of strongly and weakly adsorbed CO_2 on fresh and oxidatively degraded amine sorbents, J. Phys. Chem. C 117 (2013) 9196–9205.

[27] Y.G. Ko, S.S. Shin, U.S. Choi, Primary, secondary, and tertiary amines for CO2 capture: designing for mesoporous CO_2 adsorbents, J. Colloid Interface Sci. 361 (2011) 594–602.

[28] R. Sanz, G. Calleja, A. Arencibia, E.S. Sanz-Pérez, CO_2 adsorption on branched polyethyleneimine-impregnated mesoporous silica SBA-15, Appl. Surf. Sci. 256 (2010) 5323–5328.

[29] Y. Belmabkhout, N. Heymans, G. D. Weireld, A. Sayari, Simultaneous adsorption of H_2S and CO_2 on triamine-grafted pore-expanded mesoporous MCM-41 silica, Energy Fuels 25 (2011) 1310–1315.

[30] R. Kishor, A. K. Ghoshal, N^1-(3-Trimethoxysilylpropyl)diethylenetriamine grafted KIT-6 for CO_2/N_2 selective separation, RSC Adv., 6 (2016) 898–909.

[31] X. Yan, L. Zhang, Y. Zhang, K. Qiao, Z. Yan, S. Komarneni, Amine-modified mesocellular silica foams for CO_2 capture, Chem. Eng. J. 168 (2011) 918–924.

[32] S. Meth, A. Goeppert, G.K.S. Prakash, G.A. Olah, Silica nanoparticles as supports for regenerable CO_2 sorbents, Energy Fuels 26 (2012) 3082–3090.

[33] Y. Lin, Q. Yan, C. Kong, L. Chen, Polyethyleneimine incorporated metal–organic frameworks adsorbent for highly selective CO_2 capture, Sci. Rep. 3 (2013) 1859.

[34] W. Yan, J. Tang, Z. Bian, J. Hu, H. Liu, Carbon dioxide capture by amine impregnated mesocellular-foam-containing template, Ind. Eng. Chem. Res. 51 (2012) 3653–3662.

CHAPTER 8

POLYETHYLENIMINE FUNCTIONALIZED AS-SYNTHESIZED KIT-6 ADSORBENT FOR HIGHLY CO_2/N_2 SELECTIVE SEPARATION

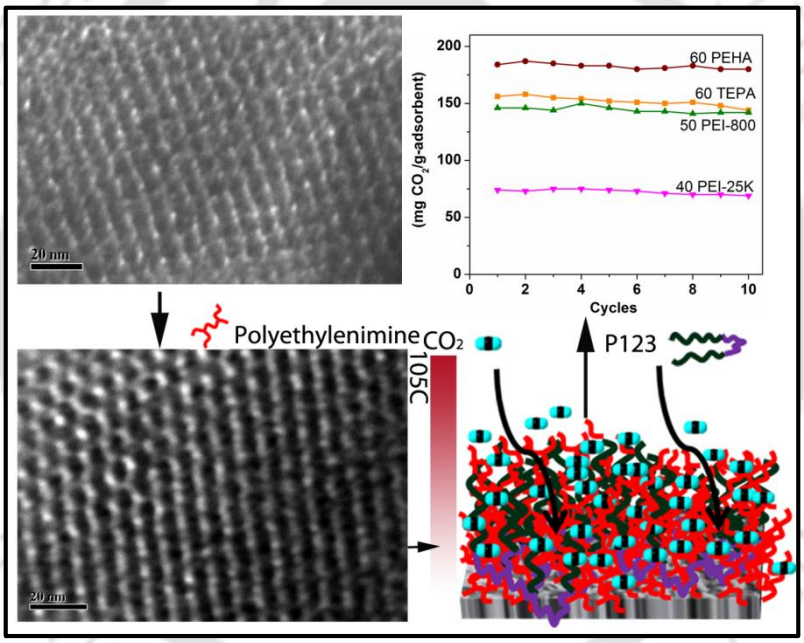

CHAPTER 8

This chapter reports synthesis of CO_2 adsorbent by impregnation of DETA, TEPA, PEHA and polyethylenimine in KIT-6 with confiscated structure directing agent in minimum time and energy. The influence of polyethylenimine on them for CO_2adsorption at wide range of temperature is discussed. This part of work has been published in ***Energy Fuels 30 (2016) 9635−9644.***

8.1. Introduction

Energy insecurity and associated environmental concerns have raised serious concerns on identifying alternate, sustainable, clean energy sources with less environmental impacts [1,2]. Carbon dioxide, the major greenhouse gas generated from burning of fossil fuels such as coal, petroleum oil and natural gas has reached a concentration of ~400 ppm in the atmosphere [2]. The earth's surfaces temperature in 2015 was the warmest since 1980, according to independent analyses by National Aeronautics and Space Administration (NASA) and National Oceanic and Atmospheric Administration (NOAA). Thus, to control the surface temperature, it is the need of the hour to control the CO_2emissions from large anthropogenic sources.

Amine functionalized mesoporous silica shows high CO_2 adsorption capacity even at low partial pressure (~ 0.15 bar) [3–5]. The mesoporous silica is functionalized by aminosilane grafting and polyethylenimine wet impregnation method. In chapters 5 and 6, the calcined KIT-6 was modified with APTES and TMPTA grafting and exhibits the maximum adsorption capacity ~ 1.5 mmol CO_2/g, and ~2.59 mmol CO_2/g, respectively at 30 ºC and 1 bar. In order for solid sorbents to be competitive with existing MEA scrubbing system, the working capacity must be in the range of 3 mmol CO_2/g of sorbent. In chapter 7, different

polyethylenimine functionalized adsorbents showed promising adsorption capacity (~ 4.4 mmol CO_2/g). However, calcination at higher temperature of mesoporous KIT-6 required huge amount of energy as well as time.

Hence, further research is needed to easily synthesize the adsorbent with enhanced CO_2 adsorption performance in wide range of temperature. Therefore, the present chapter explores the merits of different polyethylenimine functionalized as-synthesized KIT-6 (Figure 8.1) by wet impregnation method. Further, the different polyethylenimine loaded adsorbents are subjected to CO_2 adsorption over wide range of temperatures in volumetric adsorption apparatus.

8.2 Materials and Methods

8.2.1 Synthesisof adsorbent

Traditional 3D cubical as-synthesized KIT-6 (ASK) is synthesized by following the procedure of Kim et al. [6] and explained in chapter 3. Polyethylenimine is incorporated in ASK by wet impregnation method [7] as shown in Figure 8.2. The amount of polyethylenimine is calculated using the equation 'x' (wt%) = (wt of polyethylenimine ×100)/ (wt of polyethylenimine + wt of ASK). The synthesis procedure of adsorbents was comprehensively discussed in chapter 3. The resulting adsorbent was denoted as 'x' DETA, 'x' TEPA, 'x' PEHA, 'x' PEI-800 and 'x' PEI-25K.

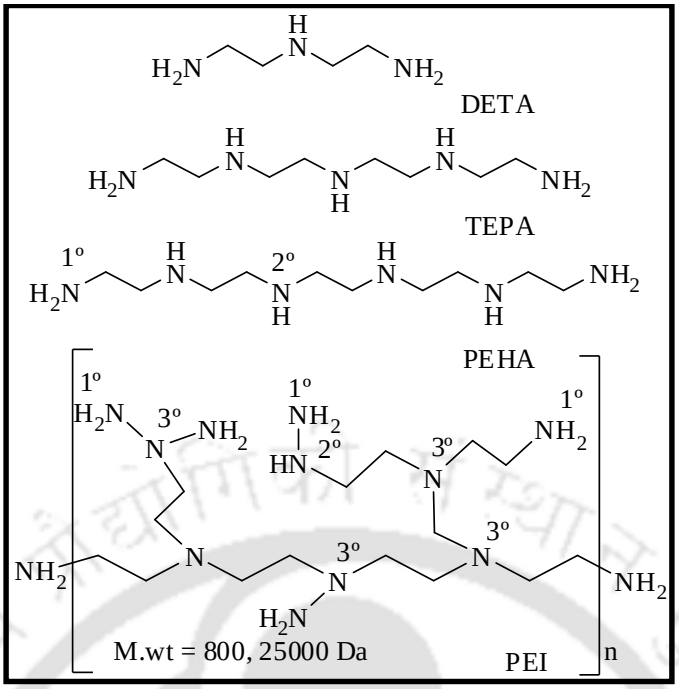

Figure 8.1 Molecular structure of different polyethylenimines

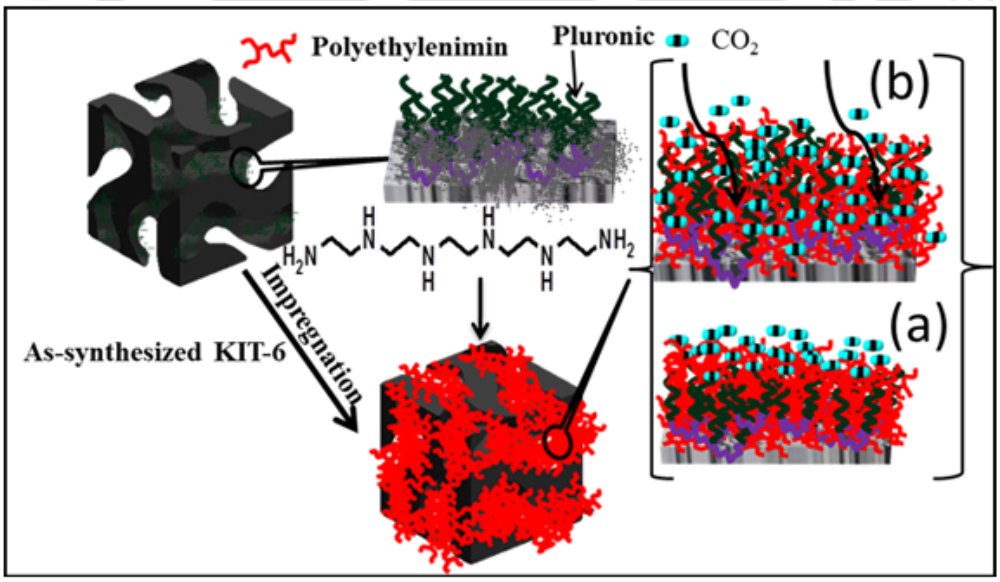

Figure 8.2 Schematic of polyethylenimine impregnation and CO_2 reaction mechanism

8.2.2 Characterizationof adsorbent

The textural properties of synthesized adsorbent are analyzed by N_2 adsorption/desorption isotherm using volumetric adsorption apparatus (Quantachrome, AutosorbiQ). Structural properties of the adsorbent are analyzed by powder X-ray diffraction spectra (Bruker D8 advance diffractometer) using CuKα (λ = 0.154250 nm) radiation between 0.5 to 5 degree. Thermal properties of the adsorbent are performed in thermogravimetric (TG, NETZSCH TG 209F1 Libra) analyzer in the temperature range 30 – 800 ºC with 10 ºC/min heating rate in N_2 atmosphere. Molecular composition of the adsorbent is identified by Fourier transform infrared (FT-IR, PerkinElmer) spectrometer in attenuated total reflection (ATR) mode in the wavenumber range 4000 – 500 cm^{-1}. Apportionment of polyethylenimine on the KIT-6 is analyzed by transmission electron microscope (TEM; JEOL, JEM2100) at 200 kV. Molecular apportionment in amine functionalized adsorbent is analyzed by surface mapping of adsorbent using field emission scanning electron microscope (FESEM, Zeiss Model: Sigma) micrograph. Heat of CO_2 reaction with adsorbent is analyzed by differential scanning calorimeter (DSC, Mettler Toledo) at 75 °C. The CO_2/N_2 adsorption performance of the adsorbent is performed in volumetric adsorption apparatus (Quantachrome, iSorbHP1-XKRLSPN100). The above analytical techniques are comprehensively discussed in Chapter 3.

8.3 Results and Discussion

8.3.1 *N_2 adsorption/desorption isotherm*

N_2 adsorption/desorption isotherms (at −196 ºC) of pure ASK is shown in Figure 4.1. The ASK clearly exhibits type IV isotherm as per IUPAC classification with H1 hysteresis loop, indicating its uniform mesoporous structure. The S_{BET}, W_{BJH} and V_t of ASK are 394 m^2/g, 6.6 nm and 0.86 cc/g, respectively. After calcination at 550 °C for 5 h, mesoporous KIT-6 shows

same structural properties with S_{BET}, W_{BJH} and V_t are 857 m^2/g, 6.6 nm and 1.25 cc/g, respectively. Even after impregnation the adsorbent shows type IV isotherm but N_2 adsorption capacity gradually decreases with increasing polyethylenimine concentration. The S_{BET} and V_t of all the adsorbents decrease gradually with increase in polyethylenimine concentration in the ASK (Figure 8.4) [7,8]. It indicates that the V_t of ASK gradually gets filled with increase in polyethylenimine concentration. However, pore size of adsorbents does not change significantly (Figure 8.3). With ~ 50 wt% polyethylenimine impregnation, the values of S_{BET}, W_d and V_t of the adsorbent are nearly zero, due to complete pore filling of the adsorbent (Figure 8.3, 8.4). Since, V_t of ASK is 0.86 cc/g as mentioned above, it can accommodate a maximum 46 wt% polyethylenimine inside the pores. Thus, in case of polyethylenimine (50 to 60 wt%) concentration, the excess amount covers only the external surface of ASK. The maximum amount of polyethylenimine retained in ASK is found to be 60 wt%. In case of 70 wt% TEPA and PEHA, adsorbents become gel type with light yellow color. However, with 50 wt% PEI-25K, most of the amine is retained outside the porous channels. It is possibly because of the large size of PEI-25K molecules compared to ASK pore size.

8.3.2 *X-ray diffraction analysis*

Low angle powder X-ray diffraction spectra of TEPA impregnated as-synthesized KIT-6 are shown in Figure 8.5. The sharp diffraction peak corresponding to d_{211} plane at 2theta 0.85º indicates that ASK is highly ordered and cubical in nature and is in agreement with previous report [9]. After impregnation, peak intensity gradually decreases with increase in TEPA concentration in the adsorbent, indicating gradual decrease of X-ray scattering towards the silica wall [8,10]. The peak corresponding to d_{211} plane is completely disappeared at above 50 wt% impregnation of TEPA. This is because of the complete surface coverage of ASK with TEPA.

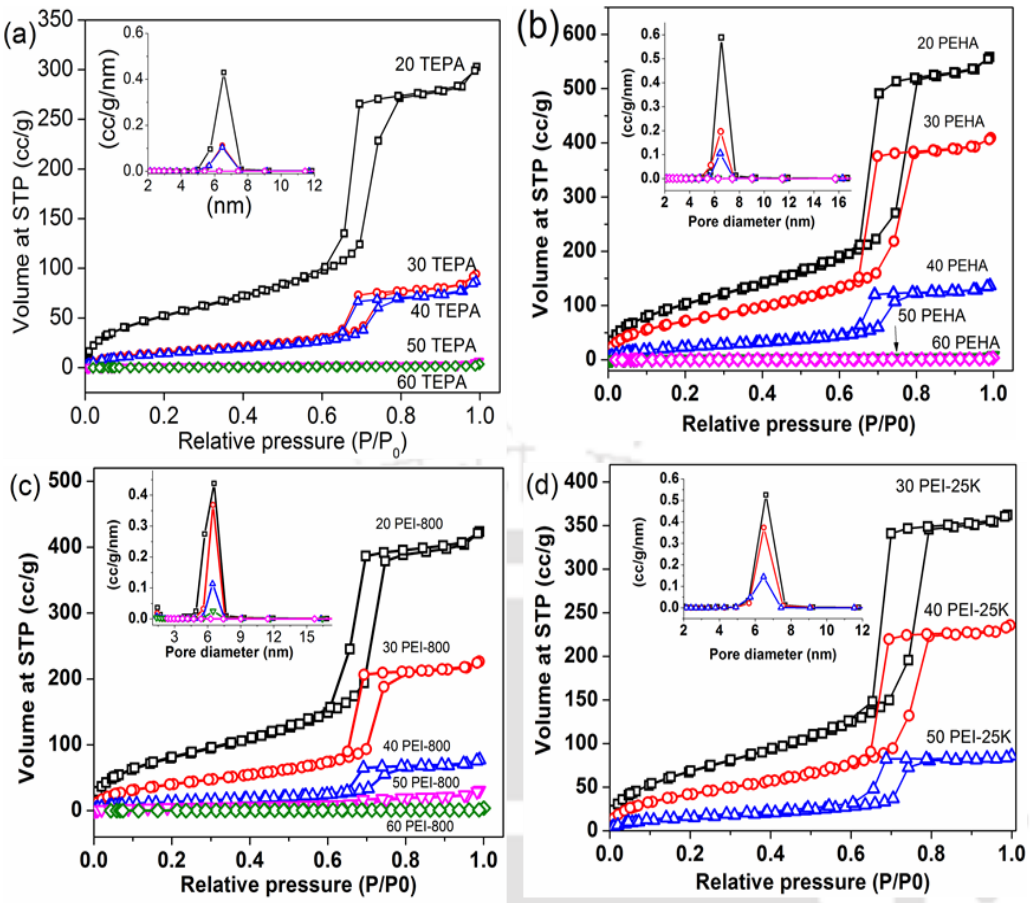

Figure 8.3 N_2 adsorption/desorption isotherm (−196 °C) of (a) TEPA (b) PEHA, (c) PEI-800 and (d) PEI-25K impregnated ASK

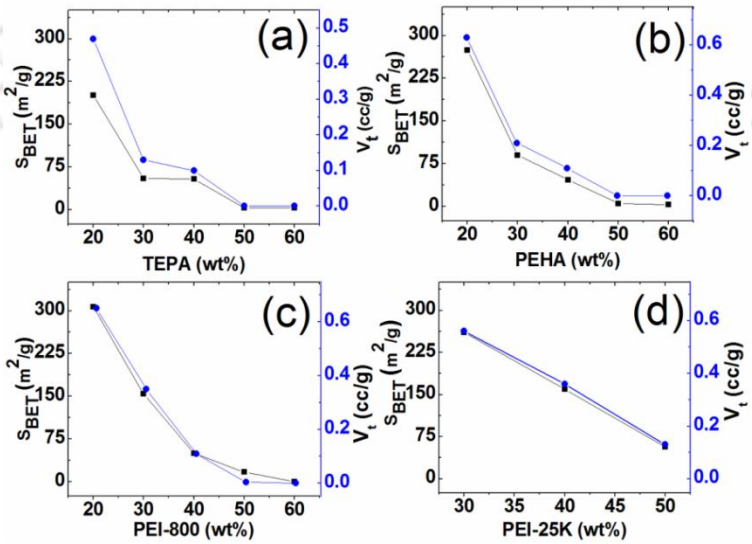

Figure 8.4 Variation of surface area and pore volume of different polyethylenimine impregnated adsorbents (a) TEPA, (b) PEHA, (c) PEI-600 and (d) PEI-25K with concentration

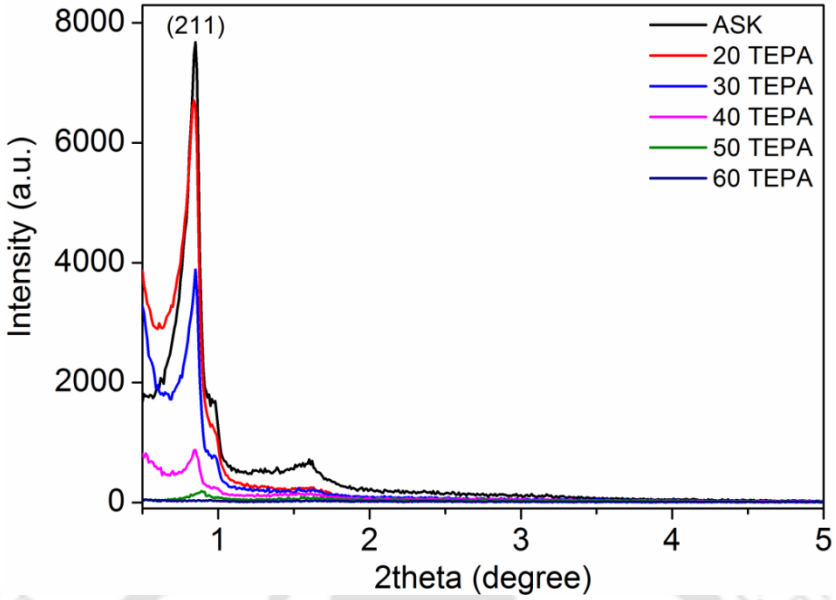

Figure 8.5 X-ray diffraction spectra of TEPA impregnated as-synthesized KIT-6

8.3.3 *Electron micrograph*

Figure 8.6 shows the electron micrograph of ASK before and after polyethylenimine impregnation. FESEM micrograph clearly shows that ASK is colloidal particle with ~1−2 μm size (Figure 8.6a'). TEM micrograph shows that the ASK contains highly ordered and interconnected pore channels (Figure 8.6b) corroborating the results from the X-ray diffraction spectra [9]. However, there is no structural change observed after different polyethylenimine impregnation in ASK as confirmed by FESEM micrograph of 60 TEPA, 60 PEHA, 50 PEI-800 and 50 PEI-25K adsorbents (Figure 8.6), although, most of ASK particles are agglomerated with each other after polyethylenimine impregnation. With increase in the molecular weight of polyethylenimine, the agglomeration of ASK solid particles is increased along with increase in the surface concentration of polyethylenimine [11]. In case of high molecular weight PEI-25K, part of PEI molecule gets inserted in the pore and part remains outside the pore. It is due to increase in agglomeration of ASK solid particles with 40 PEI-25K adsorbent.

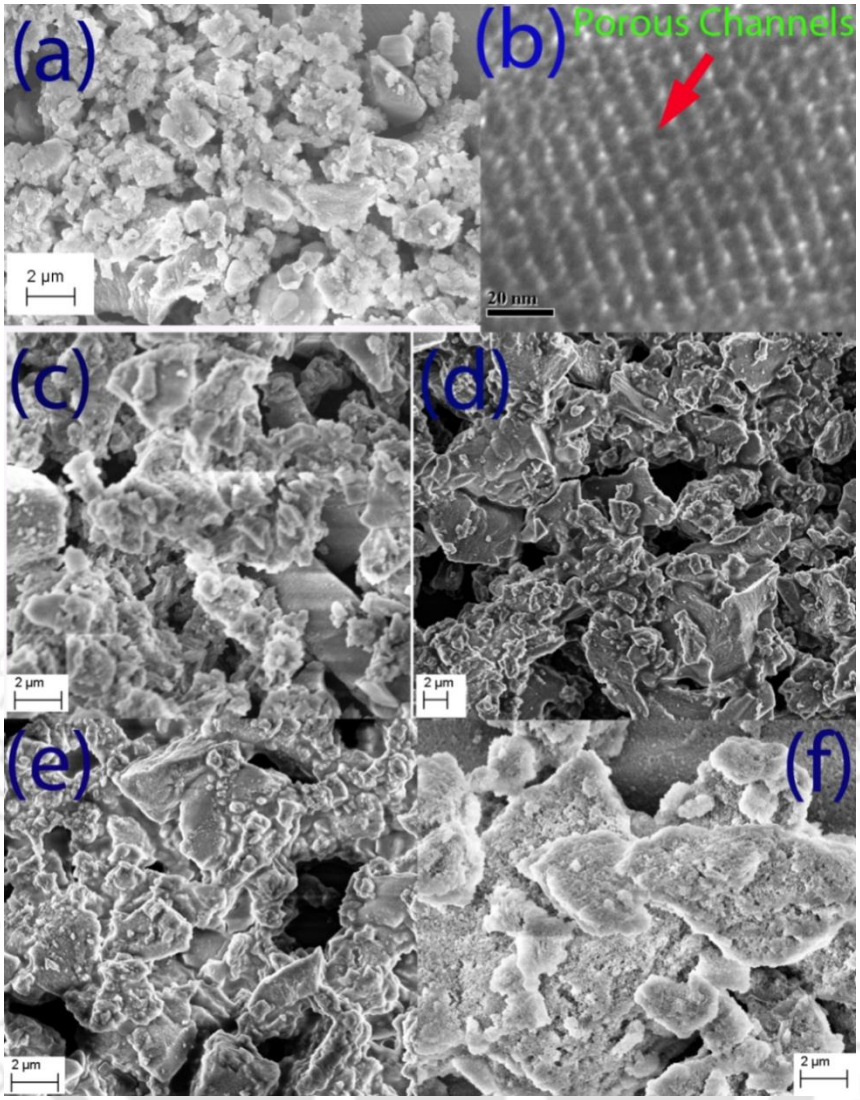

Figure 8.6 FESEM spectra of polyethylenimine impregnated (a) ASK (c) 60 TEPA, (d) 60 PEHA (d) 50 PEI-800 (f) 40 PEI-25K adsorbents and (b) TEM micrograph of ASK

8.3.4 *Attenuated total reflectance analysis*

ATR (attenuated total reflectance) spectra of polyethylenimine impregnated ASK adsorbents are shown in Figure 8.7. Formation of KIT-6 is confirmed by major characteristic bands of silica around 1050 cm^{-1}, 960 $cm^{-1}$and 795 cm^{-1} corresponding to symmetric stretching vibration (Si−O−Si), free surface silanol group (Si−OH) and asymmetric stretching vibration of Si−O−Si of mesoporous KIT-6 [11,12]. The symmetric and asymmetric vibrations of

primary amine (−NH_2) present in the polyethylenimine impregnated adsorbent are confirmed by peaks at 3420 – 3190 cm^{-1} and 1580 cm^{-1}, respectively in the spectra [13,14]. However, the presence of secondary amine (−NH−) is confirmed by peak at 1660 cm^{-1} [13,14]. The sharp band in the range of 2936 – 2820 cm^{-1} and 1460 cm^{-1} represents the stretching vibration of CH_2 and bending vibration of CH present in the polyethylenimine skeletal [15]. The peak around 1350 cm^{-1} is for carbamate formation by chemical reaction between CO_2 and amine group and 1315 cm^{-1} for stretching vibration of –NC present in adsorbents [13,14]. With the percentage increase in polyethylenimine content, the peak area gradually increases in all the adsorbent (Figure 8.7). This is mainly for the similar elemental compounds used in the preparation of amine functionalized ASK.

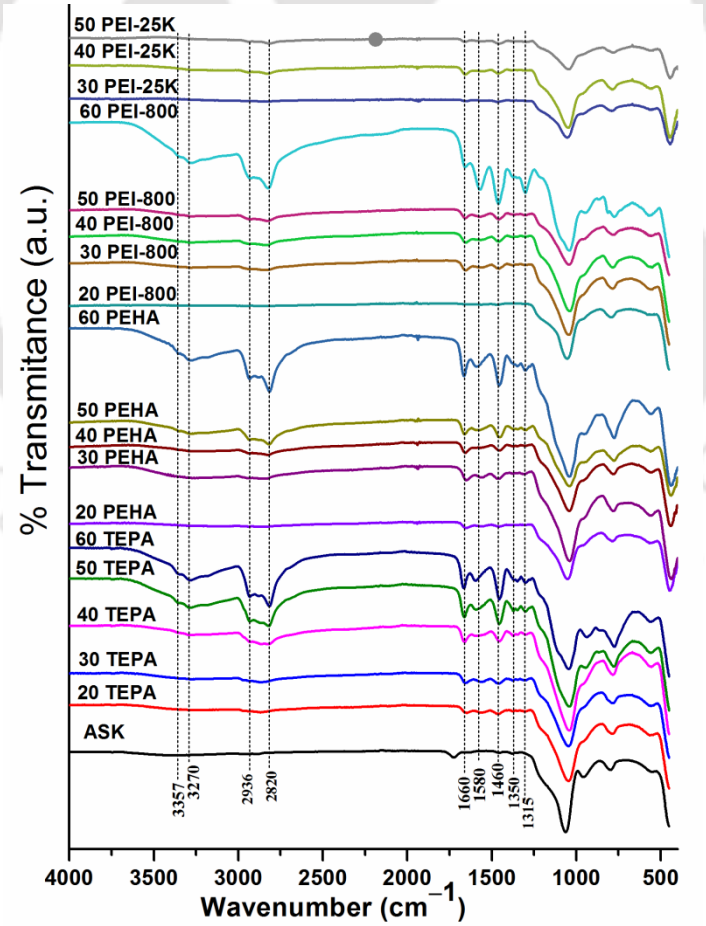

Figure 8.7 Attenuated total reflectance (ATR) spectra of polyethylenimine impregnated ASK

8.3.5 *Thermal analysis*

The thermal stability of ASK and polyethylenimine impregnated 60 TEPA, 60 PEHA, 50 PEI-800 and 50 PEI-25K adsorbents are shown in Figure 8.8. The DTG curve of adsorbent suggests that the total weight loss occurrs in two different stages. The initial weight loss up to ~130 ºC is mainly for physically and chemically pre-adsorbed CO_2, moisture and other gases [8]. The major weight loss in ASK between 150 – 500 ºC is due to thermal degradation of Pluronic P123. It is confirmed from the DTG analysis of Pluronic P123. It is completely degraded around 400 ºC (Figure 8.8b). Further weight loss in ASK at higher temperature is for surface de-hydroxylation [16]. The major weight loss between 150 – 350 ºC in adsorbent is attributable to the volatilization and decomposition of TEPA and PEHA molecules [7,15,17]. However, degradation temperature is nearly 350 ºC with polyethylenimine impregnated ASK. The thermal stability of adsorbents follows the order: TEPA < PEHA < PEI-800 < PEI-25K, i.e. stability increases with increasing molecular weight of polyethylenimine. As observed earlier, thermal stability of polyethylenimine impregnated calcined MCM-41 (~200 ºC), SBA-15 (~ 200 ºC) and KIT-6 (~ 220 ºC) is significantly lower than that of ASK (350°C) based adsorbent [7,17,19]. Thus, the presence of Pluronic P123 significantly improves the thermal stability of ASK based adsorbent by forming the Pluronic P123 and polyethylenimine composite.

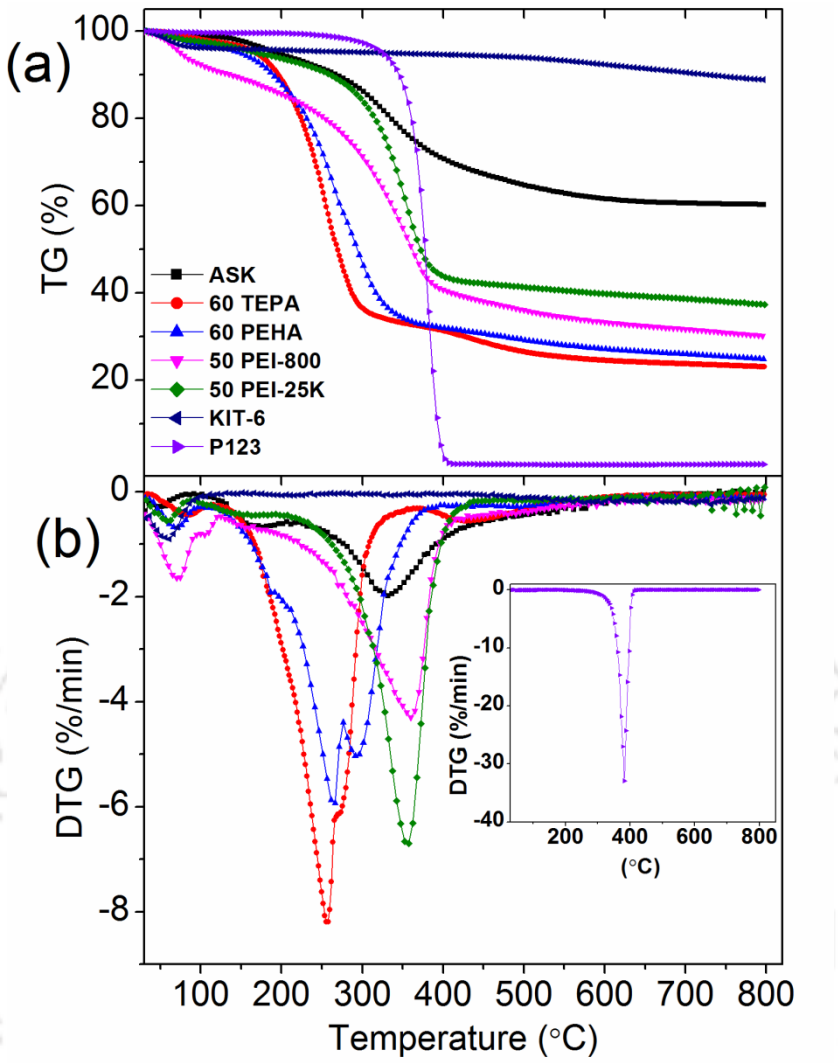

Figure 8.8 Thermo gravimetric analysis of pure and polyethylenimine impregnated as-synthesized KIT-6 in N_2 atmosphere with 10 °C/min heating rate

8.3.6 *CO_2/N_2 adsorption analysis*

8.3.6.1 *Effect of polyethylenimine loading*

The synergistic effects of as-synthesized mesoporous silica with wide varieties of polyethylenimine present in adsorbent on CO_2 sorption capacity have spurred the recent interest in exploring this hybrid material for designing the high CO_2/N_2 selective adsorbent. The pure mesoporous silica as well as polyethylenimine has low CO_2 sorption capacity,

however the polyethylenimine and mesoporous silica composite improved the sorption capacity [18]. For preliminary screening, a series of polyethylenimine (Figure 8.1) impregnated ASK with different loading in the range 20 -70 wt% are synthesized and subjected to CO_2 adsorption performance at 75 ^oC. In case of diethylenetriamine ($HN(CH_2CH_2NH_2)_2$) impregnated ASK based adsorbent, most of the amine is leached out from the adsorbent during drying and degassing of adsorbent. It was confirmed by the initial and final weight difference of the adsorbent. The above observation confirms that diethylenetriamine impregnated ASK based adsorbent possess very low thermal stability [19] and is found to be not suitable for CO_2 separation during real practical application. In case of TEPA, 60 wt% maximum loading is obtained over ASK but with further increase in concentration, the adsorbent turns in to a yellow gel. Similar behavior is also observed with PEHA. In case of 50 PEI-25K, most of the amine is retained outside the ASK as shown in the Figure 8.9. It is mainly for highly branched and ultra-large molecular size of PEI (M_w = 25K).

Figure 8.9 50 PEI-25K (Mw = 25K) impregnated as-synthesized KIT-6

The CO_2 sorption performances of all different quantities of PEI impregnated ASK are summarized in Figure 8.10. The CO_2 sorption capacity gradually increases with increase in amine loading. The maximum CO_2 sorption capacity is about 3.1, 3.15, 3.27 and 1.45 mmol CO_2/g of 60 TEPA, 60 PEHA, 50 PEI-800 and 40 PEI-25K adsorbent respectively at 75 ºC and 1 bar. In PEI-800, 50 wt% impregnated adsorbent shows the maximum adsorption capacity (3.27 mmol CO_2/g adsorbent), and 40 PEI-25K shows the maximum sorption of 1.45 mmol CO_2/g adsorbent. Further increase in polyethylenimine concentration results in the sharp reduction of CO_2 adsorption capacity which is attributed to the reduction of accessible amine sites during adsorption [18]. In addition to that, low loading of PEI-25K inside the pores of ASK also reduces the CO_2 sorption capacity of adsorbent.

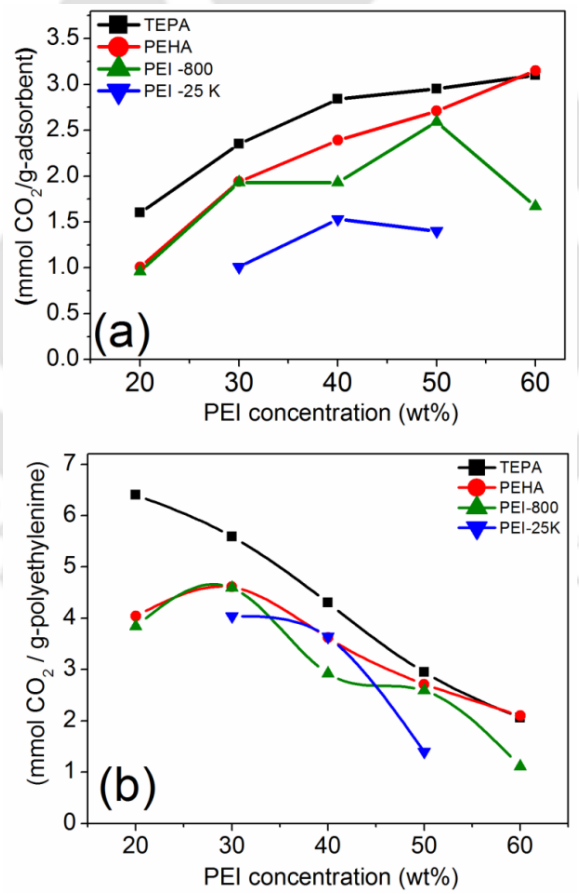

Figure 8.10 (a) CO_2 adsorption capacity and (b) different polyethylenimine efficiency of adsorbents

The polyethylenimine efficiency is defined as the ratio of the amount of CO_2 adsorbed to the polyethylenimine present in the adsorbent after impregnation [20]. It indirectly indicates the CO_2 adsorption behavior towards amine moieties by chemisorption with increasing concentration of polyethylenimine. The 20 TEPA shows the highest efficiency (ca. 6.38 mmol CO_2/g-TEPA) which decreases with increase in its concentration in the adsorbent as shown in Figure 8.10b. The similar trends are also observed for PEHA, PEI-800 and PEI-25K impregnated adsorbents. However, increase in loading and molecular weight reduces the polyethylenimine efficiency [20−22]. At low amine loading, the porosity of the adsorbent is higher compared to higher amine loading (Figure 8.4), which provides better dispersion of polyethylenimine inside the porous channels and reduces the CO_2 transfer resistance towards amines sites. Additionally, CO_2 diffusional resistance increases with increasing the molecular weight of polyethylenimine and reduces the CO_2 interaction with amine present in the lower layer of polyethylenimine [8,19,22].

It is interesting to observe that the adsorption capacity increases with increasing amine group numbers in TEPA to PEHA. However, increase in high molecular weight of polyethylenimine in adsorbent results in the drastic reduction of sorption capacity (Figure 8.10). The reduction in adsorption capacity with increasing molecular weight of polyethylenimine can be understood on the basis of its molecular structure and CO_2 reaction mechanism. TEPA and PEHA consists of primary and secondary amine groups (Figure 8.1). However, highly branched polyethylenimine (PEI-800 and PEI-25K) is a combination of primary, secondary and tertiary amines. The ratios of primary, secondary and tertiary amine are changed form 42:33:25 (PEI-800) to 31:39:30 (PEI 25K) when the molecular weight is increased from 800 to 25K Da [23]. Primary and secondary amines can react with dry CO_2 to form carbamates through the formation of zwitterionic intermediates [24]. The zwitterionic mechanism was elaborated by Caplow [25]. However, tertiary amine reacts only in aqueous

condition and reflects very low adsorption capacity [24,25]. Ko et al.[24] showed that the CO_2 sorption capacity and rate of adsorption follow the order tertiary amine < secondary amine < primary amine. Thus, the reduction in primary and secondary amine in polyethylenimine with increase in molecular weight consequently reduces the CO_2 sorption capacity of the adsorbent.

8.3.6.2 *Effect of adsorption temperature*

In order to understand the effect of temperature on sorption performance, the adsorption isotherm experiments are performed between 30 to 105 ºC with 15 ºC interval for pure CO_2 and the results are depicted in Figure 8.11. The CO_2 adsorption capacity is increased with increasing adsorption temperature from 30 ºC to 105 ºC in all the adsorbent. The similar adsorption isotherm trends were also observed with different polyethylenimine impregnated adsorbents such as calcined mesoporous silica (MCM-41, SBA-15 and MCF) activated carbon [26] and metal organic frameworks [27].

The CO_2 sorption capacity is sharply increased at low partial pressure (less than 0.1 bar) in all of the polyethylenimine functionalized ASK and then approached a saturation with a further increase in pressure. The sharp increase in adsorption capacity at low partial pressure is mainly for the chemisorption between CO_2 and amine sites present in the adsorbent [11,13,15,28]. A further increase in adsorption capacity at higher partial pressure can be for the diffusion of CO_2 inside the amine layer present in the adsorbent. The maximum adsorption capacity of 60 TEPA, 60 PEHA, 50 PEI-800 and 40 PEI-25K is (3.13 – 3.56), (3.86 – 4.20), (3.15 – 3.34) and (1.61 – 1.68) mmol CO_2/g-adsorbent, respectively between (90 – 105) ºC and 1 bar. The results suggest that the adsorption capacities of polyethylenimine impregnated ASK shows better adsorption performance than earlier reported adsorbents except disordered mesoporous silica (Table A1).

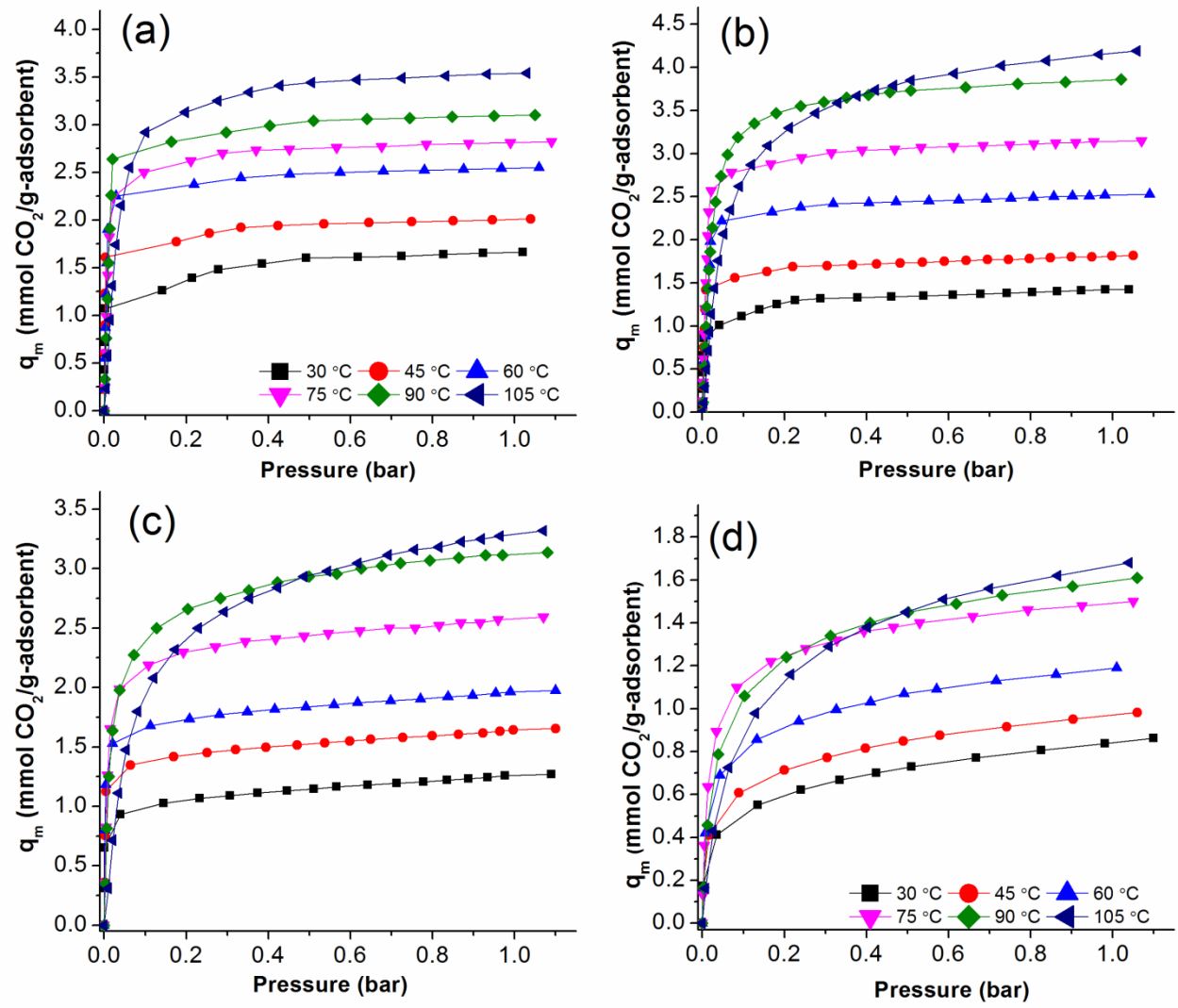

Figure 8.11 CO_2 adsorption performance of (a) 60 TEPA (b) 60 PEHA (c) 50 PEI-800 and (d) 40 PEI-25K adsorbent at different temperatures

The low temperature range is thermodynamically more favorable for the CO_2 adsorption and high temperature for desorption [13]. Additionally, adsorption capacity is also proportional to the exposed amine sites for CO_2 in polyethylenimine functionalized adsorbent [16,28,29]. The electron micrograph and N_2 adsorption isotherm clearly show polyethylenimine filled porous channels of ASK during impregnation. At low temperature, CO_2 reacts with exposed amine sites present on the adsorbent surface [7,22]. Increasing trends of CO_2 sorption

capacity indicates the increase in number of exposed amine sites with increase in adsorption temperature [8]. Increase in adsorption temperature reduces the viscosity and thereby increases the intermolecular distance between polyethylenimine molecules that exposes maximum amine sites for CO_2 adsorption in the inner layer of polyethylenimine [19,20,22]. Additionally, it also reduces the CO_2 diffusional resistance in the inner layer of polyethylenimine enabling higher temperature (90−105ºC) beneficial for CO_2 adsorption. However, further increase in the temperature to (120 ºC) leads to the sharp decrease of adsorption capacity in low partial pressure (less than 0.2 bar) as because CO_2 desorption is more favorable than adsorption (Figure 8.12).

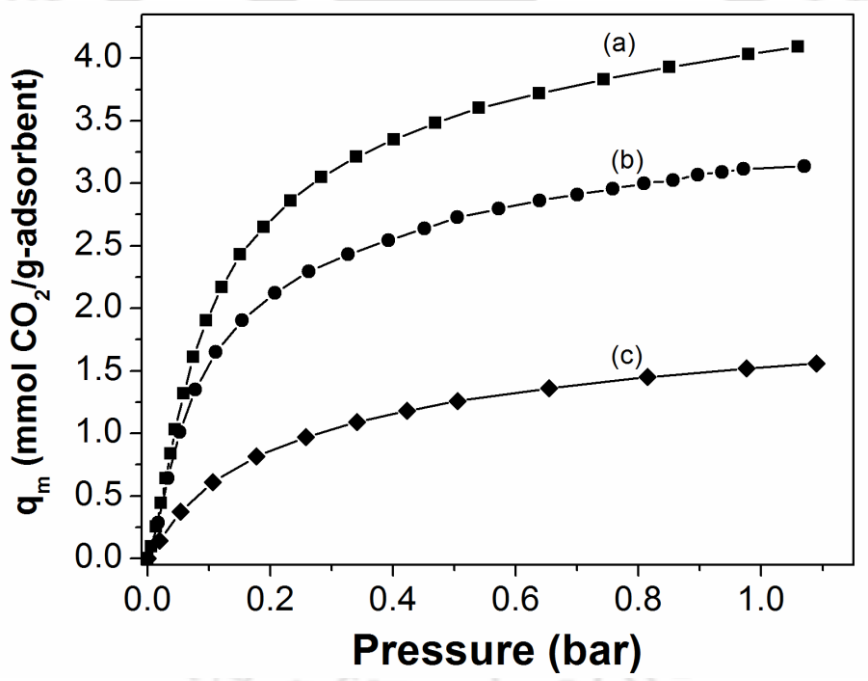

Figure 8.12 CO_2 adsorption isotherms of (a) 60 PEHA, (b) 50 PEI-800 and (c) 40 PEI-25K at 120 ºC

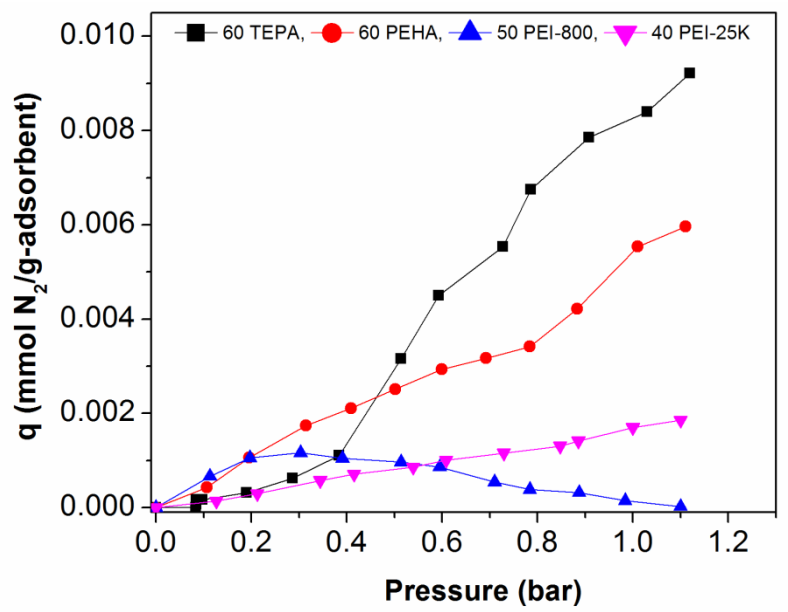

Figure 8.13 N_2 adsorption isotherm (90 ºC) of polyethylenimine impregnated as-synthesized KIT-6

The N_2 adsorption isotherm of 60 TEPA, 60 PEHA, 50 PEI-800 and 40 PEI-25K adsorbent at 90 ºC is shown in Figure 8.13. The ultralow N_2 sorption capacity at 1 bar of 60 TEPA (~ 9.2× 10^{-3} mmol N_2/g), 60 PEHA (~5.9 × 10^{-3} mmol N_2/g), 50 PEI-800 (~ 0.0 mmol N_2/g) and 40 PEI-25K (0.0 mmol N_2/g) compared to CO_2 indicates that synthesized adsorbents have very high selectivity towards CO_2 in flue gas of large anthropogenic source, where N_2 is the primary component of the mixture.

In order to understand the effect of Pluronic P123 in polyethylenimine impregnated ASK, the CO_2 adsorption of 60 wt% TEPA, 60 wt% PEHA and 50 wt% PEI-800 impregnated KIT-6 is compared at different temperatures viz. 75, 90 and 105ºC. The adsorption capacity of PEI-800 impregnated KIT-6 is significantly improved. However, the sorption of TEPA, and PEHA impregnated KIT-6 is sparsely decreased (chapter 7). It indicates that P123 have important role in CO_2 adsorption. The non-ionic P123 contains the both hydrophilic poly(ethylene glycol)chain (PEO) and hydrophobic poly(propylene glycol) chain (PPO).

During KIT-6 synthesis, PPO is present in the core while PEO in the shell of the micelle [30].After synthesis, PEO is found in the porous channel of KIT-6. During impregnation, PEO chain present on the surface gets inserted in the polyethylenimine layer as shown in Figure 8.2 and enhances the dispersion of polyethylenimine. During adsorption, PEO acts as a CO_2 carrier facilitating transport in to the inner layer of polyethylenimine [31] (Figure 8.2b, 8.14) and reduces the CO_2 diffusional resistance during adsorption and also increases the amine utilization ratio.

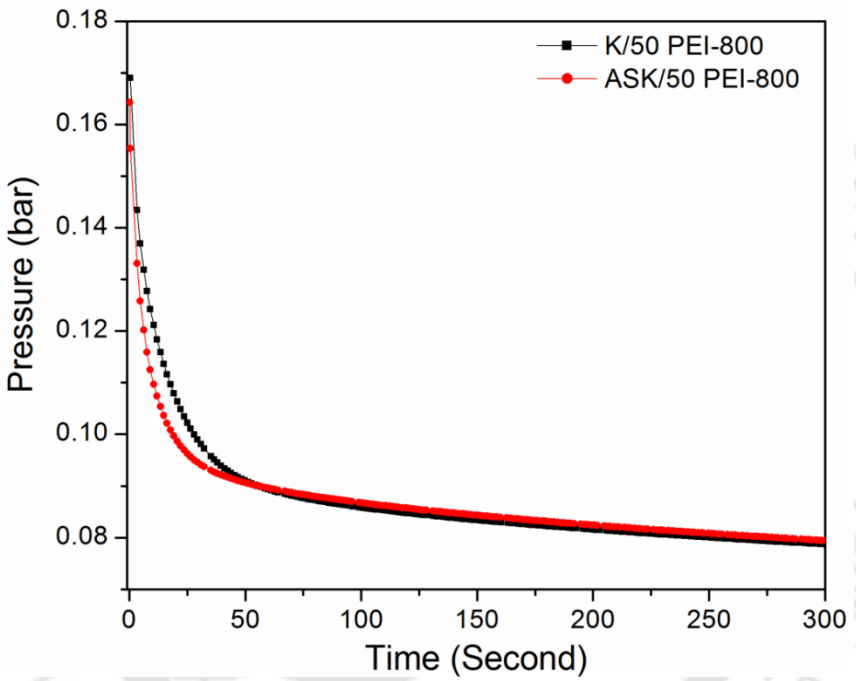

Figure 8.14 CO_2 adsorption kinetics of PEI-800 impregnated adsorbent at 75°C (■ − calcined KIT-6 and ● – as-synthesized KIT-6)

8.3.6.3 *The enthalpy of CO_2 adsorption*

The isosteric heat of adsorption (ΔHq) at a fixed adsorption capacity (q) was calculated from Clausius–Clapeyron equation: $\ln(p) = [(\Delta Hq)/RT] + C$; where C, R, p and T represent the constant, gas constant, applied pressure at constant sorption capacity and temperature, respectively [16]. The ΔHq value is evaluated from the slope of the linear plot between $\ln(p)$ vs $1/T$ at the same adsorbed capacity. The plots of different polyethyleneimine impregnated adsorbents are depicted in Figure 8.15. The ΔHq is found to be 89 kJ/mol, 124 kJ/mol, 125 kJ/mol and 94 kJ/mol for 60 TEPA, 60 PEHA, 50 PEI-800 and 40 PEI-25K adsorbent, respectively. The higher value of isosteric heat of adsorption indicates strong interaction (chemisorption) between CO_2 and amine sites present in the adsorbent [12,20,32]. The heat of adsorption of pure adsorbent such as mesoporous silica, zeolite, activated carbon and metal organic frameworks lies between 18 – 50 kJ/mol [26,29,33]. Addition of polyethylenimine in the adsorbent increases the heat of adsorption to greater than 50 kJ/mol and reaches up to 140 kJ/mol) [13,16,32,34].

Gray et al. [35] suggested that the heat required for regenerationof adsorbed CO_2 could be predicted by the following equation: $Q \approx \Delta H_r + mC_P\Delta T$, where Q is regeneration heat duity, ΔH_r is heat of reaction, m is adsorbent quantity, C_P is heat capacity, and ΔT is the change in temperature. The sensible heat ($mC_P\Delta T$) is much lower than ΔH_r for amine functionalized mesoporous silica [36].The ΔH_r is analyzed from the DSC profile (area correspond to exothermic peak) in presence of pure CO_2 at 75 °C (Figure 8.16). The CO_2 adsorption capacity of 60 TEPA, 60 PEHA and 50 PEI-800 is 124 mg/g (2.82 mmol/g), 139 mg/g (3.15 mmol/g) and 114 mg/g (2.59 mmol/g) at 75 °C and 1 bar, respectively. The ΔH_r of 60 TEPA, 60 PEHA and 50 PEI-800 is 81 kJ/mol CO_2, 61 kJ/mol CO_2 and 68 kJ/mol CO_2, respectively, which is much lower than that of 30% MEA solution (198.24 kJ/mol CO_2) [13].

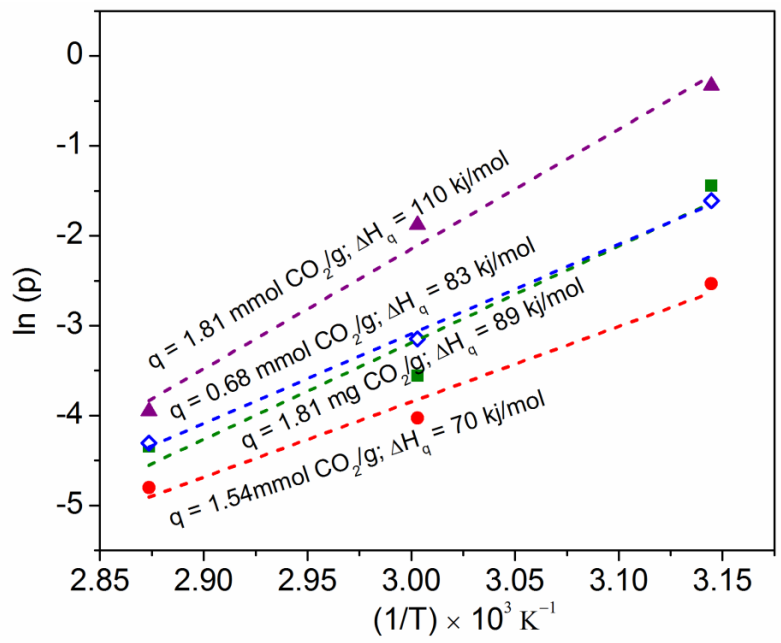

Figure 8.15 Variation of ln(p) with 1/T of different adsorbents (■ − 60 TEPA; ● − 60 PEHA; ▼ − 50 PEI-800; ♦ − 40 PEI-25K) by Clausius− Clapeyron equation

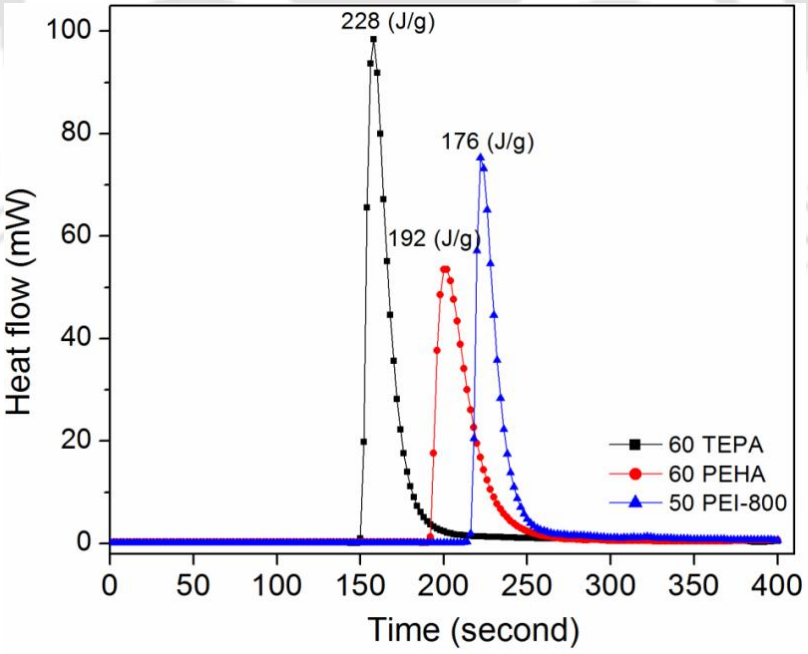

Figure 8.16 DSC profile of polyethylenimine impregnated ASK in presence of CO_2 at 75°C

8.3.6.4 *Cyclic adsorption performance*

Stable sorption capacity during cyclic adsorption/desorption performance over wide range of temperature and pressure is the desirable requirement for a good industrial adsorbent. An extensive cyclic adsorption/desorption (Ads/Des) performance of the adsorbents are performed at (90 ºC/100 ºC) and (105 ºC/100 ºC). Figure 8.17 shows the cyclic performance of the 60 TEPA, 60 PEHA, 50 PEI-800 and 40 PEI-25K adsorbent with pure CO_2. The cyclic performance reveals that the synthesized adsorbents show a very stable sorption capacity between 90 to 105 ºC adsorption temperatures. Even after 10^{th} cycles, 60 TEPA (2.95 – 3.27 mmol CO_2/g), 60 PEHA (3.75 – 4.1 mg CO_2/g), 50 PEI-800 (3.02 – 3.22 mmol CO_2/g) and 40 PEI-25K (1.6 – 1.56 mmol CO_2/g) show less than 2 − 3% reduction in sorption capacity between (90 – 105) ºC sorption temperatures. However, lower molecular weight polyethylenimine such as TEPA, PEHA impregnated calcined mesoporous silica are generally reported to have significant loss in adsorption capacity during cyclic performance [35,36]. These results suggest that the above synthesized adsorbent (60 PEHA) can a potential adsorbent for practical application.

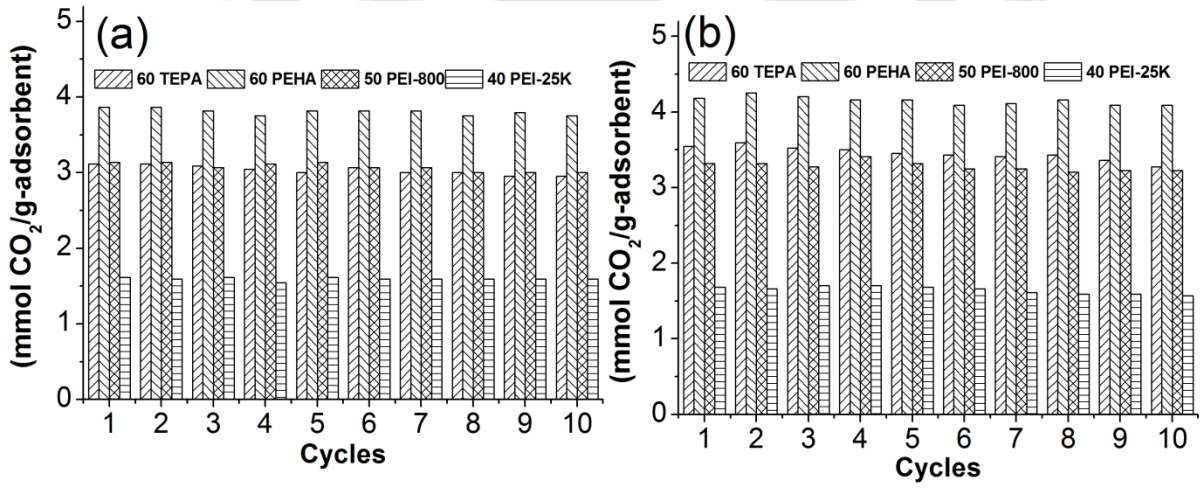

Figure 8.17 CO_2 adsorption performances at (a) 90 ºC adsorption/100 ºC desorption and (b) 105 ºC adsorption/100 ºC desorption of different adsorbents

8.4 Conclusions

In this chapter, three dimensional ASK is functionalized with TEPA, PEHA, PEI-800 and PEI-25K at different loadings by wet impregnation method and subjected to CO_2 adsorption. Increasing polyethylenimine concentration decreases the surface area and pore volume of the adsorbent by filing the porous channel of ASK. Pluronic P123 present in KIT-6 enhances the thermal stability of the polyethylenimine impregnated adsorbents. The sorption capacity of all the adsorbents (60 TEPA, 60 PEHA, 50 PEI-800 and 40 PEI-25K) increases with increasing temperature from 30 to 105 ºC. Shorter chain amine TEPA and PEHA with low molecular weight shows higher adsorption capacity than high molecular weight PEI-800 and PEI-25K. However, 60 PEHA shows the maximum sorption capacity ca. 3.86 – 4.18 mmol CO_2/g-adsorbent at 90−105 ºC and 1 bar with stable cyclic performance. Polyethylenimine impregnated adsorbents that are developed here can be synthesized energy efficiently and more easily as compared to calcined silica. The adsorbents are also highly regenerable. Thus, high sorption capacity at low partial pressure and high temperature make ASK (particularly, 60 PEHA) a promising candidate for CO_2 capture from large anthropogenic source such as coal based thermal power plant.

References

[1] Key world energy statistics 2015, The international energy agency (www.iea.org/publications/freepublications/publication/KeyWorld_Statistics_2015.pdf)

[2] P. Tans, NOAA/ESRL (www.esrl.noaa.gov/gmd/ccgg/trends/) and Keeling, R. Scripps Institution of Oceanography (scrippsco2.ucsd.edu/).

[3] P. Markewitz, W. Kuckshinrichs, W. Leitner, J. Linssen, P. Zapp, R. Bongartz, A. Schreibera, T. E. Müller, Worldwide innovations in the development of carbon capture technologies and the utilization of CO_2, Energy Environ. Sci. 5 (2012) 7281–7305.

[4] G. Zhang, P. Zhao, Y. Xu Development of amine-functionalized hierarchically porous silica for CO2 capture. J. Ind. Eng. Chem.54 (2017) 59-68.

[5] C. Chen, S. Bhattacharjee, Trimodal nanoporous silica as a support for amine-based CO2 adsorbents: Improvement in adsorption capacity and kinetics, Appl. Surf. Sci. 396 (2017) 1515–1519.

[6] T.-W. Kim, F. Kleitz, B. Paul, R. Ryoo, MCM-48-like large mesoporous silicas with tailored pore structure facile synthesis domain in a ternary triblock copolymer-butanol-water system, J. Am. Chem. Soc. 127 (2005) 7601-7610.

[7] X. Wang, X. Ma, C. Song, D. R. Locke, S. Siefert, R. E. Winans, J. Möllmer, M. Lange, A. Möller, R. Gläser, Molecular basket sorbents polyethylenimine-SBA-15 for CO_2 capture from flue gas: Characterization and sorption properties. Microporous Mesoporous Mater.169 (2013) 103–111.

[8] K. Li, J. Jiang, S. Tian, F. Yan, X. Chen, Polyethyleneimine–nanoSilica composites: A low cost and promising adsorbent for CO_2 capture. J. Mater. Chem. A 3 (2015) 2166–2175.

[9] F. Kleitz, S. H. Choi, R. Ryoo, Cubic Ia3d large mesoporous silica: Synthesis and replication to platinum nanowires, carbon nanorods and carbon nanotubes. Chem. Commun. 2003, 2136–2137.

[10] R. Sanz, G. Calleja, A. Arencibia, E.S. Sanz-Pérez, CO_2 adsorption on branched polyethyleneimine-impregnated mesoporous silica SBA-15. Appl. Surf. Sci. 256 (2010) 5323–5328.

[11] M. J. Al-Marri, M. M. Khader, M. Tawfik, G. Qi, E. P. Giannelis, CO_2 sorption kinetics of scaled-up polyethylenimine-functionalized mesoporous silica sorbent. Langmuir 31 (2015) 3569−3576.

[12] R. Kishor, A. K. Ghoshal, N^1-(3-Trimethoxysilylpropyl)diethylenetriamine grafted KIT-6 for CO_2/N_2 selective separation. RSC Adv. 6 (2016) 898–909.

[13] F. Su, C. Lu, H.-S. Chen, Adsorption, desorption, and thermodynamic studies of CO_2 with high-amine-loaded multiwalled carbon nanotubes. Langmuir 27 (2011) 8090–8098.

[14] C. S. Srikanth, S. S. C. Chuang, Infrared study of strongly and weakly adsorbed CO_2 on fresh and oxidatively degraded amine sorbents. J. Phys. Chem. C 117 (2013) 9196−9205.

[15] F. Su, C. Lu, S.-C. Kuo, W. Zeng, Adsorption of CO_2 on amine-functionalized Y-type zeolites. Energy Fuels 24 (2010) 1441–1448.

[16] L. Wang, R. T. Yang, Increasing selective CO_2 adsorption on amine-grafted SBA-15 by increasing silanol density. J. Phys. Chem. C 115 (2011) 21264–21272.

[17] X. Xu, C. Song, J. M. Andresen, B. G. Miller, A. W. Scaroni, Novel polyethylenimine-modified mesoporous molecular sieve of MCM-41 type as high-capacity adsorbent for CO_2 capture. Energy Fuels 16 (2002) 1463−1469.

[18] W.-J. Son, J.-S. Choi, W.-S. Ahn, Adsorptive removal of carbon dioxide using polyethyleneimine-loaded mesoporous silica materials. Microporous Mesoporous Mater. 113 (2008) 31–40.

[19] A. Goeppert, S. Meth, G. K. S. Prakash, G. A. Olah, Nanostructured silica as a support for regenerable high-capacity organoamine-based CO_2 sorbents. Energy Environ. Sci. 3(2010) 1949–1960.

[20] D. J. Fauth, M. L. Gray, H. W. Pennline, Investigation of porous silica supported mixed-amine sorbents for post-combustion CO_2 Capture. Energy Fuels 26 (2012) 2483−2496.

[21] J. Wang, M. Wang, W. Li, W. Qiao, D. Long, L. Ling, Application of polyethylenimine-impregnated solid adsorbents for direct capture of low-concentration CO_2. AIChE J. 61 (2015) 972−980.

[22] J. Zhao, F. Simeon, Y. Wang, G. Luo, T.A. Hatton, Polyethylenimine-impregnated Siliceous Mesocellular Foam Particles as High capacity CO_2 Adsorbents. RSC Adv. 2012, 2, 6509–6519.

[23] A.V. Harpe, H. Petersen, Y. Li, T. Kissel, Characterization of commercially available and synthesized polyethylenimines for gene delivery. J. Controlled Release 69 (2000) 309–322.

[24] Y. G. Ko, S. S. Shin, U. S. Choi, Primary, Secondary, and Tertiary amines for CO_2 capture: designing for mesoporous CO_2 adsorbents. J. Colloid Interface Sci. 361 (2011) 594–602.

[25] M. Caplow, Kinetics of carbamate formation and breakdown. J. Am. Chem. Soc. 90:24 (1968) 6795–6803.

[26] N. P. Wickramaratne, M. Jaroniec, Activated carbon spheres for CO_2 adsorption, ACS Appl. Mater. Interfaces, 5 (2013) 1849−1855.

[27] Y. Lin, H. Lin, H. Wang, Y. Suo, B. Li, C. Kong, L. Chen, Enhanced selective CO_2 adsorption on polyamine/MIL-101(Cr) composites. J. Mater. Chem. A 2 (2014) 4658–14665.

[28] A. Sayari, Y. Belmabkhout, Stabilization of amine-containing CO_2 adsorbents: Dramatic effect of water vapor. J. Am. Chem. Soc. 132 (2010) 6312–6314.

[29] R. Kishor, A. K. Ghoshal, APTES grafted ordered mesoporous silica KIT-6 for CO_2 adsorption. Chem. Eng. J. 262 (2015) 882–890.

[30] Manet, S.; Lecchi, A.; Impéror-Clerc, M.; Zholobenko, V.; Durand, D.; Oliveira, C. L. P.; Skov Pedersen, J.; Grillo, I.; Meneau, F.; Rochas, C. Structure of micelles of a nonionic block copolymer determined by SANS and SAXS. J. Phys. Chem. B 115 (2011) 11318–11329.

[31] J. Wang, D. Long, H. Zhou, Q. Chen, X. Liu, L. Ling, Surfactant promoted solid amine sorbents for CO_2 capture, Energy Environ. Sci. 5 (2012) 5742–5749.

[32] W. Yan, J. Tang, Z. Bian, J. Hu, H. Liu, Carbon dioxide capture by amine-impregnated mesocellular-foam-containing template, Ind. Eng. Chem. Res. 51 (2012) 3653−3662.

[33] Y. Park, Y. Ju, D. Park, C.-H. Lee, Adsorption equilibria and kinetics of six pure gases on pelletized zeolite 13X up to 1.0 MPa: CO_2, CO, N_2, CH_4, Ar and H_2.Chem. Eng. J. 292 (2016) 348–365.

[34] P. Bollini, S. A. Didas, C. W. Jones, Amine-oxide hybrid materials for acid gas separations. J. Mater. Chem. 21 (2011) 15100–15120.

[35] M. L. Gray, J. S. Hoffman, D. C. Hreha, D. J. Fauth, S. W. Hedges, K. J. Champagne, H. W. Pennline, Parametric study of solid amine sorbents for the capture of carbon dioxide. Energy Fuels 23 (2009) 4840–4844.

[36] K. Li, J. Jiang, F. Yan, S. Tian, X. Chen, The influence of polyethyleneimine type and molecular weight on the CO_2 capture performance of PEI-nano silica adsorbents. Applied Energy 136 (2014) 750–755

CHAPTER 9

CONCLUSIONS AND FUTURE SCOPE

CHAPTER 9

This chapter summarizes the major inferences drawn from the doctoral work and outlines the scope for future studies.

The main objective of this work was development of amine functionalized mesoporous silica (KIT-6) for carbon dioxide capture. In last 20 years, varieties of mesoporous silica were discovered. Without synthesizing any new material, this work explore the merits of the highly stable mesoporous KIT-6 with beneficial intrinsic properties such as three dimensional structure with large interconnected pore, high specific surface area and high pore volume in order to develop a good CO_2 adsorbent associated with high adsorption capacity as well as high selectivity. The major conclusions and the scope for future work based on the present research work are highlighted below.

- Synthesis procedure of highly ordered KIT-6 finally reveals that washing of as-synthesized KIT-6 improves the surface area and pore volume, hydrothermal treatment of synthesis solution alters the pore size and pore volume of KIT-6. Thermal treatment (upto 900 °C) gradually reduces the surface area, pore volume and pore size because of sintering of the structure of KIT-6. The synthesized KIT-6 possesses high mechanical stability, hydrolytic stability and thermal stability. However, low CO_2 adsorption capacity at low pressure (below 1 bar) does not suit it for practical application. Hence, it requires further improvement which is attempted in this.
- CO_2 adsorption capacity of highly stable KIT-6 is improved by grafting of APTES in both dry and aqueous solution. The loading of APTES increases with increase in water

concentration in the grafting solution. TEM micrograph shows the non-uniform apportionment of APTES in KIT-6 surface. CO_2 adsorption takes place on amine functionalized KIT-6 by the combined effect of chemisorption with amine sites and physisorption with surface. APTES grafted KIT-6 showed the stable sorption capacity of 1.56 mmol CO_2/g of adsorbent at 1 bar and 30°C.

- Adsorption capacity of amine functionalized adsorbent is directly associated with accessible amine sites with CO_2. The sorption capacity KIT-6 is further improved by grafting of TMPTA in aqueous solution showing adsorption capacity 2.59 mmol CO_2/g adsorbent at 30 °C and 1 bar, which is much higher than the sorption capacity of TMPTA grafted traditional MCM-41 and SBA-15 with 1.36 mmol CO_2/g and 1.54 mmol CO_2/g, respectively.
- Further, KIT-6 is functionalized with wide varieties of polyethylenimine such as DETA, TEPA, PEHA, PEI-800, PEI-1200 and PEI-25K by wet impregnation method. Thermal stability of adsorbent decreases with increases in molecular weight of polyethylenimine. High molecular weight PEI shows the low CO_2 sorption capacity over TEPA and PEHA impregnated KIT-6. The 60 wt% PEHA impregnated KIT-6 shows the maximum and stable sorption capacity between 4.0 to 4.5 mmol CO_2/g at 90 °C to 105 °C at 1 bar. The sorption capacity of polyethylenimine adsorbent increases with increase in adsorption temperature.
- Adsorption performance of PEHA impregnated KIT-6 are compared with MCM-41, SBA-15 and HV MCM-41. It is found that the adsorption capacity depends on the pore size of the adsorbent. Similar pore size containing adsorbents SBA-15 and KIT-6 show the nearly similar adsorption performance. Smaller pore size containing adsorbents MCM-41 and HV MCM-41 show low adsorption capacity.

- In order to avoid the calcination of mesoporous silica requiring high temperature and long time, as-synthesized (uncalcined) KIT-6 is functionalized with DETA, TEPA, PEHA, PEI-800 and PEI-25K. That show interesting adsorption performance. Presence of structure directing agent in the adsorbent improves the thermal stability of adsorbent. PEHA impregnated KIT-6 shows the maximum adsorption capacity ca. 4.2 mmol CO_2/g at 105 °C at 1 bar. However, CO_2 adsorption efficiency gradually decreases with increase in PEHA loading. Structure directing agent present in the adsorbent increases the adsorption rate. Thus, high sorption capacity at low partial pressure and high temperature designate PEHA impregnated as-synthesized KIT-6 as a promising candidate for CO_2 capture from large anthropogenic source.

Scope for Future Work

The immediate future scopes of the present work are as follows:

- CO_2 adsorption study with flue gas in order to understand the effect of the presence of impurities such as water vapor, SO_x, NO_x and CO.
- Development of adsorbent in pellet form to study the breakthrough performance in an adsorption column in order to understand the design aspects of the adsorber unit.
- Detailed design and development of the cyclic adsorption/desorption process for practical application.
- Study the adsorption mechanisam on molecular label of amine functionalized silica using monti-carlo method.

APPENDIX

A1.1 Calclation of amine loading

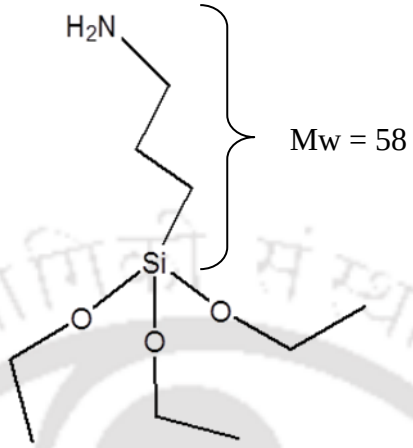

Figure A1. Molecular structure of (3-aminopropyl)triethoxysilane (APTES)

The amine loading amounts of amine-grafted sorbents were determined by the weight loss occurred at high temperature, which can be measured by TGA. With APTES grafted KIT-6 being an example, the detail of grafted amine loading of samples is provided below.

Considering the density and geometric distribution of silanols on the sorbent support, APTES grafted with 3 surface silanols when performing the silanization reaction. The weight loss of the samples was contributed to the complete removal of 3-aminopropyl group (200 ºC – 600 ºC). Thus amine loading amount of the sorbents was calculated based on the weight loss.

$$(mmol\ N/g - adsorbent) = \frac{Weight\ loss\ (wt\%)}{Molecular\ weight\ of\ propyl\ chain}$$

Table. A1 List of amine functionalized mesoporous silica and their CO_2 sorption capacity

Sorbent	**Amine**	**S_{BET} (m2/g)**	**P_d (nm)**	**V_t (cc/g)**	**Method**	**Temp (°C)**	**PCO_2 (bar)**	**Method**	**q_e (mmolCO_2/g)**	**Ref.**
Silica Gel	Mono	340	12	1.4	Grafting	22	1	volumetric	0.41	127
HMS	Mono	762	3	1.02	Grafting	20	0.91	TGA	0.86	144
HMS	Mono	1198	2.1	0.97	Grafting	20	0.91	TGA	1.59	144
Xerogel	Mono	816			Grafting	25	1	TGA	1.12	147
MCM-48	Mono	1389			Grafting	25	0.05	TGA	1.14	147
SBA-15	Mono	910	5.9	1.1	Grafting	60	0.15	GC	0.15	146
SBA-15	Mono	910	5.9	1.1	Grafting	60	0.15	GC	0.26	146
SBA-15	Tri	910	5.9	1.1	Grafting	60	0.15	GC	0.35	146
MCM-48	Mono	1349		1.03 ± 0.06	Grafting	25	0.05	volumetric	1.09	138
MCM-41	Mono	1045	30	2.5882	Grafting	30	1	Gravimetric	1.2	123
MCM-41	Mono	1204		0.79	Grafting	30	1		0.7	137
MCM-41	Mono	1045	30	2.5882	Grafting (Aqueous)	30	1	Gravimetric	1.58	129
MCM-41	Mono	1045	30	2.5882	Grafting (Aqueous)	75	1	Gravimetric	1.26	129
MCM-41	Tri	1045	30	2.5882	Grafting (Aqueous)	30	1	Gravimetric	1.78	129

Cont…

MCM-41	Tri	1045	30	2.5882	Grafting (Aqueous)	75	1	Gravimetric	2.1	129
MCM-48	Mono	1290	2.58	1.15	Grafting	25	1	MB	0.8	145
SBA-15 (Cal.)	Mono	824	7.4	0.92	Grafting	25	1	Volumetric	1.54	136
SBA-15 (Ext.)	Mono	786	7.6	1.04	Grafting	25	1	Volumetric	1.84	136
MCM-41	Mono	1506	3.3		Grafting	25	1	MB	0.57	142
SBA-12	Mono	1347	3.8		Grafting	25	1	MB	1.04	142
SBA-15	Mono	687	7.1		Grafting	25	1	MB	1.54	142
MCM-41	NH_3 (mono)	995		1.27	Ammonolysis	25	1	Volumetric	2.72	135
SBA-12	Mono	1347	3.8	0.84	Grafting	25	10% CO_2/N_2	TGA	1.04	114
SBA-12	Mono	1347	3.8	0.84	Grafting	25	10% CO_2/N_2	TGA	0.98	114
SBA-12	3(phenylamino) propyltrimethoxysilane	1347	3.8	0.84	Grafting	25	10% CO_2/N_2	TGA	0.68	114

Cont…..

PE-SBA-15	Mono	428	15.2	1.18	Grafting	45	1	Volumetric	1.49	133
PE-SBA-15	Di	428	15.2	1.18	Grafting	45	1	Volumetric	1.62	133
MCM-41	Mono	1031	3.5	0.897	Grafting	30	0.1		0.7	137
MCM-41	Mono	1031	3.5	0.897	Grafting	30	2.1		1.15	137
Platelet SBA-15	Mono	752	14.7	1.46	Grafting	25	1		1.58	131
	Di				Grafting	25	1		2.01	131
	Tri				Grafting	25	1		2.67	131
SBA-15	Mono	906	7.5	1.23	Grafting	25	1		0.99	131
	Di				Grafting	25	1		1.15	131
	Tri				Grafting	25	1		1.23	131
AMSA	Mono	628.45	20.71	3.25	co-condensation	25	1	Gas analyzer	1.95	139
						50	1	Gas analyzer	1.19	139

Cont…

Aerogels	Mono	767	42.7	4.2	Grafting	25	1	MB	0.67	132
	Di				Grafting	25	1	MB	1.2	132
	Tri				Grafting	25	1	MB	1.64	132
	Tri (Aqueous)				Grafting	25	1	MB	2.61	132
MCM-41	Di	856	2.7	0.95	Grafting	30	1	Volumetric	0.96	130
	Tri								1.01	130
	4-aminopyridine								0.07	130
	4-(methylamino) pyridine								0.36	130
	1,5,7-triazabicyclo [4.4.0]-dec-5-ene								0.4	130
SBA-15	Diamine	~ 200			Grafting	22	1	TGA	1.95	116
SBA-16	Diamine	479	0.48		Grafting	60	1	TGA	0.727	115
SNT	Mono	348		1.11	Grafting	25	1	TGA	1.45	134
	Di				Grafting	25	1	TGA	1.89	134
	Tri				Grafting	25	1	TGA	2.23	134
	Secondry				Grafting	25	1	TGA	0.95	134
	Tertary				Grafting	25	1	TGA	0.12	134

Cont…..

SNT	Mono	348		1.11	Grafting	100	1	TGA	1.13	134
	Di				Grafting	100	1	TGA	1.27	134
	Tri				Grafting	100	1	TGA	1.57	134
	Secondry				Grafting	100	1	TGA	0.55	134
	Tertary				Grafting	100	1	TGA	0.05	134
SBA-16/Cal	Diamine	715		0.54	Grafting	27	30	Microcalorimeter	3 to 4	115
SBA-16/Exc.	Diamine	574		0.49	Grafting	27	30		3 to 4	115
SBA-15	Primary	892	5.29		Grafting	25	1	TGA	0.95	124
	Secondry							TGA	0.75	124
	Tertary							TGA	0.17	124
PE-MCM-41	Triamine (Aqueous)	1134	10.88	2.26	Grafting	25	0.1	Rubotherm	2.16	122
PE-MCM-41	Triamine (Aqueous)				Grafting	25	1	Rubotherm	2.77	122
MCM-41	50wt% PEI	1480	2.75	1	Impregnation	75	1	TGA	2.54	128
SBA-15	50wt%PEI, Mw = 423 linear	950	6.6	1.31	Impregnation	75	Cin =15%	GC/ Gravimetric	3.14	155

Cont…..

KIT-6	50wt% TEPA	943	6	1	Impregnation	60	Cin = 10%	TGA	2.9	159
MCM-41	50wt% PEI, Mw = 600	1042	2.8	0.85	Impregnation	75	1	TGA	2.52	120
KIT-6	50wt% PEI, Mw =600	895	6	1.22	Impregnation	75	1	TGA	3.06	120
MCM-48	50wt% PEI, Mw =600	1162	3.1	1.17	Impregnation	75	1	TGA	2.70	120
SBA-15	60wt% PEI, Mw. = 600	753	5.5	0.94	Impregnation	75	1	TGA	2.88	120
SBA-16	50wt% PEI, Mw = 600	776	4.1	0.75	Impregnation	75	1	TGA	2.93	120
AS- SBA-15	50wt%TEPA	345	8.9	0.71	Impregnation	100		GC	151	
SBA-15	60wt%PEI, Mw = 800, Branched	775	8.9	1.1	Impregnation	75	1	volumetric	2.04	31
SBA-15	60wt%PEI, Mw = 800, Branched	775	8.9	1.1	Impregnation	75	5	volumetric	2.16	31
SBA-15	50wt% PEHA	452		0.95	Impregnation	80	1	Gas analyzer	3.50	160
Nano-silica	60wt%PEI, Mw = 600				Impregnation	75	1	TGA	3.11	156

Cont…

Nano-silica	60wt%PEI, Mw = 600				Impregnation	90	1	TGA	3.75	156
MCF	65wt%PEI, Mw = 423	950	18	2.4	Impregnation	30	1	TGA	2.61	10
MCF	65wt%PEI, Mw = 423	950	18	2.4	Impregnation	75	1	TGA	4.56	10
HMS	50wt%PEI, Mw = 423	1012	2.6	1.12	Impregnation	75	1	TGA	2.95	10
MSU-J	50wt%PEI, Mw = 423	880	9.4	1.6	Impregnation	75	1		3.11	10
SBA-15	50wt%PEI, Mw = 423	950	6.6	1.31	Impregnation	75	1		2.72	10
MCM-41	50wt%PEI, Mw = 423	1129	2.7	1.15	Impregnation	75	1	TGA	2.38	10
Disorder MS	50wt%TEPA	451.5	4.75	0.54	Impregnation	100	1	MB	4.4	25

Research Publications

1. **R. Kishor,** A. K. Ghoshal, APTES grafted ordered mesoporous silica KIT-6 for CO_2 adsorption, *Chem. Eng. J.*, 262 (**2015**) 882–890.
2. **R. Kishor**, A. K. Ghoshal, *N*[1]-(3-Trimethoxysilylpropyl)diethylenetriamine grafted KIT-6 for CO_2/N_2 selective separation, *RSC Adv.*, 6, 2016, 898–909.
3. **R. Kishor**, A. K. Ghoshal, High molecular weight polyethyleneimine functionalized three dimensional mesoporous silica for regenerable CO_2 separation, *Chem. Eng. J.*, 300 (**2016**) 236–244.
4. **R. Kishor**, A. K. Ghoshal, Polyethylenimine functionalized as-synthesized KIT‑6 adsorbent for highly CO_2/N_2 selective separation, *Energy Fuels* 30 (**2016**) 9635−9644.
5. **R. Kishor**, A. K. Ghoshal, Understanding the hydrothermal, thermal, mechanical and hydrolytic stability of mesoporous KIT-6: A comprehensive study, *Micropor. Mesopor. Mater.* 242 (**2017**) 127-135.
6. **R. Kishor**, A. K. Ghoshal, Amine modified mesoporous silica for CO_2 adsorption: The role of structural parameters, *Ind. Eng. Chem. Res.* 56, (**2017**) 6078−6087.
7. **R. Kishor**, A. K. Ghoshal, Aqueous aminosilane solution grafted three dimensional mesoporous silica for excellent adsorption performance and CO_2/N_2 selectivity, *Micropor. Mesopor. Mater.* 246 (**2017**) 137- 146.

National/International conference and workshop

1. **R. Kishor** Awareness and capacity building in carbon capture and storage: Earth process (acBCCS-2013) 15th –19th Jan, 2013, Climate Change Research Society New Delhi.
2. **R. Kishor** "Indo-finnish workshop on green chemistry", 13-14 Dec, 2013, Tezpur University.
3. **R. Kishor**, A. K. Ghoshal, Effect of nature of amine on CO_2 capture, Chemcon, 27th – 30th Dec., 2013, ICT, Mumbai. (Oral presentation)
4. **R. Kishor**, A. K. Ghoshal, CO_2 capture in amine functionalized silica, KIT-6, Harnessing natural resources for sustainable development: Global Trends 29th – 31st Jan, 2014 Cotton college, Guwahati. (Oral presentation)

5. **R. Kishor**, A. K. Ghoshal, Periodic Mesoporous Organosilicas Functionalized With Amine for CO_2 Adsorption, Sustainable development of environmental systems 20^{th} – 21^{st} June, 2014 IIT Guwahati. (Poster presentation)
6. **R. Kishor**, A. K. Ghoshal, S. Gumma, Tetraethylenepentamine-modified mesoporous silica KIT-6: Excellent material for CO_2 adsorption, Reflux 2015 27^{th} –29^{th} March, IIT Guwahati. (Oral presentation)
7. **R. Kishor**, A.K. Ghoshal, Effect of surface morphology on aminosilane grafting: Influence CO_2 adsorption capacity, Chemcon, 27th – 30th Dec., 2015, IIT Guwahati. (Poster presentation)
8. **R. Kishor,** Highly CO_2/N_2 selective separation on Mesoporous KIT-6 modified with amino groups functionalization, 3^{rd} Indo-German workshop, Advances in materials, Reaction & separation processes 23-26 Feb, 2016.
9. **R. Kishor**, A. K. Ghoshal, A major greenhouse gas "Carbon dioxide" capture by polyethylenimine impregnated KIT-6 to renewable source for useful hydrocarbons synthesis; Recycle April 1-2, 2016. (Oral presentation)
10. **R. Kishor**, A. K. Ghoshal, Adsorption of CO_2 on polyethyleneimine impregnated mesoporous silica sorbent, ICETNMST-2017, January 4-6, 2017 (Poster presentation)

Microporous and Mesoporous Materials 246 (2017) 137–146

Contents lists available at ScienceDirect

Microporous and Mesoporous Materials

journal homepage: www.elsevier.com/locate/micromeso

Aqueous aminosilane solution grafted three dimensional mesoporous silica for CO_2/N_2 separation

Rupak Kishor*, Aloke Kumar Ghoshal

Department of Chemical Engineering, Indian Institute of Technology Guwahati, Guwahati, 781039, Assam, India

ARTICLE INFO

Article history:
Received 2 June 2016
Received in revised form
23 February 2017
Accepted 16 March 2017
Available online 19 March 2017

Keywords:
Adsorbent
Aqueous grafting
Aminosilane
CO_2 adsorption
KIT-6
Selectivity

ABSTRACT

Three dimensional (3-D) mesoporous silica with large interconnecting pores are found suitable for aminosilane grafting to achieve high CO_2 adsorption with higher amine loading. In the present study, cubic KIT-6 is functionalized by (3-aminopropyl)triethoxysilane, *N*-[3-(trimethoxysilyl)propyl]ethylenediamine and N^1-(3-trimethoxysilylpropyle)diethylene triamine with various concentrations of water in aqueous solvent by post grafting method. The effect of water in grafting of aminosilane onto KIT-6 is analyzed by N_2 adsorption/desorption, TEM micrograph, TG analysis and CO_2 adsorption. The TG analysis suggests that, surface density of aminosilane increases with increase in water concentration in grafting solvent and TEM micrograph apparently shows the more intense aminosilane on mesoscopic level. The maximum adsorption capacity is 1.60, 2.09 and 2.59 mmol CO_2/g-adsorbent for WK.20AP, WK.20DA and WK.10TA, respectively at 30 °C and 1.0 bar. The CO_2/N_2 selectivity is much higher for aqueous solution grafted adsorbent. Moreover, aqueous solution grafted adsorbents are regenerable showing stable sorption performance till 20 cycles. Thus, aqueous solution grafting is a more efficient way to graft the aminosilane on mesoporous silica as well as design CO_2/N_2 selective adsorbent.

1. Introduction

Natural calamities such as gradual warming of the earth, rising of the sea level, unpredictable flood and drought situation are indicative of greenhouse effect, which is mainly caused by emission of CO_2 into the atmosphere from large anthropogenic sources such as coal based thermal power plant and crude oil refinery [1]. In order to control CO_2 concentration in atmosphere, carbon capture and utilization (CCU) is a promising technology and it is indispensable to develop a highly efficient and cost effective capture process. The basic alkanolamines based absorption process have a great potential to capture CO_2 from anthropogenic sources as well as atmosphere [2–4]. Certain drawbacks of amine based absorption process like corrosion of process equipment, amine degradation for high regeneration temperature and presence of oxygen in flue gas, high heat penalty and amine loss during regeneration and other unwanted carbonate salt formation in the solvent made it necessary to look for other alternatives [3,5].

Adsorption is a potential alternative and a large number of innovative works are being carried out to develop highly CO_2/N_2 selective adsorbents. Recently zeolites [6–8], metal organic frameworks (MOFs) [6,7,9], activated carbon (AC) [6], mesoporous metal oxide [10] emerged as potential adsorbents in CO_2 capture including covalent-organic frameworks (COFs) [11]. However, high heat penalty for regeneration of zeolites, low adsorption capacity (q_m) for AC and susceptibility to moisture for MOFs are significant drawbacks for which further alternatives are being searched. Amine immobilized adsorbents received a special attention in designing the low partial pressure based CO_2 adsorbent [12–40]. Chunsying et al. [13] designed the tetraethylenepentamine functionalized Y-type zeolite and showed the 3.3 mmol CO_2/g adsorption capacity with 50% CO_2 feed concentration. Zhang et al. [14] showed the heat of regeneration of amine functionalized adsorbent as 2.46 GJ/t CO_2 which is much lower than 3.9 GJ/tCO_2 for traditional aqueous MEA system. Jaroniec et al. [15] synthesized the periodic mesoporous benzenesilicas and functionalized them by grafting of mono, di and triaminosilane. The study showed the maximum of 3.03 mmol CO_2/g capacity with diamine grafted benzenesilicas at 25 °C and 1 bar. On the other hand, varieties of amine immobilized mesoporous silica such as MCM–series [16–18], SBA–series [12,19,21], KIT–series [22,23], MSU–F [24] and

* Corresponding author.
E-mail address: rupak.k@iitg.ernet.in (R. Kishor).

http://dx.doi.org/10.1016/j.micromeso.2017.03.023
1387-1811/

I&EC research
Industrial & Engineering Chemistry Research

Article

pubs.acs.org/IECR

Amine-Modified Mesoporous Silica for CO_2 Adsorption: The Role of Structural Parameters

Rupak Kishor* and Aloke Kumar Ghoshal

Department of Chemical Engineering, Indian Institute of Technology Guwahati, Guwahati, 781039 Assam, India

Supporting Information

ABSTRACT: The present study investigated the role of structural parameters such as pore size, pore volume, and specific surface area of mesoporous silica on the CO_2 sorption performance of various amine-functionalized adsorbents. A series of mesoporous silica with different structural properties KIT-6, MCM-41, SBA-15, and HV MCM-41 were synthesized and functionalized with pentaethylene-hexamine (PEHA) by wet impregnation. The CO_2 sorption performances of the sorbents were evaluated using high pressure gas adsorption analyzer. The sorption capacity of adsorbents follows the order: MCM-41 < HV MCM-41 < SBA-15 ≈ KIT-6 at 105 °C and 1 bar. Larger pore size reduces the mass transfer resistance, and large pore volume improves the PEHA distribution inside the pores. The high specific surface area has little impact during adsorption. Due to the 3D structure with interconnected pores, KIT-6 shows the lowest heat of regeneration (57.8 kJ/mol CO_2) during adsorption. The PEHA-impregnated KIT-6 (K-60 PEHA) shows the highest sorption capacity 4.48 mol CO_2/g at 105 °C and 1 bar. It also exhibit fairly stable sorption performance up to 10 adsorption/desorption cycles between in the temperature range of 90−105 °C.

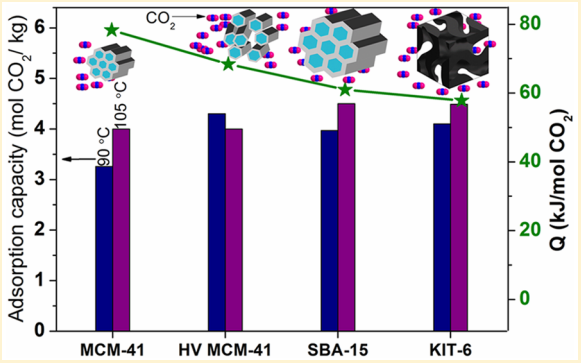

1. INTRODUCTION

At present, an aqueous alkanolamine (such as monoethanol-amine and diethanolamine) based absorption process is widely used to capture CO_2 at atmospheric condition.[1] However, the large energy requirement during solvent regeneration, corrosive nature of amines toward the equipment, and most importantly the amine loss in atmosphere during regeneration necessitates looking for an alternative process.[1,2] Amine-functionalized porous solid such as activated carbon[3,4] zeolites,[5] mesoporous silica,[6−9] and metal−organic frameworks (MOFs)[3,10] are found to be good candidates for CO_2 capture at low pressure. However, structural instability and sharp reduction in adsorption capacity under most conditions with zeolites and MOFs require further research and improvement for said application.[8]

In the past few years, amine-functionalized mesoporous silica received attentions from a large community of researchers for CO_2 capture because of its high structural stability, high surface area, and tunable pore size and pore volume.[11,12] Xu et al.[13] developed a polyethylenimine (PEI)-impregnated "molecular basket", which showed high CO_2 sorption capacity (3.0 mol CO_2/kg) and selectivity. Subsequently, several amine-functionalized mesoporous silica such as MCM-41,[14−16] SBA-15,[17] KIT-6,[7,16] MCF,[18,19] and aerogel[20] were tested in order to have an adsorbent with improved sorption performance. It was obviously observed that the sorption capacity depends on the mesoporous structure, pore size, pore volume, and type of amine.

At present, limited work has been done to understand the role of structural parameter of support on the CO_2 adsorption performance. Yan et al.[19] increased the sorption capacity from 2.51 to 4.04 mol CO_2/kg by increasing the pore volume from 1.51 to 1.82 cc/g of PEI-impregnated MCF at 75 °C and 0.15 bar, while Chen at al.[12] achieved a sorption capacity of 4.18 mol CO_2/kg at 75 °C with 60 wt % PEI loading by using three-dimensional hexagonal mesoporous silica with wormhole-like pore structure as support. Moreover, Wang et al.[21] improved the CO_2 sorption capacity of tetraethylenepentamine (TEPA)-impregnated ordered mesoporous silica from 2.31 to 3.1 mol/kg by changing the pore size from 5.6 to 7.6 nm. It should be noted that the surface area, intrinsic pore structure, and pore volume play an important role during application. In our previous study, we found that the adsorption capacity of KIT-6 was decreased with increase in molecular weight of PEI.[7] The maximum sorption capacity observed was 3.0 mol CO_2/kg (M_w of PEI = 800) at 105 °C and 1 bar, although low molecular weight TEPA- and PEHA-impregnated mesoporous silica showed much higher sorption than high molecular weight PEI.[14,22] Additionally, 3D support improved the sorption kinetics of amine-functionalized sorbent.[9,16] Thus, the above literatures clearly indicate that the structural parameters of

Received: March 1, 2017
Revised: April 20, 2017
Accepted: May 3, 2017
Published: May 3, 2017

DOI: 10.1021/acs.iecr.7b00890
Ind. Eng. Chem. Res. 2017, 56, 6078−6087

Chemical Engineering Journal 262 (2015) 882–890

Contents lists available at ScienceDirect

Chemical Engineering Journal

journal homepage: www.elsevier.com/locate/cej

APTES grafted ordered mesoporous silica KIT-6 for CO_2 adsorption

Rupak Kishor, Aloke Kumar Ghoshal *

Department of Chemical Engineering, Indian Institute of Technology Guwahati, Guwahati 781039, Assam, India

HIGHLIGHTS

- KIT-6 was synthesized and APTES grafted in both dry and aqueous solution.
- Role of water on APTES loading in KIT-6 and grafting mechanism is explained.
- APTES grafted KIT-6 exhibited a CO_2 adsorption capacity of 0.90–1.56 mmol g^{-1}.

GRAPHICAL ABSTRACT

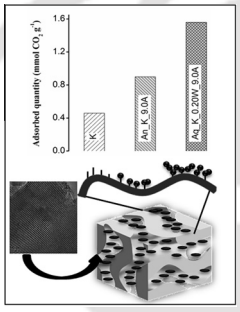

ARTICLE INFO

Article history:
Received 15 August 2014
Received in revised form 12 October 2014
Accepted 13 October 2014
Available online 22 October 2014

Keywords:
KIT-6
Mesoporous silica
Grafting
APTES
CO_2 adsorption

ABSTRACT

Pure KIT-6 was synthesized using pluronic P123 ($PEO_{20}PPO_{70}PEO_{20}$, mw ~ 5800 Da) surfactant in mild acidic condition. It was functionalized with (3-aminopropyl) triethoxysilane (APTES) by grafting in dry and aqueous solvent at 80 °C. Cubic (Ia3d) structure and uniformity of the adsorbents were analyzed by small angle powder X-ray diffraction (XRD) and high-resolution transmission electron microscopy (HRTEM). Physical properties of the adsorbents were characterized by nitrogen adsorption/desorption behavior, infrared spectroscopy (IR) and thermo gravimetric (TG) analysis. CO_2 adsorption/desorption behavior of the adsorbents was studied in a gravimetric analyzer. Optimum amine loading was substantially increased from 1.74 mmol N g^{-1} in dry grafting to 2.75 mmol N g^{-1} in aqueous grafting. The adsorption capacity was also remarkably increased from 0.90 mmol CO_2 g^{-1} (An_K_9.0A) to 1.56 mmol CO_2 g^{-1} (Aq_K_0.20W_9.0A) at 30 °C. The heat of adsorption of the process was in the range of 20–32 kJ mol^{-1}. The adsorbent showed its stability with the adsorption capacity remaining constant over 10 adsorption/desorption cycles.

1. Introduction

The rapid increase in global warming and its adverse effects on the environment, especially on the marine ecosystem has become a threat across the globe. According to earlier studies of paleoclimate data and CO_2 concentration in atmosphere, the rapid increase of global warming is mainly due to CO_2 and other greenhouse gases [1]. By observation of "Mauna Loa Observatory" Hawaii, CO_2 atmospheric concentration has already reached ~400 ppm in 2014 and it will reach 450 ppm in next few years, which is sufficient to increase global surface temperature above 2 °C of the maximum limit range [2]. In the "United Nations Climate Change Conferences, Warsaw" (COP-19) countries have taken a strong decision to control the global warming by CO_2 capture and sequestration (CCS) [3].

Coal, oil and natural gas are the major sources of energy and these provide 80% of world energy demand. These energy sectors are the major anthropogenic sources of CO_2 [4]. CCS is important to mitigate the global warming and its consequences by capture of CO_2 from large anthropogenic sources. Aqueous alkanolamines

* Corresponding author. Tel.: +91 361 2582252; fax: +91 361 2582291.
E-mail addresses: rupak.k@iitg.ernet.in (R. Kishor), aloke@iitg.ernet.in (A.K. Ghoshal).

http://dx.doi.org/10.1016/j.cej.2014.10.039
1385-8947/

Chemical Engineering Journal 300 (2016) 236–244

Contents lists available at ScienceDirect

Chemical Engineering Journal

journal homepage: www.elsevier.com/locate/cej

High molecular weight polyethyleneimine functionalized three dimensional mesoporous silica for regenerable CO_2 separation

Rupak Kishor *, Aloke Kumar Ghoshal

Department of Chemical Engineering, Indian Institute of Technology Guwahati, Guwahati 781039, Assam, India

HIGHLIGHTS

- High molecular weight amine functionalized KIT/8PEI, KIT/12PEI, KIT/250PEI adsorbent was synthesized.
- Adsorption capacity decreases with increasing the M_w of PEI.
- CO_2/N_2 selectivity increases with temperature.
- KIT/250PEI shows stable performance between 90–105 °C and 100 kPa.

ARTICLE INFO

Article history:
Received 26 February 2016
Received in revised form 8 April 2016
Accepted 9 April 2016
Available online 19 April 2016

Keywords:
CO_2/N_2 adsorption
Mesoporous silica
Polyethyleneimine
Selectivity
Cyclic performance

ABSTRACT

Polyethylenimine functionalized mesoporous silica is a potential alternative of amine based absorption process for CO_2 capture from flue gas. By impregnation of high molecular weight polyethylenimine (PEI) into three dimensional mesoporous KIT-6, a novel sorbent was prepared for highly CO_2/N_2 selective separation at moderate temperature and low partial pressure with high stability. TEM micrograph shows that, pore is covered with PEI and also a layer of PEI is formed on the surface of adsorbent without disturbing its original structure. TGA analysis confirmed that with increasing molecular weight of PEI, thermal stability of adsorbent was increased. The sorption capacity was increased with increasing the temperature form 30 to 120 °C and the adsorption mechanism is elucidated with the help of the nature of CO_2 equilibrium isotherms. The very high CO_2/N_2 selective adsorbent follows the order K/250PEI < K/12PEI < K/8PEI with maximum operating sorption capacity 3.0 mmol CO_2/g of K/8PEI at 105 °C and 100 kPa. Adsorbent showed stable sorption performance at moderate temperature (90–105)A/100D °C during 20 adsorption/desorption cycles. However, K/250PEI gives the maximum benefits in terms of stable sorption performance (2.4 mmol CO_2/g adsorbent at 105 °C and 100 kPa) and the necessary thermal stability for practical application.

1. Introduction

Release of greenhouse gases to environment results in increased average temperature of earth which is tending towards alarming limit of 2 °C [1,2]. In last few decades, the atmospheric CO_2 concentration has been increased from ~320 to ~400 ppm, and it influenced the global surface temperature, reduced the pH of ocean surface water and disturbed the ecosystem [1–6]. Majority of the greenhouse gases are released from thermal power plant, cement industries, solid waste and chemical industries where carbon dioxide (CO_2) shares 80–85% of it [4,5]. Emission of greenhouse gases to the atmosphere are required to be controlled in order to reduce its adverse effect on ecosystem and environment [2,3]. United nations climate change conference (COP 21, 2015) held at Paris was set ambitious goals to control global limit temperature rises (2 °C) which was legally agreed and signed by nearly 200 countries. To that end, carbon capture sequestration and utilization (CCSU) is a one of the possible option. Primarily post combustion CO_2 capture can target larger anthropogenic sources which emits concentrated gases [5,6].

The major component of flue gas from a thermal power plant is N_2 with ~0.10–0.15 bar partial pressure of CO_2 at moderate temperature. Amine based absorption process is commercially available for CO_2 capture [5]. But, low absorption temperature, excessive corrosion of equipment and large amounts of heat requirement during regeneration motivate for other alternatives [5–7]. Porous solid such as activated carbon, metal organic frameworks and mesoporous silica based adsorptive separation process is one such alternative [6,8–32]. In view of practical application,

* Corresponding author. Tel.: +91 361 2582300.
E-mail address: rupak.k@iitg.ernet.in (R. Kishor).

http://dx.doi.org/10.1016/j.cej.2016.04.055
1385-8947/

RSC Advances

PAPER

View Article Online
View Journal | View Issue

Cite this: *RSC Adv.*, 2016, **6**, 898

N^1-(3-Trimethoxysilylpropyl)diethylenetriamine grafted KIT-6 for CO_2/N_2 selective separation†

Rupak Kishor* and Aloke Kumar Ghoshal

Received 3rd October 2015
Accepted 14th December 2015

DOI: 10.1039/c5ra20489e

www.rsc.org/advances

In the present study N^1-(3-trimethoxysilylpropyl)diethylenetriamine was grafted on various ordered and commonly used mesoporous silica namely MCM-41 (2.2 nm), SBA-15 (6.6 nm) and KIT-6 (6.6 nm) in both anhydrous and aqueous conditions for CO_2/N_2 adsorption. The structural and physical properties before and after grafting were analyzed by nitrogen adsorption/desorption, X-ray diffraction and electron microscopy techniques. The uptake capacities of three-dimensional K30T and WK30T were 1.89 and 2.59 mol CO_2 per kg of adsorbent, respectively at 30 °C which are significantly higher than MCM-41 and SBA-15 based adsorbents. Analysis of the enthalpy of CO_2 adsorption, confirmed the adsorption in amine functionalized adsorbents by both chemical and physical interactions. Outstanding equilibrium CO_2/N_2 selectivity of functionalized KIT-6 over MCM-41 and SBA-15 opens up its practical applicability through a stable performance in several adsorptions/desorption cycles.

1. Introduction

Increasing trends of CO_2 concentration in the atmosphere are creating alarming conditions in the form of global warming across the globe. Especially in last few decades, the rate of CO_2 emission in the form of flue gas has drastically increased from large anthropogenic sources, particularly coal based thermal power plants. This is possibly due to industrialization and growth in energy demand across the globe.[1,2] As a result, the atmospheric CO_2 concentration increased from ~315 ppm in 1958 to ~400 ppm in 2015. Higher CO_2 concentrations have led to several environmental issues and therefore, reducing CO_2 emissions from the large anthropogenic sources is urgently required.

In order to control the CO_2 concentration in the atmosphere, carbon capture sequestration and utilization (CCSU) is a promising technology and is becoming indispensable to develop an efficient and cost effective separation process.[3] Basic monoethanolamine (MEA), diethanolamine (DEA) and mixed amines based absorption is in commercial operation throughout the world.[3,4] But, solid sorbent based separation process could be a potential alternative and a lot of innovative work has been carried out to develop highly CO_2/N_2 selective adsorbents. CO_2 from the anthropogenic source may be separated by a verity of solid physisorbents like zeolite,[5] porous carbon,[6,7] metal–organic frameworks (MOFs),[3,8–12] covalent organic frameworks (COFs),[13] polymer[14] and chemisorbents like alkali functionalized mesoporous silica and metal carbonates.[15–29] Microporous metal–organic frameworks shows very high sorption capacities and selectivity,[8–12] but susceptibility to moisture[8] demanding for further research for better alternatives. Alkali based metal carbonate (M_2CO_3, where M = Mg, Na, Cu, Zn *etc.*) and amine functionalized ordered mesoporous silica (OMSs) based regenerable solid sorbent are good alternatives over physisorbents for CO_2 sorption from flue gas.[15–17] Lee *et al.*[16,17] synthesized excellent adsorbent with 87–119 mg CO_2 per g sorption capacity at 60 °C and 1 bar by impregnation of potassium carbonate in ZrO_2, AC, TiO_2, Al_2O_3, MgO, SiO_2 and various zeolites. However, regeneration temperature (130–400 °C) and poor cyclic performance of adsorbents became less favourable for CO_2 capture. Amines are highly selective towards CO_2 *via* carbamate formation in low partial pressure as well as stable and easily regenerable at moderate temperature even in moist environment.[18–29] Aminosilane functionalized OMS is a suitable alternative for CO_2 sorption from anthropogenic source.

Since after the discovery of OMS by Mobil scientists in the early 1990s,[30] other OMSs like SBA-15 (ref. 22 and 27) (hexagonal), KIT-6 (ref. 28) (cubical), MCF[31] (disordered) and MSU[32] (hexagonal disordered) were also discovered. Due to high specific surface area (>600 $m^2\ g^{-1}$) and pore volume (>0.5 $cm^3\ g^{-1}$), they have attracted world-wide researcher's interest in various applications like catalysis,[33] nano-science[34] and drug delivery[35] by decorating the surface with organosilane. Yokoi *et al.*[19] synthesized the functionalized MCM-41 by direct co-condensation reaction with aminosilane and silica source during synthesis as well as by post grafting method. Among these, amine functionalized OMSs received the attention of a large community in CO_2 capture application. More recently, Linneen *et al.*[25] grafted mono, di and triaminosilane on silica aerogel with larger pore

Department of Chemical Engineering, Indian Institute of Technology Guwahati, Guwahati-781039, Assam, India. E-mail: rupak.k@iitg.ernet.in

† Electronic supplementary information (ESI) available: The effect of TMPTA concentration (Fig. S1) and TG analysis (Fig. S2). See DOI: 10.1039/c5ra20489e

energy&fuels

Article

pubs.acs.org/EF

Polyethylenimine Functionalized As-Synthesized KIT-6 Adsorbent for Highly CO_2/N_2 Selective Separation

Rupak Kishor* and Aloke Kumar Ghoshal

Department of Chemical Engineering, Indian Institute of Technology Guwahati, Guwahati-781039, Assam, India

Supporting Information

ABSTRACT: The present study targeted the synthesis of CO_2 adsorbent by impregnation of DETA, TEPA, PEHA, and polyethylenimine in KIT-6 with a confiscated structure directing agent in minimum time and energy. The adsorbents were characterized and revealed the influence of polyethylenimine with CO_2 at a wide range of temperatures. An examination by TGA confirmed that PluronicP123 present in adsorbent enhances its thermal stability and acts as a carrier for CO_2 to the inner layer of polyethylenimine during adsorption. CO_2 sorption capacity of the adsorbent was found to be dependent on the polyethylenimine loading, temperature, pressure, and the surfactant PluronicP123. At higher temperatures, adsorbents showed a positive impact for CO_2 adsorption; however, a negative effect was exhibited in amine efficiency. The sorption capacity decreased with increasing the molecular weight of polyethylenimine following the order PEI-25K (66 mg CO_2/g) < PEI-800 (114 mg CO_2/g) < TEPA (124 mg CO_2/g) < PEHA (139 mg CO_2/g) at 75 °C. However, 60 wt % PEHA impregnated KIT-6 showed the stable sorption capacity of 170−184 mg CO_2/g at 90−105 °C and 1 bar.

1. INTRODUCTION

Energy insecurity and associated environmental concerns have raised serious concerns about identifying alternate, sustainable, clean energy sources with less environmental impact.[1,2] Carbon dioxide, the major greenhouse gas generated from the burning of fossil fuels such as coal, petroleum oil, and natural gas, has reached a higher concentration of ∼400 ppm in the atmosphere.[2] The earth's surface temperature in 2015 was the warmest since 1980, according to independent analyses by the National Aeronautics and Space Administration (NASA) and National Oceanic and Atmospheric Administration (NOAA). Thus, to control the surface temperature, it is the need of the hour to control emissions from large anthropogenic sources. In the 21st session of the conference of the parties (COP-21) in 2015 including over 195 countries, a unanimous decision was taken to control CO_2 emission in the atmosphere in scientific ways.

Carbon capture and utilization (CCU) remains a promising option to control CO_2 emission, which consists of two major stages.[3−29] The primary stage involves CO_2 capture using an efficient separation process, while the secondary stage involves the conversion of captured CO_2 into various useful products with the help of effective catalysts.[3−5] Removal of CO_2 from flue gas using a commercially available amine-based absorption process has been receiving much interest among several authors.[3,7] However, the process remains energetically unfavorable due to reduced net power output attributed to several power losses in the CO_2 capture process during the amine regeneration and CO_2 compression step.[3,22,24] On the other hand, numerous adsorbents, especially activated carbon (AC),[25] carbon nanotubes (CNTs),[6] zeolite,[10,11,26] metal organic frameworks (MOFs),[10,16] and ordered mesoporous silica (MSs)[9−16,19,20] and its amine functionalized derivatives have received great attention for CO_2 adsorption under a wide range of temperatures and pressures. Mason et al.[10] showed that zeolites and most of the MOFs are highly unstable during CO_2 adsorption under flue gas conditions. However, amine functionalized mesoporous silica showed a positive effect during CO_2 adsorption under moist conditions as well as a high adsorption capacity at low partial pressure (∼0.15 bar).[10,27−29]

MS is functionalized by aminosilane grafting and the polyethylenimine wet impregnation method.[12−16,28,29] Wet impregnation received special attention over grafting for its simplicity in functionalization with low time consumption as well as high adsorption capacity. Song et al.[29] prepared the first polyethylenimine impregnated MS-based adsorbent. Later, several authors extensively studied the CO_2 adsorption on amine functionalized adsorbent.[10−19] Sayari and Belmabkhout[27] showed the enhanced CO_2 sorption capacity under moist conditions over dry ones as well as stable performance over large cycles. Son et al.[19] studied CO_2 adsorption over a wide variety of PEI-600 impregnated MCM-41, MCM-48, SBA-15, SBA-16, and KIT-6 silica. The 50 wt % PEI-600 impregnated 3D KIT-6 with large pores showed the highest adsorption capacity (135 mg CO_2/g-adsorbent) in a minimum response time.

In our previous report, the calcined KIT-6 modified with 50 wt % polyethylenimine (M_w: 800, 1200, and 25000) exhibits a CO_2 adsorption capacity of 132 mg CO_2/g, 107.8 mg CO_2/g, and 105.6 mg CO_2/g, respectively, at 105 °C and 1 bar.[14] High energy requirements and additional environmental pollutant formation during calcination (by burning of the structure directing agent) of mesoporous silica open a new window to exploring the uncalcined one. Yue et al.[16] modified the as-synthesized SBA-15 with tetraethylenepentamine impregnation

Received: August 17, 2016
Revised: October 19, 2016
Published: October 21, 2016

DOI: 10.1021/acs.energyfuels.6b02082
Energy Fuels 2016, 30, 9635−9644

Microporous and Mesoporous Materials 242 (2017) 127–135

Contents lists available at ScienceDirect

Microporous and Mesoporous Materials

journal homepage: www.elsevier.com/locate/micromeso

Understanding the hydrothermal, thermal, mechanical and hydrolytic stability of mesoporous KIT-6: A comprehensive study

Rupak Kishor*, Aloke Kumar Ghoshal

Department of Chemical Engineering, Indian Institute of Technology Guwahati, Guwahati, 781039, Assam, India

ARTICLE INFO

Article history:
Received 22 September 2016
Received in revised form
23 November 2016
Accepted 12 January 2017
Available online 16 January 2017

Keywords:
Gas adsorption
Hydrothermal stability
Mechanical stability
Mesoporous silica
Porosity
Thermal stability

ABSTRACT

The three dimensional KIT-6 with interconnected mesoporous was synthesized using triblock copolymer (P123) in mild acidic condition. The hydrothermal, thermal, mechanical and hydrolytic stability of KIT-6 were comprehensively investigated by N_2 adsorption/desorption, small-angle X-ray scattering and electron micrograph. In the initial stage of synthesis, washing of as-synthesized KIT-6 with water improves the textural property such as surface area and pore volume. The size of primary mesopores and pore volume of the material could be tailored by ageing the solution without any loss in structural morphology. KIT-6 shows the high mechanical stability up-to 4680 bar and preserves its mesopore surface area possibly due to the presence of thicker pore wall and cubical structure. KIT-6 shows the gradual decrease in surface area, pore volume and diameter with increasing calcination temperature from 823 to 1173 K, due to sintering/shrinkage of silica structure. It also shows the stable structural properties even after ageing for 6 months in atmospheric conditions and 1 month in water at room temperature. However, after 3 days of ageing in boiling water, KIT-6 still retains its porosity. In presence of ultra-high pressure, CO_2 shows good surface interaction towards KIT-6 with sorption capacity of 1.42 mol/kg (1 bar) and 10.1 mol/kg (20 bar) at 273 K without significant damage to its structure. Additionally, it also shows 2.38 wt% H_2 storage capacity at 30 bar and 77 K. The highly stable KIT-6 is considered to be a good material for catalyst support, nano structure, CO_2 separation and H_2 storage.

1. Introduction

In early 1990, the discovery of mesoporous molecular sieves (M41S) with uniform structure by researchers of the Mobil oil corporation using quaternary ammonium ($C_nH_{2n+1}(CH_3)_3NX$, X = Cl or Br) ionic template by liquid crystal templating sol-gel method was a great embodiment in material science [1,2]. Its physicochemical properties were investigated by several authors [2–17]. It has attracted great attention in wide applications like host-guest chemistry [18–20], size-selective separation [21–22], nano-material synthesis [23] and enzyme immobilization [24]. This id due to its aloof intrinsic properties such as high specific surface area (>600 m^2/g), pore volume (>0.5 cc/g) and narrow distribution of pore size (2–30 nm). Furthermore, covalently grafted organo-silane with silanol groups present on the silica surface shows improved performance during catalysis and gas separation application [19,21].

The physiochemical properties of mesoporous materials strongly affect the performance of process used for industrial applications. However, the pore characteristics (pore diameter, specific surface area, pore volume, etc.) of the material are strongly dependent on the synthesis procedures as well as post-synthesis treatments (calcination, pelletization, etc.). Moreover, traditional MCM-41(hexagonal) and MCM-48 (cubical) get their architecture collapsed and physicochemical properties destroyed in high pelletization pressure and moist conditions due to thinner pore wall [8–12,25,26]. Additionally, smaller pore opening of MCM-41 reduces the accessibility for larger reactant towards the active sites present in MCM based catalyst and adsorbent [21,22]. Numerous efforts have been reported in the literature to improve their physical properties [3–5,27–32]. MCM pores have been tailored between 1.5 and 10 nm by using the surfactants with variable chain length and swelling organic compound [3,4,27]. Jaroniec et al. [3] tailored the pore sizes of MCM-41 by hydrothermal synthesis and concluded that the high quality MCM-41 with maximum pore size up to 6.5 nm can be synthesized by

* Corresponding author.
E-mail addresses: rupak.k@iitg.ernet.in, kishorerupak@gmail.com (R. Kishor), akg_66@yahoo.com (A.K. Ghoshal).

http://dx.doi.org/10.1016/j.micromeso.2017.01.020
1387-1811/